4-7-2017

Therapeutic Modulation of Cancer Metabolism with Dichloroacetate and Metformin

Nathan Patrick Ward
University of South Florida, nward2@health.usf.edu

Therapeutic Modulation of Cancer Metabolism with Dichloroacetate and Metformin

by

Nathan Patrick Ward

A dissertation submitted in partial fulfillment
of the requirements for the degree of
Doctor of Philosophy
Department of Molecular Pharmacology and Physiology
Morsani College of Medicine
University of South Florida

Major Professor: Dominic D'Agostino, Ph.D.
Jay Dean, Ph.D.
Emma Heart, Ph.D.
Thomas Taylor-Clark, Ph.D.
Marzenna Wiranowska, Ph.D.

Date of Approval:
November 7, 2016

Keywords: Cancer metabolism, mitochondrial glucose oxidation, complex I inhibition, oxidative stress, DCA, metformin

TABLE OF CONTENTS

LIST OF TABLES

LIST OF FIGURES

LIST OF ABBREVIATIONS

CO_2 ..... Carbon Dioxide
Cu^{3+} ..... Cupric Ion
Fe^{2+} ..... Ferrous Ion
H^+ ..... Hydrogen Ion/Proton
H_2O_2 ..... Hydrogen Peroxide
HCO_3^- ..... Bicarbonate
K^+ ..... Potassium
N_2 ..... Nitrogen (gas)
$^{\cdot}NO$ ..... Nitric Oxide
O_2 ..... Oxygen
pO_2 ..... Partial Pressure of Oxygen
$^{\cdot}O_2^-$ ..... Superoxide Anion
$^{\cdot}OH$ ..... Hydroxyl Radical
$ONOO^-$ ..... Peroxynitrite
P_i ..... Inorganic Phosphate
$\Delta\Psi_m$ ..... Mitochondrial Membrane Potential
2-DG 2-Deoxyglucose
2-HG 2-Hydroxyglutarate
3-BP 3-Bromopyruvate
3-PG 3-Phosphoglycerate
5-FU ..... Hydroxyl Radical
8-OHdG 8-Hydroxydeoxyguanosine
AC ..... Adenylate Cyclase
ACC ..... Acetyl-CoA Carboxylase
Acetyl-CoA ..... Acetyl Coenzyme A
ACLY ..... ATP Citrate Lyase
ACSS2 ..... Acyl-CoA Synthetase Short-Chain Family Member 2
AICAR ..... 5-Aminoimadazole-4-Carboxamide Ribonucleotide
ANOVA ..... Analysis of Variance
ATA ..... Atmospheres Absolute
ADP ..... Adenine Diphosphate
AMP ..... Adenosine Monophosphate
AMPK ..... AMP-Activated Protein Kinase
ASCT2 ..... Glutamine/Amino Acid Transporter 2
ATM ..... Ataxia-Telangiectasia Mutated
ATP ..... Adenosine Triphosphate
BCAA ..... Branch Chain Amino Acid
βHB ..... β-hydroxybutyrate
BSO ..... Buthionine Sulfoximine
CAD ..... Carbomyl Phosphate Synthase
CAIX ..... Carbonic Anhydrase IX
cAMP ..... Cyclic AMP
CD3 ..... Cluster of Differentiation 3
CD11b ..... Cluster of Differentiation 11b
CD19 ..... Cluster of Differentation 19

CD44 ..... Cluster of Differentiation 44
CD45 ..... Cluster of Differentiation 45
CD68 ..... Cluster of Differentiation 68
CD133 ..... Cluster of Differentiation 133
CDK ..... Cyclin-Dependent Kinase
CL ..... Cardiolipin
CML ..... Chronic Myeloid Leukemia
CNS ..... Central Nervous System
CoASH ..... Coenzyme A
Complex I ..... NADH: Ubiquinone Reductase
Complex II ..... Succinate: Ubiquinone Reductase
Complex III ..... Ubiquinone: Cytochrome C Oxidoreductase
CR ..... Calorie Restriction
CS ..... Citrate Synthase
CSC ..... Cancer Stem Cell
DCA ..... Dichloroacetate
DHAP ..... Dihydroxyacetone Phosphate
DHF ..... Dihydrofolate
DHFR ..... Dihydrofolate Reductase
DLBCL ..... Diffuse Large B Cell Lymphoma
DNA ..... Deoxyribonucleic Acid
DON 6-Diazo-5-oxo-L-norleucine
ECM ..... Extracellular Matrix
EGCG Epigallo-Catechin-3-Gallate
EGFR ..... Epidermal Growth Factor Receptor
EMT ..... Epithelial-to-Mesenchymal Transition
ER ..... Endoplasmic Reticulum
ETC ..... Electron Transport Chain
EthD-1 ..... Ethidium Homodimer-1
F4/80 ..... EGF-Like Module-Containing Muncin-Like Hormone Receptor 1
FAD^+ ..... Oxidized Flavin Adenine Dinucleotide
$FADH_2$ ..... Reduced Flavin Adenine Dinucleotide
FAO ..... Fatty Acid Oxidation/ β-oxidation
FAS ..... Fatty Acid Synthesis
FASN ..... Fatty Acid Synthase
FCCP ..... Carbonyl Cyanide 4-(Fluoromethoxy)phenylhydrazone
^{18}FDG ..... ^{18}F-deoxyglucose
FDG-PET ..... Fluorodeoxyglucose Positron Emission Tomography
FH ..... Fumarate Hydratase
G6P Glucose-6-Phosphate
GAPDH ..... Glyceraldehyde Phosphate Dehydrogenase
GAM ..... Glioma-Associated Macrophage
GBM ..... Glioblastoma Multiforme
GC/MS ..... Coupled Gas Chromatography-Mass Spectroscopy
GFAP ..... Glial Fibrillary Acid Protein
GLDC ..... Glycine Decarboxlyase
GLUT ..... Glucose Transporter
GPX ..... Glutathione Peroxidase
GS ..... Glutaminase
GSC ..... Glioma Stem Cell
GSH ..... Reduced Glutathione
GSN ..... Glutamine Synthetase
GSSG ..... Oxidized Glutathione
GSTZ1 ..... Glutathione transferase zeta 1
GTPase ..... Guanosine Triphosphatase
HA ..... Hyaluronic Acid

HBOt ..... Hyperbaric Oxygen Therapy
HDAC ..... Histone Deacetylase
HIF ..... Hypoxia Inducible Factor
HIF1-α ..... Hypoxia Inducible Factor 1α
HK ..... Hexokinase
HLRCC ..... Hereditary Leiomyomatosis and Renal Cell Cancer
HRP ..... Horseradish Peroxidase
IACUC ..... Institutional Animal Care and Use Committee
IDH1 ..... Isocitrate Dehydrogenase 1
IDH2 ..... Isocitrate Dehydrogenase 2
IGF ..... Insulin-Like Growth Factor
IL-1 ..... Interleukin-1
IL-6 ..... Interleukin-6
IL-13 ..... Interleukin-13
IMM ..... Inner Mitochondrial Membrane
IMS ..... Mitochondrial Intermembrane Space
KD ..... Ketogenic Diet
KEAP1 ..... Kelch-Like ECH-Associated Protein 1
KRAS ..... Kristen Rat Sarcoma Oncogene Homolog
α-KG ..... α-Ketoglutarate
LDH ..... Lactate Dehydrogenase
LDLR ..... Low-Density Lipoprotein Receptor
LKB1 ..... Liver Kinase B1
MAPK ..... Mitogen-Activated Protein Kinase
MCL ..... Mantle Cell Lymphoma
MCT ..... Monocarboxylate Transporter
MDH ..... Malate Dehydrogenase
MDM2 ..... Mouse Double Minute 2 Homolog
ME ..... Malic Enzyme
MELAS ..... Mitochondrial Encephalopathy and Lactic Acidosis Syndrome
MGMT ..... Methylguanine-DNA-Methyltransferase
mGPD ..... Mitochondrial Glycerol-3-Phosphate Dehydrogenase
MMP ..... Matrix Metalloproteinase
mtDNA ..... Mitochondrial DNA
mTORC1 ..... Mammalian Target of Rapamycin Complex 1
MRI ..... Magnetic Resonance Imaging
NAC ..... N-Acetylcysteine
NAD^+ ..... Oxidized Nicotinamide Adenine Dinucleotide
NADH ..... Reduced Nicotinamide Adenine Dinucleotide
$NADP^+$ ..... Oxidized Nicotinamide Adenine Dinucleotide Phosphate
NADPH ..... Reduced Nicotinamide Adenine Dinucleotide Phosphate
nDNA ..... Nuclear DNA
NEFL ..... Neurofilament Light Polypeptide
NF-κB ..... Nuclear Factor κB
NNT ..... Nicotinamide Nucleotide Transhydrogenase
NOX ..... NADPH Oxidase
Nrf2 ..... Nuclear factor-like 2
NSCLC ..... Non-Small Cell Lung Cancer
OCT ..... Organic Cation Transporter
OGT ..... *O*-Linked-N-Acetylglucosaminyltransferase
OMM ..... Outer Mitochondrial Membrane
PBS ..... Phosphate Buffered Saline
PC ..... Pyruvate Carboxylase
PCA ..... Perchloric Acid
PCC ..... Pheochromocytoma
PCNSL ..... Primary Central Nervous System Lymphoma

PCOS ..... Poly-Cystic Ovary Syndrome
PDAC ..... Pancreatic Ductal Carcinoma
PDGFβ ..... Platelet Derived Growth Factor β
PDGFR ..... Platelet Derived Growth Factor Receptor
PDH ..... Pyruvate Dehydrogenase
PDK ..... Pyruvate Dehydrogenase Kinase
PDP ..... Pyruvate Dehydrogenase Phosphatase
PEP ..... Phosphoenolpyruvate
PGHDH ..... Phosphoglycerate Dehydrogenase
PFK ..... Phosphofructokinas
PHD ..... Prolyl Hydroxylase
PI3K ..... Phosphoinositide 3-Kinase
PK ..... Pyruvate Kinase
PPP ..... Pentose Phosphate Pathway
PRPS2 ..... Phosphoribosyl Pyrophosphate Synthetase 2
PRX ..... Peroxyredoxin
PTEN ..... Phosphatase and Tensin Homolog
R5P Ribose-5-Phosphate
Redox ..... Oxidative-Reduction
RNR ..... Ribonucleotide Reductase
RNS ..... Reactive Nitrogen Species
ROS ..... Reactive Oxygen Species
RTK ..... Receptor Tyrosine Kinase
SAM ..... S-Adenosylmethionine
SCLC ..... Small Cell Lung Cancer
SDH ..... Succinate Dehydrogenase
SEM ..... Standard Error of the Mean
SHMT2 ..... Serine Hydroxymethyltransferase 2
SN2 ..... System N 2 Transporter
SNP ..... Single Nucleotide Polymorphism
SOD ..... Superoxide Dismutase
SREBP-1 ..... Sterol Regulatory Element-Binding Protein-1
STAT3 ..... Signal Transducer and Activator of Transcription 3
SYT1 ..... Synaptotagmin
T2DM ..... Type II Diabetes Mellitus
TAG ..... Triacylglyceride
TAM ..... Tumor-Associated Macrophages
TBS ..... Tris-Buffered Saline
TCA Cycle ..... Tricarboxylic Acid Cycle
THF ..... Tetrahydrofolate
TIGAR ..... TP53 Induced Glycolysis Regulatory Phosphatase
TMRE ..... Tetramethyrhodamine
TMZ ..... Temozolomide
TNBC ..... Triple Negative Breast Cancer
TNFα ..... Tumor Necrosis Factor α
Treg ..... Regulatory T Cell
TRX ..... Thioredoxin
TrxR ..... Thioredoxin Reductase
TSC2 ..... Tuberous Sclerosis Complex 2
UCP ..... Uncoupling Protein
UDP ..... Uridine Diphosphate
US ..... United States
VDAC ..... Voltage-Gated Anion Channel
VEGF ..... Vascular Endothelial Growth Factor
vHL ..... von Hippel-Lindau
WHO ..... World Health Organization

xCT ..... Cysteine/Glutamate Antiporter
YKL-40 ..... Chitanase-3-like protein 1

ABSTRACT

The robust glycolytic metabolism of glioblastoma multiforme (GBM) has proven them susceptible to increases in oxidative metabolism induced by the pyruvate mimetic dichloroacetate (DCA). Recent reports demonstrate that the anti-diabetic drug metformin enhances the damaging oxidative stress associated with DCA treatment in cancer cells. We sought to elucidate the role of metformin's reported activity as a mitochondrial complex I inhibitor in the enhancement of DCA cytotoxicity in the VM-M3 model of GBM. We demonstrated that metformin potentiated DCA-induced superoxide production and that this was required for enhanced cytotoxicity towards VM-M3 cells with the combination. Similarly, rotenone enhanced oxidative stress resultant from DCA treatment and this too was required for the noted augmentation of cytotoxicity. Adenosine monophosphate kinase (AMPK) activation was not observed with the concentration of metformin required to enhance DCA activity. Moreover, addition of an activator of AMPK did not enhance DCA cytotoxicity, whereas an inhibitor of AMPK heightened the cytotoxicity of the combination. We also show that DCA and metformin reduce tumor burden and prolong survival in VM-M3 tumor-burdened mice as individual therapies. In contrast to our in vitro work, we did not observe synergy between DCA and metformin in vivo. Our data indicate that metformin enhancement of DCA cytotoxicity is dependent on complex I inhibition. Particularly, that complex I inhibition cooperates with DCA-induction of glucose oxidation to enhance cytotoxic oxidative stress in VM-M3

GBM cells. This work supports further investigation and optimization of a DCA/metformin combination as a potential pro-oxidant combinatorial therapy for GBM.

CHAPTER 1: CANCER METABOLISM

1.1 Chapter Synopsis

Herein we provide a review of the metabolic programs employed by tumors to meet the biosynthetic requirements of tumorigenesis. The metabolism of tumors is intricately linked to the hallmarks of the disease and provides cancer cells with a survival advantage in response to the stresses imposed by the tumor microenvironment. An understanding of the metabolic characteristics of tumors provides a basis for rational targeting of these metabolic dependencies as a therapeutic strategy. Current approaches in targeting cancer metabolism are also discussed in this chapter.

1.2 Altered Energy Metabolism

Cancer is traditionally considered a genetic disease, characterized by genomic instability and frequent mutation that cooperate to promote a distinct cellular environment that permits unbridled proliferation (1). Genomic sequencing of tumors has identified a multitude of drug targetable mutations that have driven research and pharmaceutical development. Unfortunately, the promise of encouraging pre-clinical findings has not often translated to clinical efficacy. This has driven the field to consider additional hallmarks of tumor development and disease progression and devise alternative strategies for cancer management (1).

Resultant from this initiative was a renewed appreciation for the distinct metabolic activity of tumors (2). Beyond the dysregulation of the cell cycle and loss of deoxyribonucleic acid (DNA) quality control that accompany cancer cell proliferation is a fundamental demand for biomass. An intricate network of metabolic pathways converges to generate the molecular building blocks required for biosynthesis (3). Cancer cell metabolism is wired in such a manner that allows for the continuous production of the nucleotides, proteins and lipid membranes necessary for proliferation whilst also generating the energy and reduction potential required for cell survival (4). The past decade of research on cancer metabolism has encompassed a methodological renaissance for characterizing the metabolic dependencies of cancer cells and the intersection between metabolism and tumor biology (5-8). Most importantly, this work has demonstrated that targeting cancer metabolism may be a sustainable therapeutic alternative for the management of the devastating disease.

1.2.1 Aerobic Fermentation

The notion of peculiar metabolism in cancer is not a recent phenomenon. Otto Warburg first observed a distinct difference in the metabolism of tumors compared to normal tissue in the early 20th century (9). Warburg reported that tumors took up significantly more circulating glucose than normal tissue, and whereas very little lactate was generated by the normal tissue, Warburg calculated that 66% of the consumed glucose was converted to lactate by the tumor. This suggests that the tumors were predominantly fermenting glucose rather than respiring on the sugar.

Glucose is the predominant energy metabolite in the body, and is preferentially metabolized by most tissues. Upon entering the cell, glucose is metabolized to pyruvate through the Embden-Meyerhof, or glycolytic pathway. Typically, pyruvate is then imported into the mitochondria where it is fully oxidized to carbon dioxide (CO_2) as long as oxygen, the final electron acceptor of the electron transport chain is not limiting. Tissues are adequately perfused under normal physiological conditions, which facilitates the delivery of oxygen and permits mitochondrial respiration of glucose. In the context of limiting oxygen, such as in muscle during vigorous exercise, pyruvate is fermented to lactate by lactate dehydrogenase (LDH).

What is remarkable about Warburg's findings is that the tumors were reported to be well perfused and thus oxygen was not limiting (9). Hence, the tumors were preferentially fermenting pyruvate to lactate in an aerobic environment. This aerobic fermentation of glucose is now widely recognized as a hallmark phenotype of most cancers and is now termed the Warburg effect (10). In fact, the robust uptake of glucose by tumors is the basis for diagnostic fluorodeoxyglucose positron emission tomography (FDG-PET) scanning (11).

A reliance on glycolytic metabolism seems counterintuitive for robust proliferation from a bioenergetics perspective. Generating the biomass required for cell division depends in part on the potential energy stored in adenosine triphosphate (ATP), a byproduct of certain catabolic reactions. Glycolysis is rather energy inefficient, generating only 2 moles (mol) of ATP per mol of glucose, whereas the complete oxidation of glucose yields ~36 mol ATP/mol glucose. Yet, cancer cells that exhibit this Warburg metabolism do not suffer from an ATP deficit (12). The conversion of pyruvate

to lactate by LDH is coupled to the oxidation of reduced nicotinamide adenine dinucleotide (NADH) to its oxidized form, NAD^+. The regeneration of NAD^+ maintains a high cytosolic NAD^+/NADH ratio that permits rapid glycolytic flux, as the glycolytic enzyme glyceraldehyde phosphate dehydrogenase (GAPDH) requires NAD^+ as a cofactor.

1.2.2 Mitochondrial Metabolism

Based on his original observation, Warburg hypothesized that aerobic fermentation in tumors was a result of an irreversible insult to oxidative capacity that prevented cancer cells from deriving sufficient energy from oxidative metabolism (13). Evidence suggests that ATP production is not a necessary function of cancer mitochondria, however mitochondrial metabolism is critical for cancer cell proliferation (14). In principle, the abundant generation of lactate as a result of the Warburg effect could restrict the flux of pyruvate into the mitochondria, where it is readily metabolized to acetyl coenzyme A (acetyl-CoA) and CO_2 via the pyruvate dehydrogenase (PDH) complex.

Acetyl-CoA is a critical carbon carrier that is utilized extensively in central carbon metabolism. Acetyl-CoA is required for continuous flux of the Citric Acid (TCA) cycle, which generates the reducing equivalents NADH and reduced Flavin adenine dinucleotide ($FADH_2$). These reducing equivalents are oxidized by protein complexes in or associated with the inner mitochondrial membrane (IMM) in reactions that couple the release of electrons with the movement of protons (H^+) from the mitochondrial matrix into the intermembrane space. The movement of these electrons through subsequent

protein complexes, that collectively make up the electron transport chain (ETC), is also coupled to the movement of H^+ across the IMM. The translocation of these H^+ generates a proton motive force and membrane potential across the IMM. ATP synthase harnesses this proton motive force to couple the movement of H+ back into the matrix with the generation of ATP from adenine diphosphate (ADP) and inorganic phosphate (P_i).

In addition to providing the reducing equivalents for oxidative phosphorylation, the TCA cycle intermediates are important for the biosynthesis of critical macromolecules. Reduced flux of glucose carbon through the PDH complex would thus restrict TCA cycling and decrease the levels of TCA cycle intermediates. Cancer cells, especially in culture, have upregulated glutamine metabolism to compensate for deficits in glucose carbon flux through the TCA cycle (15). Glutamine is an anaplerotic amino acid that is converted to glutamate in the mitochondria by glutaminase (GS). Glutamate can then be deaminated to α-ketoglutarate (α-KG), a TCA cycle intermediate. α-KG can then contribute to the replenishment of subsequent intermediates through traditional flux through the cycle or be converted to the upstream metabolite, isocitrate, through isocitrate dehydrogenase 2 (IDH2)-mediated reductive carboxylation.

In certain tumor species, the branched-chain amino acids (BCAAs) leucine and valine can be used as anaplerotic substrates (5). Moreover, glucose carbon can enter the TCA cycle in a PDH-independent manner through pyruvate carboxylase (PC), which converts cytosolic pyruvate to oxaloacetate. This oxaloacetate is then converted to malate via malate dehydrogenase (MDH). Malate can be taken up into the mitochondria

through the malate-aspartate shuttle and incorporate into the TCA cycle. Together, these pathways provide alternative means for maintaining TCA function.

The advent of isotope-labeled metabolite tracing has demonstrated that aerobic fermentation does not fully restrict glucose oxidation, rather the tracing of ^{13}C-glucose metabolic flux shows concurrent fermentation and oxidation of glucose carbon in certain cancers (16). Cellular energy metabolism is dependent on the regulated movement of electrons between metabolic intermediates and enzymatic cofactors through a series of oxidative-reduction (redox) reactions. Recent evidence suggests that mitochondrial oxidation is critical for the cell proliferation independent of the generation of ATP.

Stimulation of ETC activity through oxidation of reducing equivalents promotes redox balance through regeneration of NAD^+ and oxidized Flavin adenine dinucleotide (FAD^+), which are critical electron acceptors. Electron acceptors are necessary for continuous metabolic flux, especially in the context of meeting the biosynthetic demands of rapid proliferation (17). Oxygen serves as the terminal electron acceptor in oxidative metabolism and this reduction of oxygen is considered the most vital aspect of mitochondrial oxidative metabolism for proliferating cells (18). The amino acid aspartate is also shown to serve as an essential electron acceptor for proliferation (17, 18).

Maintenance of the mitochondrial membrane potential ($\Delta\Psi_m$) is generally dependent on the continual regulated flux of electrons through the ETC resultant from oxidative metabolism. The preservation of $\Delta\Psi_m$ is critical to the proliferative capacity of cells independent of its coupling to ATP production (19). In fact, cancer mitochondria are often hyperpolarized, suggesting inefficient flux of H^+ back into the matrix for the purposes of ATP generation (20).

In addition to glucose, fatty acids can serve as a substrate for mitochondrial oxidative metabolism. The beta-oxidation of fatty acids (FAO) yields acetyl-CoA, which is incorporated into the TCA cycle, and NADH and $FADH_2$ for electron transport and the potential generation of ATP. FAO is shown to be essential for survival and growth under conditions of metabolic stress (21). Certain haematopoietic malignancies exhibit increased FAO (22, 23). Diffuse large B cell lymphoma (DLBCL) appear to rely on FAO largely to maintain cellular ATP levels. Whereas leukemia cells often display enhanced FAO that is associated with preventing the toxic buildup of fatty acids (21). Additionally, some leukemia cells require FAO for maintenance of cytosolic redox balance in the form of citrate-dependent reduced nicotinamide adenine dinucleotide phosphate (NADPH) generation.

1.2.3 Maintenance of Redox Balance

As mentioned above, cellular metabolism is dependent on the coordinated movement of electrons through intermediate metabolites and the oxidation state of important electron carriers. Cells harness the reducing power of NADH and NAPDH for the catabolic and biosynthetic reactions necessary for growth and viability. The ratios of NAD^+/NADH and oxidized nicotinamide adenine dinucleotide phosphate ($NADP^+$)/NADPH are indicators of the redox state of the cell. Metabolic flux and the activity of bidirectional metabolic enzymes are dependent on the status of these ratios. The redox state of the cell is compartmentalized within organelles, as there are distinct metabolic mechanisms for regulating NAD^+/NADH and NADP+/NADPH in the cytosol and mitochondrial matrix for example. Yet, these are not completely independent of

each other as there are mechanisms for the exchange of metabolites between compartments that facilitate alterations to these ratios.

Maintenance of the NAD+/NADH ratio is predominantly mediated in the cytosol through glycolysis and through the TCA cycle in the mitochondrial matrix. As previously mentioned, cancer cells exhibit enhanced LDH activity, which recycles the NADH generated through glycolysis to NAD+, facilitating the rapid glycolytic flux associated with Warburg metabolism (4). The shuttling of pyruvate between the cytosol and matrix links the NAD+/NADH pools of the two compartments and is tightly regulated in cancer (24).

NADPH provides the reducing power for biosynthesis and is a critical component of cellular antioxidant capacity, both of which will be thoroughly discussed later in this review. Cytosolic NADPH is generated through two enzymatic reactions in the pentose phosphate pathway (PPP), via the conversion of malate to pyruvate by malic enzyme (ME) and oxidation of isocitrate to α-KG by IDH1. The exchange of citrate between the matrix and cytosol links the NADPH pools of the two compartments. Reductive carboxylation of glutamine is shown to contribute to the cytosolic pools of NADPH through citrate, which can be metabolized to oxaloacetate by citrate lyase and subsequently to malate via MDH. Ultimately, this citrate-derived malate is converted to pyruvate by ME, generating NADPH (25, 26). ^{13}C-glutamine tracing demonstrated that a significant fraction of mitochondrial NADPH is derived from folate metabolism (27, 28). Additional contributing factors to the matrix NADPH pool are IDH2 and the IMM-associated enzyme nicotinamide nucleotide transhydrogenase (NNT), which harnesses

the proton motive force across the IMM and the reducing power of NADH to generate NADPH.

Cellular redox state is also affected by oxidative stress, a natural byproduct of metabolism. Oxidative stress is caused by the generation of highly reactive free radical oxygen- or nitrogen-containing species (ROS, RNS) that exhibit an array of biological functions, both cell-sustaining and cytotoxic. For instance, electron transport is not a totally efficient process. Electrons can be prematurely released from the ETC to reduce molecular oxygen to superoxide anion ($\cdot O_2^-$). This occurs on the matrix side of the IMM at complex I (NADH dehydrogenase) and complex II (succinate dehydrogenase) of the ETC. Additionally, $\cdot O_2^-$ can be generated on both the matrix- and intermembrane space (IMS)-facing sides of the IMM at complex III (coenzyme Q: cytochrome c oxidoreductase). $\cdot O_2^-$ can also be generated in the cytosol and matrix through an NADPH-dependent process catalyzed by NADPH oxidases (NOXs).

In the presence of nitric oxide (NO), a byproduct of arginine metabolism, superoxide contributes to the formation of the very reactive peroxynitrite ion ($ONOO^-$). Additionally, this $\cdot O_2^-$ can be dismutated to hydrogen peroxide (H_2O_2) by superoxide dismutases (SODs). H_2O_2 can subsequently be detoxified to water through a number of enzymatic systems. Peroxiredoxins (PRXs) undergo H_2O_2-mediated oxidation that initiates a catalytic cycle in which thioredoxin (TRX), thioredoxin reductase (TrxR) and NADPH cooperate to regenerate reduced PRXs. Glutathione peroxidases (GPXs) utilize reduced glutathione (GSH) to detoxify H_2O_2. Glutathione reductase then utilizes NADPH to convert the oxidized glutathione (GSSG) to GSH. Finally, catalase can also convert to

H_2O_2 to water. Alternatively, in the presence of ferrous (Fe^{2+}) or cupric (Cu^{+}) ions, H_2O_2 can generate hydroxyl radical (·OH) through Fenton reactions.

Collectively, these detoxifying enzymes contribute to the antioxidant capacity of the cell, which prevents the accumulation of the free radicals that potentiate oxidative stress. Transcriptional regulation of these enzymes is controlled by the master regulator of cellular antioxidant machinery, nuclear factor-like 2 (Nrf2). Nrf2 activity is stimulated by oxidative stress, resulting in the upregulation of a host of detoxifying enzymes and a metabolic program that boosts antioxidant capacity. The balance between ROS and RNS generation and antioxidant detoxification greatly influences cell function and viability and is a critical component of tumorigenesis (29).

1.3 Consequences of Cancer Metabolism

Tumors exist as a heterogeneous population of cells that are under severe selection pressures that drive an evolutionary response. The mutations acquired during tumorigenesis must either confer a survival advantage or passively permit unbridled proliferation (1, 2). Tumors are subject to the constraints of natural selection and those mutations that reduce cancer cell fitness are ultimately selected against (30). Given that altered cellular metabolism is a consistent hallmark of cancer, there must be a survival benefit associated with the metabolism of neoplastic cells. Herein, I describe the consequences of cancer metabolism that provide a survival benefit to cancer cells and contribute to disease progression.

1.3.1 Proliferative Advantage

Robust glycolytic metabolism is not supremely unique to cancer cells. Rapidly proliferating cells such as lymphocytes and fibroblasts also exhibit aerobic fermentation of glucose under normal physiological conditions (31, 32). As noted previously, glycolysis is a rather energy inefficient pathway, however many glycolytic intermediates are critical biosynthetic precursors. It is proposed that increased flux of glucose through glycolysis facilitates the generation of abundant intermediates for the shunting of these metabolites into biosynthetic pathways. Moreover, the enhanced metabolism of other metabolites seen in cancer cells further contributes to the generation of amino acids, nucleotides and lipid species that are required for generating the macromolecular constituents of the cellular architecture (5-9, 15).

1.3.1.1 Amino Acid Biosynthesis and Metabolism

The accumulation of glycolytic intermediates provides cancer cells with abundant 3-phosphoglycerate, the substrate for serine and glycine biosynthesis. Serine and glycine metabolism is shown to be upregulated in many cancers and this is often associated with an overexpression of the first enzyme in the biosynthetic pathway, 3-phosphoglycerate dehydrogenase (PGHDH) (33, 34). Upon de novo synthesis, serine is taken up into the mitochondrial matrix where it is cleaved to glycine by serine hydroxymethyltransferase 2 (SHMT2). Concurrently, SHMT2 transfers the methyl side chain of serine to tetrahydrofolate (THF) generating methyl-THF, promoting the folate cycle and one-carbon metabolism. As such, serine and glycine are the predominant sources of one-carbon units, which are required for a series of biosynthetic reactions

including the generation of methionine and cysteine (35). Methionine is further metabolized to S-adenosylmethionine (SAM), the principle substrate for histone and DNA methylation, one of several links between metabolism and genetic regulation. Cysteine synthesis results from an intersection between the folate and transsulfuration cycles. Cysteine and glycine are two of the amino acid components of the tripeptide antioxidant GSH.

The third amino acid component of GSH, glutamate, can promote the uptake of cysteine in the absence of sufficient de novo synthesis. Glutamate is exchanged for cysteine via the cysteine/glutamate antiporter (xCT), which is upregulated in lymphoma, gliomas and prostate cancer (36). The increased uptake of glutamine in cancer provides abundant substrate for GS-dependent generation of glutamate. Glutamate is a critical substrate for transamination reactions, serving as a nitrogen donor for non-essential amino acid synthesis. Alternatively, glutamine serves as a direct nitrogen donor for the synthesis of asparagine. This enhanced synthesis of amino acids contributes to the robust protein synthesis required for proliferation.

To supplement amino acid pools in the face of deficiency, such as in the event of energetic stress, tumor cells upregulate autophagy (37). Autophagy permits cancer cell resilience but does not allow for proliferation as no new biomass is generated from the degradation of cellular protein. In contrast, recent evidence suggests that cancer can employ macropinocytosis, the endocytic uptake of extracellular fluid and its substituent contents, to satisfy the amino acid demand for proliferation (38).

1.3.1.2 Nucleotide Biosynthesis

The upregulation of glutamine metabolism in cancer not only contributes to TCA cycle anaplerosis and the subsequent generation of non-essential amino acids but also to the production of nucleotides. In fact, glutamine is the principle nitrogen donor for nucleotide synthesis; synthesis of uracil and thymine require a single glutamine molecule, cytosine and adenine require two, and guanine synthesis demands 3 molecules of glutamine. The transaminaton of oxaloacetate and glutamine-derived glutamate produces aspartate, which is incorporated into both purine and pyrimidine rings.

Glucose metabolism also contributes to nucleotide synthesis. The glycolytic intermediate glucose-6-phosphate (G6P) is shunted into the oxidative branch of the PPP. Increased flux through the PPP promotes the abundant generation of ribose-5-phosphate, which serves as a precursor for the pentose sugar backbone of nucleic acids. The folate cycle, which as previously noted is stimulated by enhanced serine metabolism in cancer, contributes one-carbon units to the generation of purine nucleotides. Additionally, purine ring synthesis requires the incorporation of glycine, signifying the intersection of glucose and glutamine metabolism.

1.3.1.3 Lipid Biosynthesis

In addition to protein and nucleic acids, cells require various lipid species that make up the membranous superstructure of the cell. The synthesis of fatty acids occurs in the cytosol and is typically dependent on glucose-derived acetyl-CoA. Citrate generated in the TCA cycle is exported from the mitochondria and metabolized to

oxaloacetate by ACL, releasing acetyl-CoA in the process. This acetyl-CoA is carboxylated to malonyl-CoA by acetyl-CoA carboxylase (ACC), stimulating the synthesis of the fatty acid palmitate. In the absence of sufficient glucose-derived acetyl-CoA, cancer cells have shown the ability to utilize glutamine and acetate as alternative sources of citrate for fatty acid synthesis (39-41). Fatty acids are essential components of phospholipids, which make up the lipid bilayer of the plasma membrane and cellular organelles.

Phospholipid synthesis further intersects with glucose metabolism in the metabolism of dihydroxyacetone phosphate (DHAP). DHAP, a glycolytic intermediate, is siphoned for the generation of phosphatidic acid, a critical phospholipid precursor. Moreover, serine is a direct substrate for the generation of the phospholipid, phosphatidylserine. Together, these subsidiary biosynthetic pathways of glycolysis help to generate the phospholipids required for lipid membrane assembly.

The stimulation of the oxidative PPP upon G6P accumulation not only facilitates nucleotide synthesis, but also generates 2 molecules of NADPH per G6P. Lipid synthesis is a very energy-intensive process that demands reduction potential and NADPH provides the majority of this reducing power. Synthesis of the 14-carbon fatty acid palmitiate requires 14 equivalents of NADPH. Moreover, cholesterol synthesis, which also utilizes citrate-derived acetyl-CoA, requires 26 equivalents of NADPH. Thus the enhanced glucose metabolism of cancer cells provides not only carbon, but the reducing potential required to generate the essential lipid species for proliferation.

1.3.2 Enhanced Antioxidant Capacity

As discussed previously, a natural byproduct of metabolism is the generation of ROS and RNS which contribute to a cellular state of oxidative stress. Cells must balance the generation of these reactive species with detoxification to maintain redox balance. It is well established that cancer cells generate more reactive species, especially ROS, than normal cells; both from inefficient oxidative metabolism and through enzymatic production (29). Consequently, cancer cells exhibit an extraordinary antioxidant capacity mediated by Nrf2 stimulation (42). Accumulation of H_2O_2 promotes the cysteine oxidation of the negative regulator of Nrf2, Kelch-like ECH-associated protein 1 (KEAP1). This ROS mediated oxidation of KEAP1 causes its dissociation from Nrf2, releasing KEAP1 inhibition of Nrf2 and promoting its transcriptional regulation of antioxidant machinery.

Upregulation of antioxidant enzymes does not wholly negate the induction of oxidative stress. These enzyme systems employ redox cycles that require reducing potential to drive functional cycling. This reducing potential is derived from NADPH. As previously described, the enhanced metabolism of glucose and glutamine exhibited by cancer cells promotes NADPH production and is thus critical to the antioxidant capacity of tumors (43). Furthermore, glycolytic stimulation of serine metabolism and the generation of glutamate from glutamine provide the precursors for GSH synthesis, sustaining availability of the vital antioxidant. The maintenance of redox balance in cancer cells through enhanced antioxidant capacity contributes to tumorigenesis and disease progression.

1.3.2.1 Prevention of Cytotoxic Oxidative Damage

The accumulation of ROS and RNS is detrimental to cellular viability. Though the reactivity of these species varies, their robust production nonetheless increases the probability of macromolecular oxidation. Oxidation of proteins, nucleic acid and lipid species can alter their function and fidelity. Protein degradation can result from the initiation of peptide bond cleavage by ·OH oxidation. Moreover, certain amino acid side chains are subject to radical oxidation. These oxidation events can result in the loss of structural conformation or enzymatic activity (44). Antioxidant quenching of ROS prevents the formation and accumulation of toxic products of protein oxidation such as protein carbonyls.

H_2O_2 is less reactive than other ROS and is membrane diffusible, this allows for nuclear association where it can be converted to ·OH through Fenton chemistry. ·OH is highly reactive and is known to cause DNA damage (45). Oxidation of DNA can result in crosslinking, single- or double-stranded breaks as well as less severe structural modifications to nitrogenous base, such as the formation of 8-hydroxydeoxy guanosine (8-OHdG). 8-OHdG contributes to the genomic instability and mutability of the cancer genome and is intrinsically linked to carcinogenesis (46, 47). The upregulation of antioxidant defenses in cancer permit the mutagenicity of the cancer genome, while preventing the initiation of cell death pathways associated with substantial DNA damage (48).

·OH also promotes lipid peroxidation and the generation of radical lipid species. These result in lipid fragmentation, which reduces the structural integrity of various cellular components. This is particularly detrimental to cellular membranes. The

peroxidation of phospholipids alters membrane permeability and fluidity and reduces the integrity of their associated membranes. Abundant mitochondrial ROS production is associated with the induction of apoptosis (49, 50). Temporal production of ROS at the ETC increases the probability that subsequently generated ·OH will react with the phospholipid constituents of the IMM. In the presence of profound oxidative stress, IMM integrity is lost, which disrupts the proton gradient and causes the loss of $\Delta\Psi_m$. Disruption of mitochondrial integrity also promotes the release of cytochrome c into the cytosol, where it can initiate the apoptotic cascade. The increase in antioxidant capacity, coupled with mitochondrial hyperpolarization prevents the induction of cell death in cancer cells despite robust mitochondrial ROS production (20).

1.3.2.2 Equilibration of ROS signaling

ROS and RNS generation is fundamentally associated with the induction of a stressful cellular environment that promotes macromolecular damage. However, there is accumulating evidence that ROS have alternative signaling functions when present at tightly regulated concentrations (51). This signaling function is shown to be prevalent in cancer and has profound effects on tumorigenesis (29).

Similar to its stimulation of Nrf2 activity, H_2O_2 can reversibly oxidize cysteine residues of several signaling proteins relevant to cancer. H_2O_2 potentiates aberrant signaling through the phosphoinositide 3-kinase (PI3K) pathway in cancer (52). The negative regulator of PI3K signaling, phosphatase and tensin homolog (PTEN), is a target for inhibitory H_2O_2 oxidation, which contributes to constitutive activation of PI3K. PI3K signaling promotes growth and proliferation and is hyperactivated in many tumors

(52, 53). The mitogen-activated protein kinase (MAPK) signaling axis is also regulated at the post-translational level by ROS (54). Oxidation of MAPK-associated phosphatases prevents the inactivating dephosphorylation of MAPKs, leading to unregulated MAPK signaling. MAPK signaling stimulates a transcriptional response that drives growth and proliferation. Though typically a response to growth factor signaling, MAPK activation often occurs independent of an extracellular stimulus in cancer and this is in part mediated by this ROS-mediated protein oxidation (55).

Furthermore, ROS production has been implicated in the stabilization of hypoxia inducible factor alpha (HIF1-α) through multiple proposed mechanisms. HIF-1α is a component of the hypoxia inducible factor (HIF) transcription factor, and whose regulation and transcriptional program as it relates to cancer will be more thoroughly discussed later in this review. Sequestration of Fe^{2+} for ·OH production via the Fenton reaction is shown to promote HIF-1α accumulation (56). Moreover, ROS mediates the transcription of HIF-1α in a nuclear factor κB (NF-κB)-dependent manner (57). HIF activity has profound effects on cancer metabolism and this ROS-based regulation of HIF likely potentiates tumor metabolism in a feed-forward manner.

1.3.2.3 Therapeutic Resistance

In addition to debulking surgery when appropriate, traditional therapeutic management of cancer often employs chemotherapy and radiation. Many chemotherapies elicit cytotoxicity through mechanisms that depend on the generation of ROS. For instance, the topoisomerase inhibitor doxorubicin also promotes free radical production through the chelation of Fe^{2+}, which induces ·OH production. Doxorubicin

induction of ROS likely cooperates with its interruption of DNA synthesis to promote cancer cell death through catastrophic DNA damage (58). Moreover, the platinum based alkylating agent, cisplatin, displays ROS mediated toxicity that independent of its interaction with DNA (59). Additionally, arsenic trioxide inhibits mitochondrial respiratory capacity, which potentiates superoxide production and leads to cancer cell death (60).

Radiotherapy involves the directed administration of high-energy waves or particles for the purpose of eradicating cancer cells. Irradiation promotes cytotoxic DNA damage that is mediated through two mechanisms, direct and indirect ionization. Direct ionization involves immediate DNA damage, often in the form of single-strand breaks, caused by the radiation. Indirect ionization involves the radiolysis of water, which yields ·OH, leading to DNA oxidation (61). Moreover, radiation is shown to activate NOX and potentiate continual ROS production (62).

The clinical failure of cancer therapy is often a function of chemoresistance that leads to disease recurrence. It is now widely appreciated that chemoresistance results in large part due to the robust antioxidant capacity of tumors (63). As many chemotherapies and radiotherapy are mechanistically dependent on ROS production, the upregulation of antioxidant systems in cancer cells restricts prolonged efficacy of these therapies. This is particularly true of cancer stem cells (CSCs), a distinct cellular subpopulation of tumors that have even greater antioxidant capacity than the bulk of the tumor (64). These CSCs have long been suggested to facilitate disease recurrence (65). Even if a therapy is initially successful, CSC resilience in response to therapy allows for repopulation of the tumor mass with cells resistant to treatment.

1.3.3 Alteration of the Tumor Microenvironment

Tumors are not a homogenous entity, rather they exist as a diverse population consisting not only of cancer cells but also immune and stromal constituents. Collectively these cells along with a cocktail of signaling molecules and extracellular matrix (ECM) constitute the tumor microenvironment. The confluence of these diverse cell types and signaling factors ultimately promotes tumor (66). There is also accumulating evidence that the metabolism of cancer cells has a profound effect on the tumor microenvironment and contributes to tumor aggressiveness and disease progression (15).

As previously described, a consequence of the increased glycolytic metabolism employed by tumors is the abundant generation of lactate. Intracellular accumulation of lactate is a negative regulator of glycolysis through feedback inhibition. To prevent this negative regulation, cancer cells rapidly export lactate. Lactate export is mediated by monocarboxylate transporters (MCTs). Accordingly, MCT expression is upregulated in cancer, and is essential for cancer cell proliferation (67, 68).

MCT-mediated lactate export is coupled to the movement of H^+ into the extracellular space. The rapid rate of tumor cell lactate export facilitates acidification of the tumor microenvironment. Whereas the intracellular pH of tumor cells is maintained between 7.2 – 7.3, the pH of the extracellular space of solid tumors can range from 6.5 – 6.8 (69). The concurrent mitochondrial metabolism of glucose and glutamine carbon yields excess CO_2, which freely diffuses into the extracellular space. Signals transduced from the tumor microenvironment drive the expression of carbonic anhydrase IX (CAIX),

which facilitates the conversion of CO_2 to bicarbonate (HCO_3^-) and H^+ (70). This activity exacerbates the acidification of the tumor microenvironment.

The accumulation of lactate has substantial effects on tumor-associated immune cells. As mentioned above, many immune cells exhibit a metabolism that is similar to that of cancer cells. This is particularly evident in effector T cells, which upon activation are highly glycolytic (71). Lactate transport via MCTs is dependent on a concentration gradient. Therefore, the robust export of lactate from cancer cells disrupts the export of lactate from neighboring effector T cells. The cytosolic accumulation of lactate in T cells promotes a shift towards oxidation that corresponds with cellular differentiation to a regulatory phenotype (Treg) (71). Moreover, high levels of extracellular lactate inhibit dendritic cell activation and monocyte migration (72, 73). The confluence of immune cell inhibition yields an immuno-permissive environment that prevents host detection of the growing tumor.

Increased lactate in the tumor microenvironment can promote hyaluronic acid (HA) production by tumor-associated fibroblasts (74). HA promotes cell motility and is shown to stimulate the epithelial-mesenchymal transition (EMT) that is believed to facilitate cancer metastasis (75). Moreover, the acidification of the tumor microenvironment promotes the activation of matrix metalloproteinases (MMPs), which degrade extracellular matrix and facilitate tumor cell migration and cancer metastasis (76). Thus, the metabolism of cancer cells enhances the metastatic potential of the tumor through modulation of the microenvironment.

1.4 Regulation of Cancer Metabolism

Though there are characteristics that are present across all tumor species, different tumors exhibit distinct metabolic phenotypes that differentially utilize the metabolic pathways described above. There are several inputs, both extrinsic and intrinsic, that impose particular selective pressures that dictate metabolic pathway utility in cancer. The aberrant signaling that is hallmark of the disease not only promotes rapid cell cycling and apoptotic resistance, but also greatly affects the metabolism of cancer cells. Moreover, whole body health and physiology as well as the specific tumor niche influence tumor metabolism.

1.4.1 Aberrant Signaling

The need for paracrine stimulation of growth factor signaling in cancer cells is often dispensable as very often these neoplastic cells have acquired the ability to sustain proliferative signaling in an unregulated fashion (15). This is often achieved through constitutive activation of growth factor signaling pathways irrespective of external stimuli (77). The accumulation of mutations in these pathways contribute to this aberrant signaling and not surprisingly are implicated in the metabolic phenotypes present in cancer. Some of the most commonly affected proteins have well characterized effects on energy metabolism and biosynthesis, which will be discussed below.

1.4.1.1 PI3K/Akt/mTOR Signaling Axis

The PI3K/Akt/mammalian target of rapamycin complex 1 (mTORC1) signaling axis frequently harbors mutations in cancer (ref). Typically, growth factor stimulation of associated receptor tyrosine kinases (RTKs) stimulates PI3K generation of activated lipid species that promote the plasma membrane association and subsequent activation of the serine/threonine kinase, Akt. Akt has many phosphorylation targets that are involved in the cell cycle, angiogenesis and anti-apoptotic signaling. Perhaps most critically to cancer, Akt is a potent driver of glycolytic metabolism (78). Akt mediates the translocation of glucose transporters (GLUTs) to the plasma membrane, where they facilitate the enhanced glucose uptake associated with many tumors (79). Constitutive activation of Akt promotes inhibition of the forkhead box O3 (FOXO3) transcription factor. Inactivation of FOXO3 promotes a transcriptional program that stimulates glycolytic metabolism as well as an increase in oxidative stress (80). Moreover, Akt directly activates the glycolytic enzymes, phosphofructokinase (PFK) and hexokinase (HK). Activated HK2 associates with the outer mitochondrial membrane (OMM) and the membrane spanning mitochondrial voltage-gated anion channel (VDAC). The VDAC facilitates the export of ATP generated through oxidative metabolism. Thus, HK2 association with the VDAC couples mitochondrial ATP production to glycolysis and facilitates the rapid entry of glucose into the glycolytic pathway upon GLUT-mediated import (81).

An additional target of Akt activation is mTORC1. mTORC1 activity is stimulated directly through Akt-phosphorylation as well as through the inhibitory phosphorylation of its negative regulator, tuberous sclerosis complex 2 (TSC2). mTORC1 is a master

regulator of anabolic metabolism as it stimulated protein and lipid biosynthesis in nutrient replete conditions (82). Enhanced mTORC1 activity promotes glutamine uptake and GS activity, which facilitates glutamate production and TCA cycle anaplerosis (83). Coupled to this stimulation of glutamine metabolism is mTORC1-dependent activation of the pyrimidine synthesis initiator carbomyl phosphate synthase (CAD), this ensures that nucleotide synthesis is occurs under conditions of sufficient glutamine-derived nitrogen (84, 85).

1.4.1.2 c-Myc

The proto-oncogene, c-Myc, codes for a transcription factor that is involved in the regulation of the cell cycle and apoptosis. A chromosomal translocation event involving c-Myc is associated with the development of Burkitt lymphoma (86). c-Myc is also an important regulator of glutamine and glucose metabolism in cancer. Glutamine uptake is enhanced by c-Myc through transcriptional activation of the glutamine/neutral amino acid transporter (ASCT2) and the system N 2 transporter (SN2) (87). Furthermore, c-Myc enhances the expression of GS, CAD and phosphoribosyl pyrophosphate synthetase (PRPS2), which cooperate to stimulate nucleotide synthesis (88-90). This enhanced glutamine metabolism also contributes to the antioxidant capacity of cancer cells through increasing glutamate levels for GSH synthesis (7).

Glycolytic metabolism is also enhanced by c-Myc induction of GLUT and glycolytic enzyme transcription. Moreover, c-Myc facilitates aerobic fermentation through activation of LDH and pyruvate dehydrogenase kinase 1 (PDK1), the negative regulator of PDH, which promotes cytosolic accumulation of pyruvate (91). Additionally,

c-Myc activity is associated with increased mitochondrial biogenesis, which along with the increase in glutamine metabolism enhances mitochondrial function (92).

1.4.1.3 Ras

Ras is a cellular guanosine triphosphatase (GTPase) that is an intermediary mediator of cell signaling that propagates many extracellular stimuli (93). The Kirsten rat sarcoma oncogene homolog (KRAS) member of the ras family of GTPases is implicated the tumorgenesis of non-small cell lung cancer (NSCLC) and prostate cancers (94, 95). KRAS is a driver of metabolism in these cells through stimulation of glucose uptake and the shunting of glycolytic intermediates into the PPP and hexosamine pathways. Davidson *et al*. recently demonstrated that KRAS-driven NSCLC tumors exhibit increased fermentation and oxidation of glucose compared to normal adjacent lung tissue (96). Moreover, KRAS is shown to direct glutamine-dependent aspartate synthesis. This increase in aspartate facilitates cytosolic accumulation, where it is metabolized to pyruvate to enhance the cytosolic NADPH pool (97). KRAS also appears to regulate protein and amino acid levels in NSCLC and pancreatic ductal adenocarcinoma (PDAC). Guo *et al*. showed that KRAS stimulates autophagy to maintain intracellular glutamine stores in NSCLC (94). Whereas, KRAS promotes uptake of extracellular protein through macropinocytosis in PDAC (98).

1.4.1.4 p53

The canonical tumor suppressor, p53, is traditionally associated with its regulation of the cell cycle and apoptosis in cancer. However, p53 has a profound

impact on tumor metabolism. p53 is mutated or deleted in ~50% of all human cancers and its mutant status dictates its effect on cancer metabolism. Wild-type p53 supports mitochondrial oxidation and suppresses glycolytic metabolism (99). p53 upregulates TP53 induced glycolysis regulatory phosphatase (TIGAR), which decreases the level of fructose-2,6-bisphosphate, an intermediate metabolite that stimulates glycolytic flux (100). Additionally, p53 enhances oxidative capacity through induction of SCO2, which codes for the cytochrome c oxidase assembly protein, a critical component of complex IV of the ETC (101). Wild-type p53 also promotes stabilization of Nrf2 and enhanced antioxidant capacity through activation of p21, which disrupts the KEAP1-Nrf2 interaction (102). The loss of p53 is thought to contribute to tumorigenesis through activation of glycolytic metabolism and entry of glycolytic intermediates into anabolic pathways that generate biosynthetic precursors and reducing potential in the form of NADPH (99).

1.4.1.5 PKM2

Pyruvate kinase (PK) is the rate-limiting enzyme of glycolysis, which catalyzes the conversion of phosphoenolpyruvate (PEP) to pyruvate in a substrate level-phosphorylation reaction that generates ATP. Several isoforms of PK exist, the two most relevant to cancer are the M1 and M2 isoforms. PKM1 is a highly efficient and constitutively active isoform that promotes pyruvate oxidation and prevents the buildup of glycolytic precursors (103). In contrast, The M2 isoform is inefficient and subject to inhibitory phosphorylation that promotes the accumulation of intermediates upstream of PEP (4). Though not required for tumorigenesis, PKM2 expression confers a

proliferative advantage to cancer cell by promoting PPP flux, uridine diphosphate (UDP)-glucose, glycerol and serine synthesis (104-106). The accumulation of serine activates PKM2, suggesting that PKM2 functions to promote sufficient production of serine for biosynthesis (104). There is recent evidence to suggest that PKM2 translocates to the nucleus where it directly activates the transcription of glycolytic genes including itself in a feed forward mechanism that promotes anabolic glycolytic metabolism (107). c-Myc is shown to preferentially induce expression of PKM2 over PKM1 through alternative exon splicing (108).

1.4.2 Tumor Hypoxia and HIF-1

Rapidly growing tumors require concurrent vascularization to provide nutrient support for growth. Unfortunately, the rate of angiogenesis does not match that of tumor growth and the tumor vasculature is structurally and functionally inadequate (109). This leads to a perfusion gradient for oxygen and nutrients within the tumor that promotes metabolic heterogeneity, which can be assessed in patients through magnetic resonance imaging (MRI) (109, 110). An ultimate consequence of this immature vasculature is hypoxia within areas of the tumor that are beyond the oxygen diffusion limit of 70μm from the blood supply (111). This can lead to regions of tumor necrosis when cancer cells are unable to maintain viability in the face of nutrient and oxygen restriction (112).

Tumor hypoxia contributes to the substantial activation of HIF transcriptional machinery seen in cancer (113). Under normoxic conditions, HIF-1α is hydroxylated by oxygen-dependent prolyl hydroxylases (PHDs), which promotes an interaction with the

E3 ubiquitin ligase, von Hippel-Lindau (vHL) promoting HIF-1α ubiquitination and subsequent proteasomal degradation (114). The reduction in oxygen tension thus promotes stabilization of HIF-1α, permitting formation of an active HIF transcription factor. However, this is not the only mechanism for HIF-1α activation in cancer. HIF-1α is shown to be constitutively activated through hyperactivation of mTORC1, oxidative stress, loss of vHL and the accumulation of metabolic intermediates that inhibit PHDs (115).

HIF activates transcriptional machinery that drive aerobic glycolysis, including the induction of GLUT transporters, glycolytic enzymes and PDK (113). MCT4 is also upregulated under hypoxia, which contributes to the Warburg phenotype (116). Oxidative metabolism is not necessarily lost under hypoxic conditions of <2% O_2, as the ETC can function at full capacity at oxygen levels as low as 0.5% (117). Glutamine oxidation is can sustain ATP levels under hypoxia (118). Kamphorst *et al*. demonstrated that in culture, hypoxic cancer cells utilized acetate as an alternative to glucose and glutamine for generating acetyl-CoA (39). Moreover, it has been demonstrated that ~40% of invasive ductal breast carcinomas have increased expression of Acyl-CoA synthetase short-chain family member 2 (ACSS2), which facilitates acetate metabolism for the purposes of acetyl-CoA production (119).

Oxidative stress can result from a hypoxic microenvironment (120). SHMT2 expression is upregulated under to facilitate one-carbon metabolism and NADPH production, maintaining redox balance (104). Extremely low oxygen tension (<0.2% O_2) causes endoplasmic reticulum (ER) stress and promotes the unfolded protein response,

which provides cancer cells with an adaptive advantage to maintain viability under the metabolic stress associated with hypoxia (121).

1.4.3 Comorbidities

Oncogenesis does not occur in a vacuum; even heritable cancers are influenced by the physiology of the patient. Recent epidemiological studies have demonstrated that a substantial percentage of the United States population is overweight or obese (122, 123). These burdens impose metabolic stresses that have extensive effects on physiology and have been associated with an increased risk of cancer (124). Colorectal, kidney, pancreatic, prostate as well as postmenopausal breast, endometrial, uterine and ovarian cancers have been linked to increased incidence in overweight or obese patients (123). Moreover, an estimated 20% of cancer deaths are attributable to the metabolic health of the patient (125).

These maladies are associated with increased adipogenesis, insulin resistance, increased circulating glucose and type II diabetes mellitus (T2DM). Fat deposition imposes similar energetic stresses on adipose tissue to that of a growing tumor, specifically the induction of HIF signaling (126). Adipocytes are a prominent component of the microenvironments of breast, colorectal, kidney, and ovarian cancers and thus contribute to the pool of extracellular signaling factors that drive tumor growth and metabolism (6). The pro-inflammatory cytokine Interleukin 6 (IL-6) is among several cytokines released from adipose tissue that promote the chronic state of inflammation that is often present in metabolic disease. IL-6 is shown to enhance cancer cell proliferation and invasive capacity (127). The adipocyte-derived factor endotrophin is

upregulated in breast and colorectal tumors and is associated with increased size and aggressiveness of tumors (128). Moreover, endotrophin mediated cisplatin resistance and metastasis in a mammary tumor model (ref). The induction of tumor-associated lipolysis likely provides a source of exogenous fatty acids for certain cancers; this is mediated by Xbp1 in triple negative breast cancer (TNBC) (129).

The loss of blood glucose control and insulin resistance associated with T2DM leads to increased levels of circulating glucose, insulin and insulin-like growth factors (IGFs) (131). Insulin and IGF activate PI3K/Akt signaling in cancer cells, which enhances tumor uptake of this abundant glucose and supports the biosynthetic needs for tumor expansion. High levels of fasting insulin and glucose are also associated with increased cancer risk (132).

1.4.4 Mitochondrial Dysfunction

Though substantial evidence for the role of mitochondrial metabolism in tumorigenesis has accumulated in the years since Warburg theorized that aerobic fermentation was a direct response to irreversible damage to oxidative capacity, there are also indications that mitochondrial dysfunction is present in cancer and that this dysfunction directs metabolism (133). Mitochondria exist as a dynamic network that transverse the cell to facilitate energy-demanding processes such as cell motility. The structural integrity of the mitochondrial network is maintained through regulated fission and fusion events, this morphological regulation is tightly associated with the health and oxidative capacity of the organelle (134). Morphological abnormalities of cancer mitochondria have been characterized in several tumor species (135). The mitochondria

also encapsulate its own genome (mtDNA) that is not associated with histone proteins and is thus more susceptible to oxidative damage and mutagenicity than nuclear DNA (136). As mtDNA encodes components of the ETC, disruption of mtDNA fidelity can alter oxidative capacity.

1.4.4.1 Structural Abnormalities

Electron microscopy has been employed to study mitochondrial content and morphology in tumor biopsies. These studies have demonstrated that cancer mitochondria are often less numerous, enlarged and exhibit partial or total cristolysis, the loss of IMM folding (137). Mitochondrial cristae provide increased surface area for electron transport and ATP production, the loss of this IMM folding severely hinders oxidative capacity. Moreover, the analysis of over 800 breast tumor biopsies showed that ~60% of tumor samples lacked mitochondria altogether, which would of course restrict bioenergetic and biosynthetic metabolism to the cytosol of these neoplasms (138). The mitochondrial network of cancer cells is often more fragmented than in normal cells, which is indicative of increased fission as a result of mitochondrial stress (135). Mitophagy, the process by which cells dispense of damaged mitochondria is upregulated in some cancers, and is critical to viability (134).

The lipid and protein composition of the IMM influences ETC efficiency and ATP production. Phospholipid content is an especially critical factor for ETC complex function. The mitochondrial specific phospholipid, cardiolipin (CL) is required for optimal NADH oxidation at complex I (139). Kiebish *et al*. demonstrated that compared to normal brain tissue, the mitochondria of a murine brain tumor exhibited deficiencies in

CL production (140). Reduction in CL content can contribute to mitochondrial uncoupling, or the movement of H^+ back into the matrix, independent of ATP production. Mitochondrial uncoupling is often mediated by certain uncoupling proteins (UCPs), whose expression is increased in some cancers (141, 142). Mitochondrial uncoupling is present in brown adipose tissue, where H^+ flux is harnessed to generate heat for thermoregulation rather than the production of ATP. Similarly, tumors have been characterized by thermographic detection of heat production. Interestingly, heat production was associated with more aggressive tumors (143).

1.4.4.2 Mutational Defects in Mitochondrial Metabolism

The studies mentioned above suggest that tumors can still thrive with mitochondrial deficiencies, even in the absence of mitochondria. However, work performed with mtDNA-deficient ρ° cells demonstrated that mitochondria are required for tumorigenesis, suggesting that the loss of mitochondria in these tumor samples occurred after tumor formation (144-146). Nonetheless, mutations in mtDNA-encoded components of the ETC are prevalent in cancer (147). The most commonly affected component is Complex I (133). Alteration of the rate of NADH oxidation at complex I affects the mitochondrial NADH/NAD+ ratio, which has whole cell effects on metabolic flux. Additionally, Complex I mutations were shown to promote lung and breast cancer metastasis in a ROS-dependent manner (148, 149). The extent of complex I deficiency dictates its effect on tumorigenesis; severe disruption of complex I reduced tumorigenesis compared to cells harboring mutations that only mildly disrupted complex I activity (150).

Mutations or alterations of nuclear-encoded DNA (nDNA) also impact mitochondrial metabolism. Several TCA cycle enzymes are found to be altered in many cancers (133). Citrate synthase (CS) was found to be upregulated in PDAC, where it facilitated proliferation through enhanced fatty acid synthesis (151). In contrast, the loss of CS in several cervical cancer cell lines corresponded with increased EMT and metastatic potential, suggesting that CS necessity is context dependent (152). Succinate dehydrogenase (SDH) is found to be deficient in several tumor species (153). This results in an accumulation of succinate, which is shown to elicit profound allosteric regulation of PHDs. Succinate thus inhibits PHD-dependent regulation of HIF-1α, leading to HIF stabilization and the induction of its metabolic transcriptional program (154). Furthermore, succinate accumulation results in the inhibition of oxygen-dependent DNA and histone demethlyases, which promotes hypermethylation of certain regions of nDNA (155).

Similarly, inactivating mutations of fumarate hydratase (FH) have been observed in hereditary leiomyomatosis and renal cell cancer (HLRCC) and a subset of pheochromocytomas (PCC) (156). Fumarate also exhibits a propensity to stimulate HIF-1α activity through allosteric PHD inhibition. Unique to fumarate is its ability to bind to cysteine resides through a process called succination, which modifies protein function. Of note, fumarate can succinate KEAP1, which prevents its inhibitory interaction with Nrf2 and enhances the antioxidant capacity of FH-deficient cells (157). Conversely, fumarate can succinate GSH, which was shown to enhance oxidative stress in HLRCC cells (158).

An additional enzyme associated with TCA cycling and mitochondrial metabolism that is commonly altered in cancer is IDH2. Observed mutations in both cytosolic IDH1 and mitochondrial IDH2 appear to be largely gain-of-function that promotes IDH mediated reduction of α-KG to R-2-hydroxyglutarate (2-HG). 2-HG blocks hematopoietic differentiation and promotes leukemogenesis. This is believed to be mediated through 2-HG inhibition of the oxygen-dependent DNA and histone demethylases that are also subject to fumarate and succinate inhibition (159). Again, this promotes hypermethylation of DNA, including regions important for cellular differentiation. IDH-dependent generation of 2-HG is a NADPH process, therefore robust production of 2-HG would coincide with depletion of the mitochondrial NADPH pool. This alteration of redox balance could promote oxidative stress through loss of reducing potential required to facilitate redox-cycle based antioxidant systems (160).

1.5 Therapeutic Vulnerability

Though the intricate characterization of cancer metabolism has only relatively recently become of particular interest, therapeutic targeting of cancer metabolism is not a novel strategy. Several traditional chemotherapeutics target biosynthetic pathways that disrupt cell proliferation. However, the emergence of omic technology has provided cancer biologists with knowledge of the tumor that permits specific targeting of metabolic pathways with small molecules. Cellular metabolism is ultimately dependent on nutrient availability; thus recent therapeutic initiatives have also focused on nutritional and lifestyle interventions as possible adjuvant or standalone cancer treatments.

1.5.1 Traditional Chemotherapy

The anti-folate class of chemotherapeutics has been used in the clinic since the 1950's, when it was observed that folic acid supplementation enhanced leukemia expansion (161, 162). This led to the development of the anti-folate, methotrexate, which is still employed to this day. Methotrexate inhibits dihydrofolate reductase (DHFR), which catalyzes the conversion of dihydrofolate (DHF) to THF, a critical component of one-carbon metabolism (163). As described above, the folate cycle and one-carbon metabolism is critical to nucleotide synthesis and NADPH generation, which sustain cancer proliferation (27, 28). Methotrexate is approved for the treatment of certain leukemias, lung cancer, osteosarcoma and head and neck cancers (163). Furthermore, pemetrexed, another anti-folate chemotherapy, is used as a first line-therapy for NSCLC (164).

The major consequence of anti-folate agents is the inhibition of nucleic acid synthesis as a result of nucleotide deficiencies. Nucleic acid synthesis is also the target of a number of other oft-used chemotherapies. 5-Fluorouracil (5-FU) is an inhibitor of thymidylate synthase, preventing the production of thymidine (165). Hydroxyurea inhibits ribonucleotide reductase (RNR) which is required for deoxynucleotide synthesis and is used to treat chronic myeloid leukemia (CML) (166). Furthermore, the cytidine analog, gemcitabine, also inhibits RNR in addition to its activity in disrupting DNA replication. Gemcitabine is used in advanced stage ovarian and bladder cancers as well as NSCLC (167). Together, these agents demonstrate the longstanding efficacy of targeting biosynthetic pathways as an anti-cancer strategy.

1.5.2 Molecular Targeted Therapies

The elucidation of the metabolic derangements that support rapid and sustained tumor growth has proven to be incredibly fruitful for the identification of novel targets for cancer therapy. However, as metabolism is critical to sustaining the viability of normal tissue, metabolic therapies are subject to potential toxicities. It is essential to identify metabolic vulnerabilities that are unique to cancer or to which normal tissue can sufficiently adapt. The implementation of untargeted global metabolomics as well as isotope-labeled metabolite tracing provides phenotypic context for the genomic identification of alterations to metabolic pathways. These studies will be critical for identifying individualized therapeutic regimens based on metabolic intervention.

1.5.2.1 Glycolytic Inhibitors

The glucose analog, 2-deoxyglucose (2-DG), is rapidly phosphorylated by hexokinase to 2-deoxyglucose-6-phosphate, which inhibits glycolysis through competitive inhibition of G6P metabolism (168). 2-DG is shown to reverse the Warburg effect and inhibit tumor growth. Unfortunately, clinical trials assessing the safety and efficacy of 2-DG in glioma patients demonstrated dose-limiting toxicities that compromised 2-DG efficacy, as lower doses did not demonstrate clinical benefit (169). Similarly, pre-clinical studies of the HK2 inhibitor, 3-bromopyruvate (3-BP), have demonstrated remarkable efficacy in disrupting cancer metabolism and reducing tumorigenesis (170). 3-BP is shown to cause HK2 dissociation from the OMM, preventing its interaction with VDAC and the coupling of mitochondrial ATP production

to glycolysis. As such, 3-BP disrupts mitochondrial oxidation in addition to glycolysis (171). Clinical use of 3-BP is controversial because of fears over the potential toxicity of inhibiting glycolysis in normal tissue (172).

Lactate metabolism is another potential target in cancer therapy. A study of human lymphoma and pancreatic xenografts demonstrated that inhibition of LDH with the investigative small molecule, FX11, as well as siRNA knockdown inhibited tumor progression. This was associated with the collapse of ATP production and induction of oxidative stress (173). Moreover, small molecule inhibition of MCTs disrupted glycolytic metabolism in cancer cells (174). Unfortunately, as addressed above, the metabolism of many immune cells makes them similarly susceptible to MCT inhibition (175). The pervasive necessity of glucose metabolism in normal physiology provides a narrow therapeutic window for modulators of glycolysis.

1.5.2.2 Inhibitors of Glutamine Metabolism

Glutamine metabolism is often an essential component of tumor metabolism as glutamine is required for TCA cycle anaplerosis, amino acid and nucleotide biosynthesis as well as maintenance of redox balance. Inhibition of enzymes required for glutamine metabolism has elicited pre-clinical efficacy. The experimental GS inhibitors compound 968 and BPTES disrupted glutamate production and reduced the rate of tumor growth in models of B cell lymphoma (176, 177). Additionally, targeting glutamate-dependent aminotransferases disrupted α-KG-dependent TCA cycle anaplerosis and blunted breast cancer growth (178). Furthermore, administration of 6-diazo-5-oxo-L-norleucine (DON) restricted primary tumor growth and inhibited metastasis of an aggressive brain

tumor (179). The upregulation of glutamine metabolism in cancer often coincides with restricted glucose metabolism, thus dual targeting of glucose and glutamine metabolism may exhibit greater efficacy than either alone in certain cancers.

1.5.2.3 Inhibitors of Lipid Metabolism

The necessity of fatty acid synthesis for proliferation dictates that cancer cells commit a substantial amount of carbon in the form of citrate and NADPH for de novo lipogenesis. Several experimental inhibitors of enzymes required for fatty acid synthesis (FAS) are currently under pre-clinical investigation. Interruption of cytosolic citrate catabolism through ATP citrate lyase (ACLY) inhibition restricted acetyl-CoA production for FAS and significantly reduced cancer cell proliferation (180). Inhibition of the subsequent enzymatic mediator of FAS, ACC, is shown to limit breast cancer tumorigenesis. Small molecule inhibition of fatty acid synthase (FASN), including by natural products such as green tea, was sufficient to initiate apoptosis in several cancer cell lines in addition to a reduction of xenograft tumor growth in models of NSCLC and ovarian cancer (181, 182). Moreover, FASN required NADPH as a cofactor, therefore targeting of aerobic glycolysis and/or the PPP will likely diminish cancer cell capacity for FAS, as the PPP is the predominant source of NADPH for FAS (183).

1.5.3 Lifestyle Modifications

We derive energy from the nutrients present in our diet. Excess nutrient intake and/or insufficient energy expenditure can result in adipogenesis and dysregulation of insulin signaling. As discussed previously, these can contribute to tumorigenesis and

cancer mortality. There is accumulating evidence that dietary and lifestyle interventions can promote a nutritional environment that is insufficient for carcinogenesis or disease progression (8). Suggesting that these may not only serve as a means to mitigate disease progression but to also prevent tumor formation altogether.

1.5.3.1 Exercise

Epidemiological studies have demonstrated that individuals who regularly exercise are at lower risk for breast, colorectal, endometrial and pancreatic cancers (184). Moreover, exercise may reduce the risk for disease recurrence and decrease cancer-related mortality (185). The mechanisms underlying these anti-cancer effects are not fully understood, however they are likely a result of the temporal energetic stress imposed by vigorous physical activity. Of particular note, is the regulation of insulin signaling in response to chronic exercise. Evaluation of a carcinogen-induced murine model of breast cancer showed that voluntary wheel running was associated with reduced tumor formation. The reduction in tumor incidence was associated with a reduction in circulating insulin and IGF-1 levels (186). Similar results on these circulating factors was demonstrated in breast cancer patients following regimens of aerobic or resistance exercise (187). Giganti *et al*. recently reported that exercise reduced circulating levels of MMP2 and MMP9 in breast cancer survivors, suggesting that exercise may reduce the risk of recurrent metastases (188).

There is also evidence to suggest that exercise may enhance chemotherapy efficacy (189). As mentioned above, solid tumors exhibit immature vasculature that prohibits adequate perfusion of the entire tumor mass, which induces energetic stress

and contributes to the metabolic heterogeneity of tumors. Exercise stimulates angiogenesis and improves vascular function in ischemic tissue and is shown to enhance tumor perfusion in a model of orthotropic prostate cancer (190,191). An increase in tumor perfusion would enhance drug delivery throughout the tumor. Furthermore, enhanced perfusion would promote tumor oxygenation and potentially prevent hypoxia-mediated chemoresistance of ROS-dependent chemotherapies (192). Compliance is likely to restrict the implementation of exercise for some cancer patients. Many therapeutic regimens induce fatigue and weakness, and though these symptoms would likely be attenuated with exercise, they may be serve as barriers to adjuvant exercise.

1.5.3.2 Caloric Restriction

Calorie restriction (CR), the intentional reduction of daily calorie intake by ~20-40%, is shown to increase metazoan longevity (193). Coinciding with increased longevity, CR reduces or delays the onset of age-related disorders, including cancer (194). Similar to exercise, CR reduces circulating levels of insulin and IGF-1 as well as glucose, which could compromise glycolytic metabolism in cancer. Indeed, constitutive PI3K signaling, which is a downstream mediator insulin receptor activation, conferred resistance to CR in tumors (195). Suggesting that the anti-cancer effect of CR is in part due to downregulation of insulin signaling. Weight loss is often associated with chronic CR, which has restricted its clinical use. Cancer patients are susceptible to cachexia, which is characterized by severe weight loss, muscle atrophy and loss of appetite. Thus

the implementation of CR could exacerbate this condition, which is thought to be the immediate cause of death in about ~20% of cancer patients (196).

However, there is accumulating evidence that the beneficial effects of CR can be achieved in the absence of substantial weight loss through implementation of intermittent fasting. Fasting increases lifespan in model organisms and promotes resistance to oxidative stress through downregulation of PI3K signaling (197). This metabolic regulation in normal tissue is shown to promote resistance to pro-oxidant chemotherapy, whereas fasting is shown to potentiate chemotherapy efficacy at the tumor in pre-clinical models (192, 198). Furthermore, fasting is under clinical investigation as an adjuvant to chemotherapy because of the observation that fasting mitigates dose-limiting toxicities without compromising efficacy (199).

1.5.3.3 Ketosis

A physiological consequence of the glucose restriction associated with CR and intermittent fasting is induction of ketosis, which is characterized by the increased hepatic production of ketone bodies (ketones) such as acetoacetate and β-hydroxybutyrate (βHB), to support energy metabolism in the absence of glucose. Ketosis can also result from adherence to the ketogenic diet (KD), a high fat, low carbohydrate and adequate protein diet that restricts circulating glucose levels while increasing blood levels of ketones. The KD is a first line therapy for pediatric refractory epilepsy and has also shown efficacy in treating other neurological disorders and metabolic syndrome (200-202). There is also substantial evidence to suggest that the KD elicits anti-cancer activity (203).

Similar to CR and fasting, the KD reduces circulating insulin levels. This was associated with reduced tumor growth and survival in a model of pancreatic cancer (204). Restricting glucose availability lowers the glycolytic capacity of tumors, which subsequently limits cancer cell proliferation due to a lack of biosynthetic precursors. Thus the efficacy of the ketogenic diet for highly glycolytic tumors is likely to be dependent on the restriction of glycolytic metabolism. Indeed, our laboratory has previously demonstrated that increased survival in response to the ketogenic diet was inversely proportional to blood glucose level in a model of glioblastoma (GBM) (205).

Recent evidence suggests that ketone bodies exhibit alternative functions beyond serving as energy metabolites. βHB is shown to act as a class I histone deacetlyase (HDAC) inhibitor; this activity was associated with a transcriptional response that suppressed oxidative stress (206). Moreover, it has been reported that βHB inhibits the NLRP3 inflammasome, providing a potential mechanism for the anti-inflammatory response associated with CR and the ketogenic diet (207). The epigenetic and immunomodulatory effects of βHB and the ketogenic diet in regards to tumorigenesis are currently under investigation.

The ketogenic diet is currently being evaluated in numerous clinical trials, however clinical efficacy is likely to be hampered by patient compliance. Strict adherence to the ketogenic diet is required to sustain the benefits of the diet in regards to blood metabolite levels. Imposing dietary restrictions on cancer patients may prove difficult due to the development of taste aversions and the loss of appetite associated with the disease as well as cancer therapy (208). Therefore, exogenous ketone supplementation may provide an alternative to the KD for a ketogenic cancer

intervention. We have previously demonstrated that administration of several ketone supplements can increase circulating βHB levels regardless of carbohydrate intake (209). Furthermore, Poff *et al*. showed therapeutic efficacy with a ketone ester in prolonging survival and reducing metastasis in an aggressive model of GBM (210). This study further supports the notion that ketone bodies themselves possess anti-cancer activity that merits further investigation.

1.5.4 Targeting Redox Balance

As described throughout this review, a fundamental consequence of cancer metabolism is the upregulation of pathways that contribute to the maintenance of cellular redox balance. It is now clear that moderate oxidative stress potentiates tumorigenesis and the increased antioxidant capacity of cancer cells facilitates the accumulation of non-toxic levels of ROS that permit oxidation-dependent signaling events (53). The continued utility of radiotherapy and pro-oxidant chemotherapeutics demonstrates efficacy in targeting redox balance. Rational targeting of cancer redox balance can be achieved through bidirectional modulation of oxidative stress.

Antioxidant supplementation has been suggested as therapeutic strategy to restrict ROS signaling in tumorigenesis. A series of large scale clinical trials have been conducted to evaluate the cancer preventative effects of a number of antioxidant cofactors. The Linxian trial demonstrated that a cocktail of β-carotene, vitamin E and selenium reduced total patient mortality as well as mortality associated with gastric cancer (211). In contrast, subsequent trials evaluating β-carotene in combination with vitamin E or A showed that antioxidant supplementation increased the risk for lung

cancer (212, 213). Moreover, the “Selenium and Vitamin E Cancer Prevention Trial” (SELECT) was initially lauded for demonstrating that selenium supplementation reduced prostate cancer incidence. However, further analysis of the >33,000 patient trial revealed that this was only true for a small subset of rare forms of prostate cancer. Furthermore, it was shown that vitamin E supplementation actually increased the risk for prostate cancer in men (214). Additional studies evaluating the green tea extract, epigallo-catechin-3-gallate (EGCG), curcumin and choline have demonstrated pre-clinical efficacy, however these results have yet to be replicated in the clinic.

Gorrini *et al.* have posited that ROS levels increase as tumors develop and become more aggressive, bringing them closer to the threshold for apoptotic induction. Thus as a tumor becomes more aggressive, they become susceptible to even small perturbations of redox balance (215). This has informed the development of small molecules that induce oxidative stress in cancer cells. The proteasome inhibitor bortezomib promotes the accumulation damaged protein that promotes oxidative stress and mitochondrial dysfunction in mantle cell lymphoma (MCL) (216). Subsequent studies with bortezomib demonstrated that it also disrupted ER function through exacerbation of oxidative stress and induction of the unfolded protein response (217, 218).

Similar to inducing ROS production, reducing antioxidant capacity enhances oxidative stress. The anti-inflammatory agent sulphasalazine exhibits inhibitory activity towards xCT, preventing the uptake of cysteine and restricting GSH synthesis. Sulphasalazine induction of oxidative stress is associated with a reduction of cell viability and tumor growth in models of pancreatic and small cell lung cancers (SCLC)

(219, 220). Additionally, the gold-based compound auranofin inhibits TXR and potentiates pro-oxidant therapies in head and neck cancer (221). Furthermore, inhibition of G6PDH with 6-anicotinamide restricted GSH production due to a lack of PPP-derived NADPH and reversed antioxidant-mediated resistance to doxorubicin in colon cancer cells (222). Together, these studies support a pro-oxidant approach to modulating cancer redox balance and inform the rationale for the therapeutic regimen evaluated in this thesis.

1.6 References

1. Hanahan, D. & Weinberg, RA. The hallmarks of cancer. *Cell* **100,** 57–70 (2000).
2. Hanahan, D. & Weinberg, RA. Hallmarks of cancer: the next generation. *Cell* **144**, 646-674 (2011).
3. Agathocleous, M. & Harris, WA. Metabolism in physiological cell proliferation and differentiation. *Trends Cell Biol* **23,** 484–492 (2013).
4. Lunt, SY. & VanderHeiden, MG. Aerobic glycolysis: meeting the metabolic requirements of cell proliferation. *Annu Rev Cell Dev Bi* **27,** 441–464 (2011)
5. DeBerardinis, RJ. & Chandel, NS. Fundamentals of cancer metabolism. *Sci Adv* **2,** e1600200 (2016).
6. DeNicola, GM. & Cantley, LC. Cancer's fuel choice: new flavors for a picky eater. *Mol Cell* **60,** 514–523 (2015).
7. Cairns, RA., Harris, IS. & Mak, TW. Regulation of cancer cell metabolism. *Nat Rev Cancer* **11,** 85–95 (2011).
8. Hirschey, MD. *et al.* Dysregulated metabolism contributes to oncogenesis. *Semin Cancer Biol* **35,** S129–S150 (2015).
9. Warburg, O., Wind, F. & Negelein, E. The metabolism of tumors in the body. *J Gen Physiology* **8,** 519–530 (1927).
10. Ward PS., Thompson CB. Metabolic reprogramming: a cancer hallmark even warburg did not anticipate. *Cancer Cell* **21**, 297-308 (2012).
11. Schrevens, L., Lorent, N., Dooms, C. & Vansteenkiste, J. The role of PET scan in diagnosis, staging, and management of non-small cell lung cancer. *Oncol* **9**, 633-643 (2004).
12. VanderHeiden, MG., Cantley, LC. & Thompson, CB. Understanding the Warburg effect: the metabolic requirements of cell proliferation. *Science* **324,** 1029–1033 (2009).
13. Warburg O. On the origin of cancer cells. *Science* **123**, 309-314 (1956).
14. Ahn, SA. & Metallo, CM. Mitochondria as biosynthetic factories for cancer proliferation. *Cancer Metabolism* **3**, 1-10 (2015).

15. Pavlova, NN. & Thompson, CB. The emerging hallmarks of cancer metabolism. *Cell Metab* **23**, 27-47 (2016).
16. Marin-Valencia, I. *et al.* Analysis of tumor metabolism reveals mitochondrial glucose oxidation in genetically diverse human glioblastomas in the mouse brain In Vivo. *Cell Metab* **16,** 686 (2012).
17. Birsoy, K. *et al.* An Essential role of the mitochondrial electron transport chain in cell proliferation is to enable aspartate synthesis. *Cell* **162,** 540–551 (2015).
18. Sullivan, LB. *et al.* Supporting aspartate biosynthesis is an essential function of respiration in proliferating cells. *Cell* **162,**552–563 (2015).
19. Martínez-Reyes, I. *et al.* TCA cycle and mitochondrial membrane potential are necessary for diverse biological Functions. *Mol Cell* **61,** 199–209 (2016).
20. Bonnet, S. *et al.* A mitochondria-K+ channel axis is suppressed in cancer and its normalization promotes apoptosis and inhibits cancer growth. *Cancer Cell* **11,** 37–51 (2007).
21. Pike, LS. et al. Inhibition of fatty acid oxidation by etomoxir impairs NADPH production and increases reactive oxygen species resulting in ATP depletion and cell death in human glioblastoma cells. *Biochimica Et Biophysica Acta Bba - Bioenergetics* **1807,** 726–734 (2011).
22. Samudio, I. *et al.* Pharmacologic inhibition of fatty acid oxidation sensitizes human leukemia cells to apoptosis induction. *J Clin Invest* **120,**142–156 (2010).
23. Caro, P. *et al.* Metabolic signatures uncover distinct targets in molecular subsets of diffuse large B cell lymphoma. *Cancer Cell* **22,** 547–560 (2012).
24. Matsuno, T. Oxidation of cytosolic NADH by the malate-aspartate shuttle in MC29 hepatoma cells. *Cell Biol Int Rep* **13,** 739–745 (1989).
25. Gameiro, PA. *et al*. In vivo HIF-mediated reductive carboxylation is regulated by citrate levels and sensitizes VHL-deficient cells to glutamine deprivation. *Cell Metab.* **17**, 372-385 (2013).
26. Son, J. *et al*. Glutamine supports pancreatic cancer growth through KRAS-regulated metabolic pathway. *Nature* **496**, 101-105 (2013).
27. Fan, J. *et al*. Quantitative flux analysis reveals folate-dependent NADPH production. *Nature* **510**, 298-302 (2014).
28. Lewis, CA. *et al*. Tracing compartmentalized NADPH metabolism in the cytosol and mitochondria of mammalian cells. *Mol. Cell* **55**, 253-263.
29. Trachootham, D., Alexandre, J. & Huang, P. Targeting cancer cells by ROS-mediated mechanisms: a radical therapeutic approach? *Nat Rev Drug Discov* **8,** 579–591 (2009).
30. Enriquez-Navas, P. *et al.* Exploiting evolutionary principles to prolong tumor control in preclinical models of breast cancer. *Sci Transl Medicine* **8,** 327ra24 (2016).
31. Pearce, EL. *et al*. Fueling immunity: Insights into metabolism and lymphocyte function. *Science* **342**, 1242454 (2013).
32. Ghesquière, B., Wong, BW., Kuchnio, A. & Carmeliet, P. Metabolism of stromal and immune cells in health and disease. *Nature* **511,**167–176 (2014).
33. Locasale, JW. *et al*. Phosphoglycerate dehydrogenase diverts glycolytic flux and contributes to oncogenesis. *Nat. Genet.* **43**, 869-874 (2011).

34. Jia, X. *et al.* Increased Expression of PHGDH and prognostic significance in colorectal cancer. *Transl Oncol* **9,** 191–196 (2016).
35. Tong, X., Zhao, F., & Thompson, CB. The molecular determinants of de novo nucleotide biosynthesis in cancer cells. *Curr. Opin. Genet. Dev.* **19**, 32-37 (2009).
36. Lo, M., Wang, Y. & Gout, PW. The x c− cystine/glutamate antiporter: A potential target for therapy of cancer and other diseases. *J Cell Physiol* **215**, 593–602 (2008).
37. Yang, S. *et al*. Pancreatic cancers require autophagy for tumor growth. *Genes Dev.* **25**, 717-729 (2011).
38. Commisso, C. *et al.* Macropinocytosis of protein is an amino acid supply route in Ras-transformed cells. *Nature* **497,** 633–637 (2013).
39. Kamphorst, JJ. *et al.* Quantitative analysis of acetyl-CoA production in hypoxic cancer cells reveals substantial contribution from acetate. *Cancer Metab.* **2**, 23.
40. Mullen, AR. *et al*. Reductive carboxylation enables growth in tumor cells with defective mitochondria. *Nature* **481**, 385-388 (2012).
41. Metallo, CR. *et al*. Reductive glutamine metabolism by IDH1 mediates lipogenesis under hypoxia. *Nature* **481**, 380-384 (2012).
42. DeNicola, GM. *et al*. Oncogene-induced Nrf2 transcription promotes ROS detoxification and tumorigenesis. *Nature* **475**, 106-109 (2011).
43. Patra, KC. & Hay, N. The pentose phosphate pathway and cancer. *Trends Biochem Sci* **39,**347–354 (2014).
44. Berlett, BS. & Stadtman, ER. Protein oxidation in aging, disease, and oxidative stress. *J Biol Chem* **272,** 20313–20316 (1997).
45. Guyton, KZ., and Kensler, TW. Oxidative mechanisms in carcinogenesis. *Br Med Bull* **49,** 523–44 (1993).
46. Miyake, H., Hara, I., Kamidono, S., and Eto, H. Oxidative DNA damage in patients with prostate cancer and its response to treatment. *J Urol*. **171**, 1533-1536 (2004).
47. Diakowska, D., Lewandowski, A., Kopec, W., Diakowski, W., and Chrzanowska, T. Oxidative DNA damage and total antioxidant status in serum of patients with esophageal squamous cell carcinoma. *Hepatogastroenterology* **54**, 1701-1704 (2007).
48. Sallmyr, A., Fan, J., & Rassool, FV. Genomic instability in myeloid malignancies: increased reactive oxygen species (ROS), DNA double strand breaks (DSBs) and error-prone repair. *Cancer letters **270***, 1-9 (2008).
49. Marchi S. *et al.* Mitochondrial-ROS crosstalk in the control of cell death and aging. *J Signal Transduc*t. **2012**, 329365 (2012).
50. Kroemer G., Galluzi L. & Brenner C. Mitochondrial membrane permeabilization in cell death. *Physiol Rev.* **87**, 99-163 (2007).
51. Martindale, J. & Holbrook, N. Cellular response to oxidative stress: Signaling for suicide and survival. *J Cell Physiol* **192,** 1–15 (2002).
52. Lee, S.-R. *et al.* Reversible inactivation of the tumor suppressor PTEN by H_2O_2. *J Biol Chem* **277,** 20336–20342 (2002).
53. Sullivan, LB. & Chandel, NS. Mitochondrial reactive oxygen species and cancer. *Cancer Metabolism* **2,** 1–12 (2014).

54. McCubrey, JA., LaHair, MM. & Franklin, RA. Reactive Oxygen Species-Induced Activation of the MAP Kinase Signaling Pathways.*Antioxid Redox Sign* **8,** 1775–1789 (2006).
55. Wagner, EF. & Nebreda, ÁR. Signal integration by JNK and p38 MAPK pathways in cancer development. *Nat Rev Cancer* **9,** 537–549 (2009).
56. Pan, Y. *et al.* Multiple Factors Affecting Cellular Redox Status and Energy Metabolism Modulate Hypoxia-Inducible Factor Prolyl Hydroxylase Activity In Vivo and In Vitro. *Mol Cell Biol* **27,** 912–925 (2007).
57. Bonello S. *et al*. Reactive oxygen species activate HIF-1α promoter via a functional NFκB site. *Arterioscler. Thromb. Vasc. Biol.* **27**, 755-761 (2007).
58. Kotamraju, S. *et al.* Transferrin receptor-dependent iron uptake is responsible for doxorubicin-mediated apoptosis in endothelial cells -role of oxidant-induced iron signaling in apoptosis. *J Biol Chem* **277,** 17179–17187 (2002).
59. Marullo, R. *et al.* Cisplatin Induces a Mitochondrial-ROS Response That Contributes to Cytotoxicity Depending on Mitochondrial Redox Status and Bioenergetic Functions. *Plos One* **8,** e81162 (2013).
60. Yi, J. *et al*. The inherent cellular level of reactive oxygen species: one of the mechanisms determining apoptotic susceptibility of leukemic cells to arsenic trioxide. *Apoptosis* **7**, 209-215 (2002).
61. Yoshida, T. *et* al. Mitochondrial dysfunction, a probable cause of persistent oxidative stress after exposure to ionizing radiation. *Free Radical Res* **46,** 147–153 (2012).
62. Wang, Y. *et al.* Total body irradiation causes residual bone marrow injury by induction of persistent oxidative stress in murine hematopoietic stem cells. *Free Radical Bio Med* **48,** 348–356 (2010).
63. Diehn, M. *et al.* Association of reactive oxygen species levels and radioresistance in cancer stem cells. *Nature* **458,** 780–783 (2009).
64. Shi, X. *et al*. Reactive oxygen species in cancer stem cells. *Antioxid Redox Signal.* **16**, 1215-1228 (2012).
65. Abdullah, L. & Chow, E. Mechanisms of chemoresistance in cancer stem cells. *Clin Transl Medicine* **2,** 1–9 (2013).
66. Hanahan D. & Coussens, LM. Accessories to the crime: functions of cells recruited to the tumor microenvironment. *Cancer Cell* **21**, 309-322 (2012).
67. Pinheiro, C. *et al.* Increased expression of monocarboxylate transporters 1, 2, and 4 in colorectal carcinomas. *Virchows Arch* **452,** 139–146 (2008).
68. Saedeleer, DC. *et al.* Glucose deprivation increases monocarboxylate transporter 1 (MCT1) expression and MCT1-dependent tumor cell migration. *Oncogene* **33**, 4060-4068 (2014).
69. Robey, IF. *et al.* Bicarbonate Increases Tumor pH and Inhibits Spontaneous Metastases. *Cancer Res* **69,** 2260–2268 (2009).
70. Svastová, E. *et al*. Hypoxia activates the capacity of tumor-associated carbonic anhydrase IX to acidify extracellular pH. *FEBS Lett.* **577**, 439-445 (2004).
71. Wang, T., Liu, G. & Wang, R. The intercellular metabolic interplay between tumor and immune cells. *Front. Immunol.* **5**, 358 (2014).

72. Gottfried, E. *et al*. Tumor-derived lactic acid modulates dendritic cell activation and antigen expression. *Blood*. **107**, 2013-2021 (2006).
73. Goetze, K. *et al*. Lactate enhances motility of tumor cells and inhibits monocyte migration and cytokine release. *Int. J. Oncol.* **39**, 453-463 (2011).
74. Stern, R. *et al*. Lactate stimulates fibroblast expression of hyaluronan and CD44: the Warburg effect revisited. *Exp Cell Res.* **276**, 24-31 (2002).
75. Bharadwaj, AJ. *et al.* Spontaneous Metastasis of Prostate Cancer Is Promoted by Excess Hyaluronan Synthesis and Processing. *Am J Pathology* **174,** 1027–1036 (2009).
76. Friedl, P. & Alexander, S. Cancer Invasion and the Microenvironment: Plasticity and Reciprocity. *Cell* **147,** 992–1009 (2011).
77. Yuan, TL. & Cantley, LC. PI3K pathway alterations in cancer. Variations on a theme. *Oncogene* **27,** 5497-5510 (2008).
78. Elstrom, RL. *et al.* Akt stimulates aerobic glycolysis in cancer cells. *Cancer Res* **64**, 3892-3899 (2004).
79. Robey, RB. & Hay, N. *et al.* Is Akt the "Warburg kinase"? Akt-energy metabolism interactions and oncogenesis. *Semin Cancer Biol* **19**, 25-31 (2009).
80. Khatri, S. *et al*. FOXO3a regulates glycolysis via transcriptional control of tumor suppressor TSC1. *J Biol Chem.* **285**, 15960-15965 (2010).
81. Nakashima, RA., Mangan, PS., Colombini, M. & Pedersen, PL. Hexokinase receptor complex in hepatoma mitochondria: evidence for N,N'-dicyclohexylcarbodiimide-labeling studies for the involvement of the pore-forming protein VDAC. *Biochemistry* **25**, 1015-1021 (1986).
82. Guertin, DA. & Sabatini, DM. Defining the role of mTOR in cancer. *Cancer Cell* **12**, 9-22 (2007).
83. Nicklin, P. *et al.* Bideirectional transport of amino acids regulates mTOR and autophagy. *Cell* **136**, 521-534 (2009).
84. Ben-Sahra, I., Howell, JJ., Asara, JM. & Manning, BD. Stimulation of de novo pyrimidine synthesis by growth signaling through mTOR and S6K1. *Science* **339**, 1323-1328 (2013).
85. Duran, RV. *et al.* Glutaminolysis activates Rag-mTORC1 signaling. *Mol Cell* **47**, 349-358 (2012).
86. Taub, R. *et al*. Translocation of the c-myc gene into the immunoglobulin heavy chain locus in human Burkitt lymphoma and murine plasmacytoma cells. *PNAS* **79**, 7837-7841 (1982).
87. van Geldermalsen, M. *et al*. ASCT2/SLC1A5 controls glutamine uptake and tumor growth in triple-negative basal-like breast cancer. *Oncogene* **35**, 3201-3208 (2016).
88. Eberhardy, SR. & Farnham, PJ. c-Myc mediates activation of the cad promoter via a post-RNA polymerase II recruitment mechanism. *J Biol Chem.* **276**, 48562-48571 (2001).
89. Mannava, S. *et al.* Direct role of nucleotide metabolism in c-MYC dependent proliferation of melanoma cells. *Cell Cycle* **7**, 2392-2400 (2008).
90. Gao, P. *et al*. c-Myc suppression of miR-23a/b enhances mitochondrial glutaminase expression and glutamine metabolism. *Nature* **458**, 762-765 (2009).

91. Kim, JW. *et al.* Hypoxia-inducible factor 1 and dysregulated c-Myc cooperatively induce vascular endothelial growth factor and metabolic switches hexokinase 2 and pyruvate dehydrogenase kinase 1. *Mol Cell Biol.* **27**, 7381-7393 (2007).
92. Li, F. *et al.* Myc stimulates nuclearly encoded mitochondrial genes and mitochondrial biogenesis. *Mol Cell Biol.* **25**, 6225-6234 (2005).
93. Pylayeva-Gupta, Y., Grabocka, E. & Bar-Sagi, D. RAS oncogenes: weaving a tumorigenic web. *Nat Rev Cancer* **11**, 761-774 (2011).
94. Guo, JY. *et al.* Activated Ras requires autophagy to maintain oxidative metabolism and tumorigenesis. *Genes Dev.* **25**, 460-470 (2011).
95. Ying, H. *et al.* Oncogenic Kras maintains pancreatic tumors through regulation of anabolic glucose metabolism. *Cell* **149**, 656-670 (2012).
96. Davidson, SM. *et al.* Environment impacts the metabolic dependencies of Ras-driven non-small cell lung cancer. *Cell Metab.* **23**, 517-528 (2016).
97. Son, J. *et al.* Glutamine supports pancreatic cancer growth through a KRAS-regulated metabolic pathway. *Nature* **496**, 101-105 (2013).
98. Commisso, C. *et al.* Macropinocytosis of protein is an amino acid supply route in Ras-transformed cells. *Nature* **497**, 633-637 (2013).
99. Kruiswijk, F., Labuschagne, CF. & Vousden, KH. p53 in survival, death, and metabolic health: a lifeguard with a liscence to kill. *Nat Rev Mol Cell Biol.* **16**, 393-405 (2015).
100. Bensaad, K. *et al.* TIGAR, a p53-inducible regulator of glycolysis and apoptosis. *Cell* **126**, 107-120 (2006).
101. Matoba, S. *et al.* p53 regulates mitochondrial respiration. *Science* **312**, 1650-1653 (2006).
102. Chen, W. *et al.* Direct interaction between Nrf2 and p21 (Cip1/WAF1) upregulates the Nrf2-mediated antioxidant response. *Mol Cell* **34**, 663-673 (2009).
103. Mazurek, S, Boschek, CB, Hugo, F & Eigenbrodt, E. Pyruvate kinase type M2 and its role in tumor growth and spreading. *Semin Cancer Biol.* **15**, 300-308 (2005).
104. Ye, J. *et al*. Pyruvate kinase M2 promotes de novo serine synthesis to sustain mTORC1 activity and cell proliferation. *PNAS* **109**, 6904-6909 (2012).
105. Fang, M. *et al*. The ER UDPase ENTPD5 promotes protein N-glycosylation, the Warburg effect, and proliferation in the PTEN pathway. *Cell* **143**, 711-724 (2010).
106. Marshall, S., Bacote, V. & Traxinger, RR. Discovery of a metabolic pathway mediating glucose-induced desensitization of the glucose transport system. Role of hexosamine biosynthesis in the induction of insulin resistance. *J Biol Chem.* **266**, 4706-4612 (1991).
107. Yang, W. *et al*. ERK1/2-dependent phosphorylation and nuclear translocation of PKM2 promotes the Warburg effect. *Nat Cell Biol.* **14**, 1295-1304 (2012).
108. David, CJ. *et al.* HnRNP proteins controlled by c-Myc deregulate pyruvate kinase mRNA splicing in cancer. *Nature* **463**, 364-368 (2010).
109. Lunt, SJ., Chaudary, N. & Hill, RP. The tumor microenvironment and metastatic disease. *Clin Exp Metastasis* **26**, 19-34 (2009).
110. Hensley, CT. *et al.* Metabolic heterogeneity in human lung tumors. *Cell* **64**, 681-694 (2016).

111. Vaupel, L. & Harrison, L. Tumor hypoxia: causative factors, compensatory mechanisms, and cellular response. *Oncologist* **9**, 4-9 (2004).
112. Zong, WX. & Thompson, CB. Necrotic death as a cell fate. *Genes Dev.* **20**, 1-15 (2006).
113. Semenza, GL. HIF-1: upstream and downstream of cancer metabolism. *Curr Opin Genet Dev.* **20**, 51-56 (2010).
114. Kaelin, WG Jr. The von Hippel-Lindau tumour suppressor protein: O2 sensing and cancer. *Nat Rev Cancer* **8**, 865-873 (2008).
115. Kaelin, WG Jr. & Ratcliffe, PJ. Oxygen sensing by metazoans: the central role of the HIF hydroxylase pathway. *Mol Cell* **30**, 393-402 (2008).
116. Bonen A. Lactate transporters (MCT proteins) in heart and skeletal muscles. *Med Sci Sports Exerc.* **32**, 778-789 (2000).
117. Chandel, NS., Budlinger, GR., Choe, SH. & Schumacker PT. Cellular respiration during hypoxia. Role of cytochrome oxidase as the oxygen sensor in hepatocytes. *J Biol Chem.* **272**, 18808-18816 (1997).
118. Le, A. *et al.* Tumorigenicity of hypoxic respiring cancer cells revealed by a hypoxia-cell cycle dual reporter. *PNAS* **111**, 12486-12491 (2014).
119. Schug, ZT. *et al*. Acetyl-CoA synthetase 2 promotes acetate utilization and maintains cancer cell growth under metabolic stress. *Cancer Cell* **27**, 57-71 (2015).
120. Finley, LW. *et al.* SIRT3 opposes reprogramming of cancer cell metabolism through HIF1a destabilization. *Cancer Cell* **19**, 416-428 (2011).
121. Bi, M. *et al*. ER stress-regulated translation increases tolerance to extreme hypoxia and promotes tumor growth. *EMBO J.* **24**, 3470-3481 (2005).
122. Fiegal, KM. *et al*. Prevalence of obesity among adults in the United States, 2005 to 2014. *JAMA* **315**, 2284-2291 (2016).
123. Wiseman, M. The second World Cancer Research Fund/American Institute for Cancer Research expert report. Food, nutrition, physical activity, and the prevention of cancer: a global perspective. *Proc Nutr Soc.* **67**, 253-256 (2008).
124. Pischon, T., Nothlings, U. & Boeing, H. Obesity and cancer. *Proc Nutr Soc.* **67**, 128-145 (2008).
125. Calle, EE. *et al.* Overweight, obesity, and mortality from cancer in a prospectively studied cohort of U.S. adults. *N Engl J Med.* **348**, 1625-1638 (2003).
126. Hosogai, N. *et al*. Adipose tissue hypoxia in obesity and its impact on adipocytokine dysregulation. *Diabetes* **56**, 901-911 (2007).
127. Chang, Q. *et al.* The IL-6/JAK/Stat3 feed-forward loop drives tumorignesis and metastasis. *Neoplasia* **15**, 848-862 (2013).
128. Park, J. & Scherer, PE. Adipocyte-derived endotrophin promotes malignant tumor progression. *J Clin Invest.* **122**, 4243-4256 (2012).
129. Park J., Morley, TS. & Scherer, PE. Inhibition of endotrophin, a cleavage product of collagen VI, confers cisplatin sensitivity to tumors. *EMBO Mol Med.* **5**, 935-948 (2013).
130. Chen, X. *et al.* XBP1 promotes triple-negative breast cancer by controlling the HIF1a pathway. *Nature* **508**, 103-107 (2014).
131. Giovannucci, E. *et al.* Diabetes and Cancer. *Diabetes Care* **33**, 1674-1685 (2010).

132. Gunter, MJ. *et al.* Breast cancer risk in metabolically healthy but overweight postmenopausal women. *Cancer Res* **75**, 270-274 (2015).
133. Carew, JS. & Huang, P. Mitochondrial defects in cancer. *Mol Cell* **1**, 9 (2002).
134. Chourasia, AH., Boland, ML. & Macleod, KF. Mitophagy and cancer. *Cancer Metab.* **26**, 4 (2015).
135. Arismendi-Morillo, G. Electron microscopy morphology of the mitochondrial network in human cancer. *Int J Biochem Cell Biol.* **41**, 2062-2068 (2009).
136. Griffiths, LM., Doudican, NA., Shadel, GS. & Doetsch, PW. Mitochondrial DNA oxidative damage and mutagenesis in *Saccharomyces cerevisiae*. *Methods Mol Biol.* **554**, 267-286 (2009).
137. Arismedi-Morillo, GJ. & Castellano-Ramirez, AV. Ultrastructural mitochondrial pathology in human astrocytic tumors: potentials implications pro-therapeutics strategies. *J Electron Microsc* **57**, 33-39 (2008).
138. Elliott, R. & Barnett, B. Ultrastructural observation of mitochondria in human breast carcinoma cells. *Microscopy and Microanalysis* **17**, 194-195 (2011).
139. Fry, M. & Green, DE. Cardiolipin requirement for electron transfer in complex I and II of the mitochondrial respiratory chain. *J Biol Chem.* **256**, 1874-1880 (1981).
140. Kiebish, M. *et al*. Cardiolipin and electron transport chain abnormalities in mouse brain tumor mitochondria: lipidomic evidence supporting the Warburg theory of cancer. *J Lipid Res*. **49**, 2545-2556 (2008).
141. Dalla Pozza, E. *et al*. Role of mitochondrial uncoupling protein 2 in cancer cell resistance to gemcitabine. *Biochim Biophys Acta*. **1823**, 1856-1863.
142. Samudio, I., Fiegl, M. & Andreeff, M. Mitochondrial uncoupling and the Warburg effect: molecular basis for the reprogramming of cancer cell metabolism. *Cancer Res.* **69**, 2163-2166 (2009).
143. Shada, AL. *et al.* Infrared thermography of cutaneous melanoma metastases. *J Surg Res.* **182**, e9-14 (2013).
144. Morais, R. *et al.* Tumor-forming ability in athymic mice of human cell lines devoid of mitochondrial DNA. *Cancer Res.* **54**, 3889-3896 (1994).
145. Cavalli, LR., Varella-Garcia, M. & Liang, BC. Diminished tumorigenic phenotype after depletion of mitochondrial DNA. *Cell Growth Differ.* **8**, 1189-1198 (1997).
146. Magda, D. *et al*. mtDNA depletion confers specific gene expression profiles in human cells grown in culture and in xenograft. *BMC Genomics* **9**, 521 (2008).
147. Chatterjee, A., Mambo, E. & Sidransky, D. Mitochondrial DBA mutations in human cancer. *Oncogene* **25**, 4663-4674 (2006).
148. Ishikawa, K. *et al*. ROS-generating mitochondrial DNA mutations can regulate tumor cell metastasis. *Science* **320**, 661-664 (2008).
149. He, X. *et al*. Suppression of mitochondrial complex I influences cell metastatic properties. *PLoS One* **8**, e61677 (2013).
150. Iommarini, L. *et al*. Different mtDNA mutations modify tumor progression in dependence of the degree of respiratory complex I impairment. *Hum Mol Genet.* **23**, 1453-1466 (2014).
151. Schlichtholz, B. *et al*. Enhanced citrate synthase activity in human pancreatic cancer. *Pancreas* **30**, 99-104 (2005).

152. Lin, CC. *et al.* Loss of the respiratory enzyme citrate synthase directly links the Warburg effect to tumor malignancy. *Sci Rep.* **2**, 785 (2012).
153. Bardella, C., Pollard, PJ. & Tomlinson, I. SDH mutations in cancer. *Biochim. Biophys. Acta.* **1807**, 1432-1443 (2011).
154. Kurelac, I., Romeo, G. & Gasparre, G. Mitochondrial metabolism and cancer. *Mitochondrion* **11**, 635-637 (2011).
155. Xiao, M. *et al*. Inhibition of a-KG-dependent histone and DNA demethlyases by fumarate and succinate that are accumulated in mutations of FH and SDH tumor suppressors. *Genes Dev.* **26**, 1326-1338 (2012).
156. Picaud, S. *et al*. Structural basis of fumarate hydratase deficiency. *J. Inherit. Metab. Dis.* **34**, 671-676 (2011).
157. Adam, J. *et al*. Renal cyst formation in Fh1-deficient mice is independent of the Hif/Phd pathway: roles for fumarate in KEAP1 succination and Nrf2 signaling. *Cancer Cell* **20**, 524-537 (2011).
158. Sullivan, LB. *et al.* The proto-oncometabolite fumarate binds glutathione to amplify ROS-dependent signaling. *Mol Cell* **51**, 236-248 (2013).
159. Gaude, E. & Frezza, C. Defects in mitochondrial metabolism and cancer. *Cancer & Metab.* **2**, 10 (2014).
160. Wallace, DC. Mitochondria and cancer. *Nat Rev Cancer* **12**, 685-698 (2012).
161. Farber, S. *et al*. Temporary remissions in acute leukemia in children produced by folic acid antagonist, 4-aminopteroyl-glutamic acid. *N Engl J Med.* **238**, 787-793 (1948).
162. Li, MC., Hertz, R. & Bergenstal, DM. Therapy of choriocarcinoma and related trophoblastic tumors with folic acid and purine antagonists. *N Engl J Med.* **259**, 66-74 (1958).
163. Abolmaali, SS., Tamaddon, AM. & Dinarvand, R. A review of therapeutic challenges and achievements of methotrexate delivery systems for treatment of cancer and rheumatoid arthritis. *Cancer Chemother Pharmacol.* **71**, 1115-1130 (2013).
164. Esteban, E., Casillas, M. & Cassinello, A. Pemetrexed in first-line treatment of non-small cell lung cancer. *Cancer Treat Rev.* **35**, 364-373 (2009).
165. Longley, DB., Harkin, DP. & Johnston, PG. 5-Fluorouracil: mechanisms of action and clinical strategies. *Nat Rev Cancer* **3**, 330-338 (2003).
166. Bolin, RW., Robinson, WA., Sutherland, J. & Hamman, RF. Busulfan versus hydroxyurea in long-term therapy of chronic myelogenous leukemia. *Cancer*, **50**, 1683-1686 (1982).
167. van Moorsel, CJ., Peters, GJ. & Pinedo, HM. Gemcitabine: future prospects of single-agent and combination studies. *Oncologist* **2**, 127-134 (1997).
168. Dwarakanath, BS. & Jain, V. Targeting glucose metabolism with 2-deoxy-D-glucose for improving cancer therapy. *Future Oncol.* **5**, 581-585 (2009).
169. Dwarakanath, BS. *et al.* Clinical studies for improving radiotherapy with 2-deoxy-D-glucose: present status and future prospects. *J Cancer Res Ther.* **5**, S21-26 (2009).
170. Ganapathy-Kanniappan, S. *et al*. 3-Bromopyruvate: a new targeted antiglycolytic agent and a promise for cancer therapy. *Curr Pharm Biotechnol.* **11**, 510-517 (2010).

171. Chen, Z., Zhang, H., Lu, W. & Huang, P. Role of mitochondria-associated hexokinase II in cancer cell death induced by 3-bromopyruvate. *Biochim Biophys Acta.* **1787**, 553-560 (2009).
172. Shoshan, MC. 3-Bromopyruvate: targets and outcomes. *J Bioenerg Biomembr.* **44**, 7-15 (2012).
173. Le, A. *et al*. Inhibition of lactate dehydrogenase A induces oxidative stress and inhibits tumor progression. *PNAS* **107**, 2037-2042 (2010).
174. Miranda-Gonclaves, V. *et al.* Monocarboxylate transporters (MCTs) in gliomas: expression and exploitation as therapeutic targets. *Neuro-Oncology* **15**, 172-188 (2013).
175. Murray, CM. *et al.* Monocarboxylate transporter MCT1 is a target for immunosuppression. *Nat Chem Biol.* **1**, 371-376 (2005).
176. Wang, JB. *et al.* Targeting mitochondrial glutaminase activity inhibits oncogenic transformation. *Cancer Cell* **18**, 207-219 (2010).
177. Xiang, Y. *et al*. Targeted inhibition of tumor-specific glutaminase diminishes cell-autonomous tumorigenesis. *J Clin Invest.* **125**, 2293-2306 (2015).
178. Thornburg, JM. *et al.*Targeting aspartate aminotransferase in breast cancer. *Breast Cancer Res.* **10**, R84 (2008).
179. Shelton, LM., Huysentruyt, LC. & Seyfried, TN. Glutamine targeting inhibits systemic metastasis in the VM-M3 murine tumor model. *Int J Cancer* **127**, 2478-2485 (2010).
180. Hatzivassilou, G. *et al*. ATP citrate lyase inhibition can suppress tumor cell growth. *Cancer Cell* **8**, 311-321 (2005).
181. Brusselmans, K., Vrolix, R., Verhoeven, G. & Swinnen, JY. Induction of cancer cell apoptosis by flavonoids is associated with their ability to inhibit fatty acid synthase activity. *J Biol. Chem.* **280**, 5636-5645 (2005).
182. Flavin, R., Peluso, S., Nguyen, PL. & Loda, M. Fatty acid synthease as a potential therapeutic target in cancer. *Future Oncol.* **6**, 551-562 (2010).
183. Patra, KC. & Hay, N. The pentose phosphate pathway and cancer. *Trends Biochem Sci.* **39**, 347-354 (2014).
184. Betof, AS., Dewhirst, MW. & Jones, LW. Effects and potential mechanisms of exercise training on cancer progression: a translational perspective. *Brain Behav Immun.* **30**, S75-87 (2013).
185. Byers, T. *et al*. Physical activity, biomarkers, and disease outcomes in cancer survivors: a systemic review. *J Natl Cancer Inst.* **104**, 815-840 (2012).
186. Zhu, Z. *et al*. Effects of energy restriction and wheel running on mammary carcinogenesis and host systemic factors in a rat model. *Cancer Prev Res.* **5**, 414-422 (2012).
187. Schmitz, KH., Ahmed, RL., Hannan, PJ. & Yee, D. Safety and efficacy of weight training in recent breast cancer survivors to alter body composition, insulin, and insulin-like growth factor axis proteins. *Cancer Epidemiol. Biomark. Prev*. **14**, 1672-1680 (2005).
188. Giganti, MG. *et al.* Physical exercise modulates the level of serum MMP-2 and MMP-9 in patients with breast cancer. *Oncol Lett.* **12**, 2119-2126 (2016).

189. Hockel, M., Schlenger, K., Knoop, C. & Vaupel, P. Oxygenation of the uterine cervix: evaluation by computerized O_2 tension measurements. *Cancer Res.* **51**, 6098-6102 (1991).
190. Hambrecht, R. *et al.* Effect of exercise on coronary endothelial function in patients with coronary artery disease. *N Engl. J Med.* **342**, 454-460 (2000).
191. Jones, LW. *et al.* Exercise modulation of the host-tumor interaction in an orthotopic model of murine prostate cancer. *J Appl Physiol.* **113**, 263-272 (2012).
192. Lee, C. *et al.* Fasting cycles retard growth of tumors and sensitize a range of cell types to chemotherapy. *Sci. Trans. Med.* **4**, 124-127 (2012).
193. Pallavi, R., Giorgio, M. & Pelicci, PG. Insights into the beneficial effect of caloric/dietary restriction for a healthy and prolonged life. *Front. Physiol.* **3**, 318 (2012).
194. Longo, VD. & Fontana, L. Calorie restriction and cancer prevention: metabolic and molecular mechanisms. *Trends Pharmacol. Sci.* **31**, 89-98 (2010).
195. Kalaany, NY. & Sabatini, DM. Tumors with PI3K activation are resistant to dietary restriction. *Nature* **458**, 725-731 (2012).
196. Laviano, A. *et al.* Beyond anorexia-cachexia. Nutrition and modulation of cancer patients' metabolism: supplementary, complementary or alternative anti-neoplastic therapy? *Eur. J. Pharmacol.* **668**, S87-90 (2011).
197. Tettweiler, G. *et al.* Starvation and oxidative stress resistance in Drosophila are mediated through eIF4E-binding protein, d4E-BP. *Genes Dev.* **19**, 1840-1843 (2005).
198. Shi, Y. *et al.* Starvation-induced activation of ATM/Chk2/p53 signaling sensitizes cancer cells to cisplatin. *BMC Cancer* **12**, 571 (2012).
199. Safdie, FM. *et al.* Fasting and cancer treatment in humans: a case report series. *Aging* **1**, 998-1007 (2009).
200. Groesbeck, DK., Bluml, RM. & Kossoff, EH. Long-term use of the ketogenic diet in the treatment of epilepsy. *Dev. Med. Child Neurol.* **48**, 978-981 (2006).
201. Zhao, Z. *et al*. A ketogenic diet as a potential novel therapeutic intervention in amyotrophic lateral sclerosis. *BMC Neuroscience* **7**, 29 (2006).
202. Paoli, A. Rubini, A, Volek, JS. & Grimaldi, KA. Beyond weight loss: a review of the therapeutic uses of very-low-carbohydrate (ketogenic) diets. *Eur. J. Clin. Nutr.* **67**, 789-796 (2013).
203. Allen, BG. *et al.* Ketogenic diets as an adjuvant cancer therapy: History and potential mechanisms. *Redox Biol.* **2**, 963-970 (2014).
204. Mukherjee, P. *et al*. Energy intake and prostate tumor growth, angiogenesis, and vascular endothelial growth factor expression. *J. Natl Cancer Inst.* **91**, 512-523 (1999).
205. Poff, AM., Ari, C., Seyfried, TN. & D'Agostino, DP. The ketogenic diet and hyperbaric oxygen therapy prolong survival in mice with systemic metastatic cancer. *PLoS One* **8**, e65522 (2013).
206. Shimazu, T. *et al*. Suppression of oxidative stress by B-hydroxybutyrate, an endogenous histone deacetlyase inhibitor. *Science* **339**, 211-214 (2013).
207. Youm, YH. *et al.* The ketone metabolite B-hydroxybutyrate blocks NLRP3 inflammasome-mediated inflammatory disease. *Nat Med.* **21**, 263-269 (2015).

208. Seyfried, TN. *et al.* Metabolic therapy: a new paradigm for managing malignant brain cancer. *Cancer Lett.* **356**, 289-300 (2015).
209. Kesl, SL. *et al.* Effects of exogenous ketone supplementation on blood ketone, glucose, triglyceride, and lipoprotein levels in Sprague-Dawley rats. *Nutr. Metab.* **13**, 9 (2016).
210. Poff, AM. *et al.* Ketone supplementation decreases tumor cell viability and prolongs survival of mice with metastatic cancer. *Int. J. Cancer* **135**, 1711-1720 (2014).
211. Blot, WJ. *et al.* Nutrition intervention trials in Linxian, China: supplementation with specific vitamin/mineral combinations, cancer incidence, and disease-specific mortality in the general population. *J Natl Cancer Inst.* **85**, 1483-1492 (1993).
212. The Alpha-Tocopherol Beta Carotene Cancer Prevention Study Group. The effect of vitamin E and beta catotene on the incidence of lung cancer and other cancers in male smokers. *N. Engl. J. Med.* **330**, 1029-1035 (1994).
213. Omenn, GS. *et al.* Effects of combination of beta carotene and vitamin A on lung cancer and cardiovascular disease. *N. Engl. J. Med.* **334**, 1150-1155 (1996).
214. Klein, EA. *et al.* Vitamin E and the risk of prostate cancer: the Selenium and Vitamin E Cancer Prevention Trial (SELECT). *JAMA* **306**, 1549-1556 (2011).
215. Gorrini, C., Harris, IS. & Mak, TW. Modulation of oxidative stress as an anticancer strategy. *Nat Rev Drug Disc.* **12**, 931-947 (2013).
216. Chen, Z. *et al.* Nuclear translocation of B-cell specific transcription factor, BACH2, modulates ROS mediated cytotoxic responses in mantle cell lymphoma. *PLoS ONE* **8**, e69126 (2013).
217. Vaeteewoottacham, K. *et al.* Perturbation of proteasome function by bortezomib leading to ER stress-induced apoptotic cell death in cholangiocarcinoma. *J. Cancer Res Clin Oncol.* **139**, 1551-1562 (2013).
218. Takenokuchi, M., Miyamoto, K., Saigo, K. & Taniguchi, T. Bortezomib causes ER stress-related death of Acute Promyelocytic Leukemia cells through excessive accumulation of PML-RARA. *Anticancer Res.* **35**, 3307-3316 (2015).
219. Lo, M. *et al*. Potential use of the anti-inflammatory drug, sulfasalazine, for targeted therapy of pancreatic cancer. *Curr. Oncol.* **17**, 9-16 (2010).
220. Guan, J. *et al*. The xc-cystine/glutamate antiporter as a potential therapeutic target for small-cell lung cancer: use of sulfasalazine. *Cancer Chemother. Pharmacol.* **64**, 463-472 (2009).
221. Sobhakumari, A. *et al.* Susceptibility of human head and neck cancer cells to combined inhibition of glutathione and thioredoxin metabolism. *PLoS ONE* **7**, 48175 (2012).
222. Belfi, CA. *et al.* Increased sensitivity of human colon cancer cells to DNA cross-linking agents after GRP78 up-regulation. *Biochem. Biophys. Res. Commun.* **257**, 361-368 (1999).

CHAPTER 2: GLIOMA AS A TARGET FOR METABOLIC CANCER THERAPY

2.1 Chapter Synopsis

This chapter serves to address the characteristics of malignant brain cancers that suggest that these tumors may be responsive to metabolic therapies. The VM-M3 mouse model of glioblastoma is discussed as an appropriate model for evaluating the efficacy of metabolic therapies. Lastly, we introduce dichloroacetate and metformin as a potential metabolic therapy for gliomas and discuss the central hypothesis and project aims for this dissertation.

2.2 Glioma Biology

Glioma is a collective term for brain cancers arising from cells of glial origin. Though gliomas account for only about a third of all central nervous system (CNS) tumors, they represent for the majority of malignant brain cancers (1). The detection and diagnosis of glioma is often delayed due to initial asymptomatic tumor initiation and growth. Detection often occurs upon presentation of neurological symptoms such as headache, depression, motor function deficits, hearing and vision loss, and the onset of seizures (2). These occur as a result of physiological stresses imposed by the growing tumor. The standard of care for glioma employs debulking surgery when feasible, followed by concurrent radiation and chemotherapy (3). Gliomas present distinct

morphologies and pathologies that have led to classification at the histological and morphological level. The robust effort in elucidating the process of gliomagenesis has identified several molecular hallmarks of gliomas that implicate metabolism as a potential driver of tumor progression (4).

2.2.1 Clinical Characteristics

Primary glioma nomenclature is dependent on the cell of origin. There are three glial cell types that yield tumors; astrocytes (astrocytomas), oligodendrocytes (oligodendrogliomas), and ependymal cells (ependymomas). There are also tumors that are composed of multiple glial cells in high proportion; the most common of these mixed gliomas are oligoastrocytomas (5). The World Health Organization (WHO) has developed a classification system for glioma diagnosis based on both phenotypic and genotypic characteristics. Gliomas are assigned a grade from I-IV based on the perceived aggressiveness of the tumor (6). As such, tumors of higher grades are more aggressive and are associated with a poorer prognosis. Low-grade gliomas are common in children, whereas high-grade gliomas are more frequent in adults.

Astrocytic gliomas span the complete range of WHO tumor grades. Pilocytic astrocytomas are juvenile grade I tumors that are distinct from other astrocytomas in that they are fully circumscribed and thus do not spread from the area of tumor initiation. The diffuse astrocytic gliomas (WHO grades II-IV) infiltrate the surrounding tissue. Low-grade diffuse astrocytomas (WHO grade II) are slow growing tumors that display moderate cellularity and no anaplasia. Anaplastic astrocytomas (WHO grade III) exhibit rapid growth and a high degree of dedifferentiation. The most aggressive astrocytic

tumor is glioblastoma multiforme (GBM; WHO grade IV), which in addition to rapid growth and anaplasia, also present with microvascularization of the bulk tumor and regions of necrosis. GBMs can be further typified as either primary, which are de novo tumors, or secondary, which progress from an established lower-grade tumor (7).

Oligodendrogliomas (WHO grades II or III) are also classified as diffuse gliomas and are differentiated based on the presence of anaplastic growth. Ependymomas are difficult to classify based on WHO recommendations but fall within grades I-III (5). The most recent WHO classification guidelines discourage against the diagnosis of oligoastrocytomas, as recent studies have identified molecular markers that can differentiate if a mixed glioma more closely resembles an astrocytoma or oligodendroglioma (6).

Gliomas can arise throughout the brain and spinal cord region of the CNS. Astrocytes are a ubiquitous constituent of the CNS and thus astrocytic tumors are frequently found in the brainstem, cerebellum, cerebrum and spinal cord (8). Whereas, oligodendrogliomas are most typically found in the frontal and temporal lobes of the cerebrum (9). Ependymal cells associate with the ventricles of the brain and the spinal cord, which is determinant for the location of ependymoma formation (10).

Gliomas account for 80% of malignant brain tumors despite only representing 27% of total CNS tumors. The most common malignant brain tumor is GBM, which account for ~46% of total malignant tumors with an incidence rate of 3.20 per 100,000 people in the United States (US) (1). The less aggressive diffuse astrocytomas are the second most common brain malignancies. Malignant gliomas are more prevalent in males than females and are also more common in Caucasian individuals than non-

whites (1). Moreover, the familial risk for individuals with a family history of glioma is twice that of individuals without previously reported familial incidence (11). The median age at diagnosis for GBM is 65, whereas the age at diagnosis for other gliomas tends to be 10-15 years younger. The prognosis for glioma patients is negatively correlated with age at diagnosis (12).

The focal nature of pilocytic astrocytomas typically allows for near-total resection of the tumor and is associated with a 10-year survival rate of 92.1%. The prognosis for low-grade and anaplastic astrocytomas is considerably worse, as only 47.9% and 27.9% of patients achieve 5-year survival, respectively. GBM patients face the grimmest prognosis, as only 5.1% of patients achieve 5-year survival post-diagnosis. Moreover, median survival for patients receiving radiation alone after debulking surgery is 12.1 months, whereas the addition of concurrent temozolomide (TMZ) chemotherapy only increases median survival to 14.6 months (3, 12).

Though diffuse gliomas display an exquisite propensity for invasion, marked by the extensive spread of tumor cells throughout the brain, extracranial metastasis is rare in malignant glioma (13). For instance, extracranial metastases are present in only ~0.5% of GBM cases, and the median survival of these patients is only 10.2 months (3, 14). It has been proposed that GBM metastasis from the brain is hindered by a lack of a disseminating lymphatic system in the brain, poor intravasation of intracranial vasculature due to the presence of dense dura, and that glioma cells find the microenvironment of extracranial tissue incompatible for metastases formation (13). However, GBM metastasis to bone, liver, and lung is consistently reported, suggesting that these tissues provide a sufficient niche for metastatic tumor formation (14, 15).

Rather, it is likely that the infrequency of extracranial metastasis is in part a result of the rapid mortality associated with the disease. This restricts the time for metastases formation and detection, as the average survival from time of metastases detection is only 1.5 months (13).

2.2.2 Molecular Pathology

Traditional glioma diagnosis has been dependent on histological and pathological markers that allow for the identification of a specific tumor species. For instance, GBM diagnosis has depended in part on the presence of glial fibrillary acid protein (GFAP), which is determined through histological staining (16). However, the integration of techniques that permit study of the underlying molecular changes in tumorigenesis have identified specific genetic and transcriptional characteristics of gliomas that allows for more discrete diagnosis.

Large-scale risk analyses and analysis of single nucleotide polymorphisms (SNPs) in adult gliomas has identified a possible link between childhood immunogenic events and glioma incidence. There is an apparent inverse association between childhood chicken pox incidence and glioma incidence as an adult, as the presence of IgG antibodies against the varicella-zoster virus is inversely correlated with glioma formation (17-19). Moreover, SNPs in genes associated with asthma, such as the interleukin-13 (IL-13) SNP C1112T CT, TT are inversely associated with GBM incidence (20).

Further studies have identified several glioma-associated SNPs in genes that participate in DNA repair and cell cycle regulation, both of which are dysregulated in

cancer. Variants in the excision repair cross-complementing genes ERCC1 and ERCC2, which code for the DNA excision repair proteins ERCC-1 and ERCC-2, respectively, have been found in oligodendrogliomas (21, 22). SNPs in O-6-methylguanine-DNA methyltransferase (MGMT) have also been implicated in glioma formation (23). Moreover, MGMT is often deleted or repressed in GBM, which actually confers susceptibility to the alkylating activity of TMZ and results in greater response to treatment (24). Variants of SNP309 in the promoter region of the mouse double minute 2 homolog (MDM2) gene have been implicated with astrocytoma formation in patients with Li-Fraumeni syndrome (25). MDM2 codes for an E3-ubiquitin ligase that is a negative regulator of p53 and facilitates cell cycle progression.

Additional genetic alterations in genes coding for p53 and retinoblastoma protein (Rb), another negative regulator of the cell cycle, result in the dysregulation of the cell cycle in gliomas. Several studies have demonstrated that the loss of either facilitates glioma formation in various mouse models (26, 27). Inactivating mutations in p53 are frequent in low-grade astrocytomas as well as secondary GBMs (28). Inactivation of Rb or the upregulation of its negative regulator cyclin-dependent kinase 4 (CDK4) are frequently reported in high-grade astrocytomas or oligodendrogliomas (29, 30). For instance, a study associated with the cancer genomes atlas (TCGA) project showed that of 91 secondary GBMs p53 and Rb were dysregulated in 87% and 78% of cases, respectively (31). Moreover, Rb is shown to be a target of the microRNA miR-26a, which is overexpressed in 12% of GBMs and is implicated in gliomagenesis through this repression of Rb (32).

Aberrant receptor tyrosine kinase signaling is another molecular hallmark of gliomas. In fact, the majority of GBM cell lines exhibit coactivation of at least 3 RTKs (33). The most common RTK alteration in glioma is epidermal growth factor receptor (EGFR) amplification, which was shown in two separate studies to be present in 36% of analyzed samples (23, 34). EGFR amplification is most prevalent in primary GBMs (1). Moreover, heterogeneous expression of distinct oncogenic variants of EGFR are present within single tumors. The most common mutational variant is EGFR vIII, which lacks a portion of the extracellular binding domain and is implicated in the enhanced response of certain GBMs to the EGFR inhibitor erlotinib (35).

Enhanced platelet derived growth factor receptor (PDGFR) signaling is common to low-grade astrocytomas and oligodendrogliomas (36, 37). This is resultant from enhanced expression of both PDGFR and its ligand PDGFβ, permitting autocrine and paracrine activation of the receptor within tumors (38). The enhanced activation of these RTKs stimulates signaling through the Ras-MAPK and PI3K-Akt-mTORC1 axises, which are shown to be constitutively activated in about 90% of GBMs (31). The aberrant signaling through both pathways is also mediated through PTEN loss, which is shown to be present in 36% of GBMs (31). These pathways drive tumor growth and are required for gliomagenesis (38).

Another common alteration in gliomas is the missense mutation of IDH1 at R132. This arginine residue resides in the active site of IDH1 and mutations of this residue result in the loss of H^+-bonding with isocitrate and promotes gain of function catalysis of α-KG to 2-HG (39). IDH1 mutations are present at very high proportions of grade II/III astrocytomas and oligodendrogliomas as well as secondary GBMs, but are rare in

primary GBMs (40). Consistently, IDH mutations appear to mutually exclusive with the amplification of EGFR (39). IDH1 mutant tumors tend to occur in patients that are nearly 20 years younger than those with wild type IDH1 tumors; this corresponds with a three-fold greater survival for patients with mutant IDH1 (41).

Similar to other tumor species, gliomas harbor a small population of cells that exhibit stem-like properties that have been implicated in tumor initiation and chemoresistance (42). Glioma stem cells (GSCs) often express the neural stem cell marker cluster of differentiation 133 (CD133). $CD133^{+}$ GSCs are shown to secrete vascular endothelial growth factor (VEGF), which likely contributes the high vascularity of GBMs (43, 44). Moreover, GSCs display an ability to transdifferentiate into endothelial cells and pericytes further enhancing vessel deposition. The depletion of endothelial cells restricted GBM xenograft growth in mice, suggesting that GSC-mediated vascularization is essential to tumor growth (45). GSC stemness is suggested to be a result of the increased Akt activity associated with gliomagenesis (46).

Collectively, the identification of these common molecular hallmarks and genetic alterations have provided for sub-classification of GBMs. Phillips *et al.* proposed that GBMs can be classified into three categories: proneural, proliferative, or mesenchymal (47). Under their parameters, proneural tumors display intact PTEN and normal EGFR expression. These tumors are more common in younger individuals, which corresponds with increased survival. Proliferative tumors show loss of PTEN, Akt activation and amplification of EGFR. Mesenchymal tumors are also marked by loss of PTEN, activation of Akt and EGFR amplification. These tumors also display increased CD44 and VEGF expression, which corresponds with increased vascularization (47, 48).

Verhaak *et al.* have subsequently provided rationale for a classification system with four distinct categories (49). They too propose proneural and mesenchymal classes of GBM, but also present evidence for the presence of classical and neural GBMs. Their proneural classification was based on a high frequency of PDGFRα and IDH1 mutations. Mesenchymal tumors exhibited increased expression of CD44 and chitinase-3-like protein 1 (YKL-40), which stimulates angiogenesis and astrocyte migration. Classical GBMs were marked by EGFR amplification and neural tumors showed increased expression of several neuron markers, such as the neurofilament light polypeptide (NEFL) and synaptotagmin 1 (SYT1) (49). These classification systems may serve to inform individualized GBM therapy, in hopes of improving the prognosis of the deadly disease.

2.2.3 Metabolism

The molecular factors that influence gliomagenesis are implicated in many of the metabolic dependencies exhibited by tumors. EGFR amplification and loss of p53 contribute to the highly glycolytic nature of gliomas. Enhanced EGFR signaling induces HK2 expression in GBM; increased HK2 expression is negatively correlated with patient survival (50). EGFR is also shown to stimulate NF-κB induction of HIF-1α activity in glioma. This is associated with increased PKM2 expression and nuclear translocation (51, 52). HIF-1α is likely a critical driver of glycolytic metabolism in mutant IDH1 gliomas. The reductive carboxylation of α-KG to 2-HG restricts α-KG availability. This inhibits α-KG-dependent enzymes such as PDHs, permitting accumulation of HIF-1α. HIF1 activity is responsible for increased PDKII expression in glioma (53). The glycolytic

capacity of astrocytomas is evidenced by FDG-PET imaging. Tumor grade can be predicted based on ^{18}F-deoxyglucose (^{18}FDG) uptake; GBMs show enhanced ^{18}FDG uptake compared to low-grade astrocytomas (54). Furthermore, gliomas are susceptible to MCT1 inhibition by α-cyano-4-hydroxycinnamate, which inhibits tumor growth and potentiates TMZ efficacy (55).

Glioma cells in culture exhibit robust glutamine metabolism that permits growth in the absence of glucose (56). Moreover, glutamine levels in the brain of GBM patients is shown to be significantly higher than that of normal brain (57). However, glutamine metabolism may not be as prevalent in vivo. Marin-Valencia *et al*. utilized ^{13}C-glucose tracing to demonstrate glucose-dependent TCA cycle anaplerosis as well as the synthesis of glutamine from glucose carbon in an orthotopic model of high-grade glioma (58). This is consistent with the observation that decreased glutamine synthetase (GSN) expression is associated with increased GBM patient survival (59).

GBM tumors also exhibit increased levels of unsaturated fatty acids compared to normal brain (60). EGFR stimulation of Akt activates sterol regulatory element-binding protein-1 (SREBP-1), promoting its nuclear translocation where it activates the transcription of ACC and FASN, which facilitate fatty acid synthesis (61). SREBP-1 also induces low-density lipoprotein receptor (LDLR) expression, facilitating enhanced exogenous lipid uptake in gliomas (62). SREBP-1 is also activated as a consequence of increased glycolytic metabolism. Increased flux through the hexosamine pathway cooperates with enhanced expression of O-linked-N-aceytlglucosaminyltransferase (OGT) to promote O-glycosylation (63). SREBP-1 is activated by OGT-mediated glycosylation and this increases with increasing tumor grade (64). Certain GBM cells

require fatty acid oxidation to maintain cytosolic NADPH levels in order to mitigate oxidative stress (65). Alternatively, analysis of patient GBMs showed a reliance on acetate oxidation to sustain acetyl-CoA levels for fatty acid synthesis and NADPH production (66).

Mitochondrial abnormalities are frequent in gliomas (67). Glioma mitochondria are characteristically hyperpolarized and this is most evident in $CD133^+$ GSCs, likely enhancing their chemoresistance (68). Glioma mitochondria are also shown to exhibit swelling and partial or total cristolysis (69). Yet mitochondrial metabolism is still required to maintain glioma integrity. Mitochondrial SHMT2 and glycine decarboxylase (GLDC) activity is required to prevent toxic accumulation of glycine during hypoxic conditions. This is particularly evident in pseudopalisading cells that border necrotic foci, which are a pathological hallmark of GBM (70).

The establishment of non-targeted metabolomics has permitted large-scale studies of glioma metabolism in patients. Chinnaiyan *et al*. established and analyzed the metabolomic profile of 69 glioma samples that included tumors of WHO grades II-IV (71). They noted that high-grade gliomas exhibited a distinct anabolic phenotype that corresponded with rewiring of glycolytic flux. This was evidenced by accumulation of 3-phosphoglycerate (3-PG), serine, and glycine suggestive of increased flux through the serine biosynthesis pathway. Additionally, GBMs had increased ribose-5-phosphate (R5P) and GSH, which indicates enhanced PPP activity. This was mediated through increased PKM2 expression in these tumors, which was associated with accumulation of PEP. This was particularly evident in mesenchymal GBMs. Moreover, this group was able to differentiate between low-grade and high-grade gliomas based on the level of 2-

HG present in the tumor, which corresponds with IDH1 mutant status and is again a characteristic of low-grade gliomas (39, 40, 71).

Subsequently, Zhao *et al*. analyzed 87 plasma samples from glioma patients to determine circulating metabolite profiles (72). They achieved >90% success in classifying patients with respect to grade and IDH1 status based on metabolomic profile. Circulating arginine levels were decreased in patients with high-grade glioma, which was suggested to be a result of increased demand as arginine metabolism is enhanced in GBMs and increases invasiveness (73). Serum lactate levels were also elevated in patients with high-grade gliomas, likely associated with the robust glycolytic metabolism of GBMs. Creatine metabolism distinguished mutant and wild-type IDH1 tumors. A reduction in creatine synthesis intermediates and an increase in the creatinine metabolite sarcosine were observed in the plasma of patients with mutant IDH1 tumors. Creatine levels have previously been reported to be low in high-grade gliomas, which typically harbor wild-type IDH1 (74). Interestingly, circulating 2-HG levels could not differentiate between wild-type and mutant IDH1 tumors, suggesting that 2-HG can accumulate within gliomas as was reported in the previous study. These studies can serve to provide new therapeutic targets as well as inform personalized metabolic therapy based on the metabolic dependencies of a particular patient's tumor.

2.3 The VM-M3 Model of Metastatic Glioblastoma Multiforme (GBM)

Though infrequently reported, metastasis worsens the already dire prognosis associated with GBM. Metastasis is associated with 90% of all cancer-related deaths, a direct consequence of the lack of current therapeutic efficacy towards metastatic

disease (75). A mitigating factor in the development of therapies that can effectively prevent metastasis or target the systemically disseminated tumor cells is a lack of appropriate pre-clinical models. The syngeneic VM-M3 model, which was developed by Dr. Thomas Seyfried, is derived from a spontaneous brain tumor in the VM/dk inbred strain of mice and mimics the metastatic cascade exhibited by human metastases (76, 77). VM/dk mice display an increased incidence rate of spontaneous brain tumors, which typically resemble astrocytomas (78). The original M3 tumor was adapted to cell culture to yield the VM-M3 cell line. These VM-M3 cells were transduced with a lentiviral vector containing a firefly luciferase transgene, which permits non-invasive in vivo imaging. Luciferase catalyzes the oxidation of luciferin to oxyluciferin through which light is generated. This bioluminescence can be detected and quantified to as a representation of tumor burden.

Orthotopic transplantation of VM-M3 cells into the brain of immunocompetent VM/dk mice results in the formation of a primary tumor that exhibits aggressive GBM pathology. These tumors are extraordinarily invasive, generating secondary tumors throughout the brain parenchyma of both the ipsilateral and contralateral hemispheres of transplantation. Moreover, VM-M3 cells are shown to migrate in a perivascular fashion as well as along white matter tracts, which is characteristic of GBM (79). Orthotopic transplantation is also accompanied by extracranial metastasis throughout the animal. Furthermore, subcutaneous transplantation of VM-M3 cells into the visceral fat pad of VM/dk mice results in systemic metastasis to the brain, liver, lungs, kidneys and spleen.

Though VM-M3 tumors present pathologically as GBMs, VM-M3 cells exhibit characteristics of microglia, the resident macrophages on the brain. These cells are shown to be phagocytic, a fundamental characteristic of macrophages (80). VM-M3 cells express ionized calcium-binding adaptor molecule 1 (Iba1), which is an established cell surface marker of microglia. Moreover, VM-M3 cells show expression of the macrophage markers, CD11b, CD45, CD68, and EGF-like module-containing muncin-like hormone receptor 1 (EMR1, also known as F4/80). These cell surface proteins are implicated in cell migration, cell-cell interactions and immunomodulation (81-83). For instance, CD45 disrupts antigen receptor signaling in lymphocytes and F4/80 facilitates interactions with T-cells and promotes their differentiation to Tregs (82, 83). Together these factors likely promote an immunosuppressive tumor microenvironment. VM-M3 tumors do not stain positive for the astrocyte marker GFAP, which is also generally associated with astrocytomas. However, GFAP expression is not universal in mature astrocytes and is very often absent in primary cultures of adult human brain tissue (84).

The confluence of these characteristics may suggest that VM-M3 tumors may closely resemble another class of brain tumor, such as microglioma, which is more commonly referred to as primary central nervous system lymphoma (PCNSL). PCNSLs are Non-Hodgkin lymphomas of the CNS derived from B cells. These tumors also contain an infiltrating population of $CD3^{+}$-T Cells. VM-M3 cells are negative for CD3 as well as the pan-B cell marker CD19, which is present in up to 98% of PCNSLs, suggesting that VM-M3 tumors are not PCNSLs (85, 86). Rather, VM-M3 behavior agrees with the observation that metastatic cells often resemble macrophages and that fusion events occur between macrophages and neoplastic cells (87-89). Huse and

Holland propose that gliomas incorporate a substantial number of non-neoplastic cells that become transformed in the tumor microenvironment and thus contribute to the proliferating tumor mass and influence disease progression (38). Microglia/macrophages would very likely be co-opted through this process as macrophages are very prominent components of the tumor microenvironment.

Glioma-associated macrophages (GAMs) can constitute up to 30% of the total tumor mass (90). Upon activation, macrophages undergo immunogenic polarization towards either a pro-inflammatory M1 or anti-inflammatory M2 phenotype. GAMs tend to present the M2 phenotype, which contributes to the immunosuppressive tumor microenvironment (91). Moreover, GAMs are shown to promote local invasion through degradation of the ECM (92). Consistent with the observation that mesenchymal GBMs display enhanced invasive capacity, increased GAM density is associated with this subclass of GBM (93). Thus it is likely that GAM activity contributes to the shorter median survival seen in patients with mesenchymal GBMs.

VM-M3 cell metabolism is distinctly reflective of highly glycolytic nature of GBM. Still, these cells exhibit a 2-fold preference for glucose carbon over that provided by glutamine for lipid biosynthesis suggesting that mitochondrial glucose metabolism is employed to generate the citrate required for fatty acid synthesis (94). However, consistent with the literature, glutamine metabolism increases under hypoxic conditions to combat the energetic stress (95). Moreover, VM-M3 cells synthesize triacylglycerols (TAGs) under hypoxia, likely to prevent toxic accumulation of free fatty acids such as palmitate, which is shown to induce apoptosis (94, 97). Glutamine metabolism also appears to be required for VM-M3 durability in vivo, as pharmacological inhibition of

GLS blunted tumor growth and inhibited metastasis (94). Though VM-M3 cells can withstand the stress imposed by hypoxia, they are shown to be susceptible to glucose restriction. Therapeutic implementation of the ketogenic diet with or without caloric restriction significantly prolongs and blunts metastasis in VM-M3 burdened mice (97, 98). This suggests potential utility for the VM-M3 model in screening potential cancer therapies that modulate glucose metabolism.

2.4 Dichloroacetate (DCA) and Metformin as a Therapeutic Combination for GBM

The highly glycolytic nature of gliomas suggests that they would be susceptible to perturbations in flux through glycolysis and its subsidiary pathways. However, glycolytic inhibitors have largely been ineffective in managing the disease due to drug resistance and toxicity in targeting the ubiquitous pathway. Rather than inhibiting glycolysis, the activation of mitochondrial glucose oxidation provides an alternative to rewiring glycolytic flux. As the PDH complex is the critical regulator of oxidative glucose metabolism, it provides a potential therapeutic target for altering cancer metabolism.

2.4.1 Dichloroacetate

Most cells within the body are fully differentiated and do not proliferate. These cells employ oxidative glucose metabolism to generate the ATP to maintain cellular homeostasis. This requires the full activation of the PDH complex to facilitate optimum incorporation of pyruvate carbon into the TCA cycle. The PDH complex is subject to allosteric and post translational modification-dependent regulation, the most important of which is phosphorylation of PDH. Inhibitory phosphorylation of PDH is mediated by

PDK and is removed by pyruvate dehydrogenase phosphatase (PDP). As discussed above, PDK expression is enhanced in cancer as a result of aberrant signaling. Increased PDK activity enhances Warburg metabolism and contributes to chemoresistance (53). The small-molecule pyruvate mimetic, dichloroacetate (DCA) is shown to inhibit PDK activity and is under investigation as a potential modulator of cancer metabolism. Accumulating evidence suggests that GBM may be particularly sensitive to DCA treatment (68, 99).

2.4.1.1 Mechanism of Action

The PDH complex is composed of three multi-protein enzymatic subunits localized within the mitochondrial matrix. PDH (E1 subunit) requires vitamin B_1 and lipoic acid to catalyze the rate-limiting decarboxylation of pyruvate to generate CO_2 and an acyl-lipoate molecule. Dihydrolipoyl transacetylase (E2 subunit) transfers the acetyl group from the lipoate moiety to coenzyme A (CoASH), generating acetyl-CoA and reduced lipoate. Finally, dihydrolipoyl dehydrogenase (E3 subunit) oxidizes lipoate to regenerate lipoic acid. $FADH_2$ is generated in the process and this is subsequently oxidized back to FAD^+ in a reaction coupled to the generation of NADH (100).

Excessive sustained activity will result in abundant NADH and acetyl-CoA production, both of which are negative allosteric regulators of the PDH complex. Moreover, induction of PDKs promotes phosphorylation of the E1α subunit at a series of serine residues (S232, S293, S300) that renders PDH inactive (101). PDK itself is subject to allosteric regulation as increases in the ATP/ADP as a result of excessive oxidative phosphorylation stimulate its kinase activity. Furthermore, increases in the

acetyl-CoA/CoASH and NADH/NAD^+ ratios stimulate PDK activity. Conversely, accumulation of pyruvate, NAD^+ and CoASH inhibit PDK (102). PDK is also subject to regulatory tyrosine phosphorylation (103). Fibroblast growth factor receptor, which is upregulated in cancer, exhibits promiscuous activating phosphorylation of PDK1. Additionally, aberrant stimulation of Ras signaling induces phosphoglycerate kinase translocation to the mitochondria, where it activates PDK (104).

DCA is a dichloronated organic acid that is structurally similar to pyruvate and mimics its inhibitory effects on PDK activity. Co-crystallization of DCA and PDK shows that DCA occupies the pyruvate binding site on the N-terminal regulatory domain of PDK (105). PDK sensitivity to DCA is isoform dependent; PDK2 (K_i = 200uM) is the most sensitive and PDK4 is the most resistant (K_i = 8mM) (106). DCA inhibition of PDK results in the activation of the PDH complex, increased glucose oxidation and a reduction in lactate production (107). As such, DCA reduces circulating lactate levels and is employed clinically in disorders associated with lactic acidosis such as mitochondrial encephalomyopathy and lactic acid syndrome (MELAS) (101). Moreover, DCA increases PDH complex activity in PDH complex deficiency disorders, which results in mitigation of some of the chronic neurological symptoms associated with these diseases (101, 108).

DCA is dehalogenated and biotransformed to glyoxylate by glutathione transferase zeta 1 (GSTZ1). GSTZ1 also functions as maleylacetoacetate isomerase (MAAI), catalyzing the penultimate reaction of tyrosine catabolism. Prolonged DCA exposure leads to the accumulation of tyrosine and DCA due to inhibition of GSTZ1 (109). DCA is a common contaminant of the water supply and prolonged exposure to

concentrated DCA can result in hepatotoxicity and increases the risk for liver cancers (110). However, persistent therapeutic administration of DCA is well tolerated with minimal side effects and DCA maintains FDA orphan drug status that permits clinical evaluation of its potential anti-cancer activity (111).

2.4.1.2 Anti-Cancer Activity

DCA stimulation of glucose oxidation in cancer cells is associated with inhibition of Warburg metabolism. This is characterized by reductions in both glucose uptake and lactate export (112). Though lactate production is shown to be reduced by DCA in many instances, it is not universal across cancer species. In fact, DCA induced both LDH activity and MCT1 expression as a means to compensate for the stimulation of mitochondrial pyruvate metabolism in several pancreatic and colorectal cell lines (113). Lactate efflux was still reduced in these cells leading to an increase in intracellular pH. This was likely as a result of competitive inhibition of MCT1, which facilitates DCA uptake (113). Associated with the more common observation of reduced lactate production is an increase in the cellular NADH/NAD^+ ratio, which is a strict negative regulator of LDH activity (114).

As described previously, oxidative metabolism and the stimulation of the ETC is intrinsically linked with ROS production. Consistently, DCA is shown to induce oxidative stress in cancer cells as a result of increased electron leakage from the ETC (115). This oxidative stress is shown to be cytotoxic in the vast number of studies that have evaluated DCA in cancer (114-123). Bonnet *et al*. intricately linked DCA-stimulation of mitochondrial ROS with induction of cancer cell death (114). They show that DCA

stimulated mitochondrial $\cdot O_2^-$ dependent cytosolic accumulation of H_2O_2, which led to the oxidation of the plasma membrane-associated voltage-gated potassium (K^+) channel Kv1.5. This resulted in K^+ efflux and a reduction in intracellular K+ concentration $[K^+]_I$, releasing tonic inhibition of pro-apoptotic caspases (124). This was coupled with the depletion of $\Delta\Psi_m$ and loss of mitochondrial integrity. Thus culminating with the release of cytochrome c from the intermembrane space and the activation caspase-dependent apoptosis. The induction of oxidative stress and subsequent cell death was only seen in cancer cell lines. DCA displayed no cytotoxicity towards Immortalized, but non-transformed fibroblasts, smooth muscle and epithelial cells (114). This cancer-specific cytotoxicity has been consistently reported in subsequent studies (115, 120, 121). This DCA tolerance is a result of inherent reliance on glucose oxidation in most normal cells, characterized by basal flux through the PDH complex, rendering DCA ineffective in modulating their metabolism.

DCA cytotoxicity is concentration dependent (112, 114-116). At subcytotoxic concentrations, DCA inhibits cancer cell proliferation (114, 115, 117, 119, 120). This is likely mediated by a restriction of biosynthetic glucose metabolism resultant from increased oxidation. Moreover, DCA induces autophagy in colorectal tumor cells through inhibition of mTOR, which inhibits autophagy to prevent unnecessary accumulation amino acids (113). The autophagy pathway is responsive to changes in oxidative stress as mTOR is subject to direct and indirect inactivation as a result of protein oxidation (125).

As described previously, the rewiring of cancer cell metabolism has profound effects on the tumor microenvironment. DCA inhibition of lactate export results in an

increase in extracellular pH, which was associated with reduction in the expression of HIF targets such as GLUTs and MCT1 in a mouse model of Dalton's lymphoma (118). Moreover, DCA promoted infiltration of tumor associated macrophages (TAMs) and induced M1 polarization. This resulted in greater TAM tumoricidal activity, marked by increased NO production and release of the pro-inflammatory cytokines IL-1, IL-6 and tumor necrosis factor α (TNFα) (118). These modifications of the microenvironment would render a solid tumor less aggressive. As such, DCA is shown to promote leucocyte infiltration and reduce metastatic breast cancer growth (123).

The propensity for DCA to induce oxidative stress in cancer cells suggests that it may be an attractive adjuvant to conventional pro-oxidant chemotherapies. Indeed, DCA is shown to potentiate the efficacy of several chemotherapies through exacerbation of oxidative stress (112, 115-119, 123). The hyperpolarization of cancer mitochondria as a result of Warburg metabolism contributes to therapeutic resistance through inhibition of apoptosis. DCA reverses hepatocellular carcinoma resistance to the RTK inhibitor sorafenib through reduction of $\Delta\Psi_m$ (119). Moreover, DCA sensitized radiation-resistant prostate cancer cells to irradiation through reversal of IMM hyperpolarization (126). Furthermore, DCA treatment reversed hypoxia-mediated chemoresistance to 5-FU and bevacizumab in models of gastric cancer and GBM, respectively (116, 117). Importantly, the use of glycolytic inhibitors was insufficient to reverse resistance, highlighting the necessity of activating mitochondrial glucose metabolism in overcoming the protective effects of enhanced glycolytic flux.

2.4.1.3 Clinical Implementation for Glioma

Expounding on their previous work demonstrating the cytotoxic effects of DCA on cancer cells (114), Michaelakis and colleagues conducted a pilot study evaluating DCA in 5 primary GBM patients (68). Three patients received DCA treatment following recurrence after debulking surgery, radiation and TMZ administration. One patient received DCA for three months prior to surgery and then continued following surgery with the addition of radiation and TMZ. DCA treatment was initiated at the time of radiation and TMZ after surgery in the last patient. Despite the differences in regimen, DCA reduced tumor cell proliferation, increased apoptosis and inhibited angiogenesis in these 5 patients. DCA treatment also reduced the proportion of GSCs compared to pre-surgery biopsy samples (68).

A phase I trial of 15 patients with recurrent malignant brain tumors demonstrated the safety and tolerability of DCA administration for cancer patients. No dose-limiting toxicities were observed, however low-grade fatigue was reported by a few patients. Eight of the fifteen patients remained on DCA for at least one 4-week cycle during which they all remained clinically stable (99). A subsequent dose-escalation phase I trial for various solid tumors demonstrated mild, yet dose-limiting toxicities at a dose of 25mg/kg/day, which included nausea, diarrhea and reversible non-demyelinating peripheral neuropathy. Patients that experienced early onset of these side effects were shown to express the homozygous EGM variant of GSTZ1, which was associated with increased serum trough levels of DCA. Unfortunately, there were no partial or complete responders to DCA, leading the investigators to hypothesize that DCA would not be effective as a monotherapy. Specifically, they proposed that it would be best utilized in

combination with agents that would benefit from increased glucose oxidation such as pro-oxidant chemotherapies (127).

2.4.2 Metformin

Metformin is a synthetic biguanide, an organic molecule containing two imine groups derived from *Galega officinalis*, or French lilac. Metformin is a first-line therapy for T2DM due to its activity in normalizing circulating levels of glucose and insulin. It is estimated that over 100 million patients worldwide take metformin daily (128). It displays robust physiological effects that suggest it may have therapeutic utility beyond T2DM. Metformin improves the lipid profile of patients at risk for cardiovascular disease, reduces chronic inflammation and potentially reduce cancer incidence, especially in patients with T2DM (129-131). Moreover, metformin is shown to reduce systemic estrogen levels and is being utilized in the clinic for poly-cystic ovary syndrome (PCOS) (132).

2.4.2.1 Mechanism of Action

Metformin exists physiologically as a cation, which restricts its diffusion across cellular membranes. As such, metformin is predominantly imported into the cell via a member of the family of organic cation transporters (OCTs), OCT1 (133). Within the cell, metformin is shown to accumulate within the mitochondria due to the negative membrane potential across the IMM (134). Within the mitochondrial matrix, metformin is shown to inhibit complex I of the ETC, leading to restriction of NADH oxidation (134, 135). This complex I inhibition is associated with an increase in uncoupled respiration

and partial depletion of $\Delta\Psi_m$, which restricts ATP production from oxidative phosphorylation (136). This stimulates compensatory adenylate kinase generation of ATP and subsequent accumulation of adenosine monophosphate (AMP) (134). Together, with inhibition of AMP deaminase, metformin treatment increases the AMP/ATP ratio, which induces an energetic crisis (137). The energetic crisis resultant from metformin treatment is central to the anti-diabetic effects elicited from metformin treatment.

OCT1 is highly expressed on the basolateral membrane of hepatocytes, which facilitates significant liver uptake of metformin (138). A consequence of robust hepatic uptake is a reduction in gluconeogenesis, mediated in large part by the increase in AMP/ATP ratio (139). Gluconeogenesis is stimulated by glucagon, which induces G-protein coupled receptor signaling coupled to adenylate cyclase (AC) generation of cyclic AMP (cAMP). cAMP generation by AC is dependent on ATP and is inhibited by increases in the AMP/ATP ratio. Metformin-induced accumulation of AMP thus restricts cAMP production and prevents activation of protein kinase A, which mediates signaling initiated by glucagon receptor activation. Thus, metformin activity opposes glucagon signaling.

Glucagon restricts efficient glycolytic flux to promote the accumulation of the glycolytic intermediate DHAP, a gluconeogenic substrate. Metformin enhances glycolytic metabolism and is shown to reduce hepatic levels of DHAP and other intermediates in the middle of the glycolytic pathway (140). Moreover, metformin is shown to inhibit mitochondrial glycerol-3-phosphate dehydrogenase (mGPD) in the liver, which promotes an increase in cytosolic NADH levels. This increase in NADH restricts

the reverse reaction of lactate to pyruvate catalyzed by LDH and thus inhibits the Cori cycle, which involves hepatic uptake of lactate for gluconeogenesis.

The increase in AMP/ATP ratio associated with metformin treatment also leads to the activation of AMP-activated protein kinase (AMPK) (139). Allosteric binding of AMP promotes a conformational change in AMPK that permits activating phosphorylation by liver kinase B1 (LKB1). AMPK is a critical energy sensor that has pleiotropic effects on cellular metabolism to restore energy balance. For instance, AMPK mediates metformin stimulation of glycolysis (141). Metformin is also shown to promote insulin sensitivity through AMPK-mediate normalization of insulin signaling. This stimulates Akt-mediated translocation of GLUT4 to the plasma membrane of myocytes, which permits peripheral glucose uptake (142). Though AMPK downstream targets inhibit expression of some gluconeogenesis-related genes, AMPK activation is shown to be dispensable for the reduction in hepatic gluconeogenesis associated with metformin treatment (143). Ultimately, metformin action results in the reduction of hepatic glucose output, increased peripheral glucose uptake and reversal of insulin insensitivity in diabetic patients. As T2DM is associated with cancer incidence, metformin is under extensive investigation for potential indications in cancer.

2.4.2.2 Anti-Cancer Activities

The totality of studies evaluating metformin in cancer suggest that metformin elicits both indirect and cancer call autonomous activities (128). The systemic changes in metabolism promoted by metformin treatment in patients with T2DM antagonize the release of various endocrine factors as well as energy substrates that promote

tumorigenesis. Inhibition of hepatic gluconeogenesis leads to lower circulating glucose levels, potentially starving pre-neoplastic cells of their preferential energy source. Moreover, restoring insulin sensitivity is associated with reductions in circulating insulin, limiting its mitogenic effects on insulin sensitive cancers. It has recently been appreciated that metformin also has effects on additional cell types (132, 144).

OCT1 expression in adipocytes is shown to be enhanced in obese patients, and response to metformin is positively correlated with body mass index (145). Metformin activates AMPK in subcutaneous and visceral white adipose, which results in depletion of TAG levels and increased FAO and is marked by reduction in adipocyte size (144). Adipocytes are shown to drive ovarian cancer metastasis. Omental adipose release of adipokines and cytokines is implicated in homing of metastatic ovarian cancer cells to the omentum, where adipocyte lipolysis provides fatty acids as a source of energy for these cells (146). Metformin inhibits the release of these endocrine signals, limiting ovarian cancer cell migration and proliferation (147). Metformin is also shown to downregulate the NF-κB pathway in leukocytes, restricting the production of the pro-inflammatory cytokine IL-6 (148). IL-6 signaling is shown to promote EMT and metastasis through activation of signal transducer and activator of transcription 3 (STAT3) (149). Metformin reversed IL-6 mediated EMT in NSCLC cells and prevented metastasis in lung-tumor bearing mice (150).

Metformin is also shown to activate AMPK in cancer cells, which has profound effects on their metabolism (141, 151). To restore energy balance in the face of a deficit, AMPK promotes a shift from anabolic to catabolic metabolism (142). This is marked by increases in glycolytic metabolism with concomitant restriction of glucose

oxidation in favor of FAO. Moreover, AMPK inhibits mTORC1, preventing its stimulation of protein synthesis. Metformin also disrupts the Ragulator complex, which activates mTORC1 in the presence of excess amino acids (152). Activated AMPK imparts inhibitory phosphorylation on ACC, restricting FAS and lipogenesis (153). Independently of AMPK, metformin is shown to disrupt the folate cycle, inhibiting one-carbon metabolism and nucleotide biosynthesis (154). Collectively these effects account for the cytostatic activity that metformin exhibits towards cancer cells. Despite increasing aerobic glycolysis in tumor cells, the restriction of anabolic processes prevents proliferation.

Strikingly, the metabolic rewiring induced by metformin reduces the energetic flexibility of cancer cells. In the absence of glucose, metformin exhibits cytotoxicity towards cancer cells and this cannot be rescued with other carbohydrate sources such as galactose or maltose (151). Metformin reduces oxidative and enhances reductive glutamine metabolism to generate acetyl-CoA without promoting ATP production. IDH1 mutant tumor cells are unable to efficiently use glucose to maintain TCA cycling and upregulate glutamine oxidation to compensate. As such, the presence of this mutation sensitized breast cancer cells to metformin’s cytostatic activity (155).

Retrospective studies of T2DM patients treated with metformin have suggested that metformin treatment is associated with reduced risk for certain cancers in diabetic patients. In particular, metformin treatment has been linked to lower incidence rates in breast, colorectal, prostate and endometrial cancer (156-160). However, recent commentary on these meta-analyses has proposed that these studies suffer from several forms of reporting and selection biases that confound the results. Reanalysis of

these data sets have often not replicated the original findings, thus metformin's impact on cancer risk is still controversial (161, 162). Nevertheless, many of metformin's effects could inhibit tumorigenesis.

The energetic stress induced by metformin stimulates DNA reparatory systems even in the absence of DNA damage. This likely would prevent the genomic instability necessary for cellular transformation and prevent tumorigenesis. Moreover, metformin stimulation of the DNA-repair protein ataxia-telangiectasia mutated (ATM) inhibits nucleotide synthesis through LKB1-independent activation of AMPK, restricting the nucleic acid synthesis required for rapid proliferation (163). Furthermore, metformin inhibition of folate metabolism likely selects against transformation through nucleotide restriction and reduction in DNA methylation. Again, the reduction in circulating insulin associated with metformin treatment limits the propensity for stimulation of the PI3K-Akt-mTORC1 axis associated with insulin receptor activation.

Recent evidence suggests that metformin specifically targets GSCs in models of GBM (164-166). Metformin inhibits the self-renewal capacity of GSCs and exhibits greater potency in reducing GSC proliferation compared to glioma cells, which is associated with reduced GSC xenograft growth (166). Moreover, metformin potentiates the cytotoxicity of TMZ towards glioma cells in part through induction of the miRNAs miR-124 and Let-7 (164). As CSCs exhibit enhanced antioxidant capacity and inherent chemoresistance, metformin may be a beneficial adjuvant to pro-oxidant therapies such as DCA to simultaneously target the bulk tumor and CSC subpopulation.

2.5 Central Hypothesis and Project Aims

As described, the metabolic derangements exhibited by cancer cells are intrinsically linked to the proliferative capacity and aggressiveness of tumors. Targeting specific genetic alterations in the cell cycle or signaling cascades associated with cancer has failed to yield adequate clinical efficacy as cancer is on the verge or passing heart disease as the leading cause of death in the US despite remarkable progress made in screening and detection. As anabolic metabolism is fundamental to every tumor species, it is a more promising target for therapy development. The metabolic agents DCA and metformin each exhibit anti-cancer activities dependent on the modulation of anabolic capacity. We propose that the mechanistic overlap in altering mitochondrial function in cancer suggests potential synergy between DCA and metformin. Specifically, that metformin inhibition of complex I will potentiate DCA-induced oxidative stress as a result of increased PDH activity. We hypothesize that co-administration of DCA and metformin will induce a metabolic shift towards mitochondrial oxidation in the presence of ETC dysfunction that is unsustainable in cancer cells, thus promoting cell death and blunting disease progression. The major goals of this study were to characterize the synergistic effects of DCA and metformin on VM-M3 cell metabolism and viability *in vitro* and tumor growth *in vivo*, to determine the systemic metabolic effects of DCA and metformin in Vm/dk mice, and to evaluate the efficacy of enhancing the pro-oxidant capacity of this combination. If effective, this combination would provide an alternative strategy for targeting cancer metabolism without the toxicity exhibited by previously established metabolic therapies.

2.6 References

1. Schwartzbaum, JA., Fisher, JL., Aldape, KD. & Wrensch, M. Epidemiology and molecular pathology of glioma. *Nat Clin Pract Neurol.* **2**, 494-503 (2006).
2. Omuro, A. & DeAngelis, LM. Glioblastoma and other malignant gliomas: a clinical review. *JAMA* **310**, 1842-1850 (2013).
3. Stupp, R. *et al*. Effects of radiotherapy with concomitant and adjuvant temozolomide versus radiotherapy alone on survival in glioblastoma in a randomized phase III study: 5-year analysis of the EORTC-NCIC trial. *Lancet Oncol.* **10**, 459-466 (2009).
4. Ru, P., Williams, TM., Chakravarti, A. & Guo, D. Tumor metabolism of malignant gliomas. *Cancers* **5**, 1469-1484 (2013).
5. Louis, DN. *et al.* The 2007 WHO classification of tumors of the central nervous system. *Acta Neuropathol.* **114**, 97-109 (2007).
6. Louis, DN. The 2016 World Health Organization classification of tumors of the central nervous system: a summary. *Acta Neuropathol.* **131**, 803-820 (2016).
7. Dropcho, EJ. & Soong, SJ. The prognostic impact of prior low grade histology in patients with anaplastic gliomas: a case-control study. *Neurology* **47**, 684-690 (1996).
8. Johnson, DR. & Galanis, E. Medical management of high-grade astrocytoma: current and emerging therapies. *Semin. Oncol.* **41**, 511-522 (2014).
9. Wesseling, P., van den Bent, M. & Perry, A. Oligodendroglioma: pathology, molecular mechanisms and markers. *Acta Neuropathol.* **129**, 809-827 (2015).
10. Armstrong, TS. *et al.* Adult ependymal tumors: prognosis and the M.D. Anderson Cancer Center experience. *Neuro Oncol.* **12**, 862-870 (2010).
11. Wrensch, M. *et al.* Familial and personal medical history of cancer and nervous system conditions among adults with glioma and controls. *Am J Epidemiol.* **145**, 581-593 (1997).
12. Ostrom, QT. *et al.* CBTRUS statistical report: primary brain and central nervous system tumors diagnosed in the United States in 2008-2012. *Neuro Oncol.* **17**, iv1-iv62 (2015).
13. Lun, M. *et al.* The natural history of extracranial metastasis from glioblastoma multiforme. *J Neurooncol.* **105**, 261-273 (2011).
14. Pasquier, B. *et al*. Extracranial metastasis of astrocytomas and glioblastomas: clinicopathological study of two cases and review of the literature. *Cancer* **45**, 112-125 (1980).
15. Rajagopalan, V., El Kamar, FG., Thayaparan, R. & Grossbard, ML. Bone marrow metastases from glioblastoma multiforme. A case report and reviw of the literature. *J Neurooncol*. **72**, 157-161 (2005).
16. Gullotta, F., Schindler, F., Schmutzier, R. & Weeks-Seifert, A. GFAP in brain tumor diagnosis: possibilities and limitations. *Pathol Res Pract.* **180**, 54-60 (1985).
17. Brenner, AV. *et al.* History of allergies and autoimmune diseases and risk of brain tumors in adults. *Int J Cancer*, **99**, 252-259 (2002).
18. Wiemels, JL. *et al.* History of allergies among adults with glioma and controls. *Int J Cancer* **98**, 609-615 (2002).

19. Wrensch, M. *et al.* History of chickenpox and shingles and prevalence of antibodies of varicella-zoster virus and three other herpesviruses among adults with glioma and controls. *Am J Epidemiol.* **161**, 1-10 (2005).
20. Schwartzbaum, J. *et al*. Polymorphisms associated with asthma are inversely related to glioblastoma multiforme. *Cancer Res.* **65**, 6459-6465 (2005).
21. Wang, LE. *et al*. Polymorphisms of DNA repair genes and risk of glioma. *Cancer Res.* **64**, 5560-5563 (2004).
22. Wrensch, M. *et al*. ERCC1 and ERCC2 polymorphisms and adult glioma. *Neuro Oncol.* **71**, 495-507 (2005).
23. Wiencke, J. *et al.* Molecular features of adult glioma associated with patient race/ethnicity, age, and a polymorphism in O^6-methylguanine-DNA-alkyltransferases. *Cancer Epidemiol. Biomarkers Prev.* **14**, 1774-1783 (2005).
24. Bleau, AM., Huse, JT. & Holland, EC. The ABCG2 resistance network of glioblastoma. *Cell Cycle* **8**, 2936-2944 (2009).
25. Bond, GL. *et al.* A single nucleotide polymorphism in the MDM2 promoter attenuates the p53 suppressor pathway and accelerates tumor formation in humans. *Cell* **119**, 591-602 (2004).
26. Reilly, KM. *et al.* Nfl; Trp53 mutant mice develop glioblastoma with evidence of strain-specific effects. *Nature Genet.* **26**, 109-113 (2000).
27. Xiao, A. *et al*. Astrocyte inactivation of the pRb pathway predisposes mice to malignant astrocytoma development that is accelerated by PTEN mutation. *Cancer Cell* **1**, 157-168 (2002).
28. Louis, DN. The p53 gene and protein in human brain tumors. *J. Neuropathol.* **53**, 11-21 (1994).
29. Henson, JW. *et al.* The retinoblastoma gene is involved in the malignant progression of astrocytomas. *Ann. Neurol.* **36**, 714-721 (1994).
30. Concurrent inactivation of RB1 and TP53 pathways in anaplastic oligodedroglioma. *J. Neuropathol. Exp. Neurol.* **60**, 1181-1190 (2001).
31. The Cancer Genome Atlas Research Network. Comprehensive genomic characterization defines human glioblastoma genes and core pathways. *Nature* **455**, 1061-1068 (2008).
32. Kim, H. *et al*. Integative genome analysis reveals an oncomir/oncogene cluster regulating glioblastoma survivorship. *PNAS* **107**, 2183-2188 (2010).
33. Stommel, JM. *et al.* Coactivation of receptor tyrosine kinases affects the response of tumor cells to targeted therapies. *Science* **318**, 287-290 (2007).
34. Ohgaki, H. & Kleihues, P. Epidemiology and etiology of gliomas. *Acta Neuropatol.* **109**, 93-108 (2005).
35. Mellinghoff, IK. Molecular determinants of the response of glioblastomas to EGFR kinase inhibitors. *N. Engl. J. Med.* **353**, 2012-2024 (2005).
36. Di Rocco, F., Carroll, RS., Zhang, J. & Black, PM. Platelet-derived growth factor and its receptor expression in human oligodendrogliomas. *Neurosurgery* **42**, 341-346 (1998).
37. Westermark, B., Heldin, CH. & Nister, M. Platelet-derived growth factor in human glioma. *Glia* **15**, 257-263 (1995).

38. Huse, JT. & Holland, EC. Targeting brain cancer: advances in the molecular pathology of malignant glioma and medulloblastoma. *Nat Rev Cancer* **10**, 319-331 (2010).
39. Yan, H. *et al.* IDH1 and IDH2 mutations in gliomas. *N. Engl. J. Med.* **360**, 765-773 (2009).
40. Hartmann, C. *et al.* Type and frequency of IDH1 and IDH2 mutations are related to astrocytic and oligodedroglial differentiation and age: a study of 1,010 diffuse gliomas. *Acta Neuropathol.* **118,** 469-474 (2009).
41. Hartmann, C. *et al*. Patients with IDH1 wild type anaplastic astrocytomas exhibit worse prognosis than IDH1-mutated glioblastomas, and IDH1 mutation status accounts for the unfavorable prognostic effect of higher age: implications for classification of gliomas. *Acta Neuropathol.* **120**, 707-718 (2010).
42. Bao, S. *et al*. Glioma stem cells promote radioresistance by preferential activation of the DNA damage response. *Nature* **444**, 756-760 (2006).
43. Singh, SK. *et al*. Identification of human brain tumor initiating cells. *Nature* **432**, 396-401 (2004).
44. Bao, S. *et al*. Stem cell-like glioma cells promote tumor angiogenesis through vascular endothelial growth factor. *Cancer Res.* **66**, 7843-7848 (2006).
45. Ricci-Vitiani, L. *et al*. Tumour vascularization via endothelial differentiation of glioblastoma stem cells. *Nature* **468**, 824-828 (2010).
46. Bleau, AM. *et al.* PTEN/PI3K/Akt pathway regulates the side population phenotype and ABCG2 activity in glioma tumor stem-like cells. *Cell Stem Cell* **4**, 226-235 (2009).
47. Phillips, HS. *et al.* Molecular subclasses of high-grade glioma predict prognosis, delineate a pattern of disease progression, and resemble stages in neurogenesis. *Cancer Cell* **9**, 157-173 (2006).
48. Griffloen, AW. *et al.* CD44 is involved in tumor angiogenesis; an activation antigen on human endothelial cells. *Blood* **90**, 1150-1159 (1997).
49. Verhaak, RW. *et al.* An integrated genomic analysis identifies clinically relevant subtypes of glioblastoma characterized by abnormalities in PDGFRA, IDH1, EGFR, and NF1. *Cancer Cell* **17**, 98-110 (2009).
50. Wolf, A. *et al*. Hexokinase 2 is a key mediator of aerobic glycolysis and promotes tumor growth in human glioblastoma multiforme. *J. Exp. Med.* **208**, 313-326 (2011).
51. Yang, W. *et al*. EGFR-induced and PKCepsilon monoubiquitylation-dependent NF-kB activation upregulates PKM2 expression and promotes tumorigenesis. *Mol. Cell* **48**, 771-784 (2012).
52. Yang, W. *et al*. ERK1/2-dependent phosphorylation and nuclear translocation of PKM2 promotes the Warburg effect. *Nat. Cell Biol.* **14**, 1295-1304 (2012).
53. Sutendra, G. & Michelakis, ED. Pyruvate dehydrogenase kinase as a novel therapeutic target in oncology. *Front. Oncol.* **3**, 38 (2013).
54. Padma, MV. *et al.* Prediction of pathology and survival by FDG-PET in gliomas. *J. Neurooncol.* **64**, 227-237 (2003).
55. Miranda-Goncalves, V. *et al*. Monocarboxylate transporters (MCTs) in gliomas: expression and exploitation as therapeutic targets. *Neuro. Oncol.* **15**, 172-188 (2013).

56. DeBerardinis, RJ. *et al.* Beyond aerobic glycolysis: transformed cells can engage in glutamine metabolism that exceeds the requirement for protein and nucleotide synthesis. *PNAS* **104**, 19345-19350 (2007).
57. Kallenberg, K. *et al*. Untreated glioblastoma multiforme: increased myo-inositol and glutamine levels in the contralateral cerebral hemisphere at proton MR spectroscopy. *Radiology* **253**, 805-812 (2009).
58. Marin-Valencia, I. *et al*. Analysis of tumor metabolism reveals mitochondrial glucose oxidation in genetically diverse human glioblastomas in the mouse brain in vivo. *Cell Metab.* **15**, 827-837 (2012).
59. Rosati, A. *et al*. Epilepsy in glioblastoma multiforme: correlation with glutamine synthetase levels. *J. Neurooncol.* **93**, 319-324 (2009).
60. Gopal, K., Grossi, E., Paoletti, P. & Usardi, M. Lipid composition of human intracranial tumors: a biochemical study. *Acta Neurochir.* **11**, 333-347 (1963).
61. Guo, D. *et al*. The AMPK agonist AICAR inhibits the growth of EGFRvIII-expressing glioblastomas by inhibiting lipogenesis. *PNAS* **106**, 12932-12937 (2009).
62. Guo, D. *et al.* An LXR agonist promotes GBM cell death through inhibition of an EGFR/AKT/SREBP-1/LDLR-dependent pathway. *Cancer Discov.* **1**, 442-456 (2011).
63. Ryczko, MC. *et al.* Metabolic reprogramming by hexosamine biosynthetic and golgi N-glycan branching pathways. *Sci. Rep.* **6**, 23043 (2016).
64. Padiar, AA. *et al.*Upregulated B1-6 branch N-glycan marks eary gliomagenesis but exhibited biphasic expression in the progression of astrocytic glioma. *Am. J. Cancer Res.* **5**, 1101-1016 (2015).
65. Pike, LS. *et al.* Inhibition of fatty acid oxidation by etomoxir impairsNADPH production and increases reactive oxygen species resulting in ATP depletion and cell death in human glioblastoma cells. *Biochim. Biophys. Acta* **1807**, 726-734 (2011).
66. Mashimo, T. *et al*. Acetate is a bioenergetics substrate for human glioblastoma and brain metastases. *Cell* **159**, 1603-1614 (2014).
67. Ordys, BB. *et al*. The role of mitochondria in glioma pathophysiology. *Mol. Neurobiol.* **42**, 64-75 (2010).
68. Michelakis, ED. *et al.* Metabolic modulation of glioblastoma with dichloroacetate. *Sci. Trans. Med.* **2**, 31-34 (2010).
69. Arismendi-Morillo, G. Electron microscopy of the mitochondrial network in gliomas and their vascular microenvironment. *Biochim. Biophys. Acta* **1807**, 602-608 (2011).
70. Kim, D. *et al.* SHMT2 drives glioma cell survival in ischemia but imposes a dependence on glycine clearance. *Nature* **520**, 363-367 (2015).
71. Chinnaiyan, P. *et al.* The metabolomics signature of malignant glioma reflects accelerated anabolic metabolism. *Cancer Res.* **72**, 5878-5888 (2012).
72. Zhao, H. *et al.* Metabolomics profiling in plasma samples from glioma patients correlates with tumor phenotypes. *Oncotarget* **7**, 20486-20495 (2016).
73. Pavlyk, I. *et al*. Arginine deprivation affects glioblastoma cell adhesion, invasiveness and actin cytoskeleton organization by impairment of B-actin arginylation. *Amino Acids* **47**, 199-212 (2015).

74. Yerli, H. *et al*. Evaluation of cerebral glioma grade by using normal side creatine as an integral reference in multi-voxel 1H-MR spectroscopy. *Diagn. Interv. Radiol.* **13**, 3-9 (2007).
75. Gupta, G. & Massague J. Cancer metastasis: building a framework. *Cell* **127**, 679-695 (2006).
76. Huysentruyt, LC. *et al.* Metastatic cancer cells with macrophage properties: evidence for a new murine tumor model. *Int. J. Cancer* **123**, 73-84 (2008).
77. Shelton, LM. *et al*. A novel pre-clinical in vivo mouse model for malignant brain tumor growth and invasion. *J. Neurooncol.* **99**, 165-176 (2010).
78. Fraser, H. Astrocytomas in an inbred mouse strain. *J. Pathol.* **103**, 266-270 (1971)
79. Baker, GJ. *et al.* Mechanisms of glioma formation: interative perivascular glioma growth and invasion leads to tumor progression, VEGF-independent vascularization, and resistance to antiangiogenic therapy. *Neoplasia* **16**, 543-561 (2014).
80. Ginhoux, F. & Jung, S. Monocytes and macrophages: developmental pathways and tissue homeostasis. *Nat. Rev. Immunol.* **14**, 392-404 (2014).
81. Zhang, QQ. *et al.* CD11b deficiency suppresses intestinal tumor growth by reducing myeloid cell recruitment. *Sci. Rep.* **5**, 15948 (2015).
82. Atlin, JG. & Sloan EK. The role of CD45 and CD45-associated molecules in T cell activation. *Immunol. Cell Biol.* **75**, 430-445 (1997).
83. Lin, HH. *et al.* The macrophage F4/80 receptor is required for the induction of antigen-specific efferent regulatory T cells in peripheral tolerance. *J. Exp. Med.* **201**, 1615-1625 (2005).
84. Macikova, I. *et al*. GFAP-positive astrocytes are rare or absent in primary adult human brain tissue cultures. *Biologia* **64**, 833-839 (2009).
85. Hochberg, FH., Baehring, JM. & Hochberg, EP. Primary CNS lymphoma. *Nat. Clin. Pract. Neurol.* **3**, 24-35 (2007).
86. Jahnke, K. *et al.* International study on low-grade primary central nervous system lymphoma. *Ann. Neurol.* **59**, 755-762 (2006).
87. Huysentruyt, LC., Akgoc, Z., Seyfried, TN. Hypothesis: are neoplastic macrophages/microglia present in glioblastoma multiforme? *ASN Neuro.* **3**m 183-193 (2011).
88. Huysentruyt, LC. & Seyfried, TN. Perspectives on the mesenchymal origin of metastatic cancer. *Cancer Metastasis Rev.* **29**, 695-707 (2010).
89. Munzarova, M., Lauerova, L. & Capkova, J. Are advanced malignant melanoma cells hybrids between melanocytes and macrophages? *Melanoma Res.* **2**, 127-129 (1992).
90. Glass, R. & Synowitz, M. CNS macrophages and peripheral myeloid cells in brain tumors. *Acta Neuropathol.* **128**, 347-362 (2014).
91. Cai, J. *et al.* Identification of a 6-cytokine prognostic signature in patients with primary glioblastoma harboring M2 microglia/macrophage phenotype relevance. *PLoS ONE* **10**, e0126022 (2015).
92. Hu, F. *et al.* Glioma-associated microglial MMP9 expression is upregulated by TLR2 signaling and sensitive to minocycline. *Int. J. Cancer* **135**, 2569-2578 (2014).

93. Engler, JR. *et al.* Increased microglia/macrophage gene expression in a subset of adult and pediatric astrocytomas. *PLoS ONE* **7**, e43339 (2012).
94. Shelton, LM., Husentruyt, LC. & Seyfried, TN. Glutamine targeting inhibits systemic metastasis in the VM-M3 murine tumor model. *Int. J. Cancer* **127**, 2478-2485 (2010).
95. Le, A. *et al.* Tumorigenicity of hypoxic respiring cancer cells revealed by a hypoxia-cell cycle dual reporter. *PNAS* **111**, 12486-12491 (2014).
96. Lupi, R. *et al.* Prolonged exposure to free fatty acids has cytostatic and pro-apoptotic effects on pacreactic islets: evidence that beta-cell death is caspase mediated, partially dependent on ceramide pathway, and Bcl-2 regulated. *Diabetes* **51**, 1437-1442 (2002).
97. Poff, AM., Ari, C., Seyfried, TN. & D'Agostino, DP. The ketogenic diet and hyperbaric oxygen therapy prolong survival in mice with metastatic cancer. *PLoS ONE* **8**, e65522 (2013).
98. Poff, AM. *et al*. Non-toxic metabolic management of metastatic cancer in VM mice: novel combination of ketogenic diet, ketone supplementation, and hyperbaric oxygen therapy. *PLoS ONE* **10**, e0127407 (2015).
99. Dunbar, EM. *et al.* Phase 1 trial of dichloroacetate (DCA) in adults with recurrent malignant brain tumors. *Invest New Drug* **32,** 452–464 (2014).
100. Patel, MS., Nemeriam NS., Furey, W. & Jordan, F. The pyruvate dehydrogenase complexes: structure-based function and regulation. *J. Biol. Chem.* **289**, 16615-16623 (2014).
101. Stacpoole, PW., Kurtz, TL., Han, Z. & Langaee, T. Role of dichloroacetate in the treatment of genetic mitochondrial diseases. *Adv. Drug Deliv. Rev.* **60**, 1478-1487 (2008).
102. Zhang, S. *et al.* The pivotal role of pyruvate dehydrogenase kinases in metabolic flexibility. *Nutr. Metab.* **11**, 10 (2014).
103. Hitosugi, T. *et al*. Tyrosine phosphorylation of mitochondrial pyruvate dehydrogenase kinase is important for cancer metabolism. *Mol. Cell* **44**, 864-867 (2011).
104. Li, X. *et al*. Mitochondria-translocated PGK1 functions as a protein kinase to coordinate glycolysis and the TCA cycle in tumorigenesis. *Mol. Cell* **61**, 705-719 (2016).
105. Knoechel, TR. *et al.* Regulatory roles of the N-terminal domain based on crystal structures of human pyruvate dehydrogenase kinase 2 containing physiological and synthetic ligands. *Biochemistry* **45**, 405-412 (2006).
106. Jha, MK. & Suk, K. Pyruvate dehydrogenase kinase as a potential therapeutic target for malignant gliomas. *Brain Tumor Res. Treat.* **1**, 57-63 (2013).
107. Stacpoole, PW. *et al.* A controlled clinical trial of dichloroacetate for treatment of lactic acidosis in adults. The Dichloroacetate-Lactic Acidosis Study Group. *N. Engl. J. Med.* **327**, 1564-1569 (1992).
108. Fouque, F. *et al.* Differential effect of DCA treatment on the pyruvate dehydrogenase complex in patients with severe PDHC deficiency. *Pediatr. Res.* **53**, 793-799 (2003).
109. Maisenbacher III, MW. *et al.* Pharmokinetics of oral dichloroacetate in dogs. *J. Biochem. Mol. Toxicol.* **27**, 522-525 (2013).

110. Stauber, AJ. & Bull, RJ. Differences in phenotype and cell replicative behavior of hepatic tumors induced by dichloroacetate (DCA) and trichloroacetate (TCA). *Toxicol. Appl. Pharmacol.* **144**, 235-246 (1997).
111. Abdelmalak, M. *et al.* Long-term safety of dichloroacetate in congenital lactic acidosis. *Mol. Genet. Metab.* **109**, 139-143 (2013).
112. Sanchez WY. *et al.* Dichloroacetate inhibits aerobic glycolysis in multiple myeloma cells and increases sensitivity to bortezomib. *Brit J Cancer* **108,** 1624–1633 (2013).
113. Lin, G. *et al*. Dichloroacetate induces autophagy in colorectal cancer cells and tumours. *Br. J. Cancer* **111**, 375-385 (2014).
114. Bonnet, S. *et al.* A mitochondria-K+ channel axis is suppressed in cancer and Its normalization promotes apoptosis and inhibits cancer growth. *Cancer Cell* **11,** 37–51 (2007).
115. Dai, Y. *et al.* Dichloroacetate Enhances Adriamycin-Induced Hepatoma Cell Toxicity In Vitro and In Vivo by Increasing Reactive Oxygen Species Levels. *Plos One* **9,** e92962 (2014).
116. Xuan, Y. *et al.* Dichloroacetate attenuates hypoxia-induced resistance to 5-fluorouracil in gastric cancer through the regulation of glucose metabolism. *Exp Cell Res* **321,** 219–230 (2014).
117. Kumar, K. *et al.* Dichloroacetate reverses the hypoxic adaptation to bevacizumab and enhances its antitumor effects in mouse xenografts. *J Mol Med* **91,** 749–758 (2013).
118. Kumar, A., Kant, S. & Singh, SM. Antitumor and chemosensitizing action of dichloroacetate implicates modulation of tumor microenvironment: A role of reorganized glucose metabolism, cell survival regulation and macrophage differentiation. *Toxicol Appl Pharm* **273,** 196–208 (2013).
119. Shen, YC. *et al.* Activating oxidative phosphorylation by a pyruvate dehydrogenase kinase inhibitor overcomes sorafenib resistance of hepatocellular carcinoma. *Brit J Cancer* **108,**72–81 (2013).
120. Sun, RC. *et al.* Reversal of the glycolytic phenotype by dichloroacetate inhibits metastatic breast cancer cell growth in vitro and in vivo. *Breast Cancer Res Tr* **120,** 253–260 (2010).
121. Wong, JY., Huggins, GS., Debidda, M., Munshi, NC. & De Vivo, I. Dichloroacetate induces apoptosis in endometrial cancer cells. *Gynecol Oncol* **109,** 394–402 (2008).
122. Roh, JL., Park, JY., Kim, EH., Jang, HJ. & Kwon, M. Activation of mitochondrial oxidation by PDK2 inhibition reverses cisplatin resistance in head and neck cancer. *Cancer Lett* **371,** 20–29 (2016).
123. Sun, RC., Board, PG. & Blackburn, AC. Targeting metabolism with arsenic trioxide and dichloroacetate in breast cancer cells. *Mol Cancer* **10,** 1–15 (2011).
124. Karki, P. *et al*. Intracellular K(+) inhibits apoptosis by suppressing the Apaf-1 apoptosome formation and subsequent downstream pathways but not cytochrome c release. *Cell Death Differ.* **14**, 2068-2075 (2007).
125. Jung, CH. *et al.* mTOR regulation of autophagy. *FEBS Lett.* **584**, 1287-1295 (2010).

126. Cao, W. *et al*. Dichloroacetate (DCA) sensitizes both wild-type and over expressing Bcl-2 prostate cancer cells in vitro to radiation. *Prostate* **68**, 1223-1231 (2008).
127. Chu, QS. *et al.* A phase I open-labeled, single-arm, dose-escalation, study of dichloroacetate (DCA) in patients with advanced solid tumors. *Invest New Drug* **33,** 603–610 (2015).
128. Pernicova, I. & Korbonits M. Metformin – mode of action and clinical implications for diabetes and cancer. *Nat. Rev. Endocrinol.* **10**, 143-156 (2014).
129. Glueck, CJ. *et al.* Metformin reduces weight, centripetal obesity, insulin, leptin, and low-density lipoprotein cholesterol in nondiabetic, morbidly obese subjects with body mass index greater than 30. *Metabolism* **50**, 856-861 (2001).
130. Kita, Y. *et al*. Metformin prevents and reverses inflammation in a non-diabetic mouse model of nonalcoholic steatohepatitis. *PLoS ONE* **7**, e43056 (2012).
131. Giovannuci, E. *et al*. Diabetes and cancer: a consensus report. *Diabetes Care* **33**, 1674-1685 (2010).
132. Sivalingam, VN. *et al.* Metformin in reproductive health, pregnancy and gynaecological cancer: established and emerging indications. *Hum. Reprod. Update* **20**, 853-868 (2014).
133. Shitara, Y. *et al.* Role of organic cation/carnitine transporter 1 in uptake of phenformin and inhibitory effect on complex I respiration in mitochondria. *Toxicol. Sci.* **132**, 32-42 (2013).
134. Owen, MR., Doran, E. & Halestrap, AP. Evidence that metformin exerts its anti-diabetic effects through inhibition of complex 1 of the mitochondrial respiratory chain. *Biochem J* **348,** 607–614 (2000).
135. Wheaton, WW. *et al.* Metformin inhibits mitochondrial complex I of cancer cells to reduce tumorigenesis. *Elife* **3,** e02242 (2014).
136. Batandier, C. *et al*. The ROS production induced by a reverse-electron flux at respiratory-chain complex I is hampered by metformin. *J. Bioenerg. Biomembr.* **38**, 33-42 (2006).
137. Ouyang, J., Parakhia, RA. & Ochs, RS. Metformin activates AMP kinase through inhibition of AMP deaminase. *J. Biol. Chem.* **286**, 1-11 (2011).
138. Gong, L. *et al*. Metformin pathways: pharmacokinetics and pharmacodynamics. *Pharmacogenet. Genomics* **22**, 820-827 (2012).
139. Shaw, RJ. *et al.* The kinase LKB1 mediates glucose homeostasis in liver and therapeutic effects of metformin. *Science* **310**, 1642-1646 (2005).
140. Janzer, A. *et al.* Metformin and phenformin deplete tricarboxylic acid cycle and glycolytic intermediates during cell transformation and NTPs in cancer stem cells. *PNAS* **111**, 10574-10579 (2014).
141. Jeon, SM., Chandel, NS. & Hay, N. AMPK regulates NADPH homeostasis to promote tumor cell survival. *Nature* **485**, 661-665 (2012).
142. Mihaylova, MM. & Shaw, RJ. The AMP-activated protein kinase (AMPK) signaling pathway coordinates cell growth, autophagy & metabolism. *Nat. Cell Biol.* **13**, 1016-1023 (2011).
143. Foretz, M. *et al*. Metformin inhibits hepatic gluconeogenesis in mice independently of the LKB1/AMPK pathway via a decrease in hepatic energy state. *J. Clin. Invest.* **120**, 2355-2369 (2010).

144. Moreno-Navarrete, JM. *et al.* OCT1 expression in adipocytes could contribute to increased metformin action in obese subjects. *Diabetes* **60**, 168-176 (2011).
145. Shikata, E. *et al.* Human organic cation transporter (OCT1 and OCT2) gene polymorphisms anf therapeutic effects of metformin. *J. Hum. Genet.* **52**, 117-122 (2007).
146. Nieman, KM. *et al*. Adipocytes promote ovarian cancer metastasis and provide energy for rapid tumor growth. *Nat. Med.* **17**, 1498-1503 (2011).
147. Tebbe, C. *et al.* Metformin limits the adipocyte tumor-promoting effect on ovarian cancer. *Oncotarget* **5**, 4746-4764 (2014).
148. Isoda, K. *et al*. Metformin inhibits proinflamatory responses and nuclear factor-kappaB in human vascular wall cells. *Arterioscler. Thromb. Vasc. Biol.* **26**, 611-617 (2006).
149. Bromberg, J. & Wang, TC. Inflammation and cancer. IL-6 and STAT3 complete the link. *Cancer Cell* **15**, 79-80 (2009).
150. Zhao, Z. *et al*. Metformin inhibits the IL-6-induced epithelial-mesenchymal transition and lung adenocarcinoma growth and metastasis. *PLoS ONE* **9**, e95884 (2014).
151. Zhuang, Y., Chan, DK., Haugrud, AB. & Miskimins, WK. Mechanisms by which low glucose enhances the cytotoxicity of metformin to cancer cells both *in vitro* and *in vivo*. *PLoS ONE* **9**, e108444 (2014).
152. Pierotti, MA. *et al.* Targeting metabolism for cancer treatment and prevention: metformin, an old drug with multi-faceted effects. *Oncogene* **32**, 1475-1487 (2013).
153. Loubiere, C. *et al.* Metformin-induced energy deficiency leads to the inhibition of lipogenesis in prostate cancer cells. *Oncotarget* **6**, 15652-15661 (2015).
154. Corominas-Faja, B. *et al.* Metabolomic fingerprint reveals that metformin impairs one-carbon metabolism in a manner similar to the antifolate class of chemotherapy drugs. *Aging* **4**, 480-498 (2012).
155. Cuyas, E. *et al.* Oncometabolic mutation IDH1 R132H confers a metformin-hypersensitive phenotype. *Oncotarget* **6**, 12279-12296 (2015).
156. Evans, JM., Donnelly, LA., Emslie-Smith, AM., Alessi, DR. & Morris, AD. Metformin and reduced risk of cancer in diabetic patients. *Bmj* **330,**1304–1305 (2005).
157. Libby, G. *et al.* New Users of Metformin Are at Low Risk of Incident Cancer. *Diabetes Care* **32,**1620–1625 (2009).
158. Ko, EM. *et al.* Metformin is associated with improved survival in endometrial cancer. *Gynecol Oncol* **132,** 438–442 (2014).
159. Nevadunsky, NS. *et al.* Metformin use and endometrial cancer survival. *Gynecol Oncol.* **132,**236–240 (2014).
160. Deng, D. *et al*. Association between metformin therapy and incidence, recurrence and mortality of prostate cancer: evidence from a meta-analysis. *Diabetes Metab. Res. Rev.* **31**, 595-602 (2015).
161. Suissa, S. & Azoulay, L. Metformin and the risk of cancer: time-related biases in observational studies. *Diabetes Care* **35**, 2665-2673 (2012).
162. Suissa S. & Azoulay, L. Metformin and cancer: mounting evidence against an association. *Diabetes Care* **37**, 1786-1788 (2014).

163. Sun, Y., Connors, KE. & Yang, DQ. AICAR induces phosphorylation of AMPK in an ATM-dependent, and LKB1-independent manner. *Mol. Cell Biochem.* **306**, 239-245 (2007).
164. Yu, Z. *et al.* Temozolomide in combination with metformin act synergistically to inhibit proliferation and expansion of glioma stem-like cells. *Oncol Lett* **11,** 2792–2800 (2016).
165. Yu, Z. *et al.* Metformin and temozolomide act synergistically to inhibit growth of glioma cells and glioma stem cells in vitro and in vivo. *Oncotarget* **6,** 32930–43 (2015).
166. Gritti, M. *et al.* Metformin repositioning as antitumoral agent: selective antiproliferative effects in human glioblastoma stem cells, via inhibition of CLIC1-mediated ion current. *Oncotarget* **5,** 11252–11268 (2014).

CHAPTER 3: METFORMIN ENHANCES DCA CYTOTOXICITY TOWARDS VM-M3 CELLS THROUGH POTENTIATION OF OXIDATIVE STRESS

3.1 Chapter Synopsis

Here we present data indicating the effect of a DCA and metformin combination on the viability of VM-M3 cells *in vitro* and progression of VM-M3 tumors *in vivo*. We show that metformin enhances DCA cytotoxicity towards VM-M3 cells in an oxidative stress-dependent fashion. While both metformin and DCA prolong survival of VM-M3-burdened animals as single agents, we do not demonstrate a synergistic effect of the combination on VM-M3 disease progression. The materials and methods used for the studies presented in this chapter are described in Appendix A.

3.2 Metformin Enhances DCA Cytotoxicity Towards VM-M3 Cells *in vitro*

As described, DCA exhibits anti-cancer activity towards a range of tumor species through induction of oxidative stress resultant from increased glucose oxidation. As ROS production is linked to ETC function, inhibiting ETC efficiency is likely to enhance ROS production. We hypothesized that metformin inhibition of complex I would cause energetic stress resulting in a compensatory reduction in glucose oxidation. However, we posited that the addition of DCA would overcome this compensatory response and induce glucose oxidation despite the complex I inhibition. This would result in an

increase in matrix NADH production in the presence of reduced complex I efficiency and allow for premature reduction of oxygen and enhanced production of $\cdot O_2^-$. Thus, we suggest that metformin will enhance the pro-oxidant anti-cancer activity of DCA towards neoplastic cells.

3.2.1 Figures

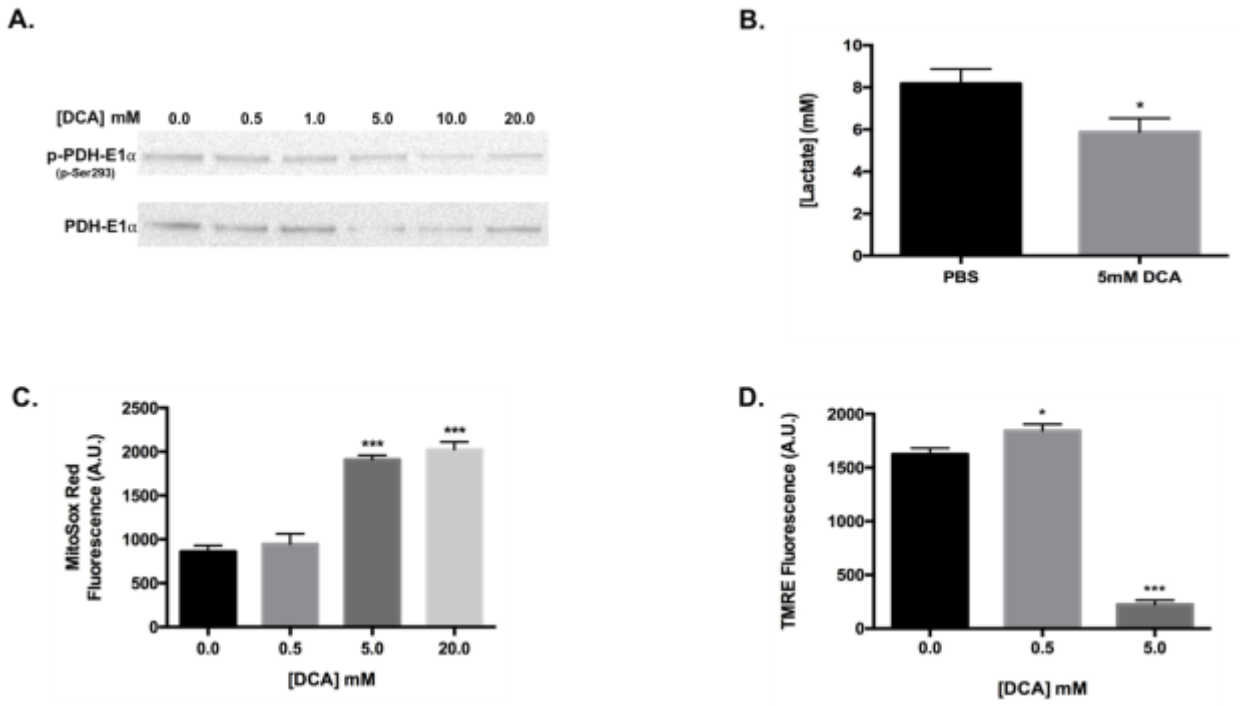

Figure 3.2.1: DCA activates the PDH complex in VM-M3 cells. (A) Western blot analysis of p-PDH-E1α (Ser293) and PDH-E1α in VM-M3 lysates following 4-hour treatment with DCA. **(B)** Quantification of lactate concentration in culture medium following 24-hour incubation with indicated treatment. **(C)** Quantification of average MitoSox Red fluorescence intensity as an indication of VM-M3 superoxide production following 1-hour incubation with DCA. **(D)** Quantification of average tetramethylrhodamine (TMRE) fluorescence intensity as an indication of mitochondrial membrane potential following 4-hour DCA treatment. **(B)** Error bars represent standard error of the mean (SEM) of three experimental replicates. **(C-D)** Error bars represent SEM of a single experiment replicated in triplicate; * $p<0.05$, and *** $p<0.001$.

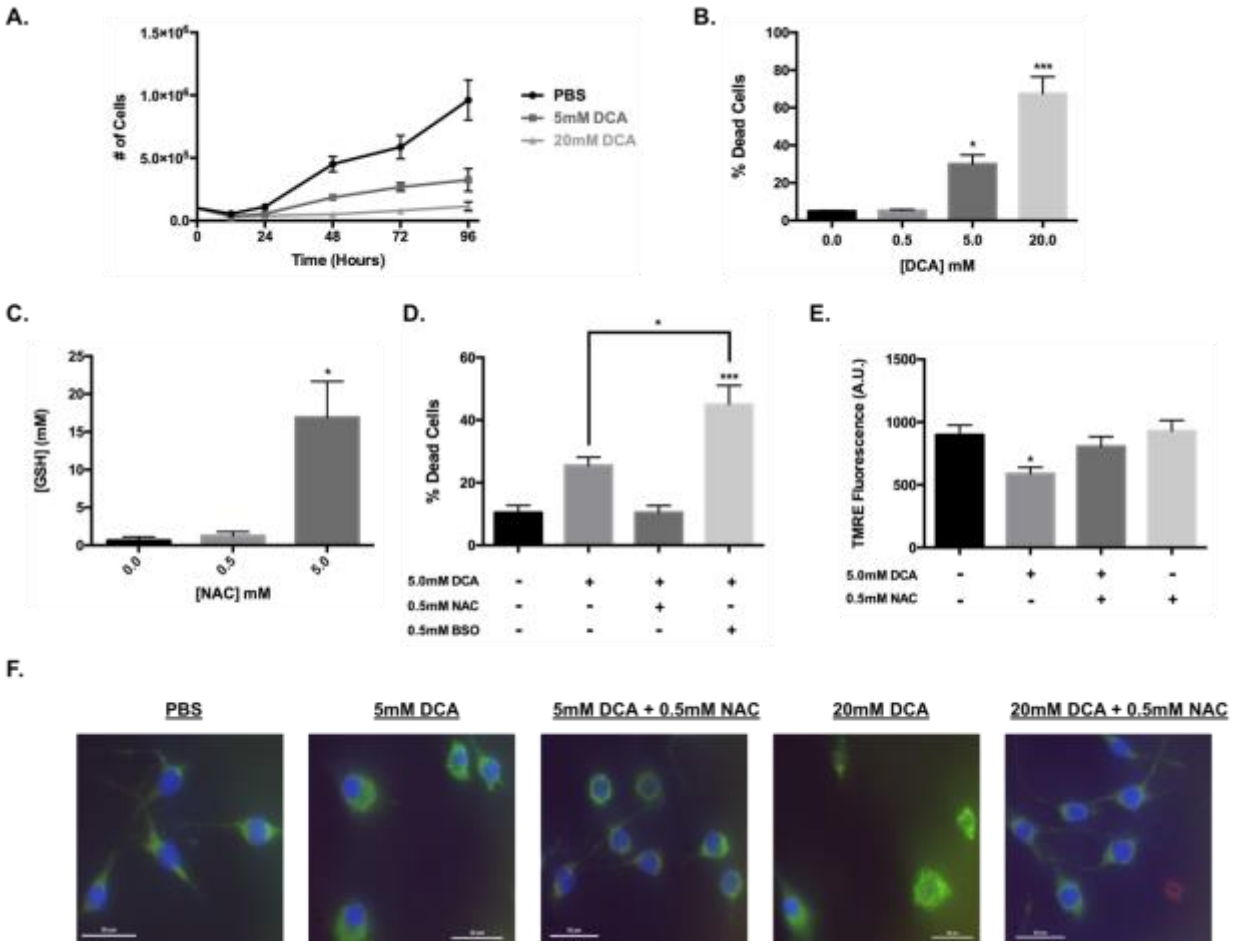

Figure 3.2.2 DCA exhibits oxidative stress-dependent cytotoxicity towards VM-M3 cells. **(A)** Analysis of VM-M3 proliferation over a 96-hour incubation with DCA. **(B)** Analysis of VM-M3 viability following 24-hour treatment with DCA. Bars represent fraction of cells stained positively for ethidium homodimer-I (Ethd-1). **(C)** Quantification of the concentration of reduced GSH in VM-M3 cells following a 4-hour incubation with NAC. **(D)** Evaluation of VM-M3 viability following 24-hour DCA treatment in the presence of modulators of glutathione availability. **(E)** Quantification of average TMRE fluorescence intensity following 4-hour DCA treatment ± N-acetylcysteine (NAC). **(F)** Representative merged immunofluorescent images of VM-M3 cells following 12-hour treatment with DCA ± NAC. Fixed cells were probed for cytochrome c (green) and mitochondrial complex Vα (red) with fluorescent antibodies and counterstained with DAPI (blue). **(A-D)** Error bars represent SEM of three experimental replicates **(E)** Error bars represent SEM of a single experiment replicated in triplicate; * $p<0.05$ and *** $p<0.001$.

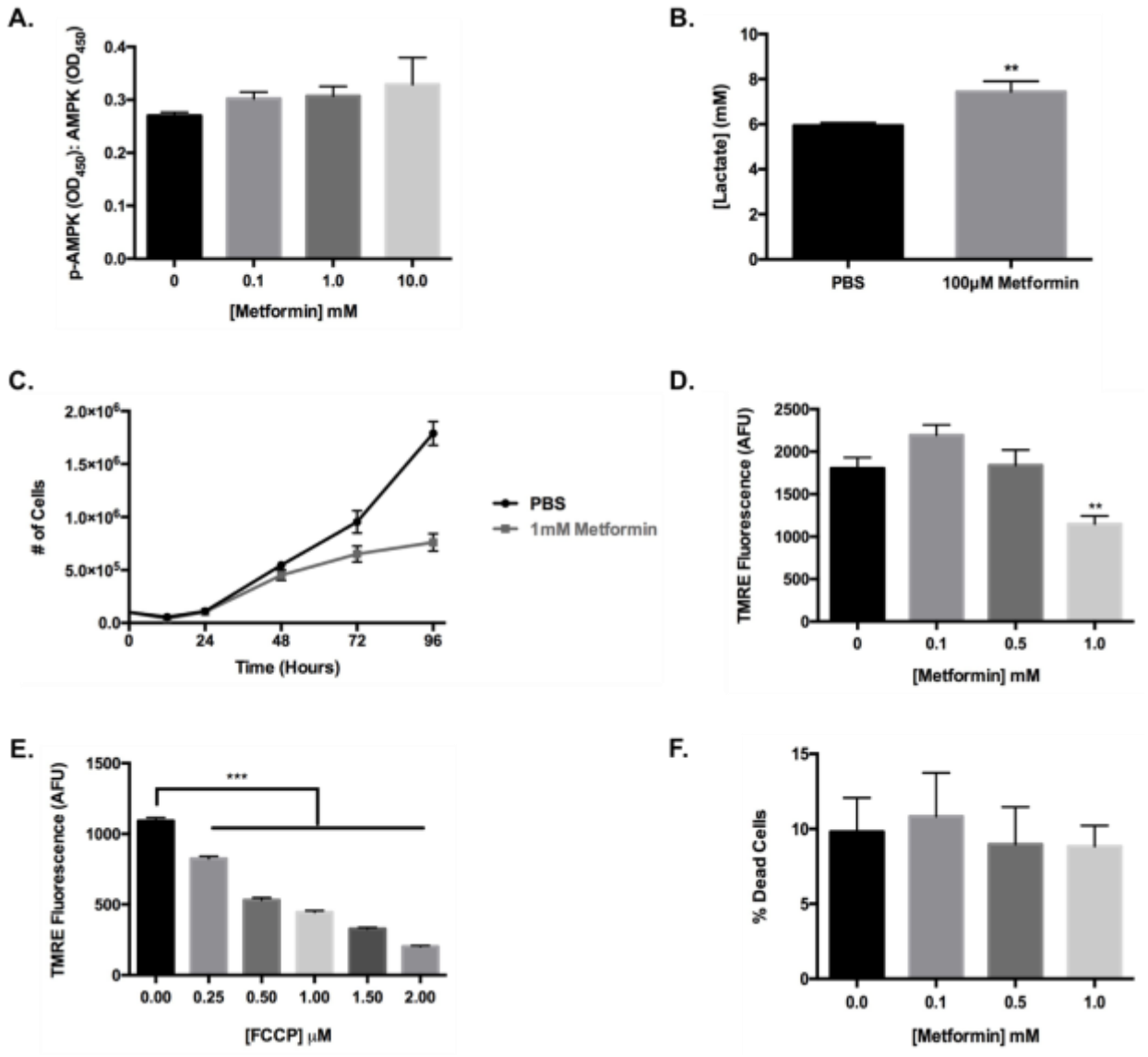

Figure 3.2.3 Metformin uncouples VM-M3 mitochondria independently of cytotoxicity.
(A) Quantification of the phosphorylation state (p-Thr172) of AMPK in VM-M3 cells following a 24-hour incubation with metformin. **(B)** Determination of the lactate concentration in culture medium following 24-hour incubation with vehicle or metformin. **(C)** Analysis of VM-M3 proliferation over a 96-hour incubation with metformin. **(D)** Quantification of average TMRE fluorescence in VM-M3 cells following a 4-hour metformin treatment. **(E)** Determination of VM-M3 cell $\Delta\Psi_m$ following a 4-hour incubation with **FCCP**. **(F)** Analysis of VM-M3 viability following 24-hour treatment with a range of metformin concentrations. **(A, D-E)** Error bars represent SEM of a single experiment replicated in triplicate. **(B-C, F)** Error bars represent SEM of three experimental replicates; **p<0.01 and ***p<0.001.

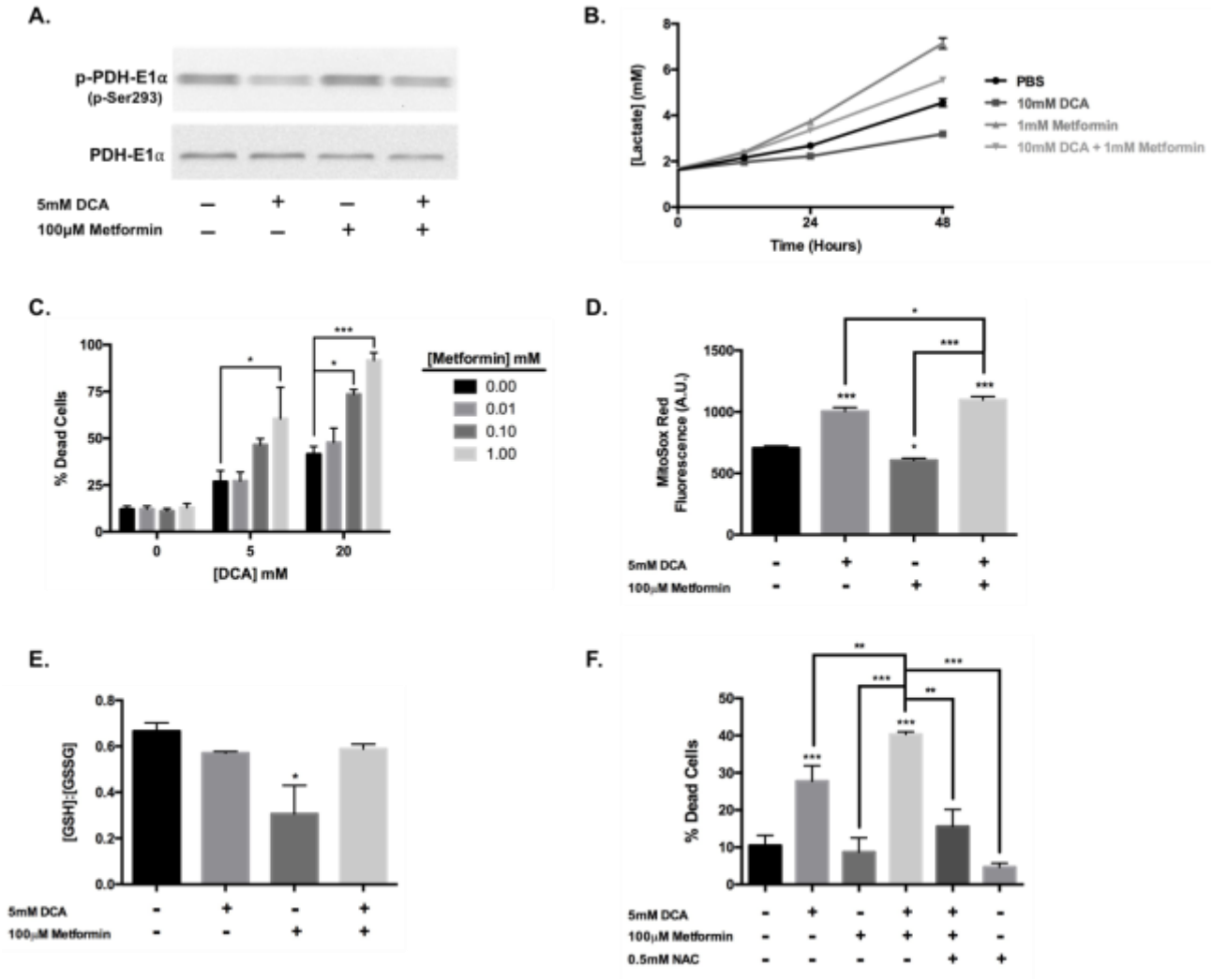

Figure 3.2.4 Metformin enhances DCA cytotoxicity towards VM-M3 cells. (A) Western blot analysis of p-PDH-E1α (Ser293) and PDH-E1α in VM-M3 cell lysates following 4-hour treatment with 5mM DCA and 100μM metformin. **(B)** Determination of lactate in the VM-M3 cell culture medium over a 48-hour incubation period with DCA and metformin. **(C)** Determination of VM-M3 cell viability after combinatorial treatment with DCA and metformin in increasing concentrations. **(D)** Quantification of superoxide production with MitoSox Red following 1-hour treatment with DCA and metformin. (E) Determination of the [GSH]:[GSSG] ratio in VM-M3 cell lysates following a 4-hour treatment with DCA and metformin. **(F)** Determination of cell death following 24-hour treatment with DCA and metformin ± NAC. **(B, D)** Error bars represent SEM of a single experiment replicated in triplicate (**C, E-F)** Error bars represent SEM of three experimental replicates; *p<0.05, **p<0.01, and ***p<0.001.

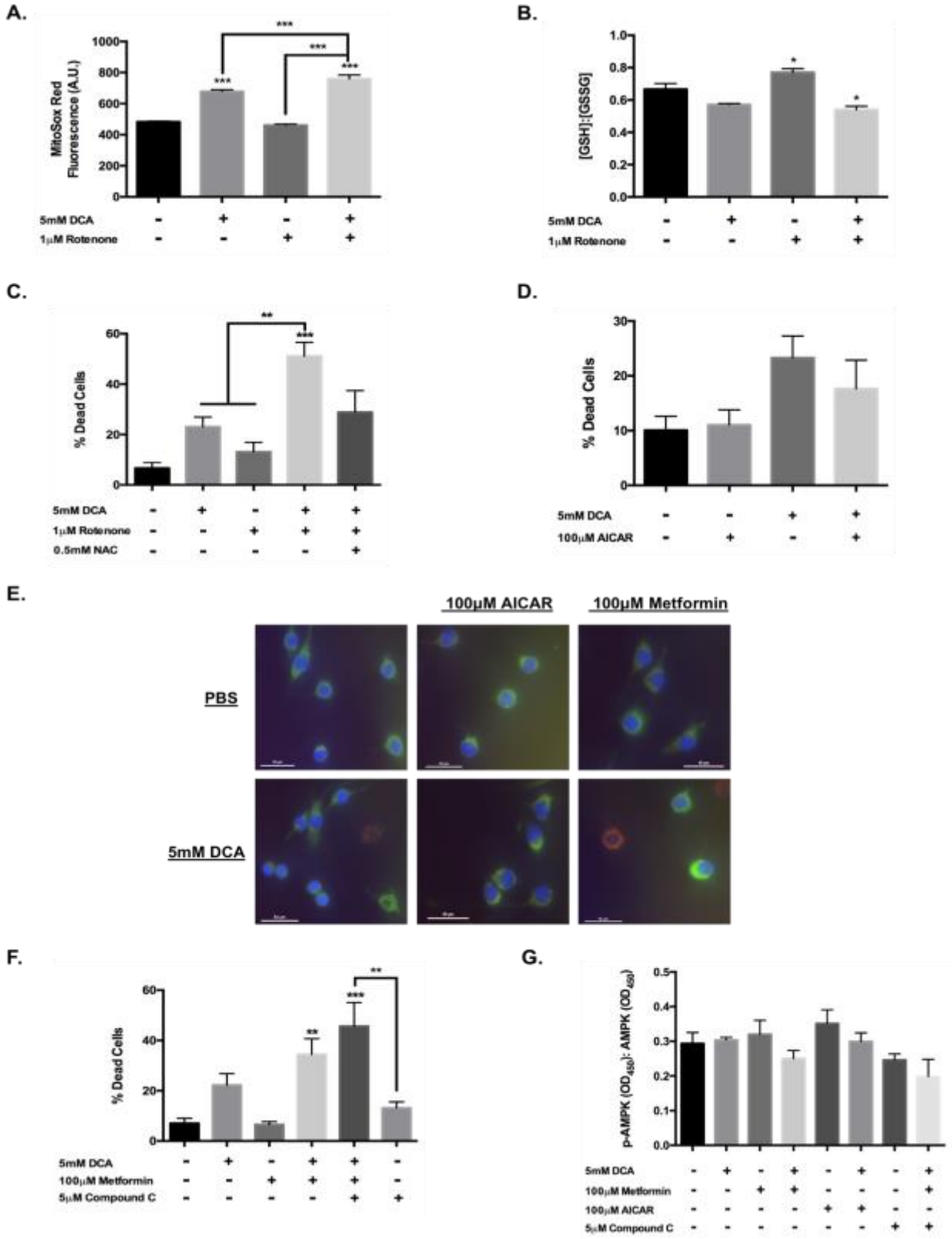

Figure 3.2.5: Complex I Inhibition, but not AMPK activation is required for metformin enhancement of DCA cytotoxicity (Continued on Next Page).

Figure 3.2.5 Complex I inhibition, but not AMPK activation is required for metformin enhancement of DCA cytotoxicity. (A) Average VM-M3 superoxide production following 1-hour treatment with DCA and rotenone. **(B)** Determination of the [GSH]:[GSSG] ratio in VM-M3 cell lysates following 4-hour treatment with DCA and rotenone. **(C)** Analysis of VM-M3 viability following a 24-hour incubation with DCA and rotenone ± NAC. **(D)** Quantification of the fraction of dead VM-M3 cells following a 24-hour treatment with DCA and AICAR. **(E)** Representative merged immunofluorescent images depicting cytochrome c localization in VM-M3 cells following 12-hour treatment with DCA ± AICAR or metformin. (F) Analysis of metformin ± compound C modulation of DCA cytotoxicity towards VM-M3 cells. **(G)** In-cell ELISA analysis of p-AMPKα (Thr172), and AMPKα in VM-M3 cells following 4-hour treatment with modulators of AMPK activation. **(A, G)** Error bars represent SEM of a single experiment replicated in triplicate **(B-D, F)** Error bars represent SEM of three experimental replicates; *p<0.05, **p<0.01 and ***p<0.001.

3.2.2 Results & Discussion

As is seen with GBM, VM-M3 cells exhibit robust basal phosphorylation of the pyruvate dehydrogenase complex (Fig. 3.2.1A). Consistent with its mechanism of action, DCA treatment reduced phosphorylation of the E1α subunit of the PDH complex in a concentration dependent manner. As PDH complex phosphorylation is associated with Warburg metabolism, we sought to determine if DCA treatment alters VM-M3 lactate production (1). A 24-hour incubation with 5mM DCA resulted in a 28.1% reduction in lactate present in the culture medium, suggesting a shift towards glucose oxidation and away from glucose fermentation (Fig. 3.2.1B).

Given that oxidative metabolism is intrinsically linked to ROS generation, we evaluated whether DCA activation of pyruvate dehydrogenase altered ROS production in VM-M3 cells. MitoSox Red fluorescent microscopy indicated a concentration-dependent increase in superoxide production following 1-hour DCA treatment (Fig. 3.21C). This suggests that DCA increases ROS production in VM-M3 cells through activation of the PDH complex.

Changes in flux through the ETC can alter mitochondrial membrane potential, therefore we utilized tetramethylrhodamine (TMRE) fluorescence microscopy to determine changes in $\Delta\Psi_m$ associated with DCA activity (2). A 4-hour incubation with

5mM DCA resulted in significant mitochondrial depolarization, whereas treatment with a lower concentration of 500μM promoted hyperpolarization of VM-M3 mitochondria (Fig. 3.2.1D). The increase in $\Delta\Psi_m$ observed with 500μM DCA treatment is indicative of increased ETC flux and associated movement of protons into the IMS, again suggesting activation of glucose oxidation. DCA-induced mitochondrial depolarization occurred after treatment with a concentration that also promoted superoxide production. As described previously, abundant oxidative stress can damage membrane lipids and thus disrupt mitochondrial membrane integrity, ultimately leading to loss of $\Delta\Psi_m$ and apoptotic initiation (3). Indeed, we show that the addition of the antioxidant N-acetylcysteine (NAC) maintained $\Delta\Psi_m$ in the presence of DCA (Fig. 3.2.2E), suggesting that the loss of membrane potential with 5mM DCA treatment is associated with the observed increase in superoxide.

Moreover, we found that DCA-induced ROS production coincided with cytotoxicity in a concentration-dependent fashion (Fig. 3.2.2B). Treatment with 5mM DCA was only mildly cytotoxic towards VM-M3 cells whereas 20mM induced significant cell death despite no apparent difference in the magnitude of ROS induction. Thus, the difference in cytotoxicity is likely resultant from sustained inhibition of PDK with the higher concentration of DCA, permitting continuous flux of pyruvate into the mitochondria. In agreement with the observed loss of membrane potential at cytotoxic concentrations, 20mM DCA promoted mitochondrial release of cytochrome c after a 12-hour incubation (Fig. 3.2.2F).

Whereas vehicle-treated controls exhibit diffuse cytochrome c and mitochondrial complex Vα co-localized fluorescence, indicative of an extensive mitochondrial network,

VM-M3 cells treated with 5mM DCA display punctate co-localized fluorescence that suggests enhanced mitochondrial fission (Fig.3.2.2F). DCA has been shown to induce mitophagy at non-cytotoxic concentrations in response to increases in oxidative stress (4). Mitophagy permits cell resilience in the presence of mitochondrial stress through enhanced mitochondrial fission facilitating the degradation of damaged portions of the mitochondrial network (5). Together, these results suggest that DCA induces oxidative stress that at upon reaching a certain threshold promotes the loss in mitochondrial integrity subsequently leading to the initiation of caspase-dependent VM-M3 cell death, which is consistent with the mechanism of cytotoxicity previously described for DCA (6-13). Below this threshold, VM-M3 cells likely employ cell survival mechanisms such as mitophagy to persist under DCA-induced oxidative stress, however these compensatory pathways likely restrict proliferative capacity. As such, treatment with 5mM DCA blunted VM-M3 proliferation, whereas treatment with 20mM completely inhibited proliferation (Fig. 3.2.2A)

To further show an association between the observed increases in oxidative stress and cell death with DCA treatment, we evaluated the effects of modifying antioxidant capacity on DCA cytotoxicity. Co-incubation of 5mM DCA with the glutathione synthesis inhibitor buthionine sulfoximine (BSO) significantly enhanced cytotoxicity. Conversely, addition of NAC, which provides an exogenous cysteine substrate for glutathione synthesis attenuated the modest increase in cell death associated with 5mM DCA treatment (Fig. 3.2.2D). This was confirmed through immunofluorescent microscopy, which showed retention of an expansive mitochondrial network with resident cytochrome c following incubation with both DCA and NAC (Fig.

3.2.2F). NAC treatment corresponded with increased levels of reduced GSH in VM-M3 cells (Fig. 3.2.2C).

We next sought to characterize the effect of metformin on VM-M3 cells. Metformin increased the proportion of phosphorylated AMPK in a concentration dependent manner, suggesting that metformin treatment promoted energetic stress in VM-M3 cells (Fig. 3.2.3A). Typical of AMPK activation, metformin enhanced lactate export, indicating an increase in glycolytic metabolism (Fig. 3.2.3B). Furthermore, VM-M3 proliferation was blunted with metformin treatment, which is consistent with the previously reported cytostatic activity of metformin resultant from restricted anabolic metabolism (Fig. 3.2.3C) (14, 15).

At a concentration of 100uM, metformin promoted mitochondrial hyperpolarization, whereas VM-M3 $\Delta\Psi_m$ decreased at a concentration of 1mM after a 4-hour incubation (Fig. 3.2.3D). This is indicative of complex I inhibition; whereby acute treatment with lower concentrations of metformin restrict electron flux, leading to accumulation of H^+ in the IMS following NADH oxidation. Increasing the concentration of metformin enhances the rate of this inhibition, resulting in a more rapid induction of energetic stress. The compensatory restriction of glucose oxidation associated with AMPK activation, leads to a reduction in ETC flux and a subsequent decrease in $\Delta\Psi_m$. Moreover, metformin is shown to slightly uncouple mitochondria to relieve the buildup of H^+ in the IMS (16). VM-M3 cells respond to the uncoupler carbonyl cyanide 4-(fluoromethoxy)phenylhydrazone (FCCP) suggesting that it is possible that metformin's effect on VM-M3 $\Delta\Psi_m$ is a result of multiple converging mechanisms (Fig. 3.2.3E). Unlike with DCA treatment, metformin depletion of $\Delta\Psi_m$ is independent of cytotoxicity

(Fig 3.2.3F). Collectively, these results suggest that metformin imposes energetic stress on VM-M3 cells through inhibition of complex I that results in AMPK activation and a rewiring of metabolism to restrict growth yet sustain viability.

As enhanced glucose oxidation is central to the anti-cancer activity exhibited by DCA towards VM-M3 cells, metformin restriction of mitochondrial glucose metabolism could prohibit any potential synergy achieved with the combination. However, we show that DCA reduces PDH phosphorylation even in the presence of metformin (Fig. 3.2.4A). Moreover, DCA attenuates the increase in lactate production associated with metformin treatment, suggesting that DCA reverses the compensatory enhancement of aerobic glycolysis induced by metformin (Fig. 3.2.4B).

Consistent with our hypothesis, the addition of metformin significantly enhanced superoxide production in DCA treated cells even though metformin alone reduces ROS levels (Fig.3.2.4D). Metformin inhibition of complex I is associated with a restriction of ROS production in the reverse direction, preventing electrons released at complex II from $FADH_2$ oxidation to reduce iron sulfur clusters associated with complex I (16). Sustained TCA cycle-dependent NADH production in the presence of complex I inhibition leads to an increase in the NADH/NAD^+ ratio, which diminishes reducing potential (17). In an attempt to maintain redox balance, electrons are prematurely lost from the ETC and generate ROS in the forward direction as a consequence (18, 19). As such, DCA induction of glucose oxidation in the presence of metformin inhibition of complex I led to the observed increase in superoxide production.

Coinciding with the increase in ROS production, DCA ± metformin reduced the [GSH]/[GSSG] ratio in VM-M3 cells, indicating an increase in oxidative stress (Fig.

3.2.4E). Strikingly, metformin treatment significantly reduced the proportion of reduced [GSH] despite the noted reduction in superoxide production. Rather, this is likely a result of diminished glutathione synthesis, which has been previously demonstrated with metformin treatment (20). This restriction of GSH production would mimic an increase in oxidative stress.

The addition of metformin significantly enhanced DCA cytotoxicity towards VM-M3 cells that was amplified with increasing concentrations of either agent (Fig. 3.2.4A). The increase in oxidative stress promoted by metformin addition to DCA treatment was shown to be necessary for this enhanced cytotoxicity as addition of NAC attenuated the loss of VM-M3 viability associated with the DCA and metformin combination (Fig. 3.2.4F). This is consistent with recent reports that demonstrated that metformin enhanced DCA cytotoxicity towards breast cancer cells in an oxidative stress-dependent manner (21, 22).

To further elucidate the contribution of complex I inhibition to metformin's enhancement of DCA cytotoxicity, we examined the impact of rotenone, a bona fide complex I inhibitor, on DCA activity. Rotenone treatment did not affect VM-M3 superoxide production alone, but significantly enhanced the pro-oxidant effect of DCA (Fig. 3.2.5A). In contrast to metformin, rotenone treatment increased the [GSH]/[GSSG] ratio in VM-M3 cells (Fig. 3.2.5B). However, like metformin, the addition of rotenone significantly augmented DCA cytotoxicity. Additionally, rotenone enhancement of DCA anti-cancer activity was partially attenuated by the antioxidant NAC, suggesting a requirement for the observed increase in oxidative stress (Fig. 3.2.5C). These results show that metformin and rotenone have a strikingly similar effect on DCA activity.

As metformin's cellular activity is traditionally associated with AMPK activation, we sought to determine if AMPK is required for metformin amplification of DCA cytotoxicity towards VM-M3 cells. The addition of DCA, which alone did not modify AMPK phosphorylation, attenuated metformin modulation of AMPK activation (Fig. 3.2.5F). 5-Aminoimidazole-4-carboxamide ribonucleotide (AICAR) is an analog of 5'-AMP and is a known activator of AMPK (23). We too show that AICAR increases stimulatory phosphorylation of AMPK and that this is blunted by DCA co-treatment (Fig. 3.2.5F). AICAR treatment did not promote VM-M3 cell death and was slightly cytoprotective in combination with DCA (Fig. 3.2.5D). This was further evidenced in immunofluorescent detection of cytochrome c localization, which depicts a reduction in mitochondrial stress with the combinatorial treatment (Fig. 3.2.5E). This is in contrast to metformin co-treatment, which increased cytochrome c release in DCA treated cells (Fig. 3.2.5E). Moreover, use of the AMPK inhibitor, compound c, further enhanced the efficacy of dichloroacetate and metformin in combination (Fig. 3.2.5F). Collectively, these results suggest that complex I inhibition, but not AMPK stimulation is necessary for metformin enhancement of DCA cytotoxicity. In fact, AMPK activation likely diminishes the synergy between the two agents, which is consistent with AMPK's role as an energy sensor and survival mediator (24). This suggests that the combination may be most effective in the absence of AMPK, such as in LKB1-deficent tumors (25).

3.3 DCA and Metformin Inhibit VM-M3 Tumor Progression As Individual Agents, But Do Not Exhibit Synergy *in vivo*

3.3.1 Figures

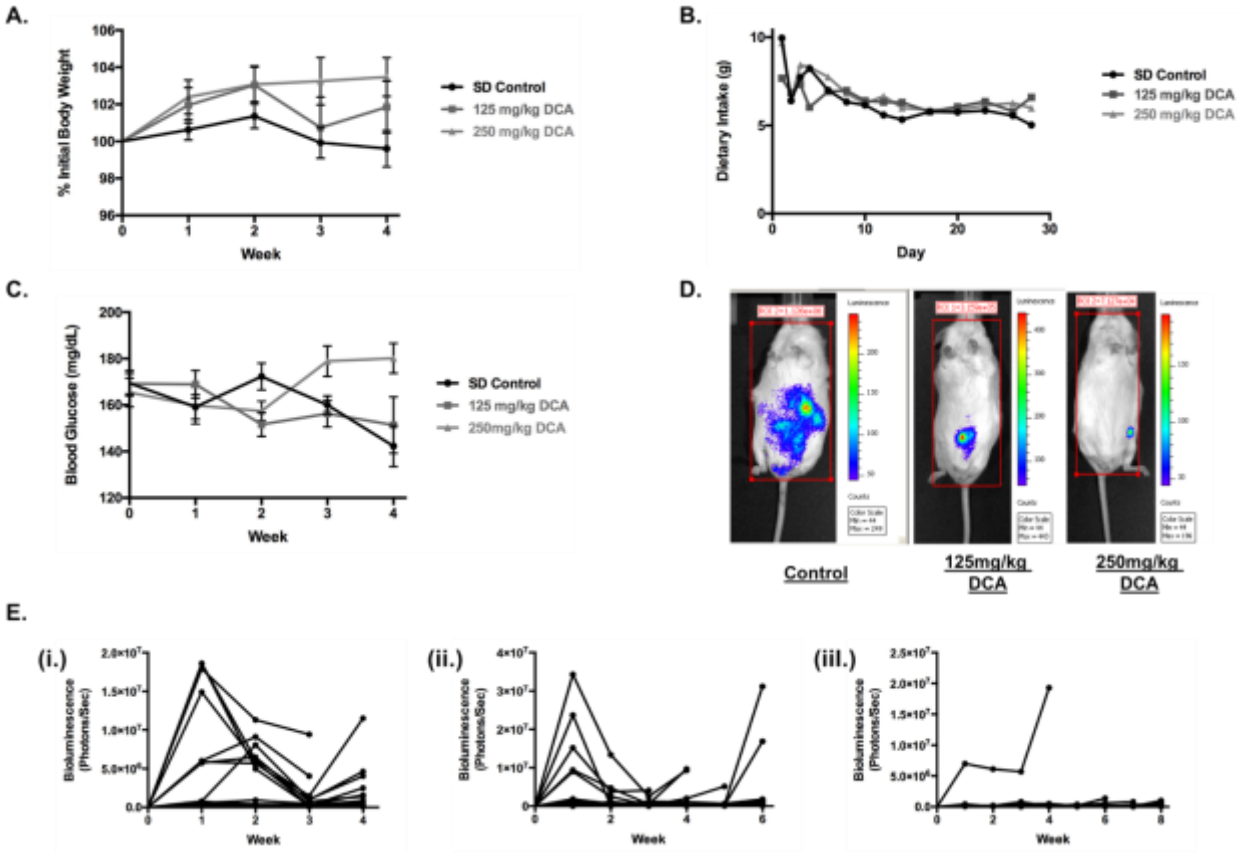

Figure 3.3.1 DCA treatment slows tumor growth in VM-M3 tumor-burdened mice. (A) Average weekly change in weight from baseline for control and DCA-treated animals for the first 4 weeks of treatment. **(B)** Average daily food intake of control and DCA-treated animals. **(C)** Average weekly blood glucose levels of control and DCA-treated mice for the first 4 weeks of treatment. **(D)** Representative bioluminescent images of control, 125mg/kg DCA and 250mg/kg DCA-treated animals at 4 weeks post VM-M3 cell implantation. **(E)** Quantification of individual weekly bioluminescent signals from (i) control (ii) 125mg/kg DCA and (iii) 250mg/kg DCA treated mice. **(A-C)** Error bars represent SEM of the treatment group.

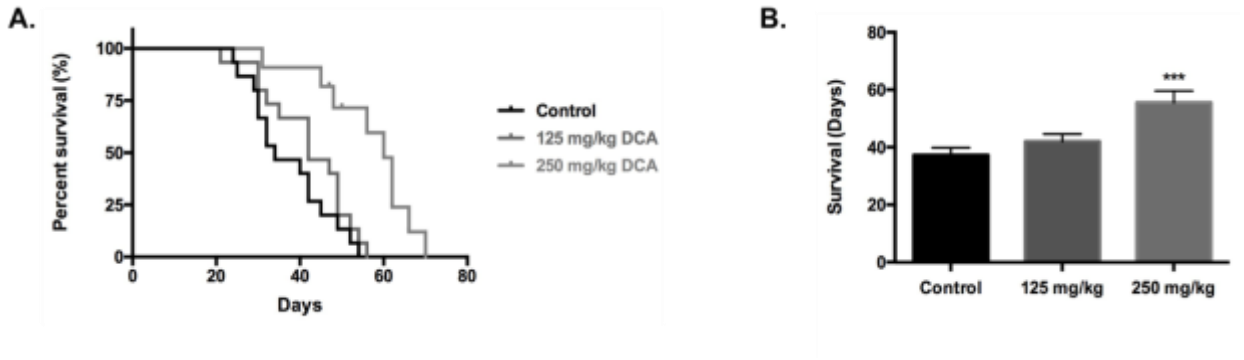

Figure 3.3.2 DCA treatment prolongs survival in VM-M3 tumor-burdened mice. (A) Kaplan-Meier survival curve of treatment groups. **(B)** Mean survival time of control and DCA-treated animals. Error bars represent SEM for each group; ***p<0.001.

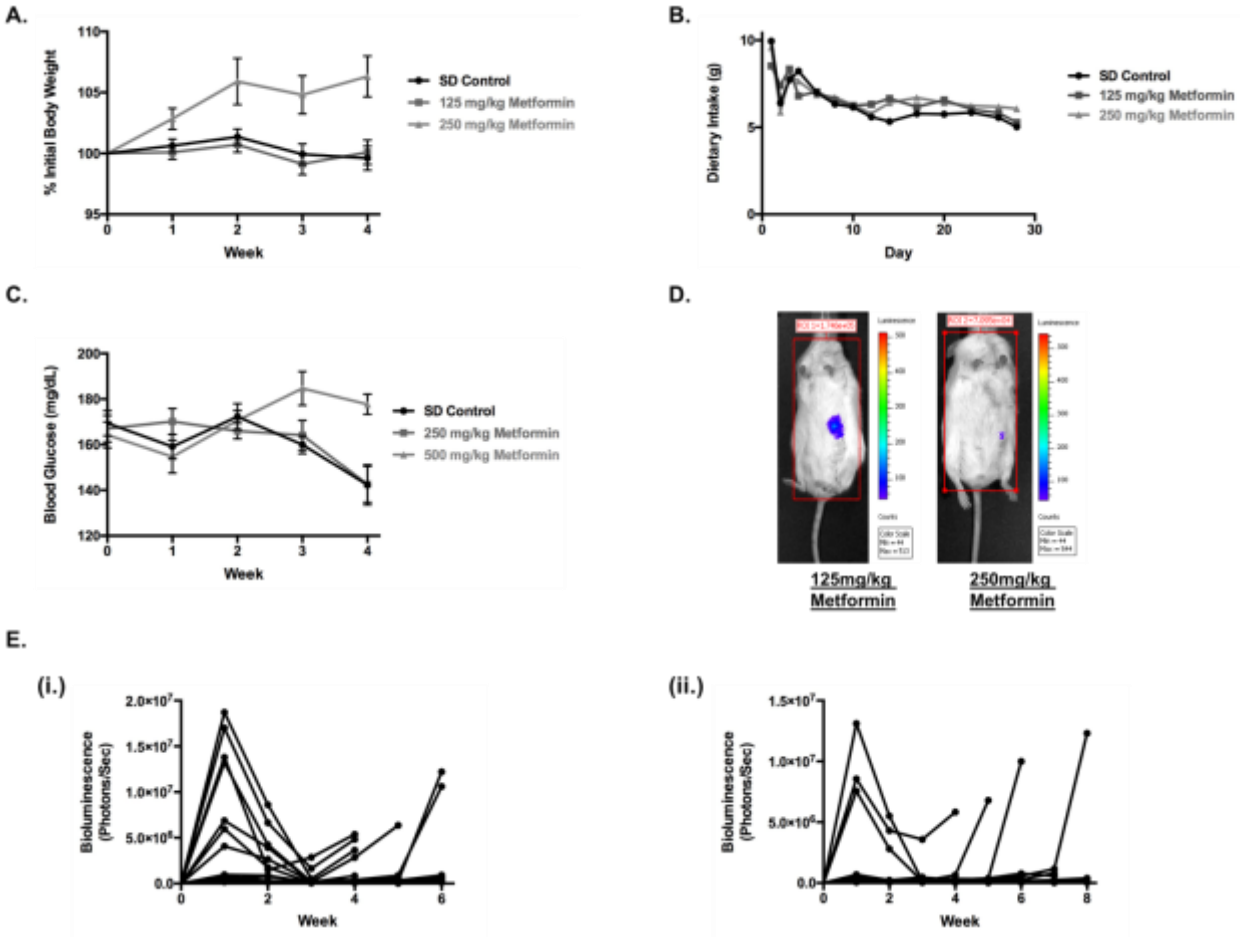

Figure 3.3.3 Metformin treatment slows tumor growth in VM-M3 tumor-burdened mice. (A) Average weekly change in weight from baseline for control and metformin-treated animals for the first 4 weeks of treatment. **(B)** Average daily food intake of control and metformin-treated animals. **(C)** Average weekly blood glucose levels of control and metformin-treated mice for the first 4 weeks of treatment. **(D)** Representative bioluminescent images of control, 125mg/kg metformin and 250mg/kg metformin-treated animals at 4 weeks post VM-M3 cell implantation. **(E)** Quantification of individual weekly bioluminescent

signals from (i) 125mg/kg DCA and (ii) 250mg/kg DCA treated mice. **(A-C)** Error bars represent SEM of the treatment group.

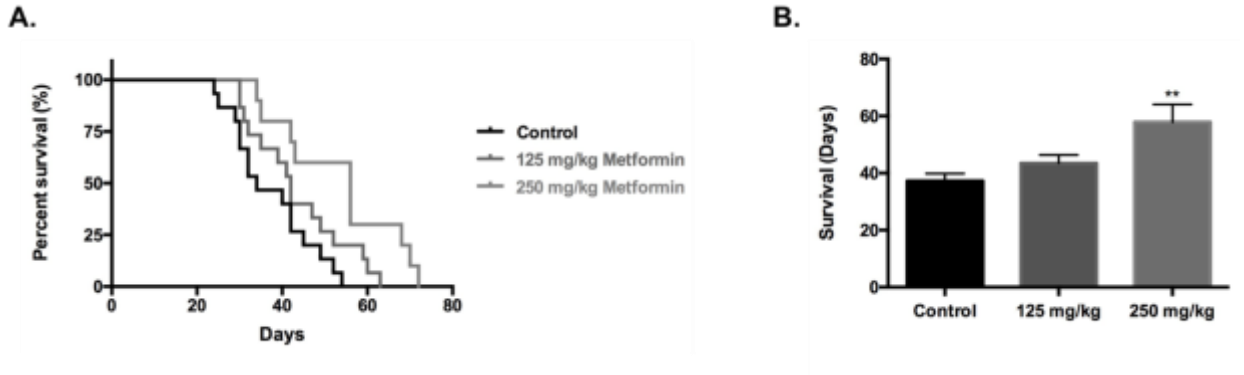

Figure 3.3.4 Metformin treatment prolongs survival in VM-M3 tumor-burdened mice. (A) Kaplan-Meier survival curve of control and metformin treatment groups. **(B)** Mean survival time of control and metformin-treated animals. Error bars represent SEM for each group; **p<0.01.

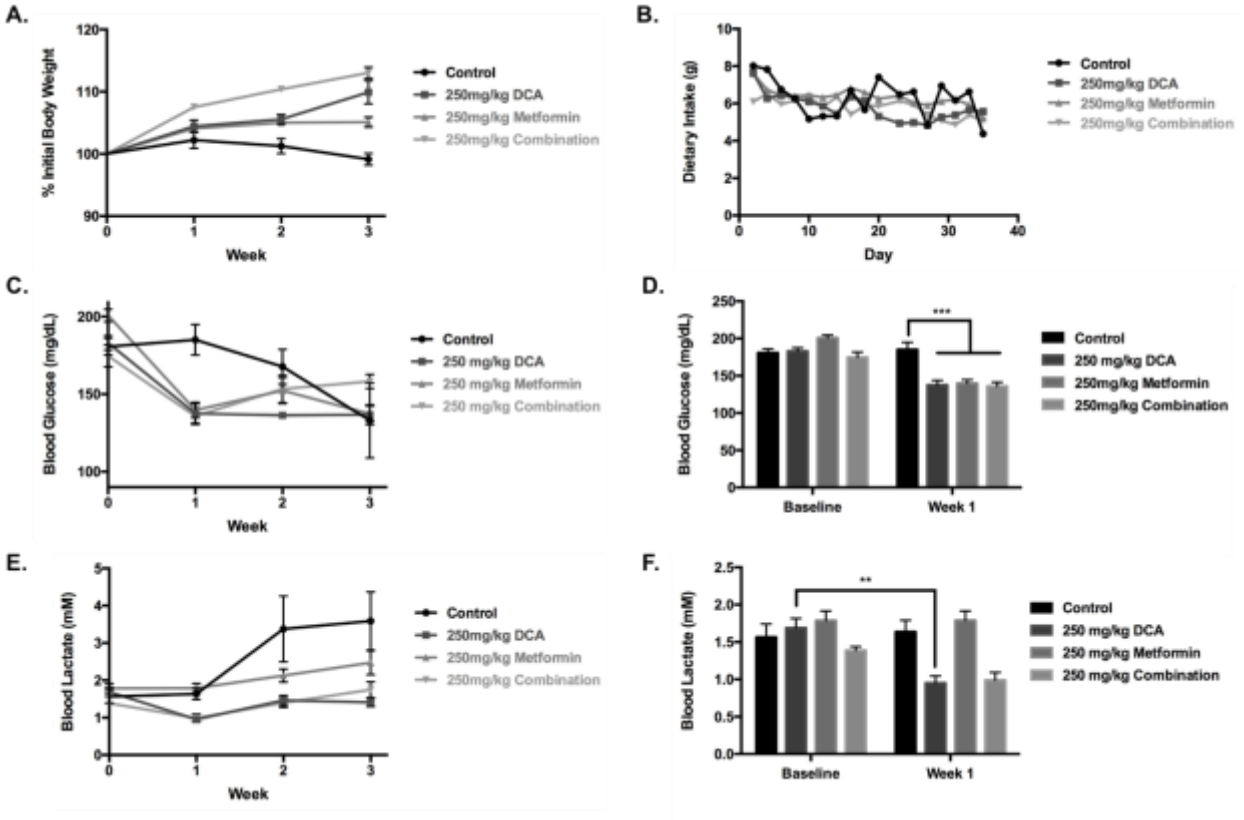

Figure 3.3.5 Metformin co-treatment does not diminish lactate-reducing effect of DCA (Continued on Next Page).

Figure 3.3.5 Metformin co-treatment does not diminish lactate-reducing effect of DCA. (A) Average weekly change in weight from baseline for control and treatment groups for the first 3 weeks of treatment. **(B)** Average daily food intake of control and treated animals. **(C)** Average weekly blood glucose levels of control and treated mice over the first 3 weeks of treatment. **(D)** Average blood glucose levels at baseline and after one week of treatment for each group. **(E)** Average blood lactate levels of control and treated animals over the first 3 weeks of treatment. **(F)** Average blood lactate levels of control and treated mice at baseline and following one week of treatment. Error bars represent SEM of the treatment group; **p<0.01 and ***p<0.001.

A.

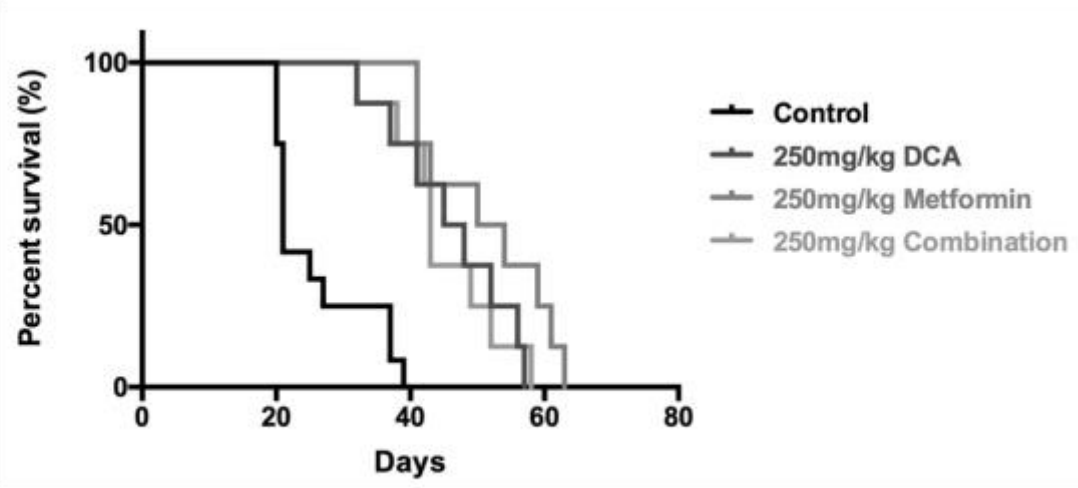

B.

Cohort	N	Median Survival	% Increase in Median Survival	Mean Survival	% Increase in Mean Survival
Control	12	21.0	-	25.8	-
250mg/kg DCA	8	46.5	121.4%	46.0	78.6%
250mg/kg Metformin	8	52.0	147.6%	51.5	100.0%
250mg/kg Combination	8	43.0	104.8%	44.6	73.2%

Figure 3.3.6 The combination of DCA and metformin does not provide further survival benefit over either individual treatment. (A) Kaplan-Meier survival curves for control, 250mg/kg DCA, 250mg/kg metformin and 250mg/kg combination treatment groups. **(B)** Notation of cohort size, median and mean survival times, and the percent increase from control for those measures.

3.3.2 Results & Discussion

To establish if our observations of *in vitro* efficacy of a DCA and metformin combination towards VM-M3 cells translated to an *in vivo* environment, we utilized the VM-M3 model of metastatic glioblastoma. As both of these agents are delivered orally in the clinic, we chose to integrate these agents into a standard rodent diet (2018 Teklad Global 18% Protein Rodent Diet; Harlan Laboratories) at a defined dose based on previous observation that a 30g mouse of this strain eats 5-6g of food per day. The addition of either agent did not alter the palatability of the diet and animals ate the expected amount of food throughout the study until near end of life (Figs. 3.3.1B, 3.3.3B, 3.3.5B). This is indicative of the anorexia associated with cancer cachexia, the multi-modal syndrome marked by debilitating loss of adipose and muscle mass seen in patients near end of life. This was further evidenced by a drop in body weight observed towards the end of life, especially in the control and 125mg/kg-dosed groups (Figs. 3.3.1A, 3.3.3A).

Both DCA and metformin were well tolerated by VM/dk mice. We did not observe any alterations in animal behavior or obvious gross physiological changes in cancer-free VM/dk mice following DCA and/or metformin treatment. Moreover, DCA and metformin treatments did not promote weight loss in these mice (Figs. 3.3.1A, 3.3.3A).

In an attempt to achieve efficacious dosing in this model, we tested low (125mg/kg) and high (250mg/kg) doses of each agent based on the findings of previous reports (10, 11, 26-28). As both DCA and metformin are established modulators of systemic metabolism, we evaluated the effects of these agents on circulating blood glucose. We did not observe an effect of DCA on systemic glucose levels during these

dosing studies (Fig. 3.3.1C). Likewise, metformin did not affect blood glucose levels at either dose (Fig. 3.3.3C). Though metformin is used clinically in T2DM patients for its activity in reducing circulating glucose, it does not always reduce blood glucose in non-diabetic patients (29).

In regards to VM-M3 tumor growth and the survival of tumor-burdened VM/dk mice, DCA and metformin behaved similarly. Low dose treatment of DCA and metformin resulted in reduced tumor burden at 4 weeks post tumor cell implantation. (Figs. 3.3.1D, 3.3.3D, Appendix B). This was associated with a reduction in bioluminescent indications of metastasis, marked by a lack of signal separate from the site of injection. 125 mg/kg DCA treatment caused a delay in VM-M3 tumor expansion (Fig. 3.3.1Eii). However, this only resulted in a non-significant 12.5% increase in survival (Fig 3.3.2B). Similarly, 125mg/kg metformin treatment promoted a slight delay in tumor expansion but only prolonged survival by 16.4% (Figs. 3.3.3Ei, 3.3.4B).

Strikingly, high doses of both DCA and metformin had a remarkable tumor suppressive effect. 250mg/kg DCA treatment likely interfered with the initial take of VM-M3 cells, as the bioluminescent signal for these animals at week 1 is markedly lower than controls (Fig. 3.3.1Ei, iii). High-dose DCA treatment prohibited expansion of primary VM-M3 tumors and distant metastasis, shown by a near complete lack of diffuse signal at 4 weeks post tumor cell implantation (Figs. 3.3.1D, 3.3.1Eiii, Appendix B)**.** This was associated with a significant 48.8% increase in mean survival of tumor-burdened mice (Fig. 3.3.2B). These data are consistent with the cytostatic effect of DCA observed in several other solid tumor models (9, 12). Alternatively, DCA increased

apoptosis in a model of Dalton's Lymphoma, suggesting that DCA likely elicits tumor-specific effects *in vivo* (10).

Administration of metformin at a dose of 250mg/kg had a mixed effect on VM-M3 tumor cell take. High-dose metformin reduced the intensity of the typical spike in signal upon injection for some of the cohort, but mimicked DCA in restricting early primary tumor growth for a greater proportion of this group (Fig. 3.3.3Eii). 250mg/kg metformin attenuation of VM-M3 tumor growth was associated with a significant 55.1% in mean survival (Fig. 3.3.4B). Metformin dosing of 250mg/kg has previously been shown to reduce tumor growth in models of colon and lung cancer (14, 30).

As the high doses of both agents were most effective in our model, we next evaluated the efficacy of a combination of DCA and metformin at doses of 250mg/kg. During this study we were forced to alter the protocol for preparing VM-M3 cells for implantation. With great frequency we began to lose bioluminescent signal from mice regardless of treatment group two weeks post-injection, suggesting a substantial host response towards the VM-M3 cells that eradicated the tumors. We hypothesized that despite washing with PBS prior to injection, residual FBS in the injection volume was promoting an antigenic response towards the VM-M3 cells (31). Thus, we serum-starved the VM-M3 cells overnight prior to injection. Indeed, this led to retention of a bioluminescent signal beyond week 2 post-injection. However, this did alter the aggressiveness of the model, as control animals succumbed to VM-M3 tumor burden quicker than before.

Median survival for control animals under the new injection protocol was 21 days compared to 34 days for the original protocol (Figs 3.3.2A, 3.3.6A). Though the model

was more aggressive, it did not present other overt differences. Control animals still exhibited signs of cachexia following initial maintenance of baseline weight, food intake and blood glucose levels until nearing end of life (Figs. 3.3.5A-C). Furthermore, the new protocol did not diminish the effects of DCA and metformin previously observed, in fact we report greater efficacy with these agents at a dose of 250mg/kg. Again, neither DCA or metformin treatment promoted weight loss or affected the dietary intake of treated animals (Figs. 3.3.5A-B).

Differing from our previous findings, both DCA and metformin promoted a significant reduction in circulating glucose levels after one week of treatment (Fig. 3.3.5D). This was maintained in the DCA-treated animals but not in metformin-treated animals suggesting that the non-diabetic mice may become tolerant to the hepatic effects of metformin over time. It has been hypothesized that DCA may influence blood glucose through activation of peripheral glucose utilization, which may be particularly useful for diabetic patients (32). The differential effects of these agents on blood glucose in mice under the two protocols may be linked to the presumed inflammation associated with our original protocol. VM-M3 cell stimulation of the host immune system may be associated with induction of the hypothalamic-pituitary-adrenocorticoid axis that results in glucocorticoid release (33, 34). These steroid hormones promote maintenance of glucose levels during immune responses in part to meet the energetic requirements of immune mediators (34). This activity may have blunted the effects of DCA and metformin on blood glucose during our dose-response studies.

As both of these agents alter glucose metabolism, we evaluated their effects on circulating lactate levels as an indicator of their respective activities. The blood lactate

levels of control animals increased with disease progression (Fig. 3.3.5E). This is likely a result of liver metastasis and disruption of hepatic function leading to inhibition of the Cori cycle. Moreover, substantial tumor burden may contribute to the increase in blood lactate as a result of the robust glycolytic metabolism of VM-M3 cells. Consistent with its mechanism of action, DCA significantly reduced blood lactate levels from baseline following one week of treatment (Fig. 3.3.5F). Metformin did not affect blood lactate levels in VM-M3 tumor-burdened mice, which is consistent with the literature despite clinical fears over lactic acidosis with metformin treatment (35). Phenformin, which is structurally similar to metformin, is 30 times more potent due to increased lipophilicity has been removed from the clinic because it induces lactic acidosis. However, reports of lactic acidosis with metformin treatment have only been associated with co-morbid kidney dysfunction (36, 37).

DCA treatment significantly prolonged survival on VM-M3 tumor-burdened mice, increasing mean survival 78.6% over controls (Figs. 3.3.6A-B). Likewise, metformin had a significant effect on the survival of cancer-burdened mice (Fig. 3.3.6A). In fact, metformin administration doubled the survival time of these mice (Fig. 3.3.6B). However, the combination of DCA and metformin did not provide a further survival benefit over either individual agent. The combination did however mimic DCA treatment in reducing both blood glucose and blood lactate levels, which suggests that similar to our *in vitro* findings, DCA can bypass the potential compensatory increase in glycolysis associated with metformin treatment.

The lack of observed synergy with the combination is likely a result of therapeutic resistance, which as previously described contributes the clinical failure of most cancer

therapies (38). The confluence of genetic heterogeneity and the tumor microenvironment contribute to heterogeneity in tumor metabolism. This is characterized by distinct regions of the tumor that exhibit differential glucose metabolism. Though the nature of the tumor vasculature system contributes to Warburg metabolism characteristic of the bulk tumor, those regions of the tumor that are well perfused often exhibit robust oxidative metabolism (39). Those regions may be inherently resistant to the effects of the combination and upon selection against the rest of the tumor, would be allowed to expand and drive progression of VM-M3 tumors. Moreover, those tumor cells that have a more robust antioxidant capacity may persist in response to the oxidative stress induced by DCA and metformin, allowing that fraction of the tumor to drive resistance. Therefore, any synergistic effect in targeting VM-M3 tumors with the combination could have been lost as a function of rapidly eradicating the susceptible proportion of the tumor population, allowing for proliferation of resistant tumor cells, ultimately leading to disease progression.

3.4 References

1. Jha, MK. & Suk, K. Pyruvate dehydrogenase kinase as a potential therapeutic target for malignant gliomas. *Brain Tumor Res. Treat.* **1**, 57-63 (2013).
2. Hüttemann, M. *et al.* Regulation of oxidative phosphorylation, the mitochondrial membrane potential, and their role in human disease. *J. Bioenerg. Biomembr.* **40,** 445–456 (2008).
3. Orrenius, S. Reactive oxygen species in mitochondria-mediated cell death. *Drug Metab. Rev.* **39,** 443–55 (2007).
4. Pajuelo-Reguera, D., Alan, L., Olejar, T. & Jezek, P. Dichloroacetate stimulates changes in the mitochondrial network morphology via partial mitophagy in human SH-SY5Y neuroblastoma cells. *Int. J. Oncol.* **46**, 2409-2418 (2015).
5. Chourasia, AH., Boland, ML. & Macleod, KF. Mitophagy and cancer. *Cancer Metab.* **26**, 4 (2015).
6. Bonnet, S. *et al.* A mitochondria-K+ channel axis is suppressed in cancer and Its normalization promotes apoptosis and inhibits cancer growth. *Cancer Cell* **11,** 37–51 (2007).
7. Dai, Y. *et al.* Dichloroacetate Enhances Adriamycin-Induced Hepatoma Cell Toxicity In Vitro and In Vivo by Increasing Reactive Oxygen Species Levels. *Plos One* **9,** e92962 (2014).
8. Xuan, Y. *et al.* Dichloroacetate attenuates hypoxia-induced resistance to 5-fluorouracil in gastric cancer through the regulation of glucose metabolism. *Exp Cell Res* **321,** 219–230 (2014).
9. Kumar, K. *et al.* Dichloroacetate reverses the hypoxic adaptation to bevacizumab and enhances its antitumor effects in mouse xenografts. *J Mol Med* **91,** 749–758 (2013).
10. Kumar, A., Kant, S. & Singh, SM. Antitumor and chemosensitizing action of dichloroacetate implicates modulation of tumor microenvironment: A role of reorganized glucose metabolism, cell survival regulation and macrophage differentiation. *Toxicol Appl Pharm* **273,** 196–208 (2013).
11. Shen, YC. *et al.* Activating oxidative phosphorylation by a pyruvate dehydrogenase kinase inhibitor overcomes sorafenib resistance of hepatocellular carcinoma. *Brit J Cancer* **108,**72–81 (2013).
12. Sun, RC. *et al.* Reversal of the glycolytic phenotype by dichloroacetate inhibits metastatic breast cancer cell growth in vitro and in vivo. *Breast Cancer Res Tr* **120,** 253–260 (2010).
13. Wong, JY., Huggins, GS., Debidda, M., Munshi, NC. & De Vivo, I. Dichloroacetate induces apoptosis in endometrial cancer cells. *Gynecol Oncol* **109,** 394–402 (2008).
14. Wheaton, WW. *et al.* Metformin inhibits mitochondrial complex I of cancer cells to reduce tumorigenesis. *Elife* **3,** e02242 (2014).
15. Zhuang, Y., Chan, DK., Haugrud, AB. & Miskimins, WK. Mechanisms by which low glucose enhances the cytotoxicity of metformin to cancer cells both *in vitro* and *in vivo*. *PLoS ONE* **9**, e108444 (2014).

16. Batandier, C. *et al*. The ROS production induced by a reverse-electron flux at respiratory-chain complex I is hampered by metformin. *J. Bioenerg. Biomembr.* **38**, 33-42 (2006).
17. Wallace, DC. Mitochondria and cancer. *Nat Rev Cancer* **12**, 685-698 (2012).
18. Martiniez-Reyes, I. *et al*. TCA cycle and mitochondrial membrane potential are necessary for diverse biological functions. *Mol. Cell* **61**, 199-209 (2016).
19. Sullivan, LB. & Chandel, NS. Mitochondrial reactive oxygen species and cancer. *Cancer Metab.* **2**, 17 (2014).
20. Corominas-Faja, B. *et al.* Metabolomic fingerprint reveals that metformin impairs one-carbon metabolism in a manner similar to the antifolate class of chemotherapy drugs. *Aging* **4**, 480-498 (2012).
21. Haugrud, AB., Zhuang, Y., Coppock, JD. & Miskimins, WK. Dichloroacetate enhances apoptotic cell death via oxidative damage and attenuates lactate production in metformin-treated breast cancer cells. *Breast Cancer Res. Tr.* **147,** 539–550 (2014).
22. Choi, YW. & Lim, IK. Sensitization of metformin-cytotoxicity by dichloroacetate via reprogramming glucose metabolism in cancer cells. *Cancer Lett.* **346,** 300–308 (2014).
23. Russell III, RR., Bergeron, R., Shulman, GI. Young, LH. Translocation of myocardial GLUT4 and increased glucose uptake through activation of AMPK by AICAR. *Am. J. Physiol.* **277**, 643-649 (1999).
24. Jeon, SM., Chandel, NS. & Hay, N. AMPK regulates NADPH homeostasis to promote tumor cell survival. *Nature* **485**, 661-665 (2012).
25. Shackelford, DB. *et al.* LKB1 Inactivation Dictates Therapeutic Response of Non-Small Cell Lung Cancer to the Metabolism Drug Phenformin. *Cancer Cell* **23,** 143–158 (2013.)
26. Chandel, NS. *et al.* Are metformin doses used in murine cancer models clinically relevant?
27. Sanchez WY. *et al.* Dichloroacetate inhibits aerobic glycolysis in multiple myeloma cells and increases sensitivity to bortezomib. *Brit J Cancer* **108,** 1624–1633 (2013).
28. Lin, G. *et al*. Dichloroacetate induces autophagy in colorectal cancer cells and tumours. *Br. J. Cancer* **111**, 375-385 (2014).
29. Viollet, B. *et al*. Cellular and molecular mechanisms of metformin: an overview. *Clin. Sci.* **122**, 253-270 (2012).
30. Zhao, Z. *et al*. Metformin inhibits the IL-6-induced epithelial-mesenchymal transition and lung adenocarcinoma growth and metastasis. *PLoS ONE* **9**, e95884 (2014).
31. Johnson, MC. *et al.* Persistence of fetal bovine serum proteins in human keratinocytes. *J. Burn Care Rehabil.* **11** 504-509 (1990).
32. Constantin-Teodosiu, D. Regulation of muscle pyruvate dehydrogenase complex in insulin resistance: effects of exercise and dichloroacetate. *Diabetes Metab. J.* **37**, 301-314 (2013).
33. Sapolsky, R. *et al*. Interlukin-1 stimulates the secretion of hypothalamic corticotropin-releasing factor. *Science* **238**, 522-524 (1987).

34. Calder, PC., Dimitradis, G. & Newsholme, P. Glucose metabolism in lymphoid and inflammatory cells and tissues. *Curr. Opin. Clin. Nutr. Metab. Care* **10**, 531-540 (2007).
35. Pernicova, I. & Korbonits M. Metformin – mode of action and clinical implications for diabetes and cancer. *Nat. Rev. Endocrinol.* **10**, 143-156 (2014).
36. Stades, AM. *et al.* Metformin and lactic acidosis: cause or coincidence? A review of case reports. *J. Intern. Med.* **255**, 179-187 (2004).
37. Alivanis, P. *et al*. Metformin-associated lactic acidosis treated with continuous renal replacement therapy. *Clin. Ther.* **28**, 396-400 (2006).
38. Gorrini, C., Harris, IS. & Mak, TW. Modulation of oxidative stress as an anticancer strategy. *Nat Rev Drug Discov* **12,** 931–947 (2013).
39. Robertson-Tessi, M., Gillies, RJ., Gatenby, RA. & Anderson, AR. Impact of metabolic heterogeneity on tumor growth, invasion, and treatment outcomes. *Cancer Res.* **75**, 1567-1579 (2015).

CHAPTER 4: SYSTEMIC METABOLIC EFFECTS OF DCA AND METFORMIN TREATMENT IN VM/DK MICE

4.1 Chapter Synopsis

In this chapter we present the findings of a metabolomics study evaluating the global effects of DCA and metformin treatment on cancer-free VM/dk mice. Changes in metabolite levels following DCA treatment suggest an increase in oxidative glucose metabolism, which is consistent with its mechanism of action. In contrast, metformin treatment restricted glucose oxidation in favor of FAO. The data also indicates that DCA modulation of glucose metabolism predominates when DCA and metformin are administered in combination. The materials and methods used for the studies presented in this chapter are described in Appendix A. The fold changes of all isolated analytes in each of the analyzed tissues is provided in Appendix C.

4.2 Metabolomics Analysis

To achieve a better understanding of the metabolic effects of DCA and metformin, we had global metabolomics analysis performed on tissue harvested from cancer-free VM/dk mice following a 3-week treatment regimen with 250mg/kg DCA, 250mg/kg metformin or the 250mg/kg combination. We collected brain, heart, kidney, liver, serum, skeletal muscle, and spleen from these mice and sent the frozen samples

to the University of Utah Health Sciences Metabolomics Core for coupled gas chromatography-mass spectroscopy (GC/MS) metabolomics. A total of 135 unique analytes were isolated from these samples and their relative concentrations were subsequently determined. We then analyzed the fold changes from control for each analyte present for all treatment groups.

One-way analysis of variance (ANOVA) with a post-hoc Tukey's multiple comparisons test was performed for each analyte present in each tissue type. This statistical analysis identified many significantly altered metabolites with widely variable fold changes. As the field of metabolomics is a relatively new, the biological relevance of fold changes in metabolite abundance determined from these analyses is still being elucidated (1). However, it is likely that even relatively small changes in abundance will have profound effects on cellular homeostasis for many metabolites given the overarching complexity and interconnectedness of cellular metabolism. For instance, a slight decrease in serine could precipitate deficiencies in lipid, nucleotide and protein metabolism as the amino acid is integrated into many divergent pathways.

GC/MS global metabolomics provides a snapshot of the tissue-wide effects of a particular treatment on a large series of metabolites. However, this method of analysis is not appropriate for the definitive determination of metabolic flux as the relative concentrations generated are from a single point in time (2). Yet, inferences of flux can still be made from these results that inform our understanding on the effects of metabolic treatments on different classes of metabolites. The concurrent analysis of multiple tissues allows for better elucidation of metabolite usage, as it is difficult to determine why a metabolite may be increased or decreased compared to controls from

serum or a single tissue type. Subsequent studies are required to investigate the functional consequences of the metabolic changes induced by agents such as DCA and metformin (3).

4.3 DCA Alteration of Glucose Metabolism Associated with a Decrease in Biosynthetic Precursors

4.3.1 Data Tables & Figures

Table 4.3.1 Fold changes in glycolytic and TCA cycle intermediates following DCA treatment. T-tests were performed for every analyte in each of the sample types from which it was detected. Dark green shading signifies significant decrease ($p<0.05$) and light green shading signifies a trend towards significant decrease ($p<0.10$). Red shading signifies significant increase ($p<0.05$) and pink shading indicates a trend towards a significant increase ($p<0.10$). Gray shading signifies that the analyte was not identified in that particular tissue.

Analyte	Brain	Heart	Kidney	Liver	Muscle	Serum	Spleen
Glucose		0.95	0.97		0.90	0.99	0.96
Glucose-6-phosphate	0.96	1.01	1.02	0.87	1.01	1.04	0.86
Fructose-6-phosphate	0.94	1.00	0.99	0.86	1.00		0.87
DHAP	0.73		1.19				
Glycerol-3-phosphate	1.02	1.00	0.99	1.05	1.02	1.00	1.04
1,3-bisphosphoglycerate	1.02	0.96	1.05			0.99	1.06
3-Phosphoglycerate	1.03	1.07	0.94	0.94	1.03		0.79
2-Phosphoglycerate		1.10	1.03	0.93	1.06		
Phosphoenolpyruvate	1.17	1.03	0.91	0.76	0.97		0.68
Pyruvic Acid	1.01	0.99	1.03	1.03	0.91	0.91	1.03
Lactic Acid	1.02	0.93	0.99	0.97	0.96	1.00	1.02
Citric Acid	0.97	1.10	1.36	0.99	1.06	0.94	0.96
cis-Aconitic Acid	1.01	1.03	1.20	0.75	0.95	0.85	0.88
Isocitric Acid	0.97	1.03	2.16	0.93		0.92	0.94
a-Ketoglutarate	1.12	1.03	1.30	1.06	1.77	0.66	0.99
Succinic Acid	1.06	0.97	1.01	1.05	1.06	1.02	1.32
Fumaric Acid	0.99	0.98	0.99	0.84	0.95	0.97	0.97
Malic Acid	0.99	1.00	1.01	0.85	0.95	0.98	0.97

Table 4.3.2 Fold changes in amino acids and related metabolites following DCA treatment. T-tests were performed for every analyte in each of the sample types from which it was detected. Dark green shading signifies significant decrease ($p<0.05$) and light green shading signifies a trend towards significant decrease ($p<0.10$). Red shading signifies significant increase ($p<0.05$) and pink shading indicates a trend towards a significant increase ($p<0.10$). Gray shading signifies that the analyte was not identified in that particular tissue.

Analyte	Brain	Heart	Kidney	Liver	Muscle	Serum	Spleen
Glutamine	1.03	1.08	1.02	1.08	0.97	0.99	0.99
Glutamate	1.03	1.05	0.99	1.06	1.06	0.85	1.04
N-acetylglutamate	1.07		1.54	0.94			1.45
Ornithine	1.11	1.05	1.00	1.00	0.93	0.96	0.96
Urea	0.99	0.99	1.00	0.98	0.98	0.92	0.99
Putrescine			1.20				
Methionine	0.99	1.00	0.96	0.85	0.95	1.04	0.94
Homocysteine	1.14	1.15	1.04		0.89	0.97	0.69
Cysteine	0.95	1.06	1.13	1.06	0.87	0.98	1.01
Serine	0.98	1.02	0.98	0.91	0.98	1.01	0.94
Homoserine	0.98	0.86	0.98	0.89	1.02	1.11	0.94
2-HG	1.03	1.11	1.16	1.17	1.10	0.71	1.13
Glycine	0.99	1.05	0.97	0.97	0.93	1.02	0.96
Sarcosine	1.04	1.03	1.12	0.91	1.01	0.91	1.11
Proline	1.02	1.02	0.96	0.94	0.96	1.02	0.93
4-hydroxyproline	1.02	1.08	1.07	0.91	1.04	1.03	0.98
Phenylalanine	1.00	1.01	0.97	0.94	0.96	1.01	0.95
Histidine	1.03	1.01	0.90		0.96	0.92	0.90
Asparagine	1.02	1.07	0.91	0.91	0.94	1.00	0.92
Lysine	1.05	1.04	0.96		0.91	0.86	0.95
Threonine	1.01	0.99	0.96	0.88	0.93	1.04	0.94
Tyrosine	0.99	0.99	0.96	1.12	0.94	1.10	0.92
Alanine	0.95	0.97	0.97	1.00	0.91	1.03	0.90
Aspartate	1.02	1.05	0.99	0.99	0.98	1.01	1.00
N-acetylaspartate	1.01	1.09	1.39	0.47	0.93		1.03
Valine	1.01	1.00	0.97	0.98	0.99	1.00	0.97
Leucine	1.00	1.02	0.96	0.97		1.00	0.97
Isoleucine	1.01	1.00	0.96	0.98	0.99	1.01	0.97

Table 4.3.3 Fold changes in fatty acids and related lipid metabolites following DCA treatment. T-tests were performed for every analyte in each of the sample types from which it was detected. Dark green shading signifies significant decrease ($p<0.05$) and light green shading signifies a trend towards significant decrease ($p<0.10$). Red shading signifies significant increase ($p<0.05$) and pink shading indicates a trend towards a significant increase ($p<0.10$). Gray shading signifies that the analyte was not identified in that particular tissue.

Analyte	Brain	Heart	Kidney	Liver	Muscle	Serum	Spleen
Lauric Acid	1.01	0.97	0.92	0.87	0.94	0.99	0.95
Myristic Acid	0.97	0.94	0.95	0.91	0.90	1.03	0.92
Palmitic Acid	0.99	1.00	0.97	0.99	0.95	0.97	0.97
Palmitelaidic Acid		0.86		0.94	0.95	1.07	0.89
Heptadecanoic Acid		1.01		0.90	0.88	0.96	0.91
Stearic Acid	0.98	1.01	1.01	0.98	0.94	0.98	0.98
Oleic Acid	0.96	0.99	0.96	1.00	0.98	0.96	0.96
Elaidic Acid	0.96	1.01	0.96	0.99	0.95	0.87	
Linoleic Acid	1.01	0.96	0.95	0.94	0.97	0.98	
Nonadecanoic Acid	0.75	1.04	0.93	0.86	0.84	0.97	0.89
Arachidonic Acid	0.99	0.99	0.99	0.93	0.82	0.93	0.97
1-palmitoyl-glycerol	1.00	1.02	1.00	1.02	0.95	0.96	0.99
1-stearoyl-glycerol	1.05	1.02	1.00	1.01	0.92	0.96	0.99
2-stearoyl-glycerol		0.90		0.73		1.15	
1-oleoyl-glycerol	0.98	0.95	0.97	1.03	0.99	0.81	0.94
2-oleoyl-glycerol	1.11	0.95	0.99	1.02	0.95	0.94	0.88
1-linoleoyl-glycerol	1.06	0.95	0.98	1.08	0.96	0.95	0.91
Glycerol	1.00	0.97	0.94	0.98	0.97	0.96	0.97
Cholesterol	1.05	1.03	0.98	0.96	0.89	0.97	1.01
β-hydroxybutyrate	1.08	1.00	1.08				1.08

Table 4.3.4 Fold changes in nucleotides and related metabolites following DCA treatment. T-tests were performed for every analyte in each of the sample types from which it was detected. Dark green shading signifies significant decrease ($p<0.05$) and light green shading signifies a trend towards significant decrease ($p<0.10$). Red shading signifies significant increase ($p<0.05$) and pink shading indicates a trend towards a significant increase ($p<0.10$). Gray shading signifies that the analyte was not identified in that particular tissue.

Analyte	Brain	Heart	Kidney	Liver	Muscle	Serum	Spleen
Adenine	1.01	1.00	1.01	1.02	0.89	1.06	1.05
Adenosine	1.00	1.03	1.31	1.08	1.13	0.90	1.46
5'-AMP	1.04	0.99	1.10	1.00	1.06		1.35
Inosine	0.99	0.93	1.00			0.92	1.03
Hypoxanthine	0.98	1.00	0.98	0.90	0.92	0.85	0.95
Xanthine	0.97	1.01	0.97	0.94	0.94	0.96	0.96
Uric Acid		1.04	1.05	0.95	1.07	0.90	1.01
Cytosine				0.96			
Thymine	0.92	1.06	1.11				1.03
Uracil	1.00	1.05	1.01	0.85	1.03	0.93	0.97

Table 4.3.5 Fold changes in PPP intermediates following DCA treatment. T-tests were performed for every analyte in each of the sample types from which it was detected. Dark green shading signifies significant decrease ($p<0.05$) and light green shading signifies a trend towards significant decrease ($p<0.10$). Red shading signifies significant increase ($p<0.05$) and pink shading indicates a trend towards a significant increase ($p<0.10$). Gray shading signifies that the analyte was not identified in that particular tissue.

Analyte	Brain	Heart	Kidney	Liver	Muscle	Serum	Spleen
Ribose-5-phosphate				0.96	0.88		
Ribose	1.00	1.01	0.94	0.85	0.66	0.79	0.91
Sedoheptulose-7-phosphate	0.94	1.00	0.99	0.96	0.57		0.96
Sedoheptulose		0.92					0.78
Eryhthrose-4-phosphate				0.84			
Erythrose	0.98		0.97			0.93	

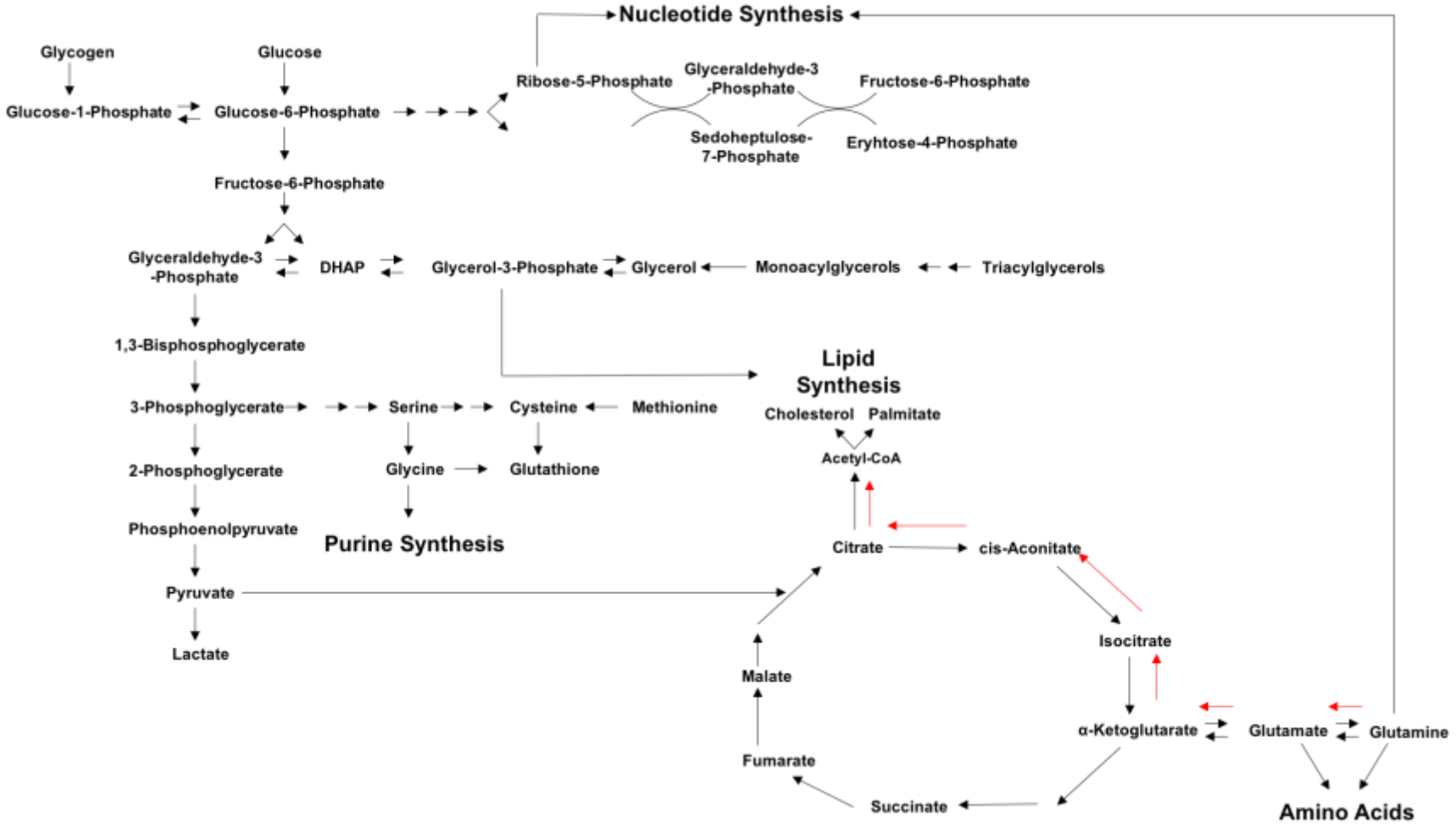

Figure 4.3.1 Schematic of biosynthetic metabolism. Representation of metabolic flux that supports biosynthesis and ultimately growth and proliferation. Black arrows represent canonical flux and red arrows represent reductive carboxylation of glutamine carbon.

4.3.2 Results & Discussion

Metabolomic analysis of tissue from VM/dk mice treated with 250mg/kg DCA indicate that DCA promotes an increase in mitochondrial glucose metabolism in these mice, which is consistent with its mechanism of action (Table 4.3.1). This is particularly evident in the liver, the predominant site of DCA action (4). DCA treatment promoted a significant reduction in early glycolytic intermediates in the liver compared to controls. This was independent of changes in hepatic lactate or pyruvate levels. However, DCA treatment did have an impact on the subsidiary pathways associated with glycolytic intermediates. We observed a significant decrease in ribose coupled with non-significant decreases in other PPP intermediates as well as a significant reduction in serine (Tables 4.3.1, 4.3.5). This was coupled with a significant increase in 2-HG, which is generated in wild-type IDH cells through a PGHDH-dependent mechanism, suggesting that DCA may restrict serine synthesis and promote alternate PGHDH function (5). This increase in 2-HG was also seen in heart, kidney and spleen samples from DCA treated mice. Furthermore, this overall change in glycolytic metabolism was mirrored in spleen (Table 4.3.1).

Coinciding with the change in glycolytic intermediates was an alteration to the TCA cycle in DCA treated liver samples. We observed a slight but significant increase in succinate, coupled with significant decreases in the subsequent intermediates, fumarate and malate (Table 4.3.1). This suggests a potential blockade of TCA cycling that may be resultant from excess glucose oxidation leading to saturation of complex II of the ETC and preventing efficient oxidation of succinate. Succinate was also elevated in the spleen and several TCA cycle intermediates upstream of succinate were significantly

increased in the kidney. Among them was α-KG, which can serve as a substrate for glutamate and glutamine production. Glutamine and glutamate levels were increased in several of the analyzed tissues suggesting diversion of excess α-KG for the generation of these amino acids (Table 4.3.2). Moreover, N-acetylglutamate was significantly increased in the kidney and was also elevated in the spleen. N-acetylglutamate is derived from acetyl-CoA and glutamate, thus the observed increase may be resultant from abundant PDH complex production of acetyl-CoA. Collectively these results suggest DCA activates glucose oxidation, likely restricting the diversion of glycolytic intermediates into biosynthetic pathways.

Interestingly, despite general increases in glutamine and glutamate levels, many non-essential amino acids derived from these two metabolites were decreased with DCA treatment (Table 4.3.2). Asparagine and proline were reduced in liver and spleen samples respectively, and alanine was reduced in muscle and spleen. This suggests that glutamine and glutamate are not being used for amino acid synthesis under DCA treatment. Moreover, most essential amino acids were also decreased in the kidney and spleen (Table 4.3.2). In contrast to the general decrease in tissue amino acids levels was a significant increase in serum tyrosine levels. This is a strong indicator of DCA action in the liver; as described above, DCA inhibits hepatic GSTZ1 and promotes tyrosine accumulation in the circulation (6).

DCA treatment decreased fatty acid levels in most tissues (Table 4.3.3). Given the observed indications of glucose oxidation, this likely is a result of reduced fatty acid uptake. Increased glucose oxidation suppresses the need for FAO to generate acetyl-CoA, thus the PDH complex is a native regulator of FAO (7). As such DCA treatment

reduces the necessity for fatty acids as an energy source. Except for slight increases in myristic and palmitelaidic acids, DCA treatment did not alter circulating levels of saturated fatty acids, suggesting no effect on adipocyte lipolysis and free fatty acid release. Moreover, despite indications of increased acetyl-CoA production, DCA did not alter palmitate levels, indicating no effect on FAS in the analyzed tissues (Table 4.3.3).

Finally, DCA treatment altered constituents of purine metabolism. We observed increases in adenosine in the kidney and spleen as well as an elevation of AMP in the spleen (Table 4.3.4). This coincided with decreases in intermediates in the purine salvage pathway in the liver and spleen. The indications of increased glucose oxidation and apparent diversion of α-KG for the generation of glutamate and glutamine suggest that DCA does not precipitate an energetic crisis. Moreover, our *in vitro* data suggest that DCA actually reduced levels of activated AMPK (Fig 3.3.5G). Thus the increase in AMP is not necessarily an indication of an energetic deficiency. Rather, it may suggest an increase in the purine nucleotide cycle, which generates fumarate for TCA cycle anaplerosis and may be induced by DCA treatment to compensate for the observed decreases in fumarate and malate (8).

Together, these data suggest that DCA activates mitochondrial glucose oxidation in VM/dk mice. This is most evident in kidney, liver and spleen tissue, whereas we show that DCA has marginal effects on brain, heart and muscle. Associated with this alteration in glucose metabolism was a general reduction in the biosynthetic precursors required for growth (Fig. 4.3.1). As biosynthesis is critical to tumor formation, the systemic metabolic effects of DCA may prevent tumorigenesis.

4.4 Metformin Treatment Alters Fuel Choice For Oxidative Metabolism

4.4.1 Data Tables

Table 4.4.1 Fold changes in glycolytic and TCA cycle intermediates following metformin treatment. T-tests were performed for every analyte in each of the sample types from which it was detected. Dark green shading signifies significant decrease ($p<0.05$) and light green shading signifies a trend towards significant decrease ($p<0.10$). Red shading signifies significant increase ($p<0.05$) and pink shading indicates a trend towards a significant increase ($p<0.10$). Gray shading signifies that the analyte was not identified in that particular tissue.

Analyte	Brain	Heart	Kidney	Liver	Muscle	Serum	Spleen
Glucose		1.06	1.04		0.93	0.98	0.95
Glucose-6-phosphate	0.94	1.35	1.01	0.96	1.06	0.96	0.96
Fructose-6-phosphate	0.89	1.40	0.93	0.92	1.10		0.97
DHAP	0.86		1.21	1.00			
Glycerol-3-phosphate	1.02	0.99	0.97	1.06	0.99	1.02	0.96
1,3-bisphosphoglycerate	1.02	0.94	0.98			0.99	0.98
3-Phosphoglycerate	0.99	1.14	0.97	1.06	1.08		0.78
2-Phosphoglycerate		1.38	0.95	0.96	1.14		
Phosphoenolpyruvate	0.85	1.12	0.95	1.09	1.05		0.67
Pyruvic Acid	0.99	1.03	1.04	0.98	0.97	1.06	0.96
Lactic Acid	1.00	0.91	0.93	0.98	0.94	0.99	0.99
Citric Acid	0.97	0.99	1.14	1.27	1.10	1.03	0.94
cis-Aconitic Acid	1.02	0.96	1.45	1.41	0.98	1.07	0.88
Isocitric Acid	0.97	0.89	1.53	1.17		1.21	0.90
a-Ketoglutarate	0.91	1.68	1.05	1.12	0.96	1.15	0.63
Succinic Acid	1.06	1.02	0.98	1.03	0.96	0.93	0.99
Fumaric Acid	0.98	0.92	0.97	1.05	0.96	1.01	0.96
Malic Acid	0.98	0.96	0.96	1.05	0.98	1.00	0.96

Table 4.4.2 Fold changes in amino acids and related metabolites following metformin treatment. T-tests were performed for every analyte in each of the sample types from which it was detected. Dark green shading signifies significant decrease ($p<0.05$) and light green shading signifies a trend towards significant decrease ($p<0.10$). Red shading signifies significant increase ($p<0.05$) and pink shading indicates a trend towards a significant increase ($p<0.10$). Gray shading signifies that the analyte was not identified in that particular tissue.

Analyte	Brain	Heart	Kidney	Liver	Muscle	Serum	Spleen
Glutamine	1.00	0.99	0.99	0.98	0.99	1.04	0.97
Glutamate	1.00	0.99	0.96	1.03	0.98	1.29	0.98
N-acetylglutamate	1.00		0.96	1.00			1.60
Ornithine	0.99	0.95	0.91	0.95	0.98	1.08	0.91
Urea	0.98	0.96	0.98	0.96	0.98	1.10	0.97
Putrescine			1.05				
Methionine	0.99	1.00	0.98	0.98	0.99	0.99	0.97
Homocysteine	0.97	0.81	0.83		1.03	0.79	0.83
Cysteine	0.88	1.01	1.01	0.92	0.92	0.88	0.91
Tryptophan	0.97	0.96	0.99	0.99	0.98	1.02	0.97
Serine	1.00	1.01	0.98	1.03	1.02	1.03	0.96
Homoserine	0.99	0.81	1.00	1.00	1.17	0.94	0.94
2-HG	1.02	0.98	1.00	0.96	0.95	1.13	0.93
Glycine	0.98	1.03	0.97	0.98	1.03	1.04	0.99
Sarcosine	1.03	0.92	0.94	0.90	0.98	0.96	0.95
Proline	1.00	0.96	0.95	0.97	0.98	1.00	0.94
4-hydroxyproline	1.01	0.97	0.96	1.04	0.99	1.14	0.95
Phenylalanine	0.98	0.98	0.97	0.97	0.98	0.97	0.97
Histidine	0.98	0.92	0.85		1.04	1.14	0.96
Asparagine	1.02	1.01	0.90	0.95	1.01	1.07	0.97
Lysine	1.00	1.02	1.00		0.98	1.24	0.97
Threonine	1.00	1.00	0.98	0.96	1.00	0.99	0.97
Tyrosine	0.99	1.00	0.98	1.11	0.99	0.92	0.96
Alanine	0.97	0.98	0.98	0.98	1.01	0.96	0.97
Aspartate	1.00	1.02	1.01	1.09	1.06	1.08	0.98
N-acetylaspartate	1.02	1.02	1.17	1.13	0.87		0.97
Valine	0.99	1.00	0.96	0.97	1.00	0.99	0.98
Leucine	0.99	1.03	0.96	0.98		0.99	0.98
Isoleucine	0.99	1.00	0.96	0.98	1.00	0.98	0.98

Table 4.4.3 Fold changes in fatty acids and related lipid metabolites following metformin treatment. T-tests were performed for every analyte in each of the sample types from which it was detected. Dark green shading signifies significant decrease ($p<0.05$) and light green shading signifies a trend towards significant decrease ($p<0.10$). Red shading signifies significant increase ($p<0.05$) and pink shading indicates a trend towards a significant increase ($p<0.10$). Gray shading signifies that the analyte was not identified in that particular tissue.

Analyte	Brain	Heart	Kidney	Liver	Muscle	Serum	Spleen
Lauric Acid	1.00	0.87	1.03	0.99	1.16	0.89	0.92
Myristic Acid	0.97	0.89	0.98	0.95	1.02	0.87	0.89
Palmitic Acid	0.97	0.97	0.97	0.99	0.98	0.97	0.96
Palmitelaidic Acid		0.87		0.91	1.03	0.83	0.87
Heptadecanoic Acid		0.91		1.07	0.97	0.95	0.91
Stearic Acid	0.98	0.97	1.00	1.00	0.97	0.97	0.96
Oleic Acid	0.93	0.94	0.96	0.97	1.03	0.94	0.93
Elaidic Acid	0.93	0.92	0.96	0.91	1.00	0.86	
Linoleic Acid	1.04	0.97	0.98	1.02	1.02	0.95	
Nonadecanoic Acid	0.87	0.91	0.96	0.96	0.94	0.94	0.90
Arachidonic Acid	0.98	0.93	0.98	0.99	0.84	0.93	0.91
1-palmitoyl-glycerol	0.98	0.97	0.97	0.99	0.97	1.02	0.99
1-stearoyl-glycerol	1.01	0.97	0.99	1.01	0.93	1.04	0.98
2-stearoyl-glycerol		0.98		0.90		1.60	
1-oleoyl-glycerol	0.93	0.95	1.00	0.95	1.05	0.81	0.88
2-oleoyl-glycerol	1.20	0.98	1.06	1.05	1.06	0.83	0.82
1-linoleoyl-glycerol	1.10	0.99	1.04	1.08	1.06	0.91	0.85
Glycerol	0.99	0.95	0.92	0.99	0.97	0.96	0.97
Cholesterol	0.99	0.98	0.91	1.04	0.92	0.96	1.00
β-hydroxybutyrate	1.01	1.00	1.01				1.03

Table 4.4.4 Fold changes in nucleotides and related metabolites following metformin treatment. T-tests were performed for every analyte in each of the sample types from which it was detected. Dark green shading signifies significant decrease ($p<0.05$) and light green shading signifies a trend towards significant decrease ($p<0.10$). Red shading signifies significant increase ($p<0.05$) and pink shading indicates a trend towards a significant increase ($p<0.10$). Gray shading signifies that the analyte was not identified in that particular tissue.

Analyte	Brain	Heart	Kidney	Liver	Muscle	Serum	Spleen
Adenine	0.99	0.91	0.99	0.97	0.96	0.85	0.99
Adenosine	0.97	0.86	1.37	1.04	1.01	1.14	1.25
5'-AMP	1.04	0.99	1.15	1.03	1.07		1.19
Inosine	0.99	0.94	1.01			0.93	1.01
Hypoxanthine	0.98	0.95	0.95	0.97	0.92	1.35	0.98
Xanthine	0.96	0.95	0.91	0.98	0.92	1.12	0.97
Uric Acid		1.02	0.98	1.00	1.08	0.95	0.97
Cytosine				0.92			
Thymine	0.97	0.82	1.01				1.03
Uracil	0.98	0.95	0.98	0.96	1.07	0.93	0.94

Table 4.4.5 Fold changes in PPP intermediates following metformin treatment. T-tests were performed for every analyte in each of the sample types from which it was detected. Dark green shading signifies significant decrease ($p<0.05$) and light green shading signifies a trend towards significant decrease ($p<0.10$). Red shading signifies significant increase ($p<0.05$) and pink shading indicates a trend towards a significant increase ($p<0.10$). Gray shading signifies that the analyte was not identified in that particular tissue.

Analyte	Brain	Heart	Kidney	Liver	Muscle	Serum	Spleen
Ribose-5-phosphate				1.03	1.00		
Ribose	0.96	0.89	0.94	0.97	0.78	1.13	0.87
Sedoheptulose-7-phosphate	0.92	0.83	1.00	1.01	0.77		1.01
Sedoheptulose		0.83					0.94
Eryhthrose-4-phosphate				1.10			
Erythrose	0.93		0.88			0.98	

4.4.2 Results & Discussion

The antidiabetic activity of metformin has been attributed largely to its action in hepatic tissue. However, metformin treatment did not have robust effects on liver metabolism in VM/dk mice. Yet, those hepatic metabolites that were altered following metformin treatment are established hallmarks of metformin activity. Metformin treatment promoted a trend towards increased AMP levels, which is often associated with metformin inhibition of complex I (Table 4.4.4) (9). We also observed a trend towards increased Glycerol-3-phosphate levels in the liver, which is consistent with the report that metformin inhibits hepatic mGPD to further induce an energetic crisis (Table 4.4.2) (10). This inhibition restricts the utilization of both glycerol and lactate as gluconeogenic substrates and may also explain the significant decrease in glycerol levels seen in many tissues following metformin treatment (Table 4.4.3). It has been proposed that metformin control of circulating glucose levels is also mediated through enhanced peripheral glucose uptake, especially in muscle (11). However, we show that metformin has very little impact on muscle metabolism. In contrast, metformin treatment had significant effects on heart and kidney metabolism.

Metformin promoted an accumulation of glycolytic intermediates upstream of pyruvate in cardiac samples (Tables 4.4.1). This could indicate an increase in glycolytic flux, which would be consistent with AMPK activation. However, it is more likely a function of reduced PK activity, resulting in this accumulation. Cardiac tissue utilizes FAO as a primary means of energy production, necessitating concurrent restriction of glucose oxidation (12). Metformin significantly reduced levels of several fatty acids in the cardiac samples, which coupled with the accumulation of glycolytic intermediates

suggests that metformin enhanced FAO in the heart. This is in line with the induction of FAO associated with metformin treatment (13). Circulating levels of fatty acids and monoacylglycerols, which are derived from TAG metabolism, were significantly decreased in VM/dk mice treated with metformin (Table 4.4.3). This is consistent with previous reports of reductions in free fatty acids with metformin treatment (9, 14). Metformin alteration of fatty acid levels is likely resultant from enhanced tissue utilization and decreases in free fatty acid release from adipocytes, which is shown to be a function of metformin stimulation of FAO in these cells (15).

Metformin treatment is also shown to alter glutamine metabolism, particularly through induction of reductive carboxylation of glutamine carbon in favor of oxidation (16). We show an accumulation of TCA cycle intermediates upstream of succinate in liver and kidney and a decrease in fumarate and malate in heart and spleen samples (Table 4.4.1). This is similar to our findings with DCA treatment, however we did not observe an increase in glutamate and glutamine. In fact, we observed a trend towards decreased glutamate in the kidney. this suggests against α-KG diversion for generation of these amino acids, rather supporting the notion of increased reductive carboxylation that would lead to increases in α-KG, isocitrate, cis-Aconitate and citrate.

In addition to the noted alterations in catabolic metabolism, metformin treatment also affected metabolites associated with anabolic processes. Despite the observed increases in glycolytic intermediates in cardiac tissue, metformin treatment was associated with a trends towards decreases in PPP intermediates in heart samples (Table 4.4.5). Furthermore, we report slight increases in circulating serine and glycine levels along with a decrease in the glycine derivative sarcosine in the liver (Table 4.4.3).

This may indicate a decrease in serine/glycine metabolism, which is consistent with a previous metabolomics study demonstrating metformin exhibits anti-folate activity (17). As serine/glycine metabolism is intricately linked to the folate cycle and one-carbon metabolism, disruption of the folate cycle also interferes with the metabolism of serine/glycine. A disruption of one-carbon metabolism could explain the observed reduction in nucleotide levels given its necessity for nucleotide synthesis (Table 4.4.4). Together, these results suggest that consistent with the literature, metformin reduces anabolic metabolism in VM/dk mice. Similar to DCA, this restriction of biosynthesis would disrupt tumorigenesis and likely contributes to the apparent reduction in cancer incidence with metformin discussed previously (18-22).

4.5 DCA modulation of glucose metabolism predominates in a DCA and metformin combination

4.5.1 Data Tables

Table 4.5.1 Fold changes in glycolytic and TCA cycle intermediates following treatment with a DCA and metformin combination. T-tests were performed for every analyte in each of the sample types from which it was detected. Dark green shading signifies significant decrease ($p<0.05$) and light green shading signifies a trend towards significant decrease ($p<0.10$). Red shading signifies significant increase ($p<0.05$) and pink shading indicates a trend towards a significant increase ($p<0.10$). Gray shading signifies that the analyte was not identified in that particular tissue.

Analyte	Brain	Heart	Kidney	Liver	Muscle	Serum	Spleen
Glucose		1.02	1.02		1.10	0.99	1.00
Glucose-6-phosphate	0.93	1.21	1.05	0.95	0.84	1.00	1.00
Fructose-6-phosphate	0.87	1.24	1.21	0.97	0.78		1.01
DHAP	1.04		1.06				
Glycerol-3-phosphate	0.99	1.03	1.01	1.02	0.90	0.97	0.95
1,3-bisphosphoglycerate	0.92	1.38	1.12			0.99	1.03
3-Phosphoglycerate	0.92	1.05	1.04	0.94	0.82		1.02
2-Phosphoglycerate		1.11	0.94	0.94	0.71		
Phosphoenolpyruvate	0.90	1.13	1.08	0.81	0.85		1.03

Pyruvic Acid	0.96	0.96	1.01	0.98	1.10	0.98	0.99
Lactic Acid	0.97	0.97	0.96	0.96	1.04	1.02	0.98
Citric Acid	0.93	1.01	0.99	0.70	1.10	0.99	0.99
cis-Aconitic Acid	0.93	1.05	1.00	0.62	1.01	0.94	0.91
Isocitric Acid	0.89	1.13	1.28	0.99		1.14	0.98
a-Ketoglutarate	0.77	0.59	0.94	1.01	2.20	1.02	1.11
Succinic Acid	0.99	0.94	1.00	1.00	0.90	0.99	1.00
Fumaric Acid	0.97	1.06	1.02	0.94	1.03	0.98	0.99
Malic Acid	0.97	1.07	1.10	0.91	1.05	0.99	0.98

Table 4.5.2 Fold changes in amino acids and related metabolites following treatment with a DCA and metformin combination. T-tests were performed for every analyte in each of the sample types from which it was detected. Dark green shading signifies significant decrease ($p<0.05$) and light green shading signifies a trend towards significant decrease ($p<0.10$). Red shading signifies significant increase ($p<0.05$) and pink shading indicates a trend towards a significant increase ($p<0.10$). Gray shading signifies that the analyte was not identified in that particular tissue.

Analyte	Brain	Heart	Kidney	Liver	Muscle	Serum	Spleen
Glutamine	0.95	1.02	1.00	1.08	1.05	1.02	1.01
Glutamate	0.96	1.02	0.98	1.00	1.16	0.96	1.00
N-acetylglutamate	0.95		1.06	0.85			1.11
Ornithine	0.90	1.04	1.03	0.97	1.04	1.03	1.01
Urea	0.93	0.98	0.97	0.95	0.99	1.02	0.95
Putrescine			1.06				
Methionine	0.96	1.01	1.00	0.93	1.01	0.96	1.01
Homocysteine	0.61	1.32	1.24		0.84	0.73	1.04
Cysteine	1.03	1.24	1.12	1.09	1.10	1.08	1.01
Tryptophan	0.96	1.03	1.00	0.98	1.02	1.00	1.04
Serine	0.95	1.03	1.03	0.99	1.05	1.02	1.01
Homoserine	0.87	0.85	0.93	0.82	1.18	0.81	0.89
2-HG	0.94	1.11	1.08	1.05	1.09	1.05	0.96
Glycine	1.02	1.07	0.99	1.00	1.02	0.99	1.00
Sarcosine	0.96	1.02	1.06	0.89	1.07	1.04	1.00
Proline	0.96	1.04	1.04	0.95	1.02	0.99	1.02
4-hydroxyproline	1.01	1.08	0.99	0.92	1.05	1.07	0.96
Phenylalanine	0.97	1.04	1.01	0.96	1.03	0.98	1.01
Histidine	0.91	1.05	1.04		1.03	1.00	1.04
Asparagine	0.96	1.08	1.06	0.97	1.07	1.02	1.04

Lysine	0.99	1.07	1.04		1.04	1.04	1.02
Threonine	0.94	0.99	0.99	0.93	0.99	0.95	0.99
Tyrosine	0.93	1.02	1.01	1.14	0.99	0.93	1.01
Alanine	0.94	1.02	1.00	0.99	1.00	0.98	0.99
Aspartate	0.97	0.97	1.01	0.98	1.07	0.92	0.99
N-acetylaspartate	0.96	0.93	0.89		1.05		0.99
Valine	0.97	1.00	0.99	0.96	1.03	0.99	1.00
Leucine	0.98	1.04	1.00	0.97		0.99	1.00
Isoleucine	0.97	1.02	0.99	0.96	1.04	0.99	1.01

Table 4.5.3 Fold changes in fatty acids and related lipid metabolites following treatment with a DCA and metformin combination. T-tests were performed for every analyte in each of the sample types from which it was detected. Dark green shading signifies significant decrease ($p<0.05$) and light green shading signifies a trend towards significant decrease ($p<0.10$). Red shading signifies significant increase ($p<0.05$) and pink shading indicates a trend towards a significant increase ($p<0.10$). Gray shading signifies that the analyte was not identified in that particular tissue.

Analyte	Brain	Heart	Kidney	Liver	Muscle	Serum	Spleen
Lauric Acid	0.98	1.07	0.96	0.98	1.09	0.87	0.91
Myristic Acid	0.96	0.99	0.98	0.88	1.02	0.87	0.96
Palmitic Acid	0.98	1.07	1.04	1.00	1.02	0.98	0.99
Palmitelaidic Acid		0.95		0.90	1.04	0.85	0.96
Heptadecanoic Acid		1.15		0.98	1.09	0.92	0.97
Stearic Acid	0.95	1.08	1.06	1.01	1.04	0.99	0.99
Oleic Acid	1.01	1.09	1.02	1.00	1.10	0.98	1.01
Elaidic Acid	1.01	1.12	1.02	1.01	1.10	0.98	
Linoleic Acid	1.00	1.06	1.01	0.97	1.09	0.97	
Nonadecanoic Acid	0.66	1.17	1.14	0.90	1.17	0.85	0.91
Arachidonic Acid	0.98	1.10	1.01	0.98	1.15	0.99	0.99
1-palmitoyl-glycerol	0.95	1.08	1.06	1.03	0.99	0.98	1.01
1-stearoyl-glycerol	0.92	1.09	1.07	1.04	0.99	1.01	1.03
2-stearoyl-glycerol		0.97		0.93		1.39	
1-oleoyl-glycerol	0.99	1.04	1.02	1.04	1.14	0.97	1.01
2-oleoyl-glycerol	0.87	0.99	1.01	0.99	1.16	0.83	1.04
1-linoleoyl-glycerol	0.91	1.00	1.01	1.03	1.13	0.86	1.01
Glycerol	0.98	1.03	0.98	0.98	1.04	0.96	1.01
Cholesterol	0.93	1.10	1.04	1.00	1.05	1.01	1.02
β-hydroxybutyrate	1.00	1.02	1.04				1.04

Table 4.5.4 Fold changes in nucleotides and related metabolites following treatment with a DCA and metformin combination. T-tests were performed for every analyte in each of the sample types from which it was detected. Dark green shading signifies significant decrease ($p<0.05$) and light green shading signifies a trend towards significant decrease ($p<0.10$). Red shading signifies significant increase ($p<0.05$) and pink shading indicates a trend towards a significant increase ($p<0.10$). Gray shading signifies that the analyte was not identified in that particular tissue.

Analyte	Brain	Heart	Kidney	Liver	Muscle	Serum	Spleen
Adenine	0.98	1.03	0.97	1.00	0.94	0.88	1.00
Adenosine	0.98	0.96	0.97	1.00	0.75	0.22	1.02
5'-AMP	0.90	0.97	1.00	1.00	0.97		0.92
Inosine	0.94	0.98	1.02			0.98	1.02
Hypoxanthine	0.99	1.07	0.99	1.01	1.09	0.96	1.01
Xanthine	0.98	1.04	0.99	0.99	1.07	0.98	1.00
Uric Acid		1.02	1.00	0.95	1.00	1.02	0.98
Cytosine				0.98			
Thymine	0.89	1.09	0.92				1.02
Uracil	0.96	1.07	1.00	1.06	1.06	0.92	0.99

Table 4.5.5 Fold changes in PPP intermediates following treatment with a DCA and metformin combination. T-tests were performed for every analyte in each of the sample types from which it was detected. Dark green shading signifies significant decrease ($p<0.05$) and light green shading signifies a trend towards significant decrease ($p<0.10$). Red shading signifies significant increase ($p<0.05$) and pink shading indicates a trend towards a significant increase ($p<0.10$). Gray shading signifies that the analyte was not identified in that particular tissue.

Analyte	Brain	Heart	Kidney	Liver	Muscle	Serum	Spleen
Ribose-5-phosphate				0.97	1.12		
Ribose	0.96	1.09	1.02	0.97	1.13	1.04	1.01
Sedoheptulose-7-phosphate	0.90	1.24	1.06	1.02	1.14		1.0
Sedoheptulose		1.10					1.06
Eryhthrose-4-phosphate				0.93			
Erythrose	0.81		1.00			0.97	

4.5.2 Results & Discussion

Central to the mechanisms of action of DCA and metformin is an opposing effect on glucose oxidation. Indeed, we show that as individual treatments, DCA and metformin differentially influence glucose metabolism. However, in combination we propose that DCA activation of the PDH complex overcomes the compensatory suppression of glucose oxidation resultant from metformin inhibition of complex I. The metabolomics analysis of tissue from VM/dk mice treated with a DCA and metformin combination support that hypothesis.

We report tissue specific differences in intermediates associated with glucose metabolism that are not mutually exclusive with an increase in glucose oxidation. Combinatorial treatment promotes a significant decrease in glycolytic intermediates independent of a decrease in glucose or pyruvate in muscle samples, suggesting efficient flux through the pathway. Similar to DCA treatment, we observed a decrease in succinate coupled with increases in α-KG and glutamate (Tables 4.5.1, 4.5.2). Moreover, fumarate and malate levels were decreased and glutamine was increased in liver samples, which is consistent with DCA treatment alone (Tables 4.3.1, 4.5.1).

In contrast, we observed an accumulation of both glycolytic and TCA cycle intermediates, including fumarate and malate following treatment with the combination in cardiac samples (Table 4.5.1). Metformin treatment promoted a similar accumulation of glycolytic intermediates, which was likely a consequence of increased FAO, marked by a decrease in fatty acid levels (4.4.1). However, many fatty acids were significantly increased in the heart with DCA and metformin. This increase was also seen in muscle and kidney tissue and coincided with a decrease in serum levels of several fatty acids

and monoacylglycerols (Table 4.5.3). These data suggest a preservation of metformin activity in lowering circulating lipid levels with the combinatorial treatment. Yet, they also indicate a restriction of FAO in favor of glucose oxidation. This is further supported by the lack of hepatic increase in glycerol-3-phosphate or AMP elevation with the combination, indicating an absence of AMPK activation in the presence of both DCA and metformin (Tables 4.5.1, 4.5.4). This is consistent with our *in vitro* finding that DCA attenuates metformin activation of AMPK in VM-M3 cells (3.2.5G).

The observed elevation in glycolytic intermediates in the heart coincided with increases in the PPP-associated metabolites ribose and sedoheptulose-7-phosphate suggesting a potential diversion of accumulated glucose-6-phosphate (Table 4.5.5). However, the combinatorial treatment did not generally alter the levels of PPP intermediates in other tissues. Nucleotide metabolism was also largely unaffected by the combination where the individual treatments reduced constituents of the purine salvage pathway (Table 4.5.4). Strikingly, the combination treatment promoted a significant reduction in a large number of metabolites in the brain, which may be indicative of an overall reduction in brain metabolism. Moreover, whereas the individual treatments had a significant influence over spleen metabolism, the combination had no discernable effect on the spleen of VM/dk mice. As the spleen is a dynamic organ that is a critical component of the immune system, the general reduction in spleen metabolite levels with individual DCA and metformin treatments may be resultant from changes in inflammation. Both DCA and metformin are shown to promote an anti-inflammatory response, which may be disrupted when administered in combination (23-25).

The efficacy of DCA and metformin as an anti-cancer therapy is dependent on active mitochondrial oxidation of glucose. Our findings suggest that DCA induces glucose oxidation even when co-administered with metformin, though this may be more pronounced in particular tissues.

4.6 References

1. van den Berg, RA. *et al.* Centering, scaling, and transformations: improving the biological information content of metabolomics data. *BMC Genomics* **7**, 142 (2006).
2. DeBerardinis, RJ. & Chandel, NS. Fundamentals of cancer metabolism. *Sci Adv* **2,** e1600200 (2016).
3. Johnson, CH., Ivanisevic, J. & Siuzdak, G. Metabolomics: beyond biomarkers and towards mechanisms. *Nat. Rev. Mol. Cell Biol.* **17**, 451-459 (2016).
4. Stacpoole, PW. The pharmacology of dichloroacetate. *Metabolism* **38**, 1124-1144 (1989).
5. Fan, J. *et al*. Human phosphoglycerate dehydrogenase produces the oncometabolite D-2-hydroxyglutarate. *ACS Chem. Biol.* **10**, 510-516 (2015).
6. Maisenbacher III, MW. *et al.* Pharmacokinetics of oral dichloroacetate in dogs. *J. Biochem. Mol. Toxicol.* **27**, 522-525 (2013).
7. Zhang, S. *et al.* The pivotal role of pyruvate dehydrogenase kinases in metabolic flexibility. *Nutr. Metab.* **11**, 10 (2014).
8. Tornheim, K. & Lowenstein, JM. The purine nucleotide cycle. The production of ammonia from aspartate by extracts of rat skeletal muscle. *J. Biol. Chem.* **247**, 162-169 (1972).
9. Zhou, G. *et al*. Role of AMP-activate protein kinase in mechanism of metformin action. *J. Clin. Invest.* **108**, 1167-1174 (2011).
10. Anila, K. *et al.* Metformin suppresses gluconeogenesis by inhibiting mitochondrial glycerophosphate dehydrogenase. *Nature* **510**, 542-546 (2014).
11. Kristensen, JM. *et al.* Two weeks of metformin treatment induces AMPK-dependent enhancement of insulin-stimulated glucose uptake in mouse soleus mescle. *Am. J. Endocrinol. Metab.* **306**, 1099-1109 (2014).
12. Goldberg, IJ., Trent, CM. & Schulze, PC. Lipid metabolism and toxicity in the heart. *Cell Metab.* **15**, 805-812 (2012).
13. Benes, J. *et al*. Effect of metformin therapy on cardiac function and survival in a volume-overload model of heart failure in rats. *Clin. Sci.* **121**, 29-41 (2011).
14. Schneider, J., Erren, T., Zofel, P. & Kaffarnik, H. Metformin-induced changes in serum lipids, lipoproteins, and apoproteins in non-insulin dependent diabetes mellitus. *Atherosclerosis* **82**, 97-103 (1990).

15. Shikata, E. *et al.* Human organic cation transporter (OCT1 and OCT2) gene polymorphisms anf therapeutic effects of metformin. *J. Hum. Genet.* **52**, 117-122 (2007).
16. Cuyas, E. *et al.* Oncometabolic mutation IDH1 R132H confers a metformin-hypersensitive phenotype. *Oncotarget* **6**, 12279-12296 (2015).
17. Corominas-Faja, B. *et al.* Metabolomic fingerprint reveals that metformin impairs one-carbon metabolism in a manner similar to the antifolate class of chemotherapy drugs. *Aging* **4**, 480-498 (2012).
18. Evans, JM., Donnelly, LA., Emslie-Smith, AM., Alessi, DR. & Morris, AD. Metformin and reduced risk of cancer in diabetic patients. *Bmj* **330,**1304–1305 (2005).
19. Libby, G. *et al.* New Users of Metformin Are at Low Risk of Incident Cancer. *Diabetes Care* **32,**1620–1625 (2009).
20. Ko, EM. *et al.* Metformin is associated with improved survival in endometrial cancer. *Gynecol Oncol* **132,** 438–442 (2014).
21. Nevadunsky, NS. *et al.* Metformin use and endometrial cancer survival. *Gynecol Oncol.* **132,**236–240 (2014).
22. Deng, D. *et al*. Association between metformin therapy and incidence, recurrence and mortality of prostate cancer: evidence from a meta-analysis. *Diabetes Metab. Res. Rev.* **31**, 595-602 (2015).
23. Zhao, Z. *et al*. Metformin inhibits the IL-6-induced epithelial-mesenchymal transition and lung adenocarcinoma growth and metastasis. *PLoS ONE* **9**, e95884 (2014).
24. Mercken, EM. *et al.* Dichloroacetate modulates the oxidative stress and inflammatory response to exercise in COPD. *Chest* **136**, 744-751 (2009).
25. Bian, L. *et al*. Dichloroacetate alleviates development of collagen II-induced arthritis in female DBA/1 mice. *Arthritis Res Ther.* **11**, R132 (2009).

CHAPTER 5: HYPERBARIC OXYGEN DOES NOT COOPERATE WITH THE COMBNATION OF DCA & METFORMIN

5.1 Chapter Synopsis

In this chapter we present data depicting the effect of hyperbaric oxygen on the efficacy of our DCA and metformin combination. Hyperbaric oxygen treatment enhanced the cytotoxicity of DCA in the presence of complex I inhibition *in vitro*. However, administration of hyperbaric oxygen to VM-M3 tumor-burdened mice did not enhance the efficacy of the DCA and metformin combination. The materials and methods used for the studies presented in this chapter are described in Appendix A.

5.2 Hyperbaric Oxygen Therapy as an Adjuvant to Cancer Therapy

As we've shown, the *in vitro* efficacy of DCA and metformin in combination is dependent on oxidative stress. To improve upon the lack of observed effect with the combination in the VM-M3 model, we hypothesized that further stimulation of oxidative stress would enhance the efficacy of DCA and metformin *in vivo*. As such, we chose to employ hyperbaric oxygen therapy as a pro-oxidant adjuvant to our proposed combinatorial anti-cancer therapy.

Hyperbaric oxygen therapy (HBOt) employs 100% O_2 at elevated pressure (>1 atm) to increase the proportion of dissolved O_2 in plasma. This overcomes the need for

hemoglobin transport of oxygen and results in increased O_2 diffusion in tissue beyond the capacity of red blood cells (1). HBOt is administered in specialized chambers that allow for pressurization to 2-3 atm absolute (ATA). Pure oxygen can be fed directly into the chamber or delivered by oxygen mask or endotracheal tube. HBOt treatments typically last for 1.5 – 2 hours (2). The clinical use of HBOt is regulated by the Undersea and Hyperbaric Medicine Society and has approved the use of HBOt for carbon monoxide poisoning, decompression sickness, non-healing wounds among other disorders (3).

There is also clear evidence that HBOt promotes a physiological response that would be detrimental to cancer, and many studies have been performed to evaluate the potential utility of HBOt as a stand-alone therapy (4). As described, the tumor vasculature is immature and inadequate, leading to incomplete perfusion of the tumor mass (5). This contributes to the HIF-1 signaling that drives many of the processes required for tumor progression. Increasing tumor perfusion promotes O_2-mediated degradation of HIF-1α, inhibiting its' tumor promoting effects. Moreover, HBOt saturation of the tumor restricts angiogenesis independent of HIF-1 through inhibition of growth-factor dependent pro-angiogenic signaling (6). Administration of HBOt in a rat mammary tumor model reduced blood vessel density, which was associated with reductions in VEGF and PDGF levels (6, 7).

Increasing tissue O_2 perfusion results in elevated O_2-tension at the cellular level. Elevating intracellular O_2 levels increases the likelihood of premature O_2 oxidation by prematurely lost electrons from the ETC. Thus, HBOt should increase superoxide production and the potential for oxidative stress. Indeed, we have previously shown that

hyperbaric oxygen increases ROS production in VM-M3 cells (8). The propensity for HBOt to enhance oxidative stress has led to its utilization as an adjuvant to chemo- and radiotherapies (4). The efficacy of platinum-based chemotherapeies appears to be particularly enhanced by HBOt, which is to be expected based on the ROS-promoting nature of those treatments. HBOt enhanced carboplatin activity in a mouse model of osteosarcoma and the efficacy of cisplatin in a human ovarian cancer xenograft (9, 10). In patients with colorectal cancer, administration of HBOt as an adjuvant to radiation significantly increased survival outcomes (11). Clinical implementation of HBOt and radiation for head and neck cancers has also proven to improve tumor control (12). HBOt-mediated oxygenation may not merely enhance the efficacy of radiotherapy at the tumor level, evidence suggests that HBOt protects normal tissue from radiation damage (13).

Gliomas have also been shown to be sensitive to HBOt. Administration of HBOt improved tumor response to carboplatin in patients with high-grade gliomas (14). As an adjuvant to radiotherapy, HBOt doubled mean survival of patients from one to two years over radiation alone (15). Moreover, our lab has demonstrated that HBOt enhances the anti-cancer effect of a ketogenic diet as well as ketone supplementation in the VM-M3 model (8, 16).

5.3 Metformin May Protect VM-M3 Cells Against the Pro-Oxidant Effects of Hyperbaric Oxygen in the Presence of DCA.

5.3.1 Figures

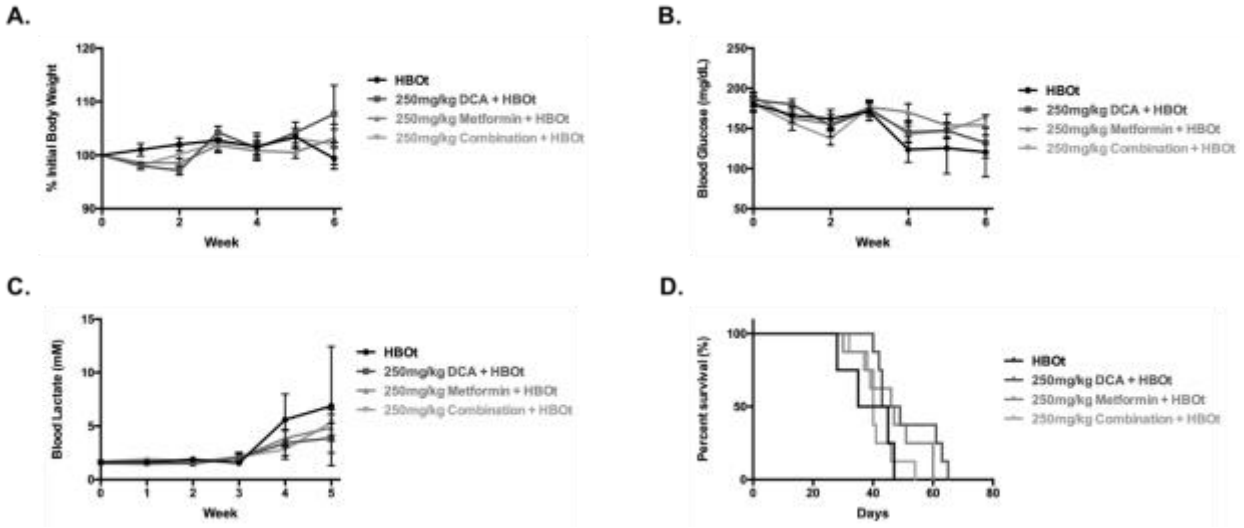

Figure 5.3.1 HBOt diminishes the effect of DCA on circulating lactate levels in tumor-burdened mice. (A). Average weekly change in weight from baseline for HBOt and metabolic therapy treatment groups for the first 6 weeks of treatment. **(B)** Average weekly blood glucose levels of control and treated mice over the first 6 weeks of treatment. **(C)** Average blood lactate levels of control and treated animals over the first 3 weeks of treatment. **(D)** Kaplan-Meier survival curves for HBOt, HBOt + 250mg/kg DCA, HBOt + 250mg/kg metformin and HBOt + 250mg/kg combination treatment groups. **(B)** Notation of cohort size, median and mean survival times, and the percent increase from control for those measures. **(A-C)** Error bars represent SEM of the treatment group.

A.

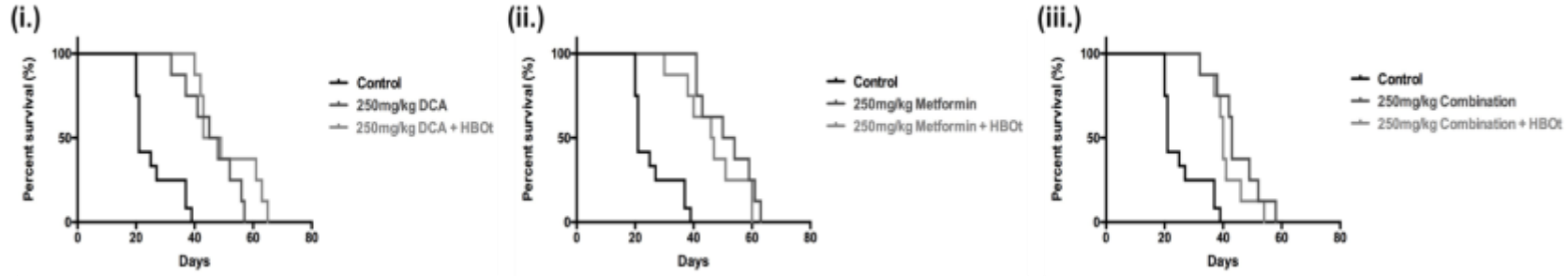

B.

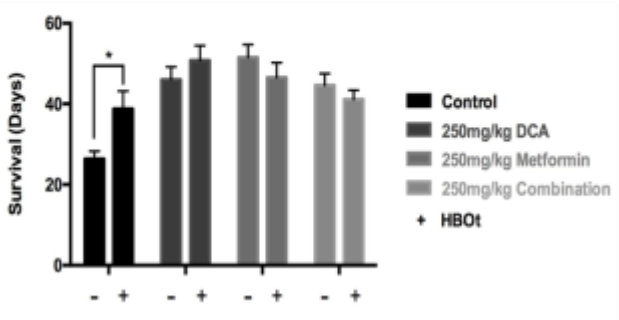

C.

Cohort	N	Median Survival	% Increase in Median Survival	Mean Survival	% Increase in Mean Survival
Control	12	21.0	-	25.8	-
HBOt	4	40.0	90.48%	38.8	50.39%
250mg/kg DCA	8	46.5	121.40%	46.0	78.60%
250mg/kg DCA + HBOt	8	46.0	119.00%	50.8	96.90%
250mg/kg Metformin	8	52.0	147.60%	51.5	100.00%
250mg/kg Metformin + HBOt	8	46.5	121.40%	46.5	80.23%
250mg/kg Combination	8	43.0	104.80%	44.6	73.20%
250mg/kg Combination + HBOt	8	40.0	90.48%	41.1	59.30%

Figure 5.3.2 HBOt co-treatment provides a slight survival benefit to DCA treated VM-M3 burdened mice. (A) Kaplan-Meier survival curves depicting the effect of HBOt on (i) 250mg/kg DCA (ii) 250mg/kg metformin and (iii) 250mg/kg combination treatment. **(B)** Notation of cohort size, median and mean survival times, and the percent increase from control for all treatment groups. **(B)** Error bars represent SEM of the treatment group; *p<0.05.

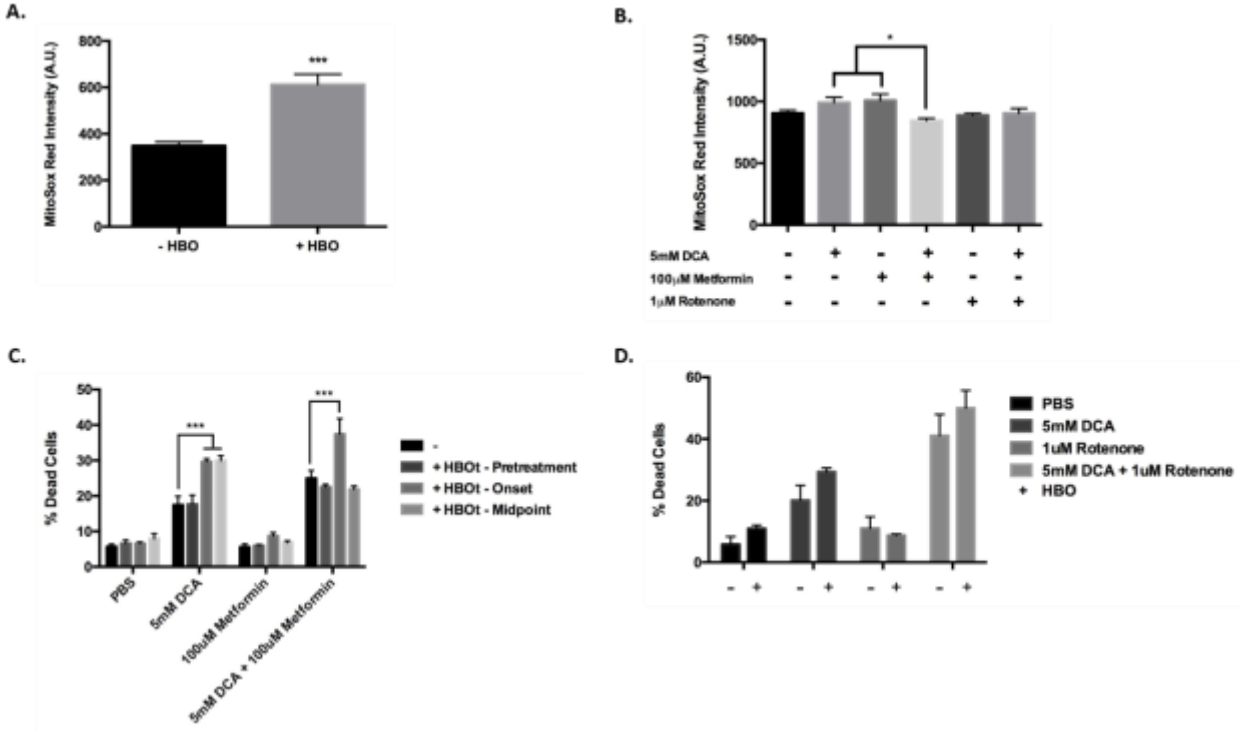

Figure 5.3.3 Hyperbaric oxygen enhancement of DCA cytotoxicity is temporal. (A) Quantification of VM-M3 superoxide production following a 1-hour treatment with hyperbaric oxygen (2.5 ATA). **(B)** Analysis of MitoSox Red fluorescence following 1-hour hyperbaric oxygen treatment (2.5 ATA) in the presence of DCA and/or metformin. **(C)** Analysis of the temporal effect of 1-hour hyperbaric oxygen treatment (2.5 ATA) on DCA ± metformin cytotoxicity towards VM-M3 cells. (D) Analysis of VM-M3 viability following a 1-hour treatment with hyperbaric oxygen at the onset of a 24-incubation with DCA ± rotenone. **(A, B)** Error bars represent SEM of a single experiment replicated in triplicate **(C, D)** Error bars represent SEM of three experimental replicates; *p<0.05 and ***p<0.001.

5.3.2 Results & Discussion

To assess the impact of HBOt on our DCA and metformin combination, we employed a previously tested therapeutic regimen (8, 16). Animals received HBOt at 2.5 ATA for 90 minutes three times a week (M, W, F) for the duration of the study starting on day 1 post tumor cell implantation. We report here that HBOt treatment significantly increased median and mean survival of VM-M3-burdened mice compared to controls (Fig. 5.3.2C). This deviates from our previous finding that showed no beneficial effect of HBOt on VM-M3 survival (8). This could be a function of variation in the subcutaneous implantation of VM-M3 cells between experiments. If VM-M3 cells enter the circulation immediately upon implantation, then they bypass the requirement for EMT. HBOt has been shown to promote a mesenchymal-to-epithelial transition that restricts the metastatic potential of tumor cells (7). Thus, if VM-M3 cells were strictly restricted to the site on implantation, HBOt treatment may inhibit VM-M3 metastasis and prolong survival in tumor-burdened mice.

Administration of HBOt was not detrimental to animal health and did promote weight loss (Fig. 5.3.1A). Consistent with our previous findings, metformin treatment promoted an initial decrease in blood glucose compared to HBOt-treated animals (Fig. 5.3.1B). However, DCA treatment did not alter blood glucose or blood lactate levels when administered with HBOt (Figs. 5.3.1B, 5.3.1C). We have demonstrated that DCA increases glucose oxidation in VM/dk skeletal muscle, which suggests that DCA reduction in blood lactate levels is mediated by enhancing oxidative efficiency in peripheral muscle tissue. As hyperoxia is shown to reduce lactate production in muscle during transient and steady-state exercise, it is possible that chronic HBOt increases

oxidative capacity of muscle tissue and diminishes DCA activity (17, 18). Consistent with the increase in survival, HBOt treatment delayed the increase in blood lactate that accompanies VM-M3 tumor progression (Fig. 5.3.1C).

Of the three therapeutic regimens, adjuvant HBOt was most beneficial to 250mg/kg DCA treatment. The addition of HBOt increased mean survival of DCA treated mice by 4.8 days (10.4%) (Fig. 5.3.2C). HBOt did not provide a benefit to metformin-treated or combination-treated animals, rather there was a slight decrease in efficacy associated with adjuvant HBOt (Fig 5.3.2C). VM-M3 tumors are extremely aggressive and metastasize rapidly upon subcutaneous transplantation (19). VM-M3 mortality is tightly associated with metastasis, thus treatment efficacy is dependent on inhibition or delay of tumor spread (8, 16, 20). DCA, metformin, and combination treatments prolong survival of tumor-burdened mice, which is exhibited in a right-shift in the survival curves of these groups. However, these Kaplan-Meier survival curves also show that these agents do not significantly alter the rate of cohort mortality, rather they delay the time to initial mortality event for the treatment cohort (Fig. 5.3.2Ai-iii). This suggests that these metabolic therapies delay onset of metastasis but do not alter the metastatic cascade upon VM-M3 dissemination. As such HBOt enhancement of DCA treatment was associated with a further delay in cohort mortality (Fig. 5.3.2Ai).

Since we hypothesized that adjuvant HBOt would enhance oxidative stress with the DCA and metformin combination, we sought to characterize the effect of hyperbaric oxygen on VM-M3 ROS production. Consistent with our previous findings, a 1-hour treatment with hyperbaric oxygen (2.5 ATA) significantly enhanced superoxide production in VM-M3 cells (Fig. 5.3.3A) (8). Incubation with DCA or metformin during

hyperbaric oxygen treatment further enhanced ROS production in VM-M3 cells (Fig. 5.3.3B). Unexpectedly, superoxide production following hyperbaric oxygen treatment was significantly lower when combined with the combination of DCA and metformin compared to either agent alone. Hyperbaric oxygen treatment also augmented the cytotoxicity of DCA and rotenone in combination (Fig.5.3.3D). This too occurred without an apparent increase in ROS production above the levels promoted by concurrent non-toxic hyperbaric oxygen treatment (Fig. 5.3.3B). Analysis of the temporal effect of hyperbaric oxygen on this combination was inconclusive (DNS).

Induction of ROS by hyperbaric oxygen treatment alone was not associated with VM-M3 cytotoxicity (Figure 5.3.3C). This is largely consistent with the literature as most studies have demonstrated that hyperbaric oxygen treatment is cancer cell neutral or cytostatic as a standalone therapy (4). We next evaluated whether the time of hyperbaric oxygen treatment had an impact on the efficacy of our metabolic agents. Elevation of the partial pressure of oxygen (pO_2) within tumors is shown to be sustained for 30-minutes following HBOt administration, thus we examined if hyperbaric oxygen pre-treatment would alter DCA and/or metformin cytotoxicity (21). Hyperbaric oxygen pre-treatment had no effect on any of the metabolic treatments following a 24-hour incubation (Fig. 5.3.3C). Delivery of hyperbaric oxygen at the onset of metabolic agent incubation significantly enhanced the cytotoxicity of DCA and the combination, whereas hyperbaric oxygen treatment 12-hours into the metabolic agent incubation only enhanced DCA cytotoxicity alone (Fig 5.3.3C). This not only suggests that the effect of hyperbaric oxygen on DCA and metformin is temporal but also that metformin is slightly protective to VM-M3 cells under hyperbaric oxygen stress.

Prolonged hyperoxia is shown to simultaneously reduce complex I/II efficiency and glycolytic capacity in the lung (2). Thus, metformin stimulation of glycolytic metabolism may protect against the potential metabolic stress induced by HBOt. We show that DCA does not fully attenuate metformin stimulation of glycolytic metabolism in VM-M3 cells over a period of 48 hours (Figure 3.2.4B). This suggests that prolonged treatment with DCA and metformin may result in a progressive increase in compensatory glycolysis that protects against the delayed delivery of hyperbaric oxygen. While we did not see increased ROS production with concurrent treatment of the combination and hyperbaric oxygen, we did observe an increase in cytotoxicity associated with this therapeutic scheme (Figs. 5.3.3B, C). This would indicate that the delivery of hyperbaric oxygen at the onset of metabolic agent treatment prevents the protective compensatory effect of metformin. These data are consistent with our *in vivo* observation that adjuvant HBOt treatment slightly reduced the efficacy of metformin and the combination (Fig. 5.3.2B). Therefore, it is necessary to consider the therapeutic regimen design in hopes of achieving translatable efficacy with this combinatorial therapy. Bolus delivery of DCA alone or the combination just prior to HBOt administration may elicit the greatest therapeutic benefit while preventing the potential delayed compensation associated with metformin treatment.

5.4 References

1. Tibbles, PM. & Edelsberg, JS. Hyperbaric-oxygen therapy. *N. Engl. J. Med.* **334**, 1642-1648 (1996).
2. Thom, SR. Hyperbaric oxygen: its mechanisms and efficacy. *Plast. Reconstr. Surg.* **127**, S131-141 (2011).
3. Gill, AL. & Bell, CN. Hyperbaric oxygen: its uses, mechanisms of action and outcomes. *QJM* **97**, 385-395 (2004).
4. Moen, I. & Stuhr, LEB. Hyperbaric oxygen therapy and cancer – a review. *Target Oncol.* **7**, 233-242 (2012).
5. Ruoslahti, E. Specialization of tumor vasculature. *Nat. Rev. Cancer* **2**, 83-90 (2002).
6. Raa, A. *et al.* Hyperoxia retards growth and induces apoptosis and loss of glands and blood vessels in DMBA-induced rat mammary tumors. *BMC Cancer* **7**, 23 (2007).
7. Moen, I. *et al*. Hyperoxic treatment induces mesenchymal-to-epithelial transition in a rat adenocarcinoma model. *PLoS ONE* **4**, e6381 (2009).
8. Poff, AM. *et al*. Non-toxic metabolic management of metastatic cancer in VM mice: novel combination of ketogenic diet, ketone supplementation, and hyperbaric oxygen therapy. *PLoS ONE* **10**, e0127407 (2015).
9. Kawasoe, Y. *et al.* Hyperbaric oxygen as a chemotherapy adjuvant in the treatment of osteosarcoma. *Oncol. Rep.* **22**, 1045-1050 (2009).
10. Selvendiran, K. *et al*. Oxygenation inhibits ovarian tumor growth by downregulating STAT3 and cyclin-D1 expressions. *Cancer Biol. Ther.* **10**, 386-389 (2010).
11. Dische, S. & Senanayake, F. Radiotherapy using hyperbaric oxygen in the palliation of carcinoma of colon and rectum. *Clin. Radiol.* **23**, 512-518 (1972).
12. Sealy, R. Hyperbaric oxygen in the radiation treatment of head and neck cancers. *Radiother. Oncol.* **20**, S75-79 (1991).
13. Bennett, MH., Feldmeier, J., Smee, R. & Milross, C. Hyperbaric oxygenation for tumour sensitization to radiotherapy. *Cochrane Database Syst. Rev.* **4**, CD005007 (2012).
14. Suzuki, Y. *et al*. Pharmacokinetic investigation of increased efficacy against malignant gliomas of carboplatin combined with hyperbaric oxygenation. *Neurol. Med Chir.* **49**, 193-197 (2009).
15. Kohshi, K. *et al.* Effects of radiotherapy after hyperbaric oxygenation on malignant gliomas. *Br. J. Cancer* **80**, 236-241 (1999).
16. Poff, AM., Ari, C., Seyfried, TN. & D'Agostino, DP. The ketogenic diet and hyperbaric oxygen therapy prolong survival in mice with systemic metastatic cancer. *PLoS One* **8**, e65522 (2013).
17. Stellingwerff, T. *et al.* Effects of hyperoxia on skeletal muscle carbohydrate metabolism during transient and steady-state exercise. *J. Appl. Physiol.* **98**, 250-256 (1985).
18. Stellingwerff, T. *et al*. Hyperoxia decreases muscle glycofenolysis, lactate production, and lactate efflux during steady-state exercise. *Am. J. Physiol. Endocrinol. Metab.* **290**, E1180-1190 (2006).

19. Huysentruyt, LC. *et al.* Metastatic cancer cells with macrophage properties: evidence for a new murine tumor model. *Int. J. Cancer* **123**, 73-84 (2008).
20. Shelton, LM., Huysentruyt, LC., Mukherjee, P. & Seyfried, TN. Calorie restriction as an anti-invasive therapy for malignant brain cancer in the VM mouse. *ASN Neuro* **2**, e00038 (2010).
21. Kinoshita, Y. *et al.* Preservation of tumor oxygen after hyperbaric oxygenation monitored by magnetic resonance imaging. *Br. J. Cancer* **82**, 88-92 (2000).
22. Das, KC. Hyperoxia decreases glycolytic capacity, glycolytic reserve and oxidative phosphorylation in MLE-12 cells and inhibits complex I and II function, but not complex IV in isolated mouse lung mitochondria. *PLoS ONE* **8**, e73358 (2013).

CHAPTER 6: CONCLUSIONS AND FUTURE DIRECTIONS

6.1 Chapter Synopsis

Herein we address the major findings of this dissertation project and the implications of these findings on the field. We also discuss logical extensions of these studies to be conducted in the future.

6.2 Conclusions and Future Directions

The goal of this dissertation project was to evaluate the potential synergy between DCA and metformin and the potential utility of the combination as an anti-cancer therapy. In line with the literature, we demonstrate a need for supraphysiological concentrations of DCA to elicit an anti-cancer effect (1-11). As dichloroacetate exists physiologically as an anion, it is relatively membrane impermeable despite its small size and requires the mitochondrial pyruvate carrier for mitochondrial uptake (12, 13). Pathak *et al*. reported that conjugating DCA to a lipophilic carrier enhanced mitochondrial transport and reduced the IC_{50} value of DCA from millimolar to the low micromolar range (14). This is well within achievable serum trough levels associated with DCA administration and reflective of the K_i of PDK2 (~200µM), the most ubiquitous isoform (12, 15, 16). Suggesting that a conjugated form of DCA may elicit a more robust anti-cancer effect at physiological concentrations.

Our *in* vitro findings suggest that complex I inhibition cooperates with DCA activation of oxidative glucose metabolism to promote catastrophic oxidative stress in VM-M3 glioblastoma cells. As described, there is extraordinary interest in targeting cancer mitochondria as a therapeutic strategy as recent evidence suggests mitochondrial metabolism is required for tumorigenesis and to meet the bioenergetics demands or rapidly proliferating tumor cells (17-19).

As mitochondrial metabolism is intrinsically linked to redox balance, a known sensitivity of cancer, targeting the organelle is likely to prove successful (20). Schöckel *et al*. recently reported that inhibition of complex I with an experimental small molecule induced cytotoxic oxidative stress and inhibited tumor growth in a model of melanoma, a highly aggressive tumor species (21). Our results also demonstrate efficacy in targeting the efficiency of electron transport in an aggressive cancer, as GBM is a highly malignant brain tumor associated with an extremely poor prognosis (22). Along those lines, Shen *et al*. have shown efficacy in the dual-targeting of GBM metabolism with DCA and a mitochondrial poison (23). Rotenone had a greater effect on VM-M3 viability in combination with a modestly cytotoxic concentration of DCA than metformin (Fig. 3.2.5C). This is likely an effect of the degree of complex I inhibition as metformin is thought to be only a mild inhibitor of complex I (24). As such, VM-M3 cells may be more sensitive to phenformin enhancement of DCA activity. Though phenformin has been removed from the clinic for induction of lactic acidosis, the activity of DCA is likely to attenuate lactate production associated with phenformin treatment (25).

While we report disappointing results in regard to the efficacy of the combination *in vivo*, Jiang *et al*. have recently reported that DCA enhanced the efficacy of

phenformin in prolonging survival in an orthotopic GSC model (25). Though we preferentially employ subcutaneous transplantation of VM-M3 cells in the abdominal fat pad, these cells can also be transplanted orthotopically (26). Future studies evaluating DCA and metformin efficacy in treating orthotopic VM-M3 tumors should be conducted before definitively discounting the potential utility of the combination. Orthotopic models allow for tumor growth in the tissue of tumor origin, which is most clinically translatable. Our metabolomics data indicate that the combination of DCA and metformin reduce overall brain metabolism in healthy VM/dk mice (Tables 4.5.1-5). This would likely alter the tumor environment and metabolic niche that supports VM-M3 tumor growth in the brain, potentially leading to a more pronounced effect of the combination on VM-M3 progression.

Additionally, manipulation of our therapeutic regimen is likely necessary to achieve optimal efficacy. Chemoresistance is an inevitability of current cancer therapies and this is often exacerbated by clinical utilization of maximally tolerated doses to promote rapid remission (27, 28). Using lower doses to maintain stable disease may be more beneficial to many patients and delay or even prevent the expansion of resistant tumor cell populations. This may also be achieved through periodic cycling of therapies that target divergent pathways, inducing differential selective pressures over the course of treatment (29, 30). Analysis of VM-M3 tumors that develop resistance to DCA and metformin can inform our selection of complementary therapies for this altered strategy.

Overall, these results support the assertion that GBMs are vulnerable to modulations of glucose metabolism (31). However, this study also highlights that metabolic therapies are susceptible to the development of chemoresistance. Thus, the

combination of DCA and metformin may be most useful as an adjuvant to current pro-oxidant therapies, for which efficacy is often fleeting due to chemoresistance mechanisms that restrict mitochondrial oxidation (3, 4, 6, 10). Our findings are consistent with several recent reports demonstrating that metformin enhances DCA efficacy in multiple cancers (32-37).

6.3 References

1. Dai, Y. *et al.* Dichloroacetate Enhances Adriamycin-Induced Hepatoma Cell Toxicity In Vitro and In Vivo by Increasing Reactive Oxygen Species Levels. *Plos One* **9,** e92962 (2014).

2. Sanchez WY. *et al.* Dichloroacetate inhibits aerobic glycolysis in multiple myeloma cells and increases sensitivity to bortezomib. *Brit J Cancer* **108,** 1624–1633 (2013).
3. Xuan, Y. *et al.* Dichloroacetate attenuates hypoxia-induced resistance to 5-fluorouracil in gastric cancer through the regulation of glucose metabolism. *Exp Cell Res* **321,** 219–230 (2014).
4. Kumar, K. *et al.* Dichloroacetate reverses the hypoxic adaptation to bevacizumab and enhances its antitumor effects in mouse xenografts. *J Mol Med* **91,** 749–758 (2013).
5. Kumar, A., Kant, S. & Singh, SM. Antitumor and chemosensitizing action of dichloroacetate implicates modulation of tumor microenvironment: A role of reorganized glucose metabolism, cell survival regulation and macrophage differentiation. *Toxicol Appl Pharm* **273,** 196–208 (2013).
6. Shen, YC. *et al.* Activating oxidative phosphorylation by a pyruvate dehydrogenase kinase inhibitor overcomes sorafenib resistance of hepatocellular carcinoma. *Brit J Cancer* **108,**72–81 (2013).
7. Sun, RC. *et al.* Reversal of the glycolytic phenotype by dichloroacetate inhibits metastatic breast cancer cell growth in vitro and in vivo. *Breast Cancer Res Tr* **120,** 253–260 (2010).
8. Bonnet, S. *et al.* A mitochondria-K+ channel axis is suppressed in cancer and Its normalization promotes apoptosis and inhibits cancer growth. *Cancer Cell* **11,** 37–51 (2007).
9. Wong, JY., Huggins, GS., Debidda, M., Munshi, NC. & De Vivo, I. Dichloroacetate induces apoptosis in endometrial cancer cells. *Gynecol Oncol* **109,** 394–402 (2008).
10. Roh, JL., Park, JY., Kim, EH., Jang, HJ. & Kwon, M. Activation of mitochondrial oxidation by PDK2 inhibition reverses cisplatin resistance in head and neck cancer. *Cancer Lett* **371,** 20–29 (2016).
11. Sun, RC., Board, PG. & Blackburn, AC. Targeting metabolism with arsenic trioxide and dichloroacetate in breast cancer cells. *Mol Cancer* **10,** 1–15 (2011).
12. Stacpoole PW. The Pharmacology of Dichloroacetate. Metabolism **38**, 1124-44 (1989).
13. Halestrap AP. The mitochondrial pyruvate carrier. Kinetics and specificity for substrates and inhibitors. *Biochem J* **148,** 85–96 (1975).
14. Pathak, RK., Marrache, S., Harn, DA. & Dhar, S. Mito-DCA: A Mitochondria Targeted Molecular Scaffold for Efficacious Delivery of Metabolic Modulator Dichloroacetate. *Acs Chem Biol* **9,** 1178–1187 (2014).
15. Dunbar, EM. *et al.* Phase 1 trial of dichloroacetate (DCA) in adults with recurrent malignant brain tumors. *Invest New Drug* **32,** 452–464 (2014).

16. Chu, QS. *et al.* A phase I open-labeled, single-arm, dose-escalation, study of dichloroacetate (DCA) in patients with advanced solid tumors. *Invest New Drug* **33,** 603–610 (2015).
17. Owen, MR., Doran, E. & Halestrap, AP. Evidence that metformin exerts its anti-diabetic effects through inhibition of complex 1 of the mitochondrial respiratory chain. *Biochem J* **348,** 607–614 (2000).
18. Martínez-Reyes, I. *et al.* TCA Cycle and Mitochondrial Membrane Potential Are Necessary for Diverse Biological Functions. *Mol Cell* **61,** 199–209 (2016).
19. Sullivan, LB. *et al.* Supporting Aspartate Biosynthesis Is an Essential Function of Respiration in Proliferating Cells. *Cell* **162,**552–563 (2015).
20. Gorrini, C., Harris, IS. & Mak, TW. Modulation of oxidative stress as an anticancer strategy. *Nat Rev Drug Discov* **12,** 931–947 (2013).
21. Schöckel, L. *et al.* Targeting mitochondrial complex I using BAY 87-2243 reduces melanoma tumor growth. *Cancer Metabolism* **3,**1–16 (2015).
22. Adamson, C. *et al.* Glioblastoma multiforme: a review of where we have been and where we are going. *Expert Opin Inv Drug* **18,** 1061–1083 (2009).
23. Shen, H. *et al.* Dual-targeting of aberrant glucose metabolism in glioblastoma. *J Exp Clin Canc Res* **34,** 1–11 (2015).
24. Viollet, B. *et al.* Cellular and molecular mechanisms of metformin: an overview. *Clin Sci* **122,** 253–270 (2012).
25. Jiang W. *et al*. Repurposing phenformin for the targeting of glioma stem cells and the treatment of glioblastoma. *Oncotarget* (2016).
26. Shelton, LM. *et al.* A novel pre-clinical in viv mouse model for malignant brain tumor growth and invasion. *J Neurooncol.* **99**, 165-176 (2010).
27. Benzekry, S. & Hahnfeldt, P. Maximum tolerated dose versus metronomic scheduling in the treatment of metastatic cancers. *J. Theor. Biol.* **335**, 235-244 (2013).
28. Gatenby, RA., Silva, AS., Gillies, RJ. & Frieden, BR. Adaptive therapy. *Cancer Res.* **69**, 4894-4903 (2009).
29. Maiti, R. Metronomic chemotherapy. *J. Pharmacol. Pharmacother.* **5**, 186-192 (2014).
30. Pasquier, E., Kavallaris, M., Andre, N. Metronomic chemotherapy: new rationale for new directions. *Nat. Rev. Clin. Oncol.* **7**, 455-465 (2010).
31. Michelakis ED. *et al.* Metabolic modulation of glioblastoma with dichloroacetate. *Sci Transl Medicine* **2,** 31-34 (2010).
32. Haugrud, AB., Zhuang, Y., Coppock, JD. & Miskimins, WK. Dichloroacetate enhances apoptotic cell death via oxidative damage and attenuates lactate production in metformin-treated breast cancer cells. *Breast Cancer Res Tr* **147,** 539–550 (2014).
33. Choi, YW. & Lim, IK. Sensitization of metformin-cytotoxicity by dichloroacetate via reprogramming glucose metabolism in cancer cells. *Cancer Lett* **346,** 300–308 (2014).
34. Hong, SE. *et al.* Targeting HIF-1a is a prerequisite for cell sensitivity to dichloroacetate (DCA) and metformin. *Biochem. Biophys. Res. Commun.* **469**, 164-170 (2016).

35. Voltan, R. *et al.* Metformin combined with sodium dichloroacetate promotes B leukemic cell death by suppressing anti-apoptotic protein Mcl-1. *Oncotarget* **7**, 18965-18977 (2016).
36. Li, B. *et al*. Dichloroacetate and metformin synergistically suppress the growth of ovarian cancer cells. *Oncotarget* **[**Epub ahead of print] (2016).
37. Hong, SE. *et al.* TRAIL restores DCA/metformin-mediated cell death in hypoxia. *Biochem. Biophys. Res. Commun.* **478**, 1389-1395 (2016).

APPENDIX A: MATERIALS AND METHODS

A.1 Ethical Statement in Regard to Animal Use

All animal used for the studies performed and analyzed in this dissertation were approved by and preformed with strict adherence to the University of South Florida's Institutional Animal Care and Use Committee (IACUC) protocol R0228.

A.2 Materials and Methods

A.2.1 Cell Culture

VM-M3/Fluc (VM-M3) cells were obtained as a gift from Dr. Thomas Seyfried (Boston College, Chestnut Hill, MA). VM-M3 cells were cultured in D-glucose, L-glutamine, and sodium pyruvate-free Dulbecco's Modified Eagle Medium (Gibco, Life Technologies) supplemented with 10% fetal bovine serum (Invitrogen), 25mM D-glucose (Fisher Scientific), 2mM L-glutamine (Gibco, Life Technologies), 1% penicillin-streptomycin (Invitrogen), and 10mM HEPES buffer (Gibco, Life Technologies). Cells were maintained at 37°C in 95% air, 5% CO_2 in a humidified incubator.

A.2.2 Western Blot Analysis

VM-M3 cells were seeded on 35-mm 6-well plates for 24 hours at a density of 10^6 cells/well. The culture media was then replaced and treatment applied. Cells were collected and lysed in 200µL of RIPA lysis buffer containing complete protease and

phosphatase inhibitors (ThermoFisher). Lysates were centrifuged at 13,200g for 15 minutes at 4°C and the supernatant collected. Protein concentration was determined by BCA assay (ThermoFisher) and 20ug of protein was loaded into a 10% Mini-PROTEAN TGX precast polyacrylamide SDS-PAGE gel (BIO-RAD). Protein was transferred to nitrocellulose membranes, blocked with 5% non-fat dairy milk in Tris-buffered saline and tween (TBS-T) and incubated overnight at 4°C with primary antibodies for PDH-E1α (Abcam, ab110330) and phospho-PDH-E1α (Ser293; Abcam, ab92696). Blots were washed with TBS-T and incubated with goat-anti-mouse and goat-anti-rabbit secondary antibodies coupled to horseradish peroxidase (HRP). HRP substrate was then applied to the blots and antibody signal was detected with the ChemiDoc MP Imaging System (BIO-RAD).

A.2.3 Lactate Export

VM-M3 cells were seeded for 24 hours on 22-mm 12-well plates in triplicate at a density of 50,000 cells/well. The culture media was then replaced and treatment applied. To determine lactate export, 10µL of treated culture media was aspirated and applied to a lactate detection strip and lactate concentration determined with a LACTATE PLUS Lactate Meter (Nova Biomedical) at time of treatment application and every 12 hours over a period of 48 hours.

A.2.4 ROS Production

Mitochondrial superoxide production was measured using the fluorescent probe, MitoSOX Red (Molecular Probes, Invitrogen). 50,000 VM-M3 cells were seeded on 18-

mm glass coverslips in 22-mm 12-well plates for 24 hours. Culture media was then replaced and treatment applied. Coverslips were then rinsed with D-PBS and stained with 2.5µM MitoSOX Red in Hank's Balanced Salt Solution (HBSS) with $Ca^{2+/}Mg^{2+}$ (Gibco, Life Technologies) for 10 minutes at 37°C. Coverslips were then inverted and mounted on glass microscope slides and MitoSOX Red fluorescence (Ex/Em: 510:580 nm) was detected with a TRITC filter and a Nikon TE2000E fluorescence microscope and a 40X objective lens. The average relative fluorescence intensity of individual cells within 8-10 fields of view were determined for each treatment.

A.2.5 Mitochondrial Membrane Potential

Mitochondrial membrane potential ($\Delta\Psi_m$) was measured using the cationic fluorescent probe tetramethylrhodamine (TMRE; Molecular Probes, Life Technologies). 50,000 VM-M3 cells were seeded on 18-mm glass coverslips in 22-mm 12-well plates for 24 hours. Culture media was then replaced and treatment applied. Coverslips were then rinsed with D-PBS and stained with 250nM TMRE in culture medium for 30 minutes at 37°C. Coverslips were counterstained with 100nM MitoTracker Green (Molecular Probes, Invitrogen) in culture media for 20 minutes at 37°C and then inverted and mounted on glass microscope slides. Cells were visualized with a Nikon TE2000E fluorescence microscope and a 40X objective lens. TMRE fluorescence (Ex/Em: 549/575 nm) was detected with a TRITC filter and MitoTracker Green fluorescence (Ex/Em: 490/516 nm) was detected with a FITC filter. The average relative fluorescence intensity of individual cells within 10 fields of view were determined for each treatment.

A.2.6 Proliferation

105 VM-M3 cells were seeded on 6-well plates and treated with DCA or metformin for 12-96 hours. At each designated time point cells were collected by physical detachment. 20µL of the cell suspension was mixed with 20µL of 0.4% Trypan blue solution (Sigma) to produce a total volume of 40uL. 20uL of the solution was applied to a hematocytometer and visualized by light microscope for cell counting. Trypan blue does not pass through the intact cell membrane of live cells and thus only stains dead cells a dark blue, permitting the identification and quantification of live cells. The number of cells present in each well was determined by standard hematocytometry.

A.2.7 Cell Viability

Cell viability was assayed with the LIVE/DEAD Viability/Cytotoxicity Kit (Invitrogen). VM-M3 cells were seeded for 24 hours on 18-mm glass coverslips in 22-mm 12-well plates at a density of 20,000 cells/well. The culture media was then replaced and treatment applied for 24 hours. Following the 24-hour treatment, cells were washed with D-PBS (Gibco, Life Technologies) and then incubated with 800µL of 2µM Calcein AM and 4µM Ethidium Homodimer-1 (EthD-1) in D-PBS for 30 minutes. Coverslips were then inverted and mounted onto glass microscope slides and cells visualized with a Nikon TE2000E fluorescence microscope and a 10X objective lens. Calcein-AM readily passes through the membrane of intact cells and is digested by cellular esterases that yield a fluorescent calcein product (Ex/Em: 495/515 nm) that can be detected with a FITC filter as an indicator of live cells. EthD-1 (Ex/Em: 525/590 nm) is cell-impermeable but emits a red fluorescence upon association with nucleic acid

following loss of membrane integrity that can be detected with a TRITC filter as an indicator of dead cells. The live/dead ratios of 8-10 distinct fields of view were determined via direct cell count for each treatment.

A.2.8 Determination of [GSH]:[GSSH]

The ratio of reduced/oxidized glutathione (GSH:GSSG) was assayed with the Glutathione Fluorometric Assay Kit (BIoVision). 10^6 VM-M3 cells were seeded in 35-mm 6-well plates for 24 hours. Culture media was then replaced and treatment applied. Cells were collected and homogenized in 100µL of ice cold Glutathione Assay Buffer. Homogenates were then transferred to pre-chilled microcentrifuge tubes containing 20µL of 6N perchloric acid (PCA) and vortexed for 10 seconds. Homogenates were spun down at 13,000 G for five minutes at 4°C. To remove potential oxidizers of GSH, the supernatants were transferred to 10KDa centrifugal filters (Millipore) and spun down at 14,000 G for 15 minutes at 4°C. 20µL of ice cold 6N KOH was added to 40µL of each sample to precipitate the PCA and then samples were spun down at 13,000 G for 2 minutes at 4°C. 10uL volume of supernatant were transferred to paired 96-well plates in duplicate to assay both GSH and GSSG in each sample. To detect GSH, 80µL of Glutathione Assay Buffer was added to the 10µL of supernatant. Whereas to detect GSSG, 60µL of assay buffer and 10µL of GSH Quencher were added to the well and incubated for 10 minutes at room temperature to quench GSH. 10µL of Reducing Agent was then added to convert GSSG to GSH. 10uL of OPA probe (o-phthalaldehyde) was added to each well and incubated for 40 minutes at room temperature, at which point the plate was read by a fluorescence plate reader at an Ex/Em spectrum of 340/420 nm.

A.2.9 Analysis of p-AMPKα:AMPKα

The activation status of AMPKα was assayed using the CytoGlow AMPKα (Phospho-Thr172) Colorimetric Cell-Based ELISA kit (Assay bioTech). 15,000 VM-M3 cells were seeded overnight on 96-well plates. Cells were then treated for 4-hours, washed twice with TBS, and fixed with 4% paraformaldehyde (w/v) in D-PBS) for 20 minutes. Cells were then washed 3X in Wash Buffer (0.2% Kathon CG/ICP, 1% Tween in TBS) and then incubated in Quenching Buffer (0.05% Sodium Azide, 1% H_2O_2 in TBS) for 20 minutes to inactivate endogenous peroxidase activity. Cells were then washed 3X with Wash Buffer and then blocked with Blocking Buffer (0.05% Sodium Azide, 0.5% Triton X-100 in TBS) for 1-hour. Cells were then incubated overnight with primary antibodies for p-AMPKα (Thr172), AMPKα or GAPDH, which served as an internal positive control. Following three washes with Wash Buffer, the cells were incubated in HRP-conjugated secondary antibodies for 90 minutes; Anti-Rabbit IgG for p-AMPK (Thr172) and AMPK, and Anti-Mouse IgG for GADPH. Cells were then washed 3X and incubated in HRP substrate (<0.02% H_2O_2 and < 0.1% 3,3',5,5'-Tetramethylbenzidine [TMB]) for 30 minutes, after which 2N sulfuric acid was added to stop the peroxidase reaction. The absorbance at 450nm was then read using a plate reader (BioTek ELx800). Cells were then washed 3X and incubated with 0.05% Crystal Violet for 30 minutes. After which, the cells were washed and then incubated with SDS to solubilize the Crystal Violet for 1-hour. The absorbance was read at 595nm to quantify cell number.

A.2.10 Survival Studies

8-10 week old VM/dk were randomly assigned to a treatment group, while maintaining age-matching, and subcutaneously implanted with 10^6 VM-M3/Fluc cells in 300µL in D-PBS in the left abdominal flank. Treatment began on the day of injection and lasted for the entirety of the study. Survival time was denoted as the time in days from cancer cell implantation to time of euthanasia. Animals were humanely euthanized by CO_2 asphyxiation upon presentation of these defined criteria: severe weight loss (>10% baseline body weight), reduced appetite, diminished grooming behavior, lethargy, lack of response to physical stimuli, loss of mobility, or development of severe ascites.

A.2.11 Drug Administration

DCA and metformin were administered orally through the animal's diet. DCA (Sigma) and metformin (Sigma) exhibit oral bioavailability and are available in a stable powdered dosage form that can be integrated into a powdered form of a standard rodent diet (2018 Teklad Global 18% Protein Rodent Diet, Harlan Laboratories). Each agent was pulverized by hand to remove any residual clumping and mixed thoroughly with the powdered diet to evenly distribute the drug. Deionized or reverse osmosis (RO) water was added in a 1:1 ratio to generate a firm paste that was fed *ad libitum*. Initial dosing was based on the observation that a 30g VM/Dk mouse will eat approximately 6g of food per day. Dietary intake was measured daily and dosing of the food was adjusted to reflect the changes in average intake of the animals. Food was replaced every other day to maintain freshness.

A.2.12 Blood Metabolite and Weight Measurements

Blood samples were collected from a perpetual tail lesion of each animal on the day prior to cancer cell implantation and every 7 days thereafter at the same time of day to control for natural fluctuations in feeding and circadian metabolism. Blood glucose was measured with the commercially available Precision Xtra Glucose (Abbot Laboratories). Blood lactate was measured with the commercially available LACTATE PLUS Lactate Meter (nova biomedical). Animals were weighed at the same 7-day interval for the duration of study with the AWS-1Kg Portable Digital Scale (AWS).

A.2.13 Tumor Burden Analysis.

The VM-M3/Fluc cells have been transfected with a lentiviral vector containing firefly luciferase, which generates a bioluminescent product from the enzymatic consumption of its substrate, luciferin. This bioluminescence can be detected and quantified by the Xenogen IVIS Lumina System (Caliper LS), permitting non-invasive *in vivo* imaging. Bioluminescent signal (photons/second) intensity is directly correlated with tumor burden and is an established measure of tumor growth in luciferase-positive tumor models. Animals will receive a 50 mg/kg intraperitoneal (i.p.) injection of D-Luciferin 12-15 minutes prior to *in vivo* imaging. Animals will be placed under light isoflurane anesthesia to immobilize the animals for image detection. The bioluminescent signal will be recorded following a 1-10 second exposure with the IVIS Lumina CCD camera. Bioluminescent images of each animal will be taken weekly as a measure of tumor burden and a means to track metastatic progression.

A.2.14 GC/MS Metabolomics Analysis

8-10 week old VM/dk were randomly assigned to a treatment group (Standard diet control, 250mg/kg DCA, 250mg/kg metformin, 250mg/kg combination) and treated for 21-days. On day 21, animals were euthanized by exanguination, during which approximately 250µL of whole blood was collected by cardiac puncture. Serum was isolated by centrifugation using Microtainer® Tubes with Serum Separator (Becton Dickinson). Serum was transferred and secured in cryovials and flash frozen in liquid nitrogen (N_2). Subsequently, brain, heart, kidney, liver, skeletal muscle, and spleen were harvested and frozen in liquid N_2. Frozen samples were sent to the University of Utah Health Sciences Metabolomics Core for GC/MS metabolomics. Samples were processed and analyzed according to an in-house protocol. A total of 135 unique analytes were isolated from these samples and their relative concentrations were subsequently determined. Welch's two-sample *t* test was used to determine differences in the relative abundance of each metabolite for each treatment group compared to standard diet control.

A.2.15 Hyperbaric Oxygen Treatment

Animals assigned to HBOt groups were subjected to hyperbaric oxygen therapy (100% O_2 at 2.5 ATA) for 90 minutes three times a week (M, W, F) in a hyperbaric chamber. Cells were subject to a single 1-hour treatment with hyperbaric oxygen (100% O_2 at 2.5 ATA).

A.2.16 Statistical Analysis

GraphPad Prism 6 software was used for all statistical analysis. Parametric tests were performed for all data sets as all groups were considered normally distributed. Paired student's *t* tests were performed for the comparison of two groups unless specifically noted. One-Way ANOVA with a post hoc Tukey's multiple comparison test was performed for the comparison of more than two groups. Two-Way ANOVA with a post hoc Tukey's multiple comparisons test was performed when two independent variables were present. Results were considered significant when $p < 0.05$.

Appendix B: Week 4 Bioluminescent Images

B.1 SD Control

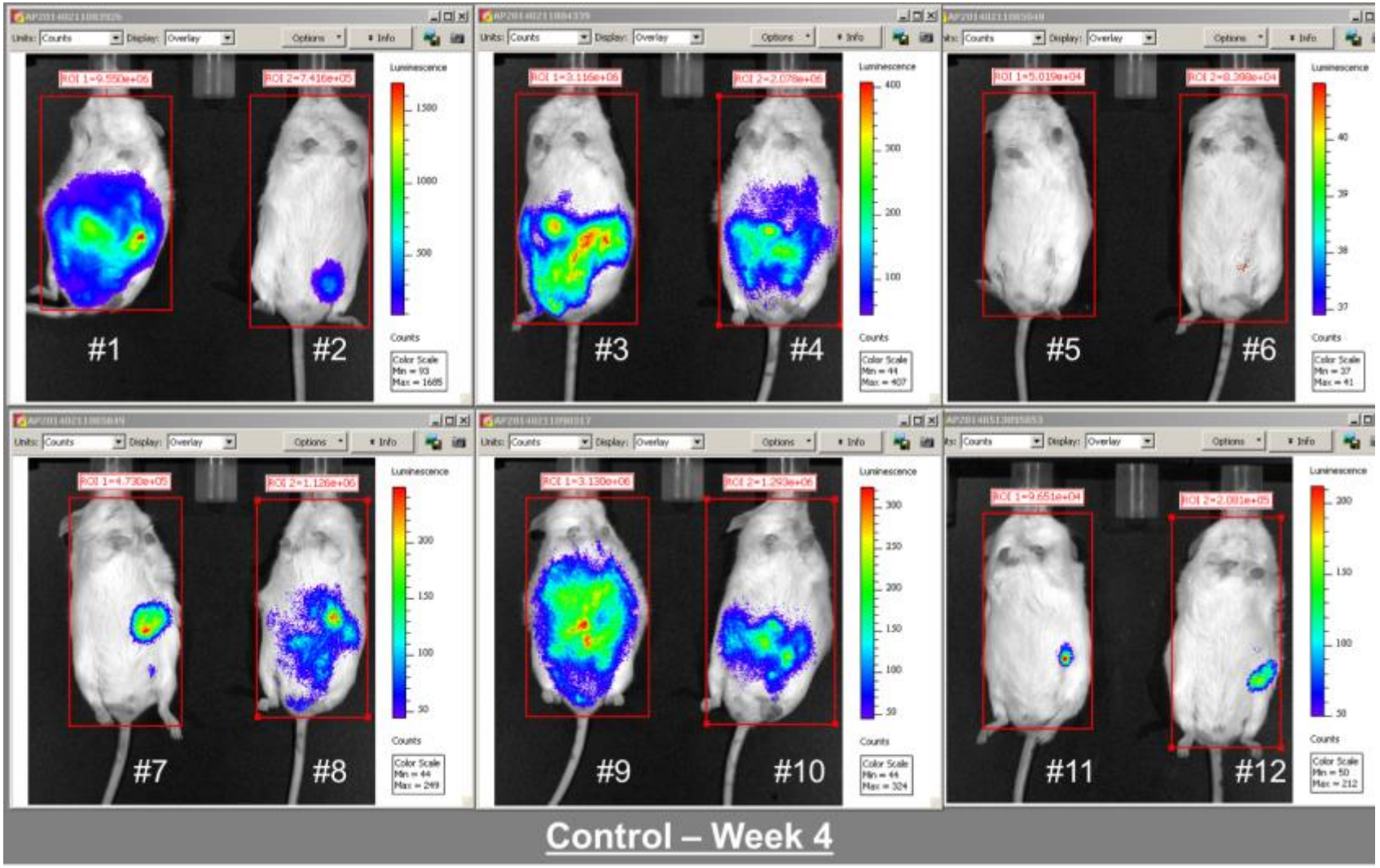

B.2 125mg/kg DCA

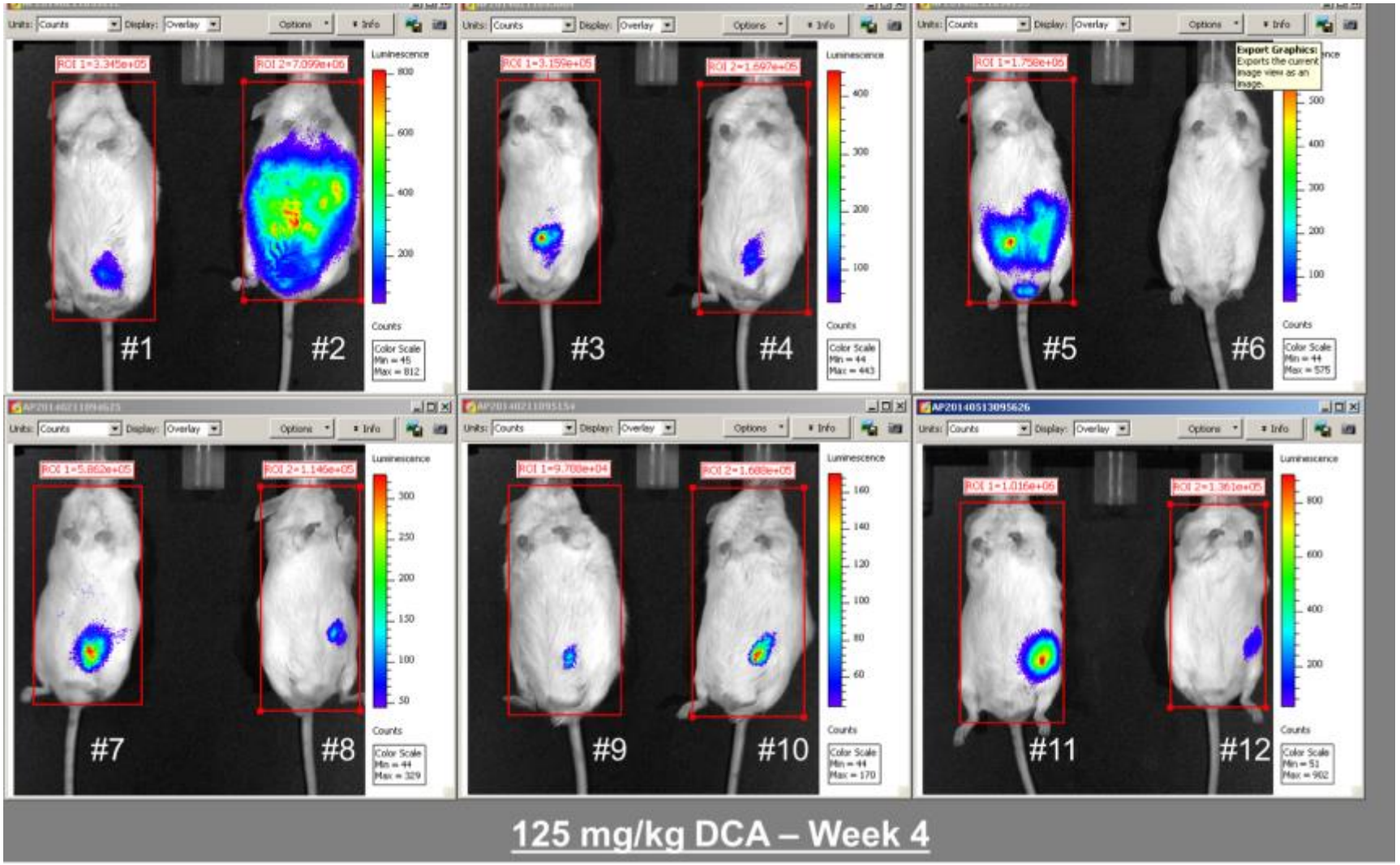

B.3 250mg/kg DCA

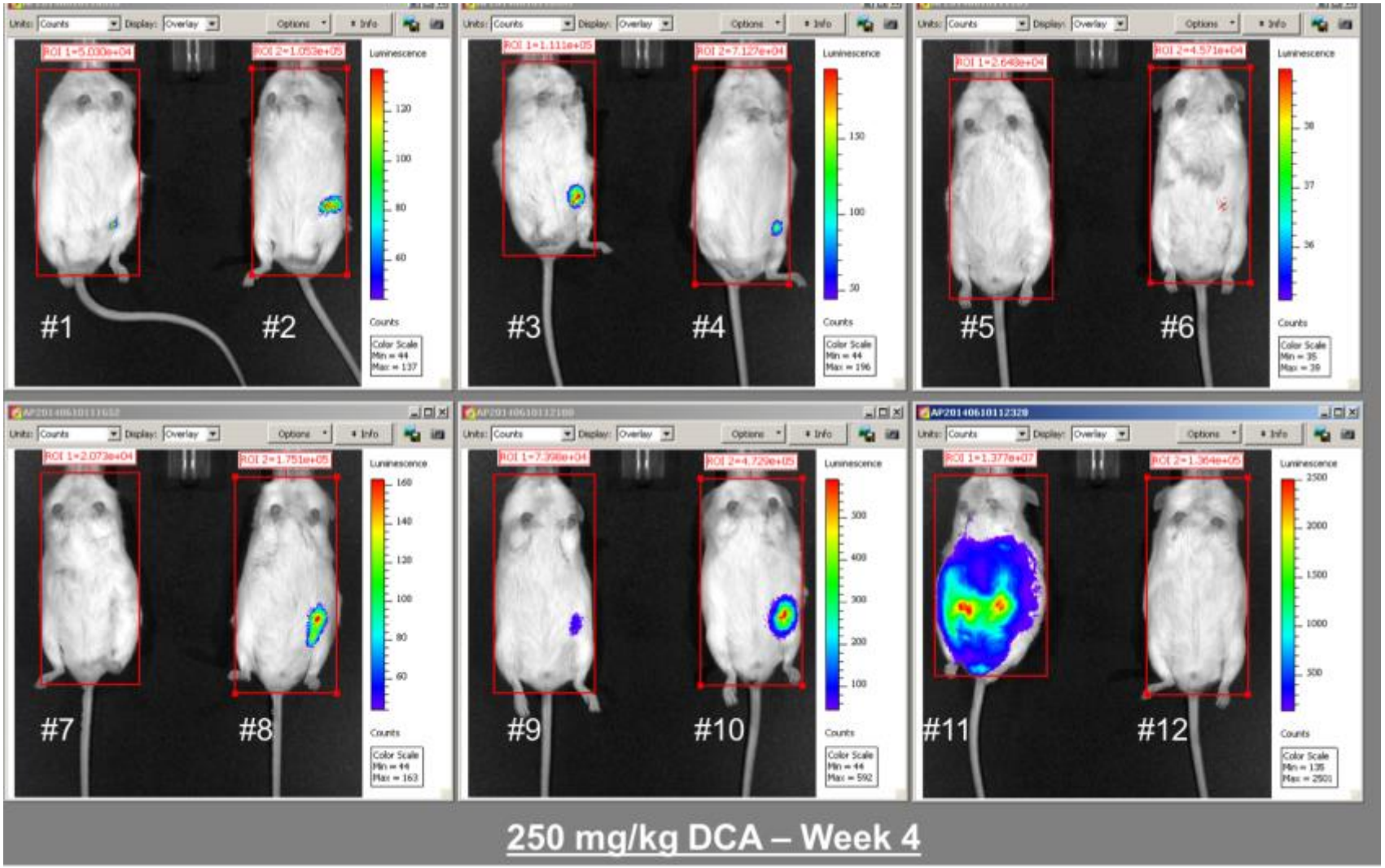

B.4 125mg/kg Metformin

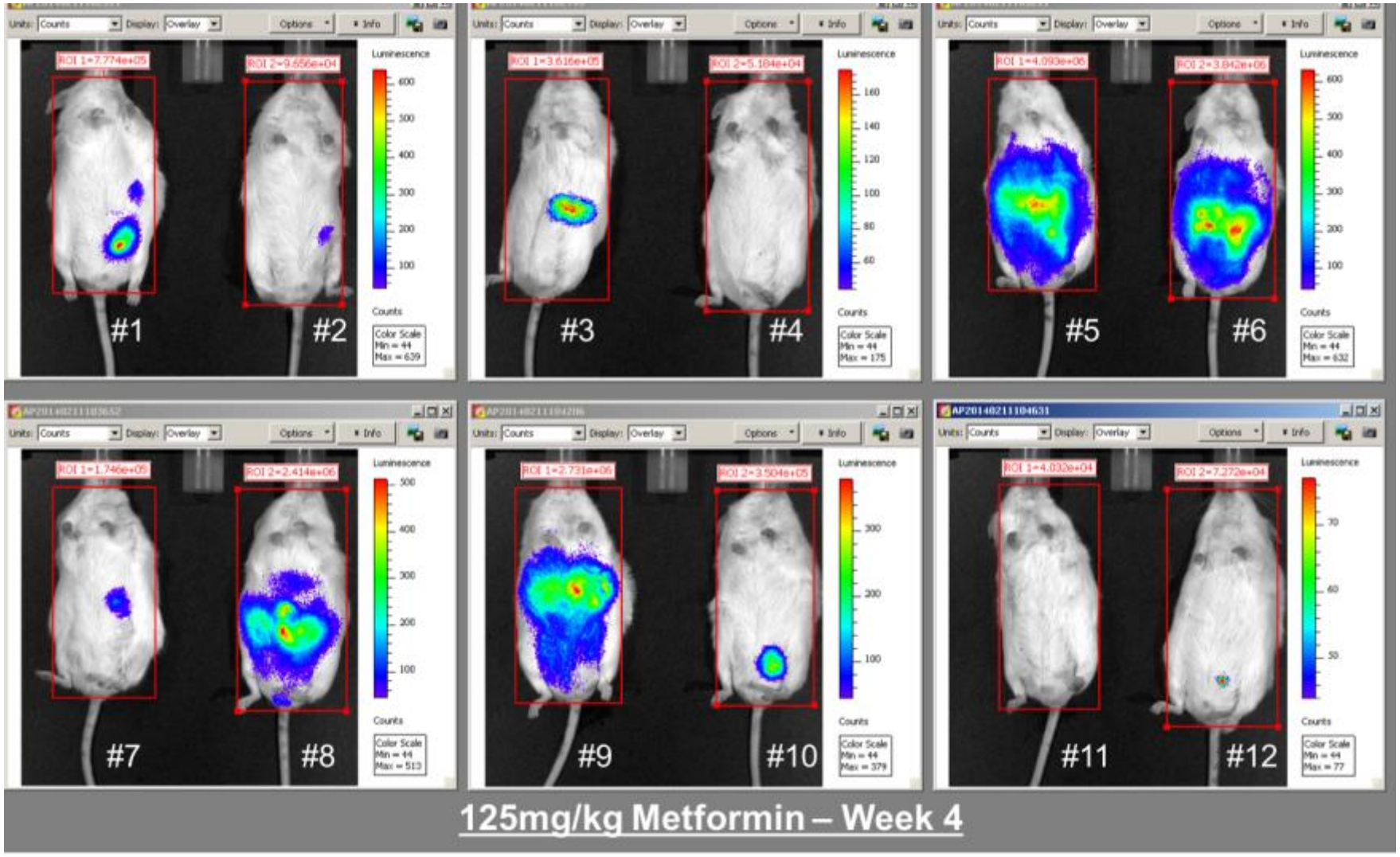

B.5 250mg/kg Metformin

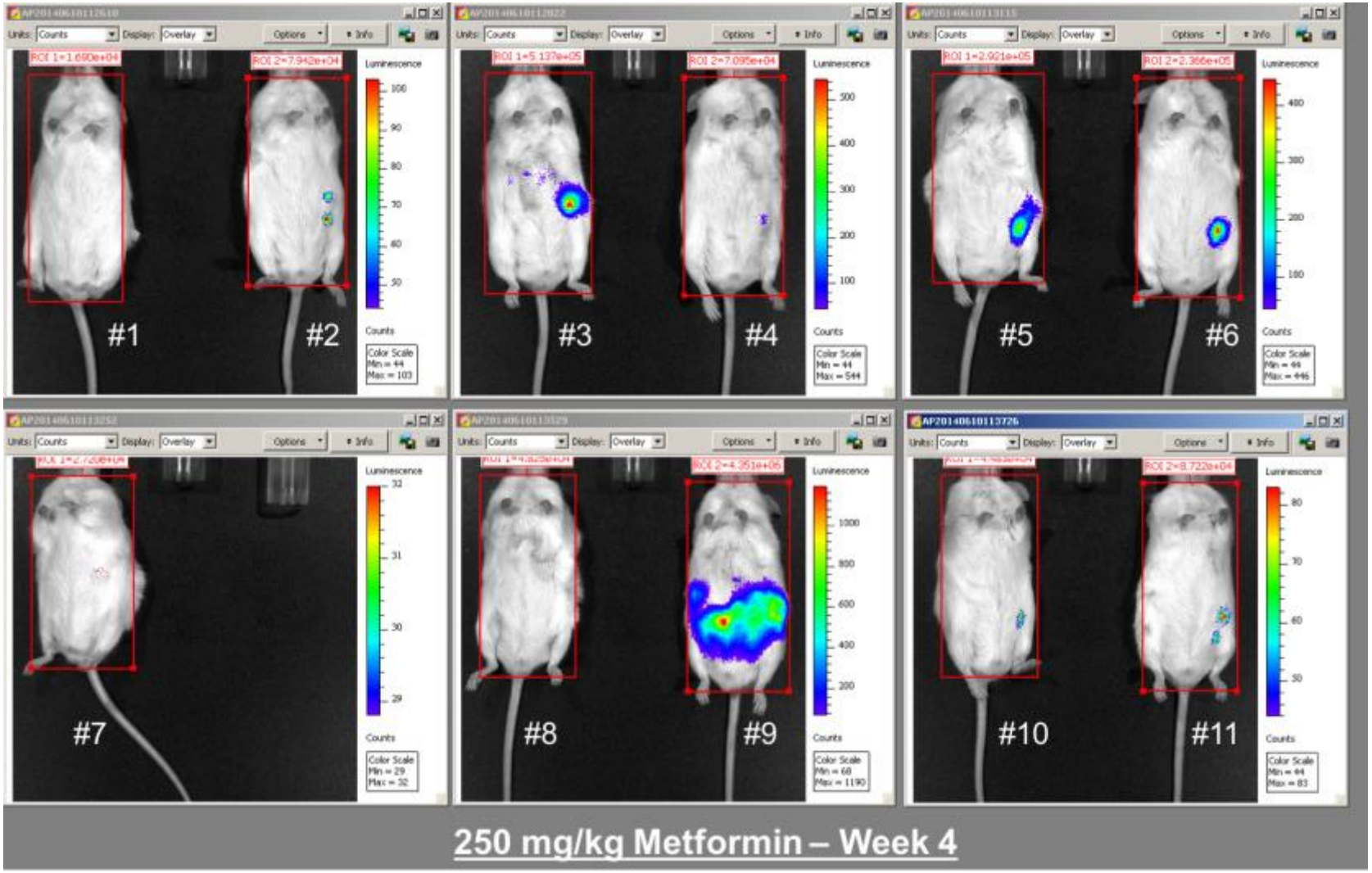

Appendix C: Metabolomics Analysis

C.1 Analysis of Brain Metabolites

Analyte	DCA/ Control	p-value	Metformin/ Control	p-value	Combo/ Control	p-value
fucose	1.07	0.8443	0.97	0.9901	0.77	0.2112
sedoheptulose-7-P	0.94	0.5062	0.92	0.3074	0.90	0.2590
glycolic acid	1.09	0.2983	1.02	0.9892	0.85	0.0739
dopamine	0.99	0.9896	0.98	0.9746	0.95	0.8734
aminomalonic acid	1.01	0.9732	1.01	0.9975	1.00	0.9980
phosphoethanolamine	1.02	0.8741	0.99	0.9924	0.93	0.0938
2-hydroxyglutarate	1.03	0.4834	1.02	0.8118	0.94	0.2150
ribose	1.00	0.9989	0.96	0.6296	0.96	0.5783
sarcosine	1.04	0.8521	1.03	0.9100	0.87	0.1339
diphosphate	1.00	0.9999	0.98	0.9956	0.86	0.4958
adenine	1.01	0.8693	0.99	0.8617	0.98	0.7294
uracil	1.00	0.9996	0.98	0.8068	0.96	0.5087
citric acid	0.97	0.7469	0.97	0.5944	0.93	0.0496
ornithine	1.11	0.0580	0.99	0.9964	0.90	0.2464
elaidic acid	0.96	0.3110	0.93	0.0122	1.01	0.7891
glutamine	1.03	0.3645	1.00	0.9987	0.95	0.2518
glyceric acid	1.00	0.9999	0.97	0.9713	0.84	0.1590
cis-Aconitic acid	1.01	0.9763	1.02	0.9427	0.93	0.2652
tryptophan	1.03	0.4579	0.97	0.3100	0.96	0.2913
arachidonic acid	0.99	0.9176	0.98	0.4375	0.98	0.7307
fumaric acid	0.99	0.9909	0.98	0.6908	0.97	0.6859
proline	1.02	0.8826	1.00	0.9998	0.96	0.7224
xanthine	0.97	0.4940	0.96	0.2290	0.98	0.6828
pantothenic acid	1.02	0.6215	1.00	0.9999	0.97	0.4835
oleic acid	0.96	0.2972	0.93	0.0113	1.01	0.7830
urea	0.99	0.7912	0.98	0.5934	0.93	0.0034
phenylalanine	1.00	0.9965	0.98	0.5286	0.97	0.2211

Fructose	1.10	0.1218	1.08	0.3081	0.99	0.9999
glucose-6-phosphate	0.96	0.7925	0.94	0.6275	0.93	0.5393
fructose-6-phosphate	0.94	0.8986	0.89	0.6527	0.87	0.5627
glucose-1-phosphate	1.05	0.8935	0.95	0.8932	0.98	0.9998
homocysteine	1.14	0.8716	0.97	0.9983	0.61	0.7661
porphobilinogen	1.16	0.7733	0.93	0.9699	0.73	0.7345
arabinose	1.02	0.9948	1.07	0.7533	0.89	0.6681
thymine	0.92	0.1517	0.97	0.7529	0.89	0.0221
Adenosine	1.00	0.9993	0.97	0.5430	0.98	0.9333
isocitric acid	0.97	0.8757	0.97	0.9312	0.89	0.1573
lauric acid	1.01	0.9969	1.00	0.9999	0.98	0.9621
histidine	1.03	0.9550	0.98	0.9822	0.91	0.3330
Myoinositol	1.00	0.9997	0.98	0.8959	0.94	0.2942
L-Glutamic acid	1.03	0.5468	1.00	0.9966	0.96	0.5422
hypoxanthine	0.98	0.4385	0.98	0.3648	0.99	0.9273
1-monopalmitoylglycerol	1.00	0.9999	0.98	0.7771	0.95	0.3172
malic acid	0.99	0.9855	0.98	0.7418	0.97	0.5753
phosphate	1.00	0.9653	1.00	0.9830	0.98	0.5799
creatinine	1.02	0.8279	1.00	0.9981	0.97	0.6093
serine	0.98	0.1759	1.00	0.9981	0.95	0.0009
myristic acid	0.97	0.5176	0.97	0.6247	0.96	0.5908
3-phosphoglycerate	1.03	0.9300	0.99	0.9974	0.92	0.5606
myo-inositol 1-phosphate	1.01	0.9639	0.98	0.7783	0.92	0.0420
nonadecanoic acid	0.75	0.6827	0.87	0.9395	0.66	0.7265
succinic acid	1.06	0.3375	1.06	0.3434	0.99	0.9986
phosphoenolpyruvate	1.17	0.8557	0.85	0.9023	0.90	0.9950
Stearic acid	0.98	0.9585	0.98	0.9684	0.95	0.8799
ascorbate	1.03	0.6393	1.01	0.9905	0.95	0.3727
oleamide	1.02	0.7621	1.00	0.9999	0.98	0.9246
asparagine	1.02	0.7263	1.02	0.8908	0.96	0.5650
lysine	1.05	0.0149	1.00	0.9977	0.99	0.9965
palmitic acid	0.99	0.9320	0.97	0.6316	0.98	0.9776
pyruvic acid	1.01	0.9874	0.99	0.9884	0.96	0.8486
1-monostearoylglycerol	1.05	0.6534	1.01	0.9990	0.92	0.5105
aspartic acid	1.02	0.5328	1.00	0.9999	0.97	0.2757
5-aminopentanoic acid	1.04	0.9816	0.99	0.9999	1.03	0.9237
cholesterol	1.05	0.8196	0.99	0.9992	0.93	0.9072
2,4-dihydroxybutanoic	1.02	0.8814	0.99	0.9423	0.90	0.0034

acid						
glycerol	1.00	0.9999	0.99	0.6540	0.98	0.7790
valine	1.01	0.8553	0.99	0.8709	0.97	0.2146
1-Linoleoyl-glycerol	1.06	0.8156	1.10	0.5130	0.91	0.7766
sorbitol	1.07	0.7590	1.07	0.6900	0.95	0.9256
glutathione	1.03	0.7243	1.00	0.9993	0.93	0.1894
cysteine	0.95	0.7434	0.88	0.0928	1.03	0.9946
glycerol 3-phosphate	1.02	0.7051	1.02	0.7161	0.99	0.9948
2-aminoadipic acid	1.01	0.9961	1.00	0.9994	0.89	0.0977
glycine	0.99	0.8645	0.98	0.6091	1.02	0.9110
N-acetylaspartate	1.01	0.8036	1.02	0.7481	0.96	0.4244
lactic acid	1.02	0.7891	1.00	0.9984	0.97	0.8668
nicotinamide	1.00	0.9954	0.99	0.8863	0.95	0.2630
homoserine	0.98	0.8189	0.99	0.9914	0.87	0.0001
5-aminovaleric acid	0.86	0.9964	1.08	0.6055	0.75	0.8873
2-hydroxybutyric acid	1.00	0.9996	0.95	0.5193	0.91	0.1659
isoleucine	1.01	0.7551	0.99	0.9401	0.97	0.3463
1-oleoyl-glycerol	0.98	0.7304	0.93	0.0140	0.99	0.9826
leucine	1.00	0.9999	0.98	0.5426	0.98	0.5711
2-monooleoylglycerol	1.11	0.7692	1.20	0.3393	0.87	0.8712
threonine	1.01	0.8830	1.00	0.9873	0.94	0.0005
inosine	0.99	0.9620	0.99	0.9619	0.94	0.0984
tyrosine	0.99	0.9556	0.99	0.9923	0.93	0.0797
serotonin	1.03	0.7441	0.91	0.9846	0.86	0.9914
1,3-bisphosphoglycerate	1.02	0.9891	1.02	0.9844	0.92	0.8074
L-methionine	0.99	0.8949	0.99	0.9840	0.96	0.3776
2-ketoglutaric acid	1.12	0.6065	0.91	0.8026	0.77	0.2468
5'-AMP	1.04	0.5000	1.04	0.4415	0.90	0.0152
3-hydroxybutyrate	1.08	0.0544	1.01	0.9660	1.00	0.9807
alanine	0.95	0.4765	0.97	0.8501	0.94	0.2663
B-alanine	1.01	0.8281	1.00	0.9858	0.96	0.0225
linoleic acid	1.01	0.9969	1.04	0.8875	1.00	0.9905
5-hydroxytryptophan	1.19	0.1997	1.00	0.9999	0.61	0.0089
N-acetylglutamate	1.07	0.1518	1.00	0.9991	0.95	0.6868
DHAP	0.73	0.0302	0.86	0.4618	1.04	0.9931
5-hydroxyindoleacetic acid	1.15	0.5873	0.99	0.9998	0.68	0.8288
mannose	1.05	0.5691	1.01	0.9984	0.87	0.0300
hydroxyproline	1.02	0.3138	1.01	0.6610	1.01	0.6680

erythrose	0.98	0.9809	0.93	0.6765	0.81	0.0719
2-hydroxysebacic acid	0.87	0.2524	0.72	0.5465	0.91	0.7184
b-Hydroxy-b-methylglutarate	1.04	0.5812	1.02	0.9028	0.90	0.1298

C.2 Analysis of Heart Metabolites

Analyte	DCA/ Control	p-value	Metformin/ Control	p-value	Combo/ Control	p-value
fucose	1.34	0.7637	0.08	0.6593	1.57	0.4946
kynurenine	0.89	0.9544	0.42	0.1144	1.16	0.8629
galactose	1.32	0.2622	0.79	0.6035	1.41	0.0276
sedoheptulose-7-P	1.00	0.9999	0.83	0.1121	1.24	0.0305
glycolic acid	1.08	0.1947	0.91	0.1248	1.04	0.6400
dopamine	1.11	0.4103	0.93	0.7454	1.07	0.4490
aminomalonic acid	1.09	0.4835	0.92	0.6252	1.14	0.1324
phosphoethanolamine	1.09	0.4019	0.96	0.8952	1.16	0.0262
2-hydroxyglutarate	1.11	0.0004	0.98	0.7632	1.11	0.0001
ribose	1.01	0.9858	0.89	0.0620	1.09	0.1915
sarcosine	1.03	0.8868	0.92	0.3303	1.02	0.8742
diphosphate	1.07	0.6124	0.95	0.8175	1.09	0.2211
adenine	1.00	0.9993	0.91	0.0017	1.03	0.5232
uracil	1.05	0.0923	0.95	0.1537	1.07	0.0057
citric acid	1.10	0.0748	0.99	0.9974	1.01	0.9244
ornithine	1.05	0.6623	0.95	0.7356	1.04	0.4966
elaidic acid	1.01	0.9941	0.92	0.0901	1.12	0.0059
glutamine	1.08	0.0299	0.99	0.9607	1.02	0.7752
glyceric acid	1.05	0.4990	0.97	0.7988	0.99	0.9999
ribitol	1.03	0.8663	0.95	0.4303	0.98	0.9992
cis-Aconitic acid	1.03	0.7633	0.96	0.6265	1.05	0.3474
tryptophan	1.03	0.1151	0.96	0.0526	1.03	0.1528
arachidonic acid	0.99	0.9956	0.93	0.0814	1.10	0.0025
fumaric acid	0.98	0.8335	0.92	0.0075	1.06	0.0382
proline	1.02	0.9412	0.96	0.4602	1.04	0.3980
Xanthine	1.01	0.9926	0.95	0.0433	1.04	0.2166
pantothenic acid	1.04	0.1233	0.99	0.8783	1.05	0.0214
oleic acid	0.99	0.9409	0.94	0.0688	1.09	0.0048
urea	0.99	0.9740	0.96	0.1011	0.98	0.8698

phenylalanine	1.01	0.9400	0.98	0.3758	1.04	0.0145
Fructose	0.89	0.0564	1.02	0.9836	0.99	0.9844
2-phosphoglycerate	1.10	0.7041	1.38	0.0029	1.11	0.5882
glucose-6-phosphate	1.01	0.9997	1.35	0.0108	1.21	0.1855
fructose-6-phosphate	1.00	0.9999	1.40	0.0171	1.24	0.2049
glucose-1-phosphate	0.98	0.9987	1.46	0.0155	1.32	0.1361
homocysteine	1.15	0.9173	0.81	0.8626	1.32	0.5164
porphobilinogen	0.93	0.9530	0.70	0.0595	1.09	0.6578
arabinose	1.11	0.8207	0.85	0.6660	1.36	0.0545
thymine	1.06	0.9243	0.82	0.2779	1.09	0.6866
Adenosine	1.03	0.9688	0.86	0.0782	0.96	0.9339
isocitric acid	1.03	0.9671	0.89	0.2563	1.13	0.0773
lauric acid	0.97	0.8575	0.87	0.0349	1.07	0.2667
histidine	1.01	0.9942	0.92	0.5010	1.05	0.6724
Myoinositol	1.04	0.4960	0.98	0.9502	1.03	0.7296
L-Glutamic acid	1.05	0.1196	0.99	0.9953	1.02	0.9144
hypoxanthine	1.00	0.9999	0.95	0.1369	1.07	0.0483
1-monopalmitoylglycerol	1.02	0.9466	0.97	0.6653	1.08	0.0424
malic acid	1.00	0.9988	0.96	0.1577	1.07	0.0041
phosphate	1.00	0.9914	0.98	0.1958	1.02	0.5934
creatinine	1.00	0.9932	0.97	0.1827	1.00	0.8933
glucose	0.95	0.6602	1.06	0.5735	1.02	0.9957
Heptadecanoic acid	1.01	0.9951	0.91	0.4668	1.15	0.0579
serine	1.02	0.3324	1.01	0.9842	1.03	0.0938
myristic acid	0.94	0.2141	0.89	0.0080	0.99	0.9999
2-ethylhexanoic acid	1.02	0.9992	0.71	0.3758	1.15	0.5832
4-hydroxyproline	1.08	0.4750	0.97	0.9611	1.08	0.3309
4-aminobutyrate	1.08	0.4830	0.97	0.9596	1.07	0.3412
3-phosphoglycerate	1.07	0.3478	1.14	0.0081	1.05	0.7141
gluconic acid	0.93	0.4737	1.03	0.9038	1.02	0.9728
myo-inositol 1-phosphate	1.02	0.9876	0.91	0.5454	1.13	0.0999
sedoheptulose	0.92	0.6189	0.83	0.0803	1.10	0.6287
Nonadecanoic acid	1.04	0.9679	0.91	0.6797	1.17	0.1122
succinic acid	0.97	0.8374	1.02	0.9335	0.94	0.4620
phosphoenolpyruvate	1.03	0.9371	1.12	0.1480	1.13	0.1298
Stearic acid	1.01	0.9744	0.97	0.7224	1.08	0.0633
2-monostearylglycerol	0.90	0.4719	0.98	0.9951	0.97	0.9999
ascorbate	0.98	0.9922	0.87	0.3372	1.08	0.6421

oleamide	1.00	0.9982	0.96	0.2943	1.01	0.7848
asparagine	1.07	0.4660	1.01	0.9972	1.08	0.1938
lysine	1.04	0.4033	1.02	0.9418	1.07	0.0560
palmitic acid	1.00	0.9989	0.97	0.7457	1.07	0.0864
pyruvic acid	0.99	0.9697	1.03	0.8094	0.96	0.8513
1-monostearoylglycerol	1.02	0.9622	0.97	0.8735	1.09	0.1091
aspartic acid	1.05	0.1170	1.02	0.7326	0.97	0.6064
5-aminopentanoic acid	1.00	0.9999	0.92	0.6834	1.05	0.6813
Cholesterol	1.03	0.8620	0.98	0.9700	1.10	0.0578
mannitol	0.90	0.0022	0.92	0.0294	0.95	0.3479
2,4-dihydroxybutanoic acid	0.98	0.9414	1.00	0.9994	0.93	0.5803
Glycerol	0.97	0.2390	0.95	0.0330	1.03	0.4364
valine	1.00	0.9841	1.00	0.9913	1.00	0.9459
1-Linoleoyl-glycerol	0.95	0.7759	0.99	0.9939	1.00	0.9988
sorbitol	0.96	0.9211	0.93	0.7120	1.03	0.8459
Glutathione	1.02	0.9326	1.00	0.9991	1.03	0.5916
cysteine	1.06	0.9534	1.01	0.9998	1.24	0.1215
Glycerol 3-phosphate	1.00	0.9999	0.99	0.9639	1.03	0.2973
2-aminoadipic acid	1.07	0.4556	1.05	0.7465	1.01	0.9266
glycine	1.05	0.6219	1.03	0.8779	1.07	0.1441
N-Acetylaspartate	1.09	0.8626	1.02	0.9988	0.93	0.9784
lactic acid	0.93	0.4503	0.91	0.2448	0.97	0.9718
nicotinamide	0.98	0.8499	0.97	0.5712	1.04	0.1705
uric acid	1.04	0.7938	1.02	0.9610	1.02	0.9955
homoserine	0.86	0.7230	0.81	0.5029	0.85	0.8492
5-aminovaleric acid	1.04	0.9949	0.97	0.9971	1.03	0.9906
2-hydroxybutyric acid	0.92	0.4297	0.94	0.6703	0.94	0.8160
isoleucine	1.00	0.9999	1.00	0.9820	1.02	0.3617
1-Oleoyl-glycerol	0.95	0.5489	0.96	0.7969	1.04	0.6100
leucine	1.02	0.6620	1.03	0.4461	1.04	0.1534
2-monooleoylglycerol	0.95	0.8930	0.98	0.9873	0.99	0.9994
Palmitelaidic acid	0.86	0.0151	0.87	0.0281	0.95	0.6465
threonine	0.99	0.9738	1.00	0.9974	0.99	0.8032
inosine	0.93	0.1978	0.94	0.3069	0.98	0.9999
tyrosine	0.99	0.9972	1.00	0.9999	1.02	0.9053
serotonin	0.99	0.9995	1.01	0.9991	0.97	0.9984
1,3-bisphosphoglycerate	0.96	0.9806	0.94	0.9377	1.38	0.0077
L-Methionine	1.00	0.9996	1.00	0.9999	1.01	0.9916

2-ketoglutaric acid	1.03	0.9989	1.05	0.9924	0.59	0.2384
5'-AMP	0.99	0.9970	0.99	0.9892	0.97	0.9574
3-hydroxybutyrate	1.00	0.9995	1.00	0.9999	1.02	0.7016
alanine	0.97	0.7302	0.98	0.7959	1.02	0.6071
B-alanine	1.02	0.8632	1.02	0.9007	1.01	0.8785
alpha-Lactose	1.13	0.9375	1.12	0.9590	1.21	0.8384
linoleic acid	0.96	0.7042	0.97	0.7399	1.06	0.3087

C.3 Analysis of Kidney Metabolites

Analyte	DCA/ Control	p-value	Metformin/ Control	p-value	Combo/ Control	p-value
fucose	0.95	0.7978	0.89	0.1676	0.99	0.9888
galactose	1.10	0.7962	0.78	0.1798	0.92	0.9569
sedoheptulose-7-P	0.99	0.9963	1.00	0.9999	1.06	0.3331
glycolic acid	1.19	0.0017	1.02	0.9710	1.02	0.4983
aminomalonic acid	1.04	0.5470	0.98	0.9387	0.96	0.8772
phosphoethanolamine	1.03	0.8563	0.99	0.9976	1.05	0.2976
2-hydroxyglutarate	1.16	0.0020	1.00	0.9999	1.08	0.1427
ribose	0.94	0.2741	0.94	0.2983	1.02	0.5995
sarcosine	1.12	0.0670	0.94	0.5815	1.06	0.2637
diphosphate	0.98	0.9330	0.97	0.5552	1.03	0.3065
adenine	1.01	0.9813	0.99	0.9837	0.97	0.8113
uracil	1.01	0.9525	0.98	0.7678	1.00	0.9353
citric acid	1.36	0.0025	1.14	0.3846	0.99	0.9922
ornithine	1.00	0.9999	0.91	0.1549	1.03	0.5472
elaidic acid	0.96	0.5408	0.96	0.6387	1.02	0.9509
glutamine	1.02	0.4920	0.99	0.8939	1.00	0.8841
glyceric acid	0.96	0.7963	0.96	0.8686	0.98	0.9978
ribitol	0.91	0.2696	0.87	0.0371	0.98	0.9989
cis-Aconitic acid	1.20	0.5047	1.45	0.0148	1.18	0.3697
tryptophan	1.01	0.9595	0.99	0.9095	1.02	0.8990
arachidonic acid	0.99	0.9928	0.98	0.7840	1.01	0.6527
fumaric acid	0.99	0.9802	0.97	0.6859	1.02	0.7119
proline	0.96	0.8730	0.95	0.7487	1.04	0.3930
Xanthine	0.97	0.4412	0.91	0.0028	0.99	0.9985
pantothenic acid	1.01	0.9569	0.98	0.8630	0.98	0.9882
oleic acid	0.96	0.5374	0.96	0.6384	1.02	0.9523
urea	1.00	0.9999	0.98	0.6810	0.99	0.9087

phenylalanine	0.97	0.5989	0.97	0.5052	1.01	0.8161
Fructose	0.99	0.9879	0.94	0.1221	1.00	0.9624
2-phosphoglycerate	1.03	0.9778	0.95	0.8327	1.12	0.2715
glucose-6-phosphate	1.02	0.9646	1.01	0.9992	1.05	0.4810
fructose-6-phosphate	0.99	0.9999	0.93	0.9403	1.21	0.1309
glucose-1-phosphate	0.51	0.0516	0.90	0.9443	0.95	0.9925
homocysteine	1.04	0.9920	0.83	0.5717	1.24	0.0938
thymine	1.11	0.5317	1.01	0.9984	0.92	0.9632
Adenosine	1.31	0.0121	1.37	0.0016	0.97	0.9188
isocitric acid	2.16	0.0029	1.53	0.2694	1.28	0.5048
lauric acid	0.92	0.1229	1.03	0.8387	0.96	0.7708
histidine	0.90	0.4826	0.85	0.1806	1.04	0.5690
Myoinositol	0.99	0.9941	0.99	0.9451	1.03	0.6201
L-Glutamic acid	0.99	0.9775	0.96	0.0943	0.98	0.9376
hypoxanthine	0.98	0.4431	0.95	0.0066	0.99	0.9999
1-monopalmitoylglycerol	1.00	0.9998	0.97	0.8214	1.06	0.0700
malic acid	1.01	0.9832	0.96	0.6488	1.10	0.8560
phosphate	0.96	0.0025	0.96	0.0004	1.00	0.9576
creatinine	1.05	0.5080	0.95	0.4185	1.00	0.8553
glucose	0.97	0.5579	1.04	0.3048	1.02	0.6614
serine	0.98	0.8571	0.98	0.7070	1.03	0.2482
myristic acid	0.95	0.3009	0.98	0.8415	0.98	0.9251
4-hydroxyproline	1.07	0.1365	0.96	0.4275	0.99	0.9960
4-aminobutyrate	1.07	0.1369	0.96	0.4284	0.99	0.9960
3-phosphoglycerate	0.94	0.6791	0.97	0.9273	1.04	0.5250
gluconic acid	0.99	0.9903	1.03	0.6142	1.00	0.9794
myo-inositol 1-phosphate	1.00	0.9991	1.01	0.9970	1.06	0.1665
Nonadecanoic acid	0.93	0.8982	0.96	0.9766	1.14	0.2344
succinic acid	1.01	0.9861	0.98	0.5000	1.00	0.9867
phosphoenolpyruvate	0.91	0.6958	0.95	0.9234	1.08	0.4190
Stearic acid	1.01	0.9546	1.00	0.9990	1.06	0.0113
oleamide	1.00	0.9985	0.99	0.7803	0.98	0.8143
asparagine	0.91	0.4030	0.90	0.2267	1.06	0.3354
lysine	0.96	0.5146	1.00	0.9995	1.04	0.2683
palmitic acid	0.97	0.5699	0.97	0.3509	1.04	0.1064
pyruvic acid	1.03	0.5474	1.04	0.2712	1.01	0.9754
1-monostearoylglycerol	1.00	0.9999	0.99	0.9957	1.07	0.0864
aspartic acid	0.99	0.8415	1.01	0.9785	1.01	0.6998

5-aminopentanoic acid	1.01	0.9977	0.98	0.9235	0.92	0.3603
Cholesterol	0.98	0.9635	0.91	0.2249	1.04	0.4760
2,4-dihydroxybutanoic acid	0.94	0.5317	0.96	0.7470	0.98	0.9986
Glycerol	0.94	0.0001	0.92	0.0001	0.98	0.5316
valine	0.97	0.3378	0.96	0.0834	0.99	0.9998
1-Linoleoyl-glycerol	0.98	0.9948	1.04	0.9168	1.01	0.9913
sorbitol	1.02	0.9642	1.00	0.9999	1.00	0.9740
cysteine	1.13	0.0002	1.01	0.9860	1.12	0.0001
Glycerol 3-phosphate	0.99	0.9842	0.97	0.6638	1.01	0.7569
2-aminoadipic acid	0.99	0.9937	0.97	0.8764	0.92	0.4944
glycine	0.97	0.4369	0.97	0.2081	0.99	0.7659
N-Acetylaspartate	1.39	0.0501	1.17	0.6228	0.89	0.7529
lactic acid	0.99	0.8591	0.93	0.0001	0.94	0.0003
nicotinamide	0.98	0.7527	0.96	0.2799	0.99	0.9994
uric acid	1.05	0.4441	0.98	0.9312	1.00	0.9999
homoserine	0.98	0.9434	1.00	0.9999	0.93	0.6657
5-aminovaleric acid	0.97	0.9638	1.09	0.6067	0.91	0.6976
2-hydroxybutyric acid	0.97	0.8005	0.98	0.8548	0.93	0.3330
isoleucine	0.96	0.1825	0.96	0.0843	0.99	0.9999
1-Oleoyl-glycerol	0.97	0.9675	1.00	0.9999	1.02	0.9853
leucine	0.96	0.0903	0.96	0.1387	1.00	0.9251
2-monooleoylglycerol	0.99	0.9983	1.06	0.8435	1.01	0.9925
threonine	0.96	0.5682	0.98	0.8864	0.99	0.9812
inosine	1.00	0.9998	1.01	0.9930	1.02	0.9980
tyrosine	0.96	0.6453	0.98	0.8647	1.01	0.8393
serotonin	0.98	0.9607	1.00	0.9999	0.98	0.9842
1,3-bisphosphoglycerate	1.05	0.7643	0.98	0.9888	1.12	0.0509
L-Methionine	0.96	0.5924	0.98	0.8014	1.02	0.9194
2-ketoglutaric acid	1.30	0.0143	1.05	0.9476	0.94	0.9852
5'AMP	1.10	0.1996	1.15	0.0164	1.00	0.9917
3-hydroxybutyrate	1.08	0.0698	1.01	0.9948	1.04	0.3909
alanine	0.97	0.6234	0.98	0.8027	1.00	0.9387
B-alanine	1.03	0.5836	1.06	0.1645	1.04	0.4877
alpha-Lactose	0.83	0.6031	0.89	0.8316	0.85	0.7773
linoleic acid	0.95	0.2803	0.98	0.8497	1.01	0.9874
5-hydroxytryptophan	1.04	0.9918	1.10	0.8615	1.00	0.9849
N-acetylglutamate	1.54	0.0394	0.96	0.9950	0.89	0.9960
DHAP	1.19	0.1651	1.21	0.0932	1.06	0.6370

mannose	0.99	0.9996	0.89	0.2241	1.01	0.9996
erythrose	0.97	0.9103	0.88	0.0865	1.00	0.9532
b-Hydroxy-b-methylglutarate	1.29	0.0123	1.08	0.7980	1.01	0.8403
2-phosphoglycerol	1.02	0.9907	1.07	0.6990	0.94	0.9504
rhamnose	1.09	0.5978	1.04	0.9518	1.06	0.5459
3,4-dihydroxybutanoic acid	1.06	0.9386	1.06	0.9378	1.16	0.2648
Indoxyl sulfate	1.14	0.2204	1.09	0.5115	1.10	0.2436
nicotinic acid	0.71	0.1565	0.45	0.0010	0.87	0.9259
putrescine	1.20	0.2365	1.05	0.9525	1.06	0.7641
threitol	1.05	0.8523	0.96	0.9271	1.00	0.9842

C.4 Analysis of Liver Metabolites

Analyte	DCA/ Control	p-value	Metformin/ Control	p-value	Combo/ Control	p-value
fucose	0.82	0.0584	0.88	0.2714	1.01	0.9999
kynurenine	0.84	0.6423	0.80	0.4775	0.94	0.9230
sedoheptulose-7-P	0.96	0.5294	1.01	0.9825	1.02	0.9153
glycolic acid	1.23	0.0077	0.95	0.8839	0.97	0.9810
dopamine	0.89	0.0030	0.90	0.0108	0.91	0.0476
aminomalonic acid	1.02	0.9645	1.00	0.9998	1.01	0.9999
phosphoethanolamine	0.84	0.0207	1.11	0.1799	0.92	0.4800
2-hydroxyglutarate	1.17	0.0011	0.96	0.7992	1.05	0.4644
ribose	0.85	0.0001	0.97	0.7327	0.97	0.7068
sarcosine	0.91	0.0178	0.90	0.0133	0.89	0.0193
diphosphate	1.02	0.6626	0.99	0.8741	1.05	0.0844
adenine	1.02	0.9287	0.97	0.6430	1.00	0.9941
uracil	0.85	0.0433	0.96	0.9020	1.06	0.5652
citric acid	0.99	0.9994	1.27	0.0896	0.70	0.2464
ornithine	1.00	0.9915	0.95	0.0220	0.97	0.3366
elaidic acid	0.99	0.9940	0.91	0.0291	1.01	0.9999
glutamine	1.08	0.0001	0.98	0.6665	1.08	0.0002
glyceric acid	0.79	0.0170	0.95	0.8910	0.91	0.4572
cis-Aconitic acid	0.75	0.9999	1.41	0.2359	0.62	0.6662
tryptophan	0.99	0.8196	0.99	0.9899	0.98	0.5664
arachidonic acid	0.93	0.0003	0.99	0.9590	0.98	0.4811
fumaric acid	0.84	0.0047	1.05	0.6993	0.94	0.7117

proline	0.94	0.1668	0.97	0.6337	0.95	0.3650
Xanthine	0.94	0.0148	0.98	0.5886	0.99	0.9155
pantothenic acid	1.01	0.9997	1.03	0.9480	1.17	0.0249
oleic acid	1.00	0.9962	0.97	0.3646	1.00	0.9996
urea	0.98	0.7857	0.96	0.4313	0.95	0.2893
phenylalanine	0.94	0.0125	0.97	0.4284	0.96	0.1150
Fructose	0.85	0.0003	0.94	0.2973	1.00	0.9954
2-phosphoglycerate	0.93	0.6528	0.96	0.4175	0.94	0.9476
glucose-6-phosphate	0.87	0.0060	0.96	0.6461	0.95	0.7127
fructose-6-phosphate	0.86	0.0438	0.92	0.4222	0.97	0.9453
glucose-1-phosphate	0.80	0.0043	0.97	0.9307	0.98	0.9993
Adenosine	1.08	0.3607	1.04	0.8052	1.00	0.8998
isocitric acid	0.93	0.9797	1.17	0.8179	0.99	0.9876
lauric acid	0.87	0.2586	0.99	0.9986	0.98	0.8813
Myoinositol	0.95	0.0343	0.99	0.8927	0.95	0.0980
L-Glutamic acid	1.06	0.0655	1.03	0.5111	1.00	0.9999
hypoxanthine	0.90	0.0007	0.97	0.5538	1.01	0.9550
1-monopalmitoylglycerol	1.02	0.2926	0.99	0.7959	1.03	0.0513
malic acid	0.85	0.0044	1.05	0.6227	0.91	0.3598
phosphate	0.98	0.4540	1.00	0.9794	1.01	0.9924
creatinine	0.93	0.4936	0.91	0.2810	0.94	0.8461
Heptadecanoic acid	0.90	0.0645	1.07	0.2799	0.98	0.8973
serine	0.91	0.0168	1.03	0.6512	0.99	0.9427
myristic acid	0.91	0.0241	0.95	0.3923	0.88	0.0013
4-hydroxyproline	0.91	0.2162	1.04	0.8230	0.92	0.4095
4-aminobutyrate	0.91	0.2164	1.04	0.8206	0.92	0.4100
3-phosphoglycerate	0.94	0.8514	1.06	0.8486	0.94	0.6621
gluconic acid	0.95	0.0174	0.98	0.4713	0.96	0.2219
myo-inositol 1-phosphate	1.00	0.9980	1.05	0.3074	1.06	0.2564
Nonadecanoic acid	0.86	0.0011	0.96	0.5469	0.90	0.0206
succinic acid	1.05	0.0495	1.03	0.3543	1.00	0.9985
phosphoenolpyruvate	0.76	0.1395	1.09	0.8492	0.81	0.1489
Stearic acid	0.98	0.3117	1.00	0.9996	1.01	0.9180
2-monostearylglycerol	0.73	0.0001	0.90	0.1811	0.93	0.3082
ascorbate	0.98	0.9403	0.92	0.2544	0.97	0.9669
asparagine	0.91	0.0490	0.95	0.3803	0.97	0.7611
palmitic acid	0.99	0.2988	0.99	0.5934	1.00	0.9456
pyruvic acid	1.03	0.7517	0.98	0.8756	0.98	0.9895

1-monostearoylglycerol	1.01	0.9207	1.01	0.9717	1.04	0.1681
aspartic acid	0.99	0.9627	1.09	0.0006	0.98	0.5956
5-aminopentanoic acid	0.86	0.2555	0.89	0.4730	0.82	0.0907
Cholesterol	0.96	0.3979	1.04	0.4079	1.00	0.9822
Glycerol	0.98	0.2602	0.99	0.9768	0.98	0.6743
valine	0.98	0.7830	0.97	0.4465	0.96	0.0845
1-Linoleoyl-glycerol	1.08	0.4269	1.08	0.4134	1.03	0.8605
sorbitol	0.78	0.0048	0.91	0.3928	0.96	0.9154
Glutathione	1.10	0.0078	0.93	0.1006	1.07	0.0804
cysteine	1.06	0.5107	0.92	0.2872	1.09	0.1879
Glycerol 3-phosphate	1.05	0.1196	1.06	0.0965	1.02	0.8398
2-aminoadipic acid	1.01	0.9925	0.95	0.6367	0.91	0.4773
glycine	0.97	0.3641	0.98	0.7457	1.00	0.9748
lactic acid	0.97	0.4854	0.98	0.6433	0.96	0.1461
nicotinamide	0.91	0.0002	0.96	0.1733	0.98	0.8085
uric acid	0.95	0.2174	1.00	0.9999	0.95	0.2158
homoserine	0.89	0.0844	1.00	0.9999	0.82	0.0053
2-hydroxybutyric acid	0.96	0.4085	0.95	0.2634	0.92	0.0302
isoleucine	0.98	0.7155	0.97	0.4893	0.96	0.1953
1-Oleoyl-glycerol	1.03	0.8696	0.95	0.6798	1.04	0.9384
leucine	0.97	0.3381	0.98	0.6566	0.97	0.2443
2-monooleoylglycerol	1.02	0.9584	1.05	0.6361	0.99	0.9999
Palmitelaidic acid	0.94	0.2189	0.91	0.0247	0.90	0.0042
threonine	0.88	0.0013	0.96	0.5700	0.93	0.0310
tyrosine	1.12	0.5364	1.11	0.6295	1.14	0.4355
serotonin	0.99	0.9941	1.03	0.8687	1.01	0.9989
2,3-pyridinedicarboxylic acid	1.04	0.9530	1.09	0.7450	0.88	0.5447
L-Methionine	0.85	0.0001	0.98	0.8630	0.93	0.0959
2-ketoglutaric acid	1.06	0.9818	1.12	0.8636	1.01	0.9399
5'-AMP	1.00	0.9881	1.03	0.3199	1.00	0.9994
alanine	1.00	0.9961	0.98	0.8034	0.99	0.9712
B-alanine	0.93	0.0615	0.95	0.1735	0.98	0.7565
linoleic acid	0.94	0.0017	1.02	0.6720	0.97	0.1251
N-acetylglutamate	0.94	0.4342	1.00	0.9992	0.85	0.0067
mannose	0.89	0.0001	0.96	0.1294	0.99	0.9499
b-Hydroxy-b-methylglutarate	0.78	0.1679	0.97	0.9923	0.84	0.4502
N-acetylglycine	1.06	0.6698	1.07	0.6005	1.13	0.0918

3-indoleproprionic acid	0.58	0.0260	0.77	0.3781	0.25	0.0001
cytosine	0.96	0.7636	0.92	0.1575	0.98	0.9894
D-Ribose 5-phosphate	0.96	0.5520	1.03	0.6859	0.97	0.8715
erythrose-4-phosphate	0.84	0.4706	1.10	0.8011	0.93	0.9781
nicotinic acid	0.74	0.0052	0.77	0.0138	1.00	0.9998

C.5 Analysis of Skeletal Muscle Metabolites

Analyte	DCA/ Control	p-value	Metformin/ Control	p-value	Combo/ Control	p-value
sedoheptulose-7-P	0.57	0.0135	0.77	0.3057	1.14	0.5615
glycolic acid	1.05	0.6922	0.98	0.9815	1.09	0.0778
aminomalonic acid	0.91	0.1780	1.03	0.9306	1.05	0.7114
phosphoethanolamine	0.89	0.7915	1.04	0.9910	1.22	0.1610
2-hydroxyglutarate	1.10	0.2890	0.95	0.8429	1.09	0.1959
ribose	0.66	0.0017	0.78	0.0625	1.13	0.3122
sarcosine	1.01	0.9824	0.98	0.8106	1.07	0.0787
diphosphate	0.94	0.5044	1.00	0.9999	1.04	0.5898
adenine	0.89	0.5129	0.96	0.9564	0.94	0.9818
uracil	1.03	0.9498	1.07	0.7014	1.06	0.6544
citric acid	1.06	0.7887	1.10	0.4069	1.10	0.2917
ornithine	0.93	0.6413	0.98	0.9842	1.04	0.8007
elaidic acid	0.95	0.5915	1.00	0.9995	1.10	0.0493
glutamine	0.97	0.7903	0.99	0.9701	1.05	0.2040
glyceric acid	0.73	0.0050	0.70	0.0016	1.00	0.9999
ribitol	0.95	0.3597	0.93	0.1939	0.99	0.9944
cis-Aconitic acid	0.95	0.2951	0.98	0.8541	1.01	0.9604
tryptophan	1.00	0.9978	0.98	0.8786	1.02	0.5647
arachidonic acid	0.82	0.0851	0.84	0.1498	1.15	0.1417
fumaric acid	0.95	0.5728	0.96	0.7130	1.03	0.6493
proline	0.96	0.6729	0.98	0.9574	1.02	0.9871
Xanthine	0.94	0.4134	0.92	0.2853	1.07	0.2773
pantothenic acid	1.00	0.9998	1.00	0.9990	1.04	0.1055
oleic acid	0.98	0.9055	1.03	0.7717	1.10	0.0034
urea	0.98	0.6578	0.98	0.8213	0.99	0.9177
phenylalanine	0.96	0.1888	0.98	0.6327	1.03	0.4118
Fructose	0.78	0.0663	0.84	2745.0000	1.01	0.9682
2-phosphoglycerate	1.06	0.8348	1.14	0.2513	0.71	0.0064

glucose-6-phosphate	1.01	0.9991	1.06	0.4755	0.84	0.0250
fructose-6-phosphate	1.00	0.9999	1.10	0.7019	0.78	0.2426
glucose-1-phosphate	0.98	0.9963	1.05	0.8929	0.82	0.2025
homocysteine	0.89	0.9078	1.03	0.9976	0.84	0.6498
Adenosine	1.13	0.9189	1.01	0.9999	0.75	0.6723
lauric acid	0.94	0.8939	1.16	0.3019	1.09	0.6830
histidine	0.96	0.8977	1.04	0.9247	1.03	0.8487
Myoinositol	0.94	0.3718	0.95	0.4914	1.04	0.3794
L-Glutamic acid	1.06	0.0929	0.98	0.8863	1.16	0.0001
hypoxanthine	0.90	0.0820	0.92	0.2150	1.09	0.0997
1-monopalmitoylglycerol	0.95	0.1372	0.97	0.6744	0.99	0.9998
malic acid	0.95	0.6397	0.98	0.9461	1.05	0.3474
phosphate	0.95	0.1770	0.97	0.6487	1.02	0.6470
creatinine	0.95	0.2403	0.97	0.7109	1.02	0.6981
glucose	0.90	0.1928	0.93	0.4549	1.10	0.2471
Heptadecanoic acid	0.88	0.2097	0.97	0.9439	1.09	0.3155
serine	0.98	0.7009	1.02	0.7465	1.05	0.0331
myristic acid	0.90	0.0219	1.02	0.9428	1.02	0.8872
4-hydroxyproline	1.04	0.9533	0.99	0.9995	1.05	0.7800
4-aminobutyrate	1.04	0.9521	0.99	0.9996	1.06	0.7783
3-phosphoglycerate	1.03	0.9150	1.08	0.3427	0.82	0.0061
gluconic acid	0.90	0.1214	0.96	0.7744	1.08	0.2944
myo-inositol 1-phosphate	0.87	0.3592	0.93	0.8032	1.17	0.1277
Nonadecanoic acid	0.84	0.5164	0.94	0.9560	1.17	0.2739
succinic acid	1.06	0.6510	0.96	0.8484	0.90	0.0956
phosphoenolpyruvate	0.97	0.9056	1.05	0.7069	0.85	0.0423
Stearic acid	0.94	0.2880	0.97	0.8279	1.04	0.5196
asparagine	0.94	0.5398	1.01	0.9994	1.07	
lysine	0.91	0.1346	0.98	0.9616	1.04	0.5031
palmitic acid	0.95	0.1188	0.98	0.7364	1.02	0.6500
pyruvic acid	0.91	0.4112	0.97	0.9265	1.10	0.2335
1-monostearoylglycerol	0.92	0.3464	0.93	0.5039	0.99	0.9982
aspartic acid	0.98	0.9325	1.06	0.3726	1.07	0.1050
5-aminopentanoic acid	0.69	0.0254	0.91	0.8115	1.13	0.6714
Cholesterol	0.89	0.1308	0.92	0.3928	1.05	0.4636
mannitol	0.95	0.3842	0.97	0.8415	0.99	0.9956
Glycerol	0.97	0.3583	0.97	0.3813	1.04	0.0753
valine	0.99	0.8894	1.00	0.9998	1.03	0.2282

1-Linoleoyl-glycerol	0.96	0.9499	1.06	0.8140	1.13	0.1636
sorbitol	0.96	0.5080	1.04	0.5624	0.99	0.9860
Glutathione	1.01	0.9956	1.00	0.9999	1.08	0.0263
cysteine	0.87	0.6437	0.92	0.8689	1.10	0.8305
Glycerol 3-phosphate	1.02	0.9681	0.99	0.9982	0.90	0.0577
2-aminoadipic acid	0.95	0.6789	0.97	0.9085	1.12	0.0230
glycine	0.93	0.1605	1.03	0.8010	1.02	0.8622
N-Acetylaspartate	0.93	0.9815	0.87	0.8805	1.05	0.8976
lactic acid	0.96	0.5215	0.94	0.2263	1.04	0.3183
nicotinamide	0.98	0.7045	0.99	0.9216	1.03	0.2389
uric acid	1.07	0.4135	1.08	0.2238	1.00	0.9968
homoserine	1.02	0.8835	1.17	0.9145	1.18	0.8157
5-aminovaleric acid	0.58	0.0002	0.78	0.0752	0.78	0.1621
2-hydroxybutyric acid	0.99	0.9957	0.97	0.9679	1.07	0.6402
isoleucine	0.99	0.9816	1.00	0.9975	1.04	0.0677
1-Oleoyl-glycerol	0.99	0.9940	1.05	0.7725	1.14	0.0346
leucine	0.99	0.9243	1.00	0.9998	1.04	0.0533
2-monooleoylglycerol	0.95	0.9047	1.06	0.8321	1.16	0.1532
Palmitelaidic acid	0.95	0.7154	1.03	0.9238	1.04	0.7823
threonine	0.93	0.0149	1.00	0.9977	0.99	0.9902
tyrosine	0.94	0.1026	0.99	0.9912	0.99	0.9999
2,3-pyridinedicarboxylic acid	0.68	0.3687	0.81	0.7518	1.04	0.9474
L-Methionine	0.95	0.1221	0.99	0.9675	1.01	0.9303
2-ketoglutaric acid	1.77	0.3030	0.96	0.9996	2.20	0.0451
5'-Adenosine monophosphate	1.06	0.6208	1.07	0.4762	0.97	0.9995
alanine	0.91	0.0298	1.01	0.9751	1.00	0.9958
B-alanine	1.04	0.4351	1.04	0.5037	1.06	0.2611
linoleic acid	0.97	0.7041	1.02	0.8129	1.09	0.0057
3-indoleproprionic acid	0.34	0.4136	0.62	0.9884	1.33	0.3875
D-Ribose 5-phosphate	0.88	0.5408	1.00	0.9999	1.12	0.2516

C.6 Analysis of Serum Metabolites

Analyte	DCA/ Control	p-value	Metformin/ Control	p-value	Combo/ Control	p-value
fucose	0.93	0.7870	0.93	0.3021	1.04	0.9440
kynurenine	1.25	0.1921	0.96	0.9864	0.96	0.9810
glycolic acid	0.82	0.0004	1.23	0.9984	1.08	0.4053
2-hydroxyglutarate	0.71	0.2583	1.13	0.0468	1.05	0.8672
ribose	0.79	0.2290	1.13	0.3796	1.04	0.9236
sarcosine	0.96	0.8387	1.05	0.9998	1.04	0.8901
diphosphate	0.97	0.0417	1.08	0.2852	1.05	0.2617
adenine	0.80	0.7420	0.85	0.8541	0.88	0.9304
uracil	1.00	0.9999	0.93	0.6334	0.92	0.5310
citric acid	0.94	0.2807	1.03	0.1565	0.99	0.9545
ornithine	0.96	0.2028	1.08	0.6910	1.03	0.8216
elaidic acid	0.87	0.9716	0.86	0.0005	0.98	0.8436
glutamine	0.99	0.4369	1.04	0.7656	1.02	0.8716
glyceric acid	0.93	0.0157	1.20	0.2187	1.00	0.9999
ribitol	0.88	0.3969	1.13	0.9999	0.96	0.9430
cis-Aconitic acid	0.85	0.6509	1.07	0.3253	0.94	0.7273
tryptophan	0.96	0.4343	1.02	0.1301	1.00	0.9964
arachidonic acid	0.93	0.0516	0.93	0.1449	0.99	0.9943
fumaric acid	0.97	0.9881	1.01	0.9767	0.98	0.9607
proline	1.02	0.9999	1.00	0.8848	0.99	0.9802
Xanthine	0.96	0.7494	1.12	0.9215	0.98	0.8418
pantothenic acid	0.97	0.9291	1.01	0.9256	0.99	0.9635
oleic acid	0.96	0.8109	0.94	0.1072	0.98	0.8386
urea	1.10	0.2633	1.01	0.9987	1.02	0.9688
phenylalanine	1.01	0.0589	0.97	0.3379	0.98	0.2221
Fructose	1.05	0.7486	0.95	0.9999	0.95	0.6362
glucose-6-phosphate	1.04	0.7807	0.96	0.9999	1.00	0.9999
homocysteine	0.97	0.9965	0.79	0.8195	0.73	0.7297
arabinose	1.01	0.9923	0.98	0.9972	1.08	0.6825
Adenosine	0.90	0.8873	1.14	0.9995	0.22	0.0119
lauric acid	0.99	0.3028	0.89	0.2265	0.87	0.1486
histidine	0.92	0.1679	1.14	0.8654	1.00	0.9999
Myoinositol	0.93	0.1029	1.09	0.9503	0.99	0.9987
L-Glutamic acid	0.85	0.0106	1.29	0.6493	0.96	0.9543
hypoxanthine	1.35	0.3892	1.35	0.8924	1.11	0.9508

1-monopalmitoylglycerol	0.96	0.8763	1.02	0.6424	0.98	0.8486
malic acid	0.98	0.9999	1.00	0.9426	0.99	0.9973
phosphate	1.01	0.6371	1.02	0.3308	0.95	0.0111
creatinine	1.33	0.0818	1.11	0.8551	0.99	0.9999
glucose	0.99	0.5499	0.98	0.2260	0.99	0.8909
Heptadecanoic acid	0.96	0.4017	0.95	0.0442	0.92	0.0579
serine	1.01	0.1483	1.03	0.0610	1.02	0.6699
myristic acid	1.03	0.0704	0.87	0.1568	0.87	0.0765
4-hydroxyproline	1.03	0.0598	1.14	0.0112	1.07	0.4634
4-aminobutyrate	1.03	0.0584	1.14	0.0111	1.07	0.4633
gluconic acid	1.05	0.0034	0.92	0.4925	0.97	0.3722
myo-inositol 1-phosphate	0.98	0.6201	1.06	0.8282	1.04	0.8074
Nonadecanoic acid	0.97	0.6885	0.94	0.2985	0.85	0.0314
succinic acid	1.02	0.0964	0.93	0.2136	0.99	0.9946
Stearic acid	0.98	0.9929	0.97	0.1996	0.99	0.7677
2-monostearylglycerol	1.15	0.6291	1.60	0.3201	1.39	0.8444
asparagine	1.00	0.5019	1.07	0.4884	1.02	0.9566
lysine	0.86	0.0636	1.24	0.8984	1.04	0.9758
palmitic acid	0.97	0.9692	0.97	0.0984	0.98	0.5474
pyruvic acid	0.91	0.6778	1.06	0.9202	0.98	0.9666
1-monostearoylglycerol	0.96	0.7142	1.04	0.9999	1.01	0.9837
aspartic acid	1.01	0.4279	1.08	0.3076	0.92	0.3266
5-aminopentanoic acid	0.90	0.1466	0.88	0.0571	0.84	0.0102
Cholesterol	0.97	0.9186	0.96	0.0146	1.01	0.9090
Glycerol	0.96	0.0702	0.96	0.0004	0.96	0.0727
valine	1.00	0.8461	0.99	0.7985	0.99	0.4700
1-Linoleoyl-glycerol	0.95	0.0077	0.91	0.0001	0.86	0.0001
cysteine	0.98	0.3829	0.88	0.2215	1.08	0.7031
Glycerol 3-phosphate	1.00	0.9806	1.02	0.9677	0.97	0.8534
2-aminoadipic acid	1.01	0.9435	0.98	0.9915	0.88	0.0269
glycine	1.02	0.5690	1.04	0.1814	0.99	0.9952
lactic acid	1.00	0.9954	0.99	0.9815	1.02	0.8312
uric acid	0.90	0.0573	0.95	0.4801	1.02	0.9621
homoserine	1.11	0.6006	0.94	0.7353	0.81	0.0008
2-hydroxybutyric acid	0.90	0.0918	0.92	0.1499	0.95	0.5847
isoleucine	1.01	0.6660	0.98	0.8369	0.99	0.8063
1-Oleoyl-glycerol	1.02	0.9704	0.81	0.0002	0.97	0.8192
leucine	1.00	0.6904	0.99	0.8884	0.99	0.6604
2-monooleoylglycerol	0.88	0.0120	0.83	0.0002	0.83	0.0001

Palmitelaidic acid	1.07	0.0372	0.83	0.2075	0.85	0.0808
threonine	1.04	0.8740	0.99	0.5550	0.95	0.0266
inosine	1.02	0.9982	0.93	0.9270	0.98	0.9964
tyrosine	1.10	0.0392	0.92	0.9224	0.93	0.0385
1,3-bisphosphoglycerate	0.99	0.9765	0.96	0.1551	0.99	0.9009
2,3-pyridinedicarboxylic acid	1.14	0.6327	1.00	0.9999	0.88	0.7103
L-Methionine	1.04	0.9347	0.99	0.4923	0.96	0.1042
2-ketoglutaric acid	0.66	0.2471	1.15	0.0147	1.02	0.9906
alanine	1.03	0.0360	0.96	0.9741	0.98	0.2972
B-alanine	0.98	0.2961	1.15	0.4254	0.94	0.8593
linoleic acid	0.98	0.4677	0.95	0.0823	0.97	0.3642
erythrose	0.93	0.9993	0.98	0.9160	0.97	0.9971
N-acetylglycine	1.01	0.1540	2.06	0.1080	1.84	0.6261
3,4-dihydroxybutanoic acid	0.97	0.5609	1.06	0.8800	1.12	0.0899
isocitrate	0.92	0.3130	1.21	0.9331	1.14	0.9998
lactate	0.96	0.7042	0.97	0.1046	0.98	0.8569

C.7 Analysis of Spleen Metabolites

Analyte	DCA/ Control	p-value	Metformin/ Control	p-value	Combo/ Control	p-value
fucose	1.10	0.7144	0.80	0.2318	1.10	0.6816
kynurenine	1.09	0.9775	0.50	0.1707	1.33	0.4298
sedoheptulose-7-P	0.96	0.5403	1.01	0.9640	1.00	0.9767
glycolic acid	1.05	0.5037	0.96	0.7242	1.00	0.9996
dopamine	1.06	0.9227	0.91	0.8091	1.13	0.5215
aminomalonic acid	0.99	0.9632	0.98	0.9305	1.01	0.9894
phosphoethanolamine	1.00	0.9976	0.94	0.0464	0.98	0.5770
2-hydroxyglutarate	1.13	0.0051	0.93	0.1786	0.96	0.4649
ribose	0.91	0.4706	0.87	0.2361	1.01	0.9999
sarcosine	1.11	0.0013	0.95	0.2663	1.00	0.9651
diphosphate	1.06	0.1980	1.04	0.6296	1.04	0.5131
adenine	1.05	0.3672	0.99	0.9747	1.00	0.9990
uracil	0.97	0.0656	0.94	0.0003	0.99	0.8987
citric acid	0.96	0.7789	0.94	0.4944	0.97	0.9271
ornithine	0.96	0.6370	0.91	0.0825	1.20	0.7870
glutamine	0.99	0.9750	0.97	0.2397	1.01	0.9959
glyceric acid	1.02	0.9518	1.01	0.9809	1.05	0.6100
ribitol	1.00	0.9999	0.89	0.4184	1.07	0.8295
cis-Aconitic acid	0.88	0.9042	0.75	0.5793	0.97	0.9988
tryptophan	0.99	0.9975	0.97	0.9204	1.04	0.6094
arachidonic acid	0.97	0.7647	0.91	0.0871	0.99	0.8265
fumaric acid	0.97	0.2407	0.96	0.0199	0.99	0.7731
proline	0.93	0.0329	0.94	0.1805	1.02	0.5086
Xanthine	0.96	0.0255	0.97	0.0632	1.00	0.9927
pantothenic acid	1.03	0.4738	0.97	0.6217	1.02	0.8473
oleic acid	0.96	0.8277	0.93	0.4828	1.01	0.9999
urea	0.99	0.9707	0.97	0.1402	0.95	0.0255
phenylalanine	0.95	0.0211	0.97	0.2853	1.01	0.8722
Fructose	0.80	0.0019	0.89	0.1401	1.09	0.1476
glucose-6-phosphate	0.86	0.0237	0.96	0.7717	1.00	0.9923
fructose-6-phosphate	0.87	0.0305	0.97	0.8772	1.01	0.9847
glucose-1-phosphate	0.82	0.0153	0.93	0.5779	0.99	0.9999
homocysteine	0.69	0.0332	0.83	0.4271	1.04	0.9013
porphobilinogen	0.94	0.8997	0.76	0.0495	0.96	0.9587
arabinose	0.89	0.5025	0.91	0.6558	1.04	0.9922

thymine	1.03	0.7807	1.03	0.7929	1.02	0.8883
Adenosine	1.46	0.0037	1.25	0.2155	1.02	0.9988
isocitric acid	0.94	0.9058	0.90	0.6472	0.98	0.9060
lauric acid	0.95	0.9574	0.92	0.8371	0.91	0.7309
histidine	0.90	0.0996	0.96	0.8494	1.04	0.5767
Myoinositol	1.03	0.3193	1.00	0.9920	1.02	0.4896
L-Glutamic acid	1.04	0.0148	0.98	0.4921	1.00	0.9971
hypoxanthine	0.95	0.0101	0.98	0.4112	1.01	0.7227
1-monopalmitoylglycerol	0.99	0.8448	0.99	0.5824	1.01	0.6649
malic acid	0.97	0.1534	0.96	0.0318	0.98	0.3227
phosphate	0.99	0.5997	0.98	0.0420	1.00	0.8927
creatinine	1.03	0.7126	0.90	0.0072	0.95	0.2903
glucose	0.96	0.7857	0.95	0.5411	1.00	0.9924
Heptadecanoic acid	0.91	0.1057	0.91	0.1539	0.97	0.8741
serine	0.94	0.0090	0.96	0.1797	1.01	0.8056
myristic acid	0.92	0.3855	0.89	0.1457	0.96	0.7163
4-hydroxyproline	0.98	0.6612	0.95	0.0261	0.96	0.3092
4-aminobutyrate	0.98	0.6645	0.95	0.0265	0.96	0.3095
3-phosphoglycerate	0.79	0.0094	0.78	0.0118	1.02	0.9380
gluconic acid	0.96	0.7898	0.93	0.4178	1.01	0.9891
myo-inositol 1-phosphate	1.00	0.9999	1.00	0.9997	1.04	0.5077
sedoheptulose	0.78	0.0002	0.94	0.5748	1.06	0.5490
Nonadecanoic acid	0.89	0.0286	0.90	0.0541	0.91	0.1035
succinic acid	1.32	0.0229	0.99	0.9995	1.00	0.9956
phosphoenolpyruvate	0.68	0.0119	0.67	0.0147	1.03	0.9530
Stearic acid	0.98	0.3925	0.96	0.0585	0.99	0.9383
ascorbate	1.07	0.5664	0.93	0.6205	1.01	0.9977
oleamide	0.99	0.9767	0.96	0.0471	0.99	0.9446
asparagine	0.92	0.2282	0.97	0.8451	1.04	0.5414
lysine	0.95	0.0869	0.97	0.5726	1.02	0.5853
palmitic acid	0.97	0.5168	0.96	0.2849	0.99	0.9042
pyruvic acid	1.03	0.9253	0.96	0.8395	0.99	0.8770
1-monostearoylglycerol	0.99	0.9048	0.98	0.5433	1.03	0.1509
aspartic acid	1.00	0.9855	0.98	0.2784	0.99	0.9345
5-aminopentanoic acid	0.90	0.1606	0.90	0.2008	0.98	0.9820
Cholesterol	1.01	0.7466	1.00	0.9953	1.02	0.3400
mannitol	0.89	0.1459	0.87	0.0621	0.83	0.0066
2,4-dihydroxybutanoic acid	0.90	0.0182	0.96	0.5348	0.98	0.9893

Glycerol	0.97	0.1936	0.97	0.1646	1.01	0.9757
valine	0.97	0.1022	0.98	0.4106	1.00	0.8916
1-Linoleoyl-glycerol	0.91	0.6205	0.85	0.2256	1.01	0.9941
sorbitol	1.03	0.9368	0.93	0.4966	1.01	0.9999
Glutathione	1.01	0.9937	1.00	0.9999	1.01	0.9999
cysteine	1.01	0.9483	0.91	0.0087	1.01	0.9982
Glycerol 3-phosphate	1.04	0.9039	0.96	0.9218	0.95	0.6756
2-aminoadipic acid	0.99	0.9347	0.96	0.1894	0.93	0.0094
glycine	0.96	0.0084	0.99	0.7956	1.00	0.9541
N-Acetylaspartate	1.03	0.8519	0.97	0.9303	0.99	0.9304
lactic acid	1.02	0.5628	0.99	0.9497	0.97	0.2837
nicotinamide	1.03	0.0764	1.01	0.8573	1.01	0.9077
uric acid	1.01	0.9564	0.97	0.6759	0.98	0.5842
homoserine	0.94	0.1698	0.94	0.2401	0.89	0.0134
5-aminovaleric acid	0.83	0.4887	0.85	0.6276	0.85	0.7276
2-hydroxybutyric acid	0.96	0.6273	0.93	0.1178	0.90	0.0184
isoleucine	0.97	0.1582	0.98	0.2910	1.01	0.8550
1-Oleoyl-glycerol	0.94	0.7551	0.88	0.2200	1.01	0.9996
leucine	0.97	0.0790	0.98	0.3264	1.00	0.9792
2-monooleoylglycerol	0.88	0.5454	0.82	0.2208	1.04	0.9999
Palmitelaidic acid	0.89	0.4594	0.87	0.3559	0.96	0.8343
threonine	0.94	0.0119	0.97	0.3657	0.99	0.9994
inosine	1.03	0.4942	1.01	0.9296	1.02	0.9583
tyrosine	0.92	0.0275	0.96	0.5909	1.01	0.7659
serotonin	1.03	0.3692	0.98	0.7143	1.01	0.9986
1,3-bisphosphoglycerate	1.06	0.1772	0.98	0.8078	1.03	0.9578
L-Methionine	0.94	0.0182	0.97	0.4094	1.01	0.9187
2-ketoglutaric acid	0.99	0.9999	0.78	0.6432	1.11	0.9365
5'-AMP	1.35	0.0009	1.19	0.1272	0.92	0.5256
3-hydroxybutyrate	1.08	0.1846	1.03	0.8713	1.04	0.9042
alanine	0.90	0.0030	0.97	0.7374	0.99	0.9992
B-alanine	1.00	0.9924	1.01	0.9014	0.97	0.1967
N-acetylglutamate	1.45	0.3600	1.27	0.7664	0.83	0.9225
b-Hydroxy-b-methylglutarate	1.03	0.8967	0.93	0.4795	0.96	0.7487
rhamnose	0.87	0.7392	0.85	0.5975	1.14	0.6789
Galactitol	1.02	0.9804	0.92	0.2973	0.99	0.9791
phenylpyruvate	0.86	0.8543	0.55	0.2737	0.78	0.5934